Universidad de Valencia
Departamento de Física Teórica

Estudio de la Dinámica
de los quarks
mediante teorías
de campos efectivas

Tesis doctoral presentada por
Juan José Sanz Cillero.

Director: **Antonio Pich Zardoya**.

28 de junio del 2004

Contents

Chapter 1

Prólogo y antecedentes

1.1 QCD como teoría de las interacciones fuertes

A través de muchos experimentos se ha hecho patente que la Cromodiámica Cuántica (QCD) parece ser la teoría adecuada para describir los procesos hadrónicos [1]. En la región de altas energías ($E \gg 1$ GeV) se puede ver que la teoría acepta una descripción perturbativa en términos de quarks y gluones.

En esta línea se han realizado muchos y exitosos cálculos perturbativos a varios órdenes en el parámetro de expansión, la constante de la interacción fuerte α_s. Estos resultados teóricos en la zona de altas energías -cortas distancias- han sido cotejados con muchos experimentos dando un notable acuerdo en todos ellos. No obstante, a través de análisis basados en las ecuaciones del Grupo de Renormalización, es bien sabido que el acoplamiento renormalizado $\alpha_S(\mu)$ crece a medida que la energía disminuye, de tal manera que alrededor de $E \lesssim 2$ GeV la expansión perturbativa en $\alpha_S(\mu)$ falla; debido a la no-conmutatividad de la simetría gauge de color $SU(N_C)$ la interacción entre quarks y gluones se vuelve más y más intensa a bajas energías –largas distancias–.

El resultado de esa interacción tan fuerte a largas distancias es lo que se denomina confinamiento. Los quarks y los gluones se ven por tanto "confinados" en el interior de los hadrones. Son éstos precisamente los grados de libertad asintóticos que se observan en la física macroscópica (de largas distancias en relación al tamaño hadrónico, del orden del Fermi). Así por tanto, los estados inicial y final en nuestros experimentos de bajas energías no van a ser quarks y gluones sino hadrones sin carga de color.

Teóricamente uno esperaría que existiera una transformación que ligara el lagrangiano de QCD y sus parámetros con las propiedades de los estados hadrónicos. A través de esta transformación se convertiría una interacción no perturbativa entre quarks y gluones a largas distancias en una interacción perturbativa entre estados hadrónicos. Cuál puede ser esta transformación o qué nuevo parámetro de expansión se ha de considerar es algo sobre lo que todavía hay controversia. En este trabajo

se presenta un amplio resumen de algunos de los métodos con que se ha tratado de afrontar este problema. Aún así, debido a la complejidad de la interacción no-perturbativa todavía no se ha encontrado un resultado general que resuelva este puzle que sigue siendo QCD.

En el capítulo 2 se introducirá y estudiará la acción de QCD así como algunas de sus propiedades. En concreto estudiaremos una simetría que posee el lagrangiano en el límite de masas cero, la simetría quiral. Sin embargo esta simetría se rompe espontáneamente debido a fenómenos no-perturbativos y el vacío de la teoría deja de ser invariante. Aunque no se conoce exactamente cómo se produce esta ruptura espontánea de la simetría quiral (SχSB) lo que actualmente nadie duda es que esto es así, ante el aluvión de indicios teóricos y fenomenológicos [2, 3, 4].

Así mismo en ese capítulo se estudiarán ciertas propiedades que muestra QCD en el límite en el que el número de colores N_C se hace infinito [5]. En ese límite los *loop*s fermiónicos vienen suprimidos por factores $1/N_C$ y en la visión hadrónica la contribución dominante viene dada por los procesos a orden árbol, sin *loop*s de hadrones, que vienen suprimidos por $1/N_C$. Éste es el contaje que emplearemos en la teoría efectiva a energías del orden de la masa de las resonancias y que conviene no confundir con la expansión en potencias de momentos que aparecerá en la Teoría Quiral de Perturbaciones. Hasta cierto punto el contaje en $1/N_C$ se corresponderá con un contaje en número de *loop*s, aunque también pueda haber contribuciones subdominantes de los diagramas con mesones a orden árbol.

1.2   Teorías efectivas: La simetría quiral

Un método ampliamente utilizado de afrontar el problema ha sido a través de teorías efectivas [6, 7]. Requiriendo las simetrías de la interacción subyacente – el lagrangiano de QCD en este caso– uno siempre puede contruir con los grados de libertad relevantes a las energías consideradas el lagrangiano más general que preserva esa simetría (aunque a priori nada impide que la acción efectiva pueda tener un número infinito de términos).

En física hadrónica se emplean estos grados de libertad para construir los lagrangianos efectivos. Las constantes no vienen fijadas por la simetría y deben por lo tanto ser fijadas mediante experimentos o por otros argumentos teóricos.

Para afrontar QCD a bajas energías, durante estas décadas pasadas se han ido desarrollando una serie de teorías efectivas de campos (EFT) basadas en la simetría quiral del lagrangiano de QCD para los quarks ligeros [7, 8, 9]. Cuando se trabaja por debajo del umbral de producción del quark *charm* uno puede integrar los tres sabores pesados –*charm*, *bottom* y *top*– y continuar con un lagrangiano efectivo de QCD con sólo tres sabores ligeros [10, 11].

Las masas de estos quarks son mucho menores que la escala dinámica Λ_{QCD} que genera la interacción no perturbativa, con lo que los términos de masa se pueden tomar como una modificación pequeña al lagrangiano y tratarse perturbativamente.

Así, en el límite de masas cero QCD presenta una simetría extra de sabor, la simetría quiral, que permite "rotar" independientemente los espinores derechos e izquierdos. Sin embargo esta simetría del lagrangiano no se observa físicamente ya que se encuentra espontáneamente rota, es decir, el vacío de la teoría no es invariante bajo este grupo de transformaciones $SU(n_f) \times SU(n_f)$. El subgrupo que continúa siendo una simetría de la teoría es el subgrupo vectorial $SU(n_f)_V$. Debido a ello se genera una serie de bosones de Goldstone (NGB), o más exactamente pseudo-bosones de Goldstone (pNGB), ya que la simetría no es exacta sino aproximada.

Este desarrollo dio lugar a una EFT para describir las interacciones entre los Goldstones a muy bajas energías (por debajo del umbral de cualquier otro estado hadrónico) y que estuviera basada en la simetría quiral. Se denominó teoría de perturbaciones quiral (χPT). Primeramente se construyó para el caso de dos sabores ligeros u/d, con el grupo de transformaciones $SU(2)_L \times SU(2)_R$ [8]. Posteriormente se repitió el trabajo también para el caso de tres sabores $u/d/s$ bajo la simetría $SU(3)_L \times SU(3)_R$ [9].

Para el caso de dos sabores el numero de generadores rotos es tres y aparecen ese número de Goldstones, que se pueden identificar fácilmente en el espectro físico con los tres piones. En el caso de tres sabores aparecen ocho pNGB que se identifican con el octete de pseudoescalares ligeros (π, K, η_8). Debido a que el quark strange es algo más pesado los kaones y la eta tienen masas ostensiblemente superiores a las de los piones, manteniéndose aún así con masas bastante por debajo de las del resto de hadrones.

χPT describe los observables mediante una expansión en potencias de los momentos y las masas de los pseudo-escalares sobre una escala característica quiral $\Lambda_\chi \sim 4\pi F_\pi \sim 1.2$ GeV, siendo $F_\pi \simeq 92.4$ MeV la constante de desintegración del pion. Dentro del lagrangiano que permite la simetría no todas las piezas van a ser igualmente relevantes a bajas energías. Las piezas con menor número de derivadas darán las contribuciones dominantes para $E \ll \Lambda_\chi$. Se establece así un contaje en potencias de momentos que se denomina contaje quiral y que falla alrededor de $E \sim 0.5$ GeV, al aproximarnos al primer multiplete de resonancias. Al nivel de *loop*s se observa que está ordenación se mantiene y que las correcciones radiativas a un determinado orden en momento son de tamaño similar al de los contratérminos. Con esto el contaje queda bien definido al nivel cuántico. Para un amplio resumen en χPT se pueden consultar las referencias [6, 12, 13, 14, 15].

1.3 Teoría quiral de resonancias: una teoría para mesones

Como se ha dicho antes la expansión quiral empieza a fallar según aumentamos la energía de los procesos. Para seguir manteniendo un nivel de precisión dado hay que realizar el cálculo hasta ordenes quirales cada vez más altos [16, 17, 18].

Sin embargo hay un punto en que no se pueden seguir ignorando el efecto del intercambio no-local de resonancias. Desde la década de los años cincuenta se ob-

servó que en algunos canales las amplitudes presentaban picos concentrados entorno
a determinadas regiones con momento total al cuadrado $s \sim M^2$ y una anchura de
la región $\Delta s \sim M\Gamma$. Estos resultados experimentales sugirieron que estos picos de
amplitud podían estar producidos por el propagador de una partícula intermedia
en el canal–s con los números cuánticos del canal. Cuando la energía del proceso
está cercana al polo del propagador se produciría un maximo en la amplitud. Las
energías a las que se producían estos picos era para $M \sim 1$ GeV, mucho mayores
que las masas del octete de pseudoescalares ligeros. Estas partículas empezaron a
ser incluidas en los modelos teóricos y fueron llamadas resonancias.

En los ochenta, además de desarrollarse χPT, se empezaron los primeros trabajos
en que se construían teorías efectivas incluyendo los bosones de Goldstone de la SχSB
y la resonancia vectorial $\rho(770)$ basándose en la simetría quiral y considerando dos
sabores ligeros [8].

Trabajos posteriores lo extendieron al caso $SU(3)$ y añadieron otros canales
aparte del vectorial $J^{PC} = 1^{--}$, como el axial-vector 1^{++}, el escalar 0^{++} y reso-
nancias pseudoescalares 0^{-+} [19]. A esta teoría se le denominó la Teoría Quiral de
Resonancias (RχT).

La expansión en momentos falla cuando se aumenta la energía de los procesos
por lo que el contaje quiral se vuelve inadecuado para estudiar los observables a
energías del orden de las masas de las resonancias. Sin embargo, en Ref. [5] fue
sugerida una expansión alternativa para los elementos de matriz en QCD –y para
sus descripciones efectivas– en potencias de $1/N_C$, donde N_C es el número de colores
en QCD, considerando $N_C \alpha_S$ constante. Aunque físicamente uno tiene $N_C = 3$
y se esperaría una lenta convergencia de la serie, fenomenológicamente se tienen
muchos motivos para creer que ésta es mucho más rápida y que ya las contribuciones
a primer orden en $1/N_C$ dan una muy buena descripción de un gran número de
fenómenos [5, 20, 21].

Estudios posteriores en RχT y χPT han permitido encontrar restricciones al
orden dominante en $1/N_C$ sobre algunos de los acoplamientos mediante comparación
con el comportamiento a cortas distancias de QCD [21, 22, 23].

1.4   Canal vectorial: Anchura y resultado perturbativo

RχT da una buena descripción de varios observables simplemente al orden do-
minante en $1/N_C$ (LO). Sin embargo falla cuando la energía del proceso está muy
cerca de la capa de masas de la resonancia. Como pasa en cualquier descripción
en teoría de perturbaciones de cualquier teoría cuántica de campos, falla cuando
hay diagramas que no son *one − particle − irreducible* (1PI) y el propagador de la
partícula intermeda se situa sobre la capa de masas. Estas situaciones se resuelven a
través de una resumación a todos los ordenes en teoría de perturbaciones de Dyson-
Schwinger [24, 25]. Esta resumación proporciona a todas las partículas inestables,
cuyos propagadores internos pueden ponerse sobre la capa de masas, una parte

absortiva imaginaria en el propagador de la resonancia, a veces denominada con el nombre de anchura.

Esta resumación debe hacerse también en RχT esencialmente del mismo modo pero siguiendo una serie de pautas adicionales. En Refs. [26, 105] se estudió el canal vectorial $J^{PC} = 1^{--}$ y se proporcionó una anchura para cualquier valor del momento para la primera resonancia vectorial, la $\rho(770)$. En el presente trabajo y en las publicaciones que han derivado de ella se siguió el espíritu de la resumación realizada en Ref. [26] extendiéndola a un estudio de canales acoplados pion-pion y kaón-kaón, y aplicándola al caso de la primera resonancia vectorial. De igual modo se han aplicado estas técnicas al canal escalar en un capítulo siguiente.

En el caso vectorial los resultados mostrados en este trabajo concuerdan con los obtenidos en Ref. [26], donde se sumaban las anchuras parciales a piones y a kaones obtenidas mediante estudios separados de canales desacoplados. Otros resultados similares se pueden encontrar en las Refs. [27, 28, 29].

Las resumaciones de Dyson mostrarán como la interación de estado final y la modificación de los propagadores se produce de un modo universal. Con esto se quiere decir que la modificación del propagador de cada partícula dependerá no de los estados inicial o final del proceso sino de los estados intermedios accesibles.

También se mostrará que este tipo de resumaciones de Dyson-Schwinger satiface exactamente unitariedad y que por lo tanto reproducimos los resultados obtenidos mediante métodos basados en unitariedad como el Método de la Amplitud Inversa [30], resumaciones de Bethe-Salpeter [31] o el método N/D [32]. Se mostrará cómo se recuperan sus resultados y cómo se explica la relación física entre sus parametros y los acoplamientos del lagrangiano de RχT.

Sin embargo, en las resumación de Dyson surge el problema de la renormalización de *loops* de Goldstones. Es en ese punto cuando uno se plantea si es posible construir una autentica teoría de campos para las interacciones fuertes en términos de mesones. Por ello en el capítulo 6 se estudiará un elemento de matriz, el factor de forma vectorial, a un *loop*. Se analizarán los problemas y complicaciones que surgen en el cálculo de procesos a segundo orden en $1/N_C$, así como sus posibles soluciones.

El resultado de esta parte del trabajo será por una parte una serie de determinaciones, bien fundadas teóricamente, de los acoplamientos y masas del primer multiplete vectorial al siguiente orden en $1/N_C$ (no sólo a primer orden como se había hecho hasta ahora). Por otro lado se pondrán de manifiesto cuáles son las líneas de investigación y sobre qué detalles de la teoría efectiva hay que realizar un trabajo más profundo si se quiere llevar los estudios en $1/N_C$ más alla del orden dominante.

1.5   Canal escalar: Poniendo en práctica lo aprendido en el sector vectorial

En el canal escalar iso-escalar $J^{PC} = 0^{++}$ tendremos que considerar dos resonancias con esos números cuánticos, la resonancia octete y la singlete, ambas dentro del mismo nonete quiral. Veremos que debido a la ruptura explícita de la simetría quiral por masas de quarks una resonacia octete puede convertirse en una singlete a traves de un *loop* de pNGB (el correlador entre la corriente octete y la singlete no es cero). Esto va a producir una mezcla entre ambos estados, que ahora dejarán de ser los autoestados físicos de masa. La obtención de estos autoestados va a complicar el procedimiento de obtención de las anchuras que se seguía en el caso vectorial.

Mostraremos cómo es posible realizar un análisis del factor de forma escalar a energías del orden de la masa de las resonancias escalares, aplicando las técnicas desarrolladas en el estudio del canal vectorial. De este modo, en el capítulo 7 se muestra como es posible realizar una resumación de Dyson con estados intermedios de dos Goldstones ($\pi\pi$, $K\overline{K}$ y $\eta\eta$). Esta descripción diagramática implementa de modo automático unitariedad y analiticidad, de modo que tras las debidas consideraciones se puede relacionar con facilidad este resultado resumado con el obtenido por otros trabajos basados en otros métodos [30, 31, 32].

Sin embargo en un primer análisis se puede estudiar los observables a energías por debajo del umbral $K\overline{K}$ y trabajar en QCD con dos quarks ligeros, *up* y *down*. Es más, bajo esta aproximación, se puede aplicar una simplicación extra que es trabajar en el límite de masas de pion nulas.

Así, en este capítulo se muestran los resultados que se obtienen de la comparación de la fase experimental [35] en la región elástica y el resultado teórico de la resumación de Dyson. Se comprobará que la descripción teórica es bastante buena, obteniéndose así, una estimación de la masa del primer multiplete escalar (siempre teniendo en cuenta que en el cálculo hay un grado de incertidumbre debido a tomar los piones sin masa en lugar de con sus masas físicas).

Por último, al final del capítulo se mostrará cómo es posible obtener información sobre el multiplete de resonancias escalares a partir de otros observables y otras técnicas diferentes, pero manteniéndose bajo el marco de la RχT. Así, se estudiarán los resultados obtenidos en simulaciones en el retículo para las constantes de desintegración del pion y del kaón. Se verá que es posible dar una explicación con una sólida fundamentación teórica a la dinámica que se viene observando en este tipo de observables para altos valores de las masas de los quarks *up* y *down*. El estudio al orden dominante en $1/N_C$ mostrará que bajo este contaje es posible reproducir los comportamientos observados. Del mismo modo, será posible extraer algunas determinaciones fenomenológicas (a partir de las simulaciones en el retículo) de la masa del primer multiplete $q\bar{q}$ de escalares y de los parámetros quirales.

1.6   Interacciones entre mesones B y Goldstones: Estudio de simulaciones en el retículo

En el capitulo 8 se presentará un estudio que se realizó en colaboración con J.F. Donoghue y A. Ross, y que llevó a la publicación del trabajo que se puede ver en la Ref. [33]. En él se hizo un estudio de las constantes de desintegración del meson B, f_B, y su constante de mezcla $B^0 - \overline{B}^0$, B_B. Se tomaron resultados de simulaciones en el retículo [34], que han de ser generados para valores no físicos de las masas de los quarks *up* y *down*. Por ello en este trabajo se analizó cómo era posible realizar una extrapolación hasta altos valores de masas de los quarks ligeros basándose en Teoría efectiva Quiral para mesones pesados (HMχPT). Con esta teoría se describen de modo efectivo las interacciones entre los mesones pesados, D o B, y el octete de pseudo-escalares ligeros, en el régimen energético cuando estos transportan una fracción del momento total mucho menor que la escala quiral $\Lambda_\chi \sim 1$ GeV.

Sin embargo, al igual que pasa con la Teoría de Perturbaciones Quiral habitual, las descripción efectiva falla cuando los momentos o las masas de del octete de psedo-escalares ligeros se vuelve muy grande. Se observa así en los resultados de las simulaciones en el retículo que hay un cambio de régimen para $m_\pi \gtrsim 0.5$ GeV. El comportamiento logarítmico prescrito por HMχPT desaparece.

Para describir este nuevo régimen, al mismo tiempo que se mantiene el buen comportamiento de HMχPT a bajos valores de las masas, se realizó el cálculo en la teoría efectiva pero regularizando las integrales de los *loops* con un $cut-off$ suave de forma dipolar, Λ_{cut}. Este parámetro se mantuvo a un valor finito entorno a $\Lambda_{cut} \sim 1$ Gev y se tomó como una constante que permitía parametrizar el punto en que los *loops* de HMχPT dejaban de ser relevantes y a partir del cual el comportamiento del observable se volvía lineal en m_π^2.

Aunque esto es un *ansatz* para describir los resultados de simluaciones en el retículo basándose en cáculos de teorías efectivas y añadiendo ciertas suposiciones razonables, los buenos resultados obtenidos en el capitulo 7 para el analisis de las simulaciones para las constantes F_π y F_K permite suponer que existe una fundamentación física más profunda para este *ansatz*; la descripción en $1/N_C$ podría ser una útil técnica a ser tenida en cuenta a la hora de analizar resultados de la física de B's.

1.7   Resumen de objetivos

Por tanto, resumiendo los puntos anteriormente explicados, los objetivos de la presente tesis de doctorado se centran en:

- Mejorar la descripción efectiva de las interacciones de resonancias. Se busca aumentar la precisión y la consistencia de la teoría a través del análisis de observables a un *loop*, así como el estudio de las complicaciones que surgen.

- A través de este análisis se puede obtener importante información con una sólida base teórica sobre los acoplamientos, masas y propiedades de los mesones vectoriales.

- De igual modo, se emplearán en el canal escalar las técnicas desarrolladas en el sector vectorial (que tiene una fundamentación mucho más establecida que la que uno tiene en el sector de *spin* cero). A través de ellas se obtendran algunas determinaciones de los parámetros de este tipo de resonancias, en concreto de aquéllas con iso-spin $I = 0$.

- Finalmente se plantea un primer acercamiento a las simulaciones de *Lattice* desde el planteamiento del contaje en $1/N_C$. Se busca con ello mostrar cómo es posible aplicar estas técnicas para describir desde un punto de vista más físico los comportamientos lineales observados en las simulaciones numéricas y descritos por *ansatze* de uno u otro tipo

Chapter 2

Quantum Chromodynamics and chiral symmetry

2.1 The QCD lagrangian

Quantum Chromodynamics (QCD) has been proved to be the theory to describe the strong interactions. It describes the strong interaction by a set of fermions –the quarks– and gauge bosons –the gluons–.

When the energy of the experiments increased it was realized that the hadrons were not really point-like particles but they rather had a composite structure. They were built by smaller fermions which were called quarks. The proton and neutron contained three of them of two different classes, *up* and *down*. The discovery of the baryon Δ^{++} with spin and isospin 3/2, and baryon number $B = 1$, showed that the description in terms of three single *up* constituents was inconsistent with the Fermi Exclusion Principle unless they were three different *up* particles: It became necessary to describe a quark not by a single Dirac spinor but by three of them –*Red*, *Green* and *Blue*, as they were going to be called–. These $N_C = 3$ different "colours" could be put together into a N_C vector of a new space –the colour space–,

$$q = \begin{pmatrix} q_{Red} \\ q_{Green} \\ q_{Blue} \end{pmatrix}, \qquad (2.1)$$

being q the *up* or *down* quark.

It is important to distinguish the three kinds of tensor structures that arise here: Dirac spinor structure, flavour structure (*up* or *down*), and colour structure (*Red*, *Green* and *Blue*).

Since it was impossible to identify the particular colour of each component of the Δ^{++} particle, there had to be at least a global symmetry $SU(N_C)_C^{global}$ in the colour space. It becomes obvious that the kinetic term for the coloured spinors is invariant

under colour transformations when it is expressed in the colour-vector notation:

$$\mathcal{L}_{quark}^{Kin} \; = \; i\,\bar{q}\,\slashed{\partial}\,q \; - \; m_q\,\bar{q}\,q\,. \tag{2.2}$$

When requiring the colour symmetry to be local, $SU(N_C)_C^{local}$ ($SU(N_C)$ since now on), one has to introduce the corresponding gauge bosons G_μ^a, with $a = 1, ..., (N_C^2 - 1)$. They transform under the adjoint representation of the group and provide a fair explanation of how the strong interaction occurs.

To compensate the action of the derivative over the local transformation one needs to construct the $SU(N_C)$ covariant derivative:

$$D^\mu\,q \; \equiv \; \left[\partial^\mu \; - \; i\,g_s\,\frac{\lambda_a}{2}G_a^\mu(x)\right]\,q \; \equiv \; [\partial^\mu \; - \; i\,g_s\,G^\mu(x)]\,q\,, \tag{2.3}$$

with the $N_C \times N_C$ matrix $[G^\mu(x)]_{\alpha\beta} \equiv [\frac{\lambda_a}{2}]_{\alpha\beta}G_a^\mu(x)$. Notice that the covariant derivative D^μ is also a $N_C \times N_C$ matrix in the colour space and that this operator depends on the position. The gauge transformation of the fields is:

$$
\begin{aligned}
q(x) & \longrightarrow & q'(x) = & \quad U(x)\,q(x)\,, \\[2mm]
\bar{q}(x) & \longrightarrow & \bar{q}'(x) = & \quad \bar{q}(x)\,U^\dagger(x)\,, \\[2mm]
G^\mu(x) & \longrightarrow & G^\mu(x)' = & \quad U(x)\,G^\mu(x)\,U^\dagger(x) \; - \; \frac{i}{g_s}(\partial^\mu U(x))\,U^\dagger(x)\,, \\[2mm]
D^\mu & \longrightarrow & (D^\mu)' = & \quad U(x)\,D^\mu\,U^\dagger(x)\,,
\end{aligned} \tag{2.4}
$$

with the gauge transformation $U(x) \in SU(N_C)$. The coupling g_s will be called the strong coupling constant and in non-abelian theories the charge of all the fermions must equal, i.e., all the quarks must couple with the same strength to the gluons.

To end with, one must consider the strength field tensor of the gluon field:

$$
\begin{aligned}
G^{\mu\nu}(x), & \equiv \; \frac{i}{g_s}\,[D^\mu, D^\nu] = \partial^\mu G^\nu - \partial^\nu G^\mu \; - \; ig_s[G^\mu, G^\nu] \equiv \frac{\lambda^a}{2}\,G_a^{\mu\nu}(x)\,, \\[2mm]
G_a^{\mu\nu}(x) & \equiv \; \partial^\mu G_a^\nu - \partial^\nu G_a^\mu \; + \; g_s f^{abc}\,G_b^\mu\,G_c^\nu\,,
\end{aligned} \tag{2.5}
$$

which transforms as

$$G^{\mu\nu}(x) \quad \longrightarrow \quad G^{\mu\nu}(x)' = \quad U(x)\,G^{\mu\nu}(x)\,U^\dagger(x)\,, \tag{2.6}$$

under the colour group, and, therefore, the colour trace $\mathrm{Tr}(G^{\mu\nu}G_{\mu\nu}) = \frac{1}{2}G_a^{\mu\nu}G_{\mu\nu}^a$ remains invariant. This tensor provides the kinetic term for the gauge bosons keeping the desired gauge invariance.

Therefore the QCD lagrangian for the quarks of n_f different flavours reads:

$$\mathcal{L}_{QCD} \; = \; -\frac{1}{2}\,\mathrm{Tr}(G^{\mu\nu}\,G_{\mu\nu}) \; + \; \sum_f \bar{q}_f\,(i\gamma^\mu D_\mu \; - \; m_f)\,q_f\,. \tag{2.7}$$

Those are all the non-irrelevant operators that one may construct keeping $SU(N_C)$ gauge invariance. Actually the symmetry allows as well one extra piece, but it violates CP and experimentally it has been proved to be completely neglectful. There is not a clear reason for this operator to be so suppressed and it is usually refered as the strong CP problem. The influence of this θ-term has not been considered in this thesis.

The last step is the inclusion of the gauge-fixing and Faddeev-Popov terms in order to properly quantize the fields. They remove the unphysical polarizations of the gauge bosons by fixing the gauge and introducing a set of anticonmuting scalar fields –the *Ghosts*–. None of these terms contains quark fields.

2.2 Non-perturbative regime of QCD

Hence, Quantum Chromodynamics (QCD) describes properly the strong interactions between the quarks and the gluons through a non-abelian gauge theory with symmetry $SU(N_C)$, being $N_C = 3$ the number of colours in the Standard Model (SM). There we have six different flavours for the quarks: *up, down, strange, charm, bottom* and *top* (from lighter to heavier). The existence of these flavours is nowadays quite well established and their masses are known within well controlled uncertainties. The three heavier ones own masses above 1.5 GeV. Moreover, since the strong interactions do not change the flavour they must be produced in $Q\bar{Q}$ pairs, which puts their production within a loop beyond 3 GeV. Therefore, when studying QCD around 1 GeV the heavy quarks *charm/bottom/top* may be integrated out of the theory and the observables may be described by an effective QCD theory with $n_f = 3$ light flavours. Sometimes one may even integrate out the *strange* quark if the analysis is to be done at very low energies, having a $n_f = 2$ flavours effective field theory (EFT) of full QCD.

The non-abelian interaction of the gluons generate large radiative corrections at low energies. When analysing the strong coupling constant with the renormalization group techniques one observes that it grows when decreasing the scale, becoming so large that the perturbative series breaks down around 1 GeV.

The variation with the scale is given by the beta-function:

$$\mu \, \frac{d\alpha}{d\mu} \;=\; \alpha\beta(\alpha) \tag{2.8}$$

which can be obtained from the perturbative calculation: $\beta(\alpha) = \beta_1 \frac{\alpha}{\pi} + \beta_2 \left(\frac{\alpha}{\pi}\right)^2 + ...$, with $\alpha \equiv g_s^2/4\pi$. At one loop we only obtain the first coefficient:

$$\beta_1 \;=\; \frac{2}{3}\,T_F\,n_f \,-\, \frac{11}{6}\,C_A \;=\; \frac{2n_f - 11N_C}{6}\,, \tag{2.9}$$

with the $SU(N_C)$-group constants $T_F = \frac{1}{2}$, $C_A = N_C$. In the standard model β_1 is negative and then the coupling increases when the scale decreases. For $N_C = 3$

the theory would need a number of flavours $n_f \geq 17$ to change this behaviour. Therefore, QCD with just light quarks –with the heavy flavours integrated out– or without quarks at all (quenched approximation from Lattice) maintain the same non-perturbative behaviour at low energies as full QCD in the SM.

The solution to the renormalization group equation (RGE) from Eq. (2.8) at one loop is then:

$$
\alpha(\mu) = \frac{\alpha(\mu_0)}{1 - \frac{\beta_1}{2\pi}\,\alpha(\mu_0)\,\ln\left(\mu^2/\mu_0^2\right)} = \frac{-\dfrac{2\pi}{\beta_1}}{-\dfrac{2\pi}{\beta_1\alpha(\mu_0)} + \ln\left(\mu^2/\mu_0^2\right)} = \frac{-\dfrac{2\pi}{\beta_1}}{\ln\left(\mu^2/\Lambda_{QCD}^2\right)},
$$

$$(2.10)$$

where there arises a dynamical QCD scale Λ_{QCD} due to the non-abelian interaction, defined from $0 < -\frac{2\pi}{\beta_1\alpha(\mu_0)} = \ln\mu_0^2 - \ln\Lambda_{QCD}^2$, this is, $\Lambda_{QCD} \equiv \mu_0 \exp\left\{\frac{\pi}{\beta_1\alpha(\mu_0)}\right\}$. The values $(\mu_0, \alpha(\mu_0))$ provide the initial conditions to the RGE. Thus, the non-perturbative interaction generates the so-called Landau pole at low energies, where the coupling constant becomes infinite.

Actually, the extrapolation of the one loop coupling to the non-perturbative region is not valid. In addition, higher perturbative orders modify the position of the Landau pole. What everybody agrees is that the renormalized constant becomes large in the low energy range and that the perturbative description is not valid any longer. Thence an effective description will be necessary for this region in terms of the proper degrees of freedom, the hadrons.

2.3   Decomposition in chiral components

The QCD lagrangian for n_f flavours can be written as:

$$\mathcal{L}_{QCD} = \mathcal{L}_{QCD}^0 + \ \Delta\mathcal{L}^{m_q} \ ,$$

$$\mathcal{L}_{QCD}^0 = i\overline{\Psi}\slashed{D}\,\Psi - \tfrac{1}{4}G_{\mu\nu}^a G_a^{\mu\nu} + \mathcal{L}_{GF} + \mathcal{L}_{FP} \ , \qquad (2.11)$$

$$\Delta\mathcal{L}^{m_q} = -\overline{\Psi}\mathcal{M}\Psi \ ,$$

where $\overline{\Psi} \equiv (\bar{u}, \bar{d}...)$ is a flavour vector containing the n_f different fermionic coloured fields, and $\mathcal{M} = \text{diag}\{m_u, m_d, m_s...\}$ is a diagonal $n_f \times n_f$ matrix in the flavour space, where m_i is the mass of each quark. $\mathcal{L}_{GF}$ and $\mathcal{L}_{FP}$ are the gauge-fixing and Faddeev-Popov terms which contain only gluon and ghost fields.

Notice that the QCD lagrangian has been split into two pieces. The quark mass contributions have been separated in $\Delta\mathcal{L}^{m_q}$. When observing the physical values of the light $u/d/s$ quark masses one realizes that they are much smaller than the dynamical scale $\Lambda_{QCD} \sim 0.5$ GeV generated by the non-perturbative interaction. Therefore one may consider the massless QCD lagrangian and later on introduce the quark masses as a small perturbation.

Let us now express the Dirac spinors in the QCD lagrangian in terms of chiral components in order to behold the new symmetry that arises in $\mathcal{L}^0_{QCD}$. The left and right components of a Dirac spinor are given by the projectors:

$$\begin{cases} q_L = \frac{1}{2} \left(1 - \gamma_5 \right) q \,, \\ q_R = \frac{1}{2} \left(1 + \gamma_5 \right) q \,. \end{cases} \tag{2.12}$$

and the corresponding conjugate spinors $\bar{q}_{L,R} = q^\dagger_{L,R} \gamma_0$ are:

$$\begin{cases} \bar{q}_L = \bar{q} \left(1 + \gamma_5 \right) \frac{1}{2} \,, \\ \bar{q}_R = \bar{q} \left(1 - \gamma_5 \right) \frac{1}{2} \,. \end{cases} \tag{2.13}$$

Therefore, the product between spinors with the same chirality vanishes: $\bar{q}_L q_L = \bar{q}_R q_R = 0$. Thence the mass term $m_q \bar{q} q$ only contains the crossed combinations: $\bar{q} q = \bar{q}_L q_R + \bar{q}_R q_L$.

The contrary happens to the kinetic term. The effect of the γ^μ on the right hand side of $\bar{q}_{L,R}$ is:

$$\begin{cases} \bar{q}_L \gamma^\mu = \bar{q} \gamma^\mu \left(1 - \gamma_5 \right) \frac{1}{2} \,, \\ \bar{q}_R \gamma^\mu = \bar{q} \gamma^\mu \left(1 + \gamma_5 \right) \frac{1}{2} \,, \end{cases} \tag{2.14}$$

and therefore the crossed combinations now disappear with the massless lagrangian becoming:

$$\mathcal{L}^0_{QCD} = i\overline{\Psi}_L \not{D}\, \Psi_L + i\overline{\Psi}_R \not{D}\, \Psi_R - \frac{1}{4} G^a_{\mu\nu} G^{\mu\nu}_a + \mathcal{L}_{GF} + \mathcal{L}_{FP} \,, \tag{2.15}$$

having $\overline{\Psi}_{L,R} \equiv (\bar{u}^{L,R}, \bar{d}^{L,R}...)$. where $\Psi_{L,R}$ are the left and right projections of each of the Dirac spinors in the flavour vector Ψ. This is telling us that the lagrangian does not allow a mass-less left-spinor to flip into a right-spinor and viceversa, so the left and right sectors do not talk each other. Nonetheless, the physical world contains a small mass term which mixes the different chiralities:

$$\Delta\mathcal{L}^{m_q} = -\overline{\Psi}_L \mathcal{M} \Psi_R - \overline{\Psi}_R \mathcal{M} \Psi_L \,. \tag{2.16}$$

In addition one will have to consider also the interaction with the electroweak sector of the SM. This can be easily implemented, but by now let us analyse the massless QCD situation where all the remaining interactions have been switched off.

In addition to these terms, the non-perturbative QCD regime is going to change the structure of the physical vacuum $|0\rangle$, because the interaction allows a non-negligible left-right flip.

2.4 Chiral symmetry

In the massless quark limit the term $\Delta\mathcal{L}^{m_q}$ disappears and the lagrangian $\mathcal{L}_{QCD}$ gains a set of new symmetries.

First, it is possible to perform global phase redefinitions independently in the left and right fields:

$$\psi_L \longrightarrow \psi_L^{'} = exp(i\theta_L)\ \psi_L \quad , \tag{2.17}$$

$$\psi_R \longrightarrow \psi_R^{'} = exp(i\theta_R)\ \psi_R \quad . \tag{2.18}$$

This group is $U(1)_L \otimes U(1)_R = U(1)_V \otimes U(1)_A$. The transformations with $\theta_L = \theta_R$ belong to $U(1)_V \equiv U(1)_{L+R}$, and the ones with $\theta_L = -\theta_R$ to $U(1)_A \equiv U(1)_{R-L}$. The $U(1)_V$ symmetry remains even with non-zero masses and gives rise to the baryonic number conservation. However, the subgroup $U(1)_A$ is anomalous and it is broken at the quantum level.

The current associated to the $U(1)_V$ symmetry is $B^\mu = \overline{\Psi}\gamma^\mu\Psi$, with the conserved baryonic charge $B = \int d\vec{x}^3\ B^0 = \int d\vec{x}^3\ \Psi^+\Psi$.

The lagrangian owns as well an invariance under the action of the chiral group $G \equiv SU(n_f)_L \otimes SU(n_f)_R$,

$$\psi_L \longrightarrow \psi_L^{'} = g_L\psi_L \quad , \tag{2.19}$$

$$\psi_R \longrightarrow \psi_R^{'} = g_R\psi_R \quad , \tag{2.20}$$

with the global transformations $g_L \in SU(n_f)_L$ and $g_R \in SU(n_f)_R$.

The Noether currents associated to the chiral group are:

$$J_X^{a\mu} = \overline{\Psi}_X\gamma^\mu\frac{\lambda^a}{2}\Psi_X \quad (X = L, R\ ; \quad a = 1, ..., n_f^2 - 1) \quad , \tag{2.21}$$

where $\frac{\lambda^a}{2}$ are the generators of the group $SU(n_f)$ and the indices $X = L, R$ point out the type of current. These currents provide the corresponding Noether charges $Q_X^a = \int d\vec{x}^3 J_X^{a0}(x)$, satisfying the commutation relations

$$[Q_X^a, Q_Y^b] = if_{abc}\delta_{XY}Q_X^c \quad , \tag{2.22}$$

with f_{abc} the $SU(n_f)$ structure constants.

A chiral transformation (g_L, g_R) can be observed in an alternative way, as a combination of two transformations: a vector transformation $g_h \in H \equiv SU(n_f)_{R+L}$, followed by an axial one $\Xi \in G/H$. One calls vector transformations $g_h = (h, h)$ to those with $g_L = g_R$, and axial transformations $\Xi = (\xi, \xi^{-1})$ to those with $g_L = g_R^{-1}$. Any element $g = (g_L, g_R)$ of the chiral group accepts the decomposition

$$(\xi, \xi^{-1}) \cdot (h, h) = (\xi h, \xi^{-1} h) \overset{h=\xi g_R}{=} (\xi^2 g_R, g_R) \overset{\xi^2 = g_L g_R^{-1}}{=} (g_L, g_R)\,. \tag{2.23}$$

which is unique, being h and ξ given by the relations $\xi^2 = g_L g_R^{-1}$ and $h = \xi g_R$. One may be tempted then to write the group G as the direct product of the vector subgroup times the axial one. However this is not true: Although this is right for the vector subgroup, the axial transformations do not form a closed subgroup. Only joining both types of transformation one gets a closed group, G.

Therefore, it is possible to express the full group G in terms of vector and axial generators. The corresponding vector and axial currents, J_μ^a and J_μ^{5a} respectively, are then

$$J_\mu^a \equiv J_{\mu R}^a + J_{\mu L}^a = \overline{\Psi}\gamma^\mu \frac{\lambda^a}{2}\Psi \ , \tag{2.24}$$

$$J_\mu^{5a} \equiv J_{\mu R}^a - J_{\mu L}^a = \overline{\Psi}\gamma^\mu \gamma_5 \frac{\lambda^a}{2}\Psi \ , \tag{2.25}$$

with the γ_5 definition given by $\gamma_5 q_R = +q_R$, $\gamma_5 q_L = -q_L$.

In the chiral limit these currents are conserved. However in physical QCD they obey partially conserved relations:

$$\partial_\mu \left(\bar{q}_j\gamma^\mu q_i\right) = i\left(m_{q_j} - m_{q_i}\right)\bar{q}_j q_i \qquad , \qquad \partial_\mu \left(\bar{q}_j\gamma^\mu \gamma_5 q_i\right) = i\left(m_{q_j} + m_{q_i}\right)\bar{q}_j \gamma_5 q_i \ . \tag{2.26}$$

There are two types of charges associated to these currents: The vector charges $Q_V^a = Q_R^a + Q_L^a$ and the axial ones $Q_A^a = Q_R^a - Q_L^a$. Under parity they transform as scalars and pseudo-scalar respectively for vector and axial charges:

$$Q_V^a = \int d\vec{x}^3 \, J_0^a(x^0, \vec{x}) \quad \longrightarrow \quad P\, Q_V^a \, P^{-1} = \int d\vec{x}^3 \, J_0^a(x^0, -\vec{x}) = Q_V^a \, ,$$

$$Q_A^a = \int d\vec{x}^3 \, J_0^{5a}(x^0, \vec{x}) \quad \longrightarrow \quad P\, Q_A^a \, P^{-1} = \int d\vec{x}^3 \left(-J_0^{5a}(x^0, -\vec{x})\right) = -Q_A^a \, . \tag{2.27}$$

This feature will be relevant when observing their actions over the vacuum.

These charges satisfy now some different commutation rules:

$$[Q_V^a, Q_V^b] = if_{abc}Q_V^c \quad , \tag{2.28}$$

$$[Q_A^a, Q_A^b] = if_{abc}Q_V^c \quad , \tag{2.29}$$

$$[Q_A^a, Q_V^b] = if_{abc}Q_A^c \quad . \tag{2.30}$$

These charges are going to commute with the massless QCD hamiltonian H_{QCD}^0 due to the current conservation:

$$[Q_V^i, H_{QCD}^0] = [Q_A^i, H_{QCD}^0] = 0 \qquad i = 1, ..., n_f^2 - 1 \quad . \tag{2.31}$$

Vafa and Witten [36] proved that the lowest energy state (the vacuum $|0\rangle$ by definition) had to be necessarily invariant under vector transformations:

$$Q_V^i \, |0\rangle = 0 \, . \tag{2.32}$$

Nonetheless, there are two alternative possibilities for the action of the axial charges. The two available realizations are shown in Tab. (2.1) [37]. The non-perturbative interaction is going to play a fundamental role and the physically observed realization is the Nambu-Goldstone one; the chiral symmetry becomes spontaneously broken due to the strong interaction and the vacuum turns out to be non-trivial.

$Q_{\mathrm{A}}^i \left|0\right\rangle = 0$	$Q_{\mathrm{A}}^i \left|0\right\rangle \neq 0$
Wigner-Weyl realiz. of G	Nambu-Goldstone realiz. of G
Symmetric bound state	Asymmetric bound state
$\left\langle 0\right| \overline{\Psi}_R \Psi_L \left|0\right\rangle = 0$	$\left\langle 0\right| \overline{\Psi}_R \Psi_L \left|0\right\rangle \neq 0$
Ordinary symmetry	Spontaneous Symmetry Breaking
Spectrum:	Spectrum:
Parity degeneration	Nambu-Goldstone bosons
Degenerate multiplets of G	Degenerate multiplets of $\mathrm{SU}(3)_{L+R} \subset G$

Table 2.1: Alternative realizations of the chiral group $G = \mathrm{SU}(3)_R \times \mathrm{SU}(3)_L$.

2.5   Spontaneous chiral symmetry breaking

The massless limit –with exact chiral symmetry– is a very good approximation for the *up* and *down* quark sector, with masses of the order of $\hat{m} = (m_u + m_d)/2 \sim$ 10 MeV. They are clearly much smaller than the QCD scale, of some hundreds of MeV. This approximation is also still suitable –but not as good– for the *strange* quark $m_s \sim 150$ MeV [82].

When considering the massless limit the unique energy scale in the theory is then Λ_{QCD}. It is generated dynamically through the strong interaction and it does not know anything about the quark masses, just depends on the size of $\alpha_s(\mu_0)$ at a reference scale μ_0. The masses of the heavy hadrons (the baryons and the $u/d/s$ resonances –with $M \sim 1$ GeV–) are mainly proportional to Λ_{QCD} and the quark masses only produce tiny modifications.

The phenomenology below the first resonance multiplet , the vectors of the $\rho(770)$ multiplet, shows only a spectrum of eight light pseudo-scalars, much lighter than any other hadron. The three lightest –the pions– form a nearly degenerate multiplet $(\pi^0, \pi^\pm)$, and the remaining five, $(K^+, K^-, \overline{K}^0, K^0, \eta)$, own larger masses and contain strange-ness (the kaons) or a $s\bar{s}$ component (the η).

This group of mesons can be easily classified in an octet of $SU(3)_V$. Actually, the light pions form a triplet of the isospin group $SU(2)_V$. When exchanging the quarks in the triplet (u, d, s) one has the analogous transformation in the mesons corresponding to the octet representation. For instance, the exchange $d \leftrightarrow -s$, which can be seen in Fig. (2.1), is reflected in the mesons as the exchanges $\pi^\pm \leftrightarrow -K^\pm$, $K^0 \leftrightarrow -\bar{K}^0$ and a more complicate change for the neutral pion and the η.

Now one may wonder about what happens when applying axial transformations. When applying a general axial transformation over a particle of the octet we would generate a state with a component of opposite parity. A mirror scalar octet should be found in that case. However it is not observed in the QCD spectrum. The closest group of scalars is placed around 1 GeV, and the difference cannot be attributed to the explicit chiral symmetry breaking from the quark mass term. These mirror
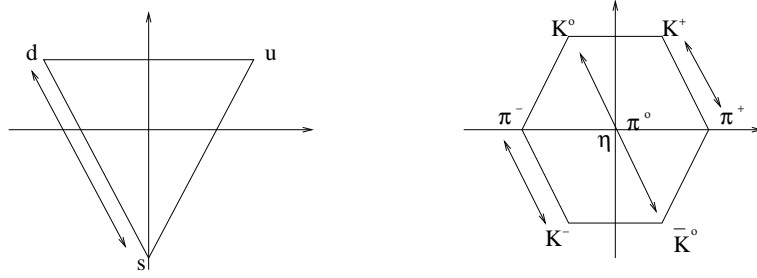
Figure 2.1: Actuation of the $SU(3)_{L+R}$ transformation $d \leftrightarrow -s$ over the quarks and the light pseudo-scalars.

scalars are not found even for the pions for which the chiral limit is rather good.

Therefore the approximate chiral symmetry of the lagrangian is not beheld in the physical spectrum, which does not show the expected degeneration in parity.

A given symmetry may be not observed in the spectrum for two reasons. On one side the symmetry may be explicitly broken in the lagrangian, i.e., not being invariant under the symmetry. On the other side the symmetry may be spontaneously broken, i.e, the physical vacuum is not trivial and is not invariant under these transformations.

The explicit breaking in QCD cannot explain the spectrum and therefore one finds that the non-perturbative interactions generate dynamically a spontaneous breaking of the chiral symmetry (SχSB).

The necessity of SχSB can also be observed by other arguments. One may analyse the vacuum expectation value (v.e.v.) of some QCD operators. In a given QFT, if the physical vacuum $|0\rangle$ is invariant under a given group G then the unique operators $\mathcal{O}$ that can get a non-zero v.e.v. are those being G-invariant:

$$\left.\begin{array}{c} G\,|0\rangle \;=\; |0\rangle \\[2mm] \mathcal{O} \neq G\,\mathcal{O}\,G^{-1} \end{array}\right\} \qquad \Longrightarrow \qquad \langle 0|\,\mathcal{O}\,|0\rangle \;=\; 0 \quad . \tag{2.33}$$

This can be expressed in other way: If an operator owns a non-zero v.e.v. then either the operator $\mathcal{O}$ is G-invariant or the the vacuum is not G-invariant.

$$\langle 0|\,\mathcal{O}\,|0\rangle \neq 0 \qquad \Longrightarrow \qquad \left\{ \begin{array}{c} G\,|0\rangle \neq |0\rangle\,, \\[2mm] \text{or} \\[2mm] \mathcal{O} = G\,\mathcal{O}\,G^{-1}\,. \end{array}\right. \tag{2.34}$$

Since the theory is invariant under Lorentz transformations, parity and charge conjugation, the unique candidates that can gain a non-zero v.e.v. are scalar operators. The simplest ones to analyse are those with the form $\bar{q}_i q_i$, which can be put

together in the form $\overline{\Psi}\Psi$. This operator is not invariant under the full chiral group $G = SU(n_f)_L \times SU(n_f)_R$ but just under its vector subgroup $H \equiv SU(n_f)_{L+R} \subset G$.

Therefore, if this non-G-invariant operator gets a non-zero v.e.v. one may conclude that the vacuum is not invariant under G. However, since this operator is invariant under H, the vacuum may still remain invariant under this subgroup even if the operator gets a v.e.v. different from zero, as it was required from other analyses [36]. This v.e.v. is therefore an order parameter of the chiral symmetry phase transition and it is usually named as the quark condensate.

There are many indications from QCD studies pointing out that in fact this v.e.v does not vanish. Thus, recent Lattice calculations [80] have obtained the value $\langle \bar{q}q \rangle \simeq -(250 \text{ MeV})^3$. The QCD sum rules have also yielded a value of the same order, $\langle \bar{q}q \rangle_{1 \ GeV} \simeq -(250 \text{ MeV})^3$ [2]. Some analyses of the divergence of the vector and axial quark current correlators provide the related invariant quantity $\langle \widehat{\bar{q}q} \rangle = -[(194 \pm 8) \text{ MeV}]^3$ [3], which is proportional to the quark condensate and point out a clear non-zero value. In addition, once assumed the hypothesis of SχSB it is possible to develop an EFT that when compared with the phenomenology provides a consistent non-vanishing v.e.v. [8, 9].

Therefore, one finds an overwhelming amount of hints that point out that the chiral symmetry becomes spontaneously broken; there is a set of Nambu-Goldstone bosons (NGB) and the way the symmetry is broken will be an essential ingredient to implement when constructing the corresponding low energy EFT.

In other words, the state of minimal energy, $|0\rangle$, is not invariant under G, just under H. As we saw before, the axial charges commute with the massless QCD hamiltonian [37]. These charges Q_A^i generate $i = 1, ...(n_f^2 - 1)$ states $Q_A^i |0\rangle$ different from the vacuum $|0\rangle$, with the same energy $E = 0$ as the bound state:

$$H_{QCD}^0 Q_A^i |0\rangle = Q_A^i H_{QCD}^0 |0\rangle = 0 \quad . \tag{2.35}$$

The spectrum contains eight states for $n_f = 3$, $Q_A^1 |0\rangle$, ... $Q_A^8 |0\rangle$ with $E = 0$, i.e., eight massless particles, the Nambu-Goldstone bosons from the SχSB. Moreover, these states have the same quantum numbers as the axial charges that create them: spin zero, odd parity and they transform as the adjoint representation of the group –octet in $SU(3)$, triplet in $SU(2)$–.

Summarising: The QCD lagrangian owns the chiral symmetry G but the physical spectrum and the vacuum must be invariant only under the vector subgroup H. The SχSB generate $(n_f^2 - 1)$ Nambu-Goldstone bosons. This breaking is due to the non-perturbative QCD dynamics and its mechanisms remain still not well understood.

2.6   The $N_C \to \infty$ limit in QCD

Many experiments have shown that the number of colours in physical QCD has to be $N_C = 3$ [1]. However, although being extremely successful in the high energy region, nobody has been able to fully solve the strong interaction at low energies.

Many years ago 't Hooft and Witten [5] proposed a limit where QCD suffered large simplifications. They studied QCD in the limit of large number of colours $N_C \gg 1$, but keeping $\alpha_s N_C$ as an $\mathcal{O}(1)$ constant (this means that α_s scales as $1/N_C$). The assumption was that the physical theory with $N_C = 3$ was qualitatively and quantitatively close to the theory in the $N_C \to \infty$ limit. Thus, solving the large N_C theory one could recover the bulk of physical QCD. In this limit the theory could be expressed as a series of powers of $1/N_C$, providing a formally well founded expansion. When considered the physical expansion $1/N_C = 1/3$ one would have a maybe slowly convergent series but which would provide a clear estimate about the size of the neglected terms in the perturbative calculations. The NLO contribution, $\sim \mathcal{O}(1/3)$, may become large due to an unexpected large coefficient, but it is much more difficult that the NNLO, $\sim \mathcal{O}(1/3^2)$ turns out to be as big as the LO, $\sim \mathcal{O}(1)$.

Many works have shown that the convergence is much better than expected and that the LO provides the main contribution [23, 21, 59]. The authors even suggested the possibility of further suppressions due to factors $\frac{1}{(4\pi)^2}$ from the loop kinematics. However, this point is still not clear at all.

The $1/N_C$ expansion is based on the fact that when there is a loop with some state running inside, it is not equally important when it is a quark or a gluon, since the number of them are N_C and $(N_C^2 - 1) \sim N_C^2$ respectively. From a more careful study one realizes that every quark loop is suppressed by a $1/N_C$ factor whereas the planar gluon loops are $\mathcal{O}(1)$ in the $1/N_C$ counting. There are also some other gluon diagrams (the non-planar diagrams) which start contributing beyond LO in $1/N_C$.

A clarifying example is the gluon self-energy. The diagram with two gluons has a factor $g_s \sim \sqrt{1/N_C}$ in each vertex and an extra combinatorial factor N_C from the summation $f^{acd} f^{bcd} = C_A \delta^{ab} = N_C \delta^{ab}$. However, the combinatorial factor that arises from the quark-antiquark loop is $\mathcal{O}(1)$, coming from the summation $\mathrm{Tr}(\frac{\lambda^a}{2} \frac{\lambda^b}{2}) = T_F \delta^{ab} = \frac{1}{2} \delta^{ab}$. One may construct diagrams including a larger number of loops and prove that, in general, every quark loop is suppressed by $1/N_C$ and that the non-planar gluon topologies (they cannot be painted on a plane without cutting or jumping over a propagator) are order $1/N_C^2$. As result of this, the gluon self-energy is $\mathcal{O}(1)$ in the $1/N_C$ expansion and it is dominated by the gluon loops.

Another indication of the dominance of the gluon diagrams in QCD is that the low energy behaviour of the strong coupling constant is mainly ruled by the gluon loops. The one loop contribution to the β-function from the quark loops is much smaller than that from the gluons ($2n_f \ll 11N_C$). Actually the confining feature of QCD is essentially due to the gluon interactions. The increasing of N_C makes the theory more confining and increases the QCD scale Λ_{QCD}. Actually the quarks and gluons are confined within the hadrons because the number of colours is "large enough". For $N_C = 2$ the theory would become weakly interacting at low energies for $n_f \geq 11$ (for $N_C = 3$ it was $n_f \geq 17$).

There are a series of phenomenological results that seem to hint that the $1/N_C$ expansion is a good approximation to what happens in the physical world:

1. **In hadronic physics one observes a suppression of the $q\bar{q}$ sea:** In the $N_C \to \infty$ limit the pair creation disappears and the $q\bar{q}$ sea does not exist any longer. For some years the Lattice simulations have being emulating QCD but in the quenched approximation (this is, without quark loops), with results quite close to the experimental ones. Even nowadays, that the quark loops can be simulated, one observes that the influence from the sea $q\bar{q}$ pairs is small.

2. Due to this same reason the quarks in the hadrons do not suffer interactions with the $q\bar{q}$ loops in the large N_C limit and therefore the exotic states with a large number of quarks (e.g. $q\bar{q}q\bar{q}$) decouple of the $q\bar{q}$ mesons.

3. **Zweig rule:** The mesons become classified in $U(3)$ nonets. In the $N_C \to \infty$ limit the axial anomaly disappears and the group $U(n_f)_L \otimes U(n_f)_R$ is reestablished [4].

4. **Two body decay dominance:** There is the experimental fact that the unstable meson decays are mainly to two bodies almost on their mass-shells. Some of these products may be unstable resonances, giving further decays afterwards.

   In the large N_C limit the amplitude for an unstable meson going to two mesons is $\mathcal{O}(1/\sqrt{N_C})$, whereas a higher number of final mesons would give a larger suppression in $1/N_C$.

5. **Spontaneous chiral symmetry breaking:** In the $N_C \to \infty$ limit it was proven that a $U(n_f)_L \otimes U(n_f)_R$ chiral theory had an spectrum of n_f^2 massless pseudo-scalar particles, which could be put together within a $U(n_f)$ multiplet [4]. These particles are nothing else but the NGB from the SχSB.

All these hints point out the thorough efficiency of the $1/N_C$ arguments. In the next chapters we will see that, at energies around the mass of the resonances, it is not trivial what kind of perturbative counting to handle. The $1/N_C$ expansion will prove to be a quite successful tool to describe the hadronic processes in that range.

Chapter 3

Chiral Perturbation Theory

As it was realized in the last chapter, in the massless limit the QCD lagrangian gains an extra symmetry, the chiral symmetry. Actually the lagrangian owns small mass terms but the chiral symmetry limit is still a fair approximation for the light quarks. However, QCD does not show this invariance nor small deviations from it. The symmetry becomes spontaneously broken and the vacuum turns non trivial. Thence, a set of massless NGB appears in the spectrum. Nonetheless, they are not exactly massless but the NGB have small masses, since there is a tiny explicit symmetry breaking in the real QCD lagrangian. For this reason these particles are very often called pseudo-Nambu-Goldstone bosons (pNGB).

In this chapter one will find the way to construct their EFT. This is the Chiral Perturbation Theory (χPT) and, as it happens with the EFTs, it accepts more than one unique realization. However, all the set of equivalent EFTs must provide exactly the same on-shell amplitudes.

The range of validity of the theory is provided by a characteristic chiral symmetry breaking scale Λ_χ and all the hadronic scales in QCD are proportional to it. When computing loops of Goldstone bosons one will obtain an expansion in inverse powers of $\Lambda_\chi \sim 4\pi F \sim 1.2$ GeV, being $F \simeq F_\pi = 92.4$ MeV the pion decay constant. At low energies there are also contributions from the heavy mass resonance to the local counterterms which introduce a scale of the same size, $\Lambda_\chi \sim M_R \sim 1$ GeV. For sake of this, the expansion in powers of the momenta of χPT naturally breaks down when approaching to the first resonance multiplet, $M_V \sim 770$ MeV. At high energies one has non-local interactions through the exchange of heavy resonances. At low energies they generate contributions to the low energy constants, being these contributions "suppressed" by p^2/M_R^2, denoting p the external momenta of the considered process.

A last comment before passing to the construction of the EFT. As it was reminded before, a peculiarity of these EFTs is that the Green functions are not really described by a unique effective lagrangian. There is an infinite number of realizations in which the symmetry can be implemented. In the next chapter we will

add the resonance fields. There will be some ambiguities around the definition of the resonance fields and the resonance lagrangian. Moreover, there will be some ambiguities about what is a local NGB interaction and what is resonance interaction. There are several options to describe the Green functions and all of them are right if the Green functions are equivalently described, obeying their QCD requirements.

3.1   Effective description of the Goldstone bosons

At the end of the last chapter we saw that the QCD chiral symmetry became spontaneously broken to the vector subgroup $H = SU(n_f)_{R+L}$.

Below the first resonance multiplet ($E < M_\rho \simeq 770$ MeV) the QCD spectrum contains the octet of light pseudo-scalars (π, K, η_8), which in the last chapter was related to the Nambu-Goldstone bosons from the SχSB. The pions, with $m_\pi \simeq 138$ MeV, are somewhat lighter, whereas the kaons, with $m_K \simeq 496$ MeV, and the η_8, with $m_\eta \simeq 547$ MeV, form the heavier components of the octet.

Among the full QCD spectrum we are now interested in these light degrees of freedom, including the resonances in the next chapter. These are the relevant ones for the processes at very low energies.

The quark masses can be considered as small compared to the dynamical QCD scale Λ_{QCD}, $m_u(1 \text{ GeV}) = (5.0 \pm 2.5)$ MeV [82], $m_d(1 \text{ GeV}) = (8.5 \pm 2.5)$ MeV [82], $m_s(1 \text{ GeV}) = (160^{+28}_{-35})$ MeV [74, 75]. On the contrary, the remaining quarks own masses much larger than this scale, $m_c(m_c) = (1.23 \pm 0.09)$ GeV [81], $m_b(m_b) = (4.0 - 4.4)$ GeV [82], $m_t(m_t) = (168.2^{+9.6}_{-7.4})$ GeV [82], so the heavy quark sector is decoupled from the theory, and only the light quarks are considered.

The decoupling theorem (Appelquist-Carazzone theorem [10, 11]) states that a theory with a light field ϕ and a heavy field Φ, with masses m and M respectively, can be described at low energies ($E \ll M$) in terms of just the light degrees of freedom. Take a high energy theory with action $S[\phi, \Phi]$. The parameter λ will denote the set of couplings for terms that contain at least one field Φ and g for those operators with only light fields ϕ. Then, the theorem says that the Green function with only light particles on the external legs can be given by an effective action $\widetilde{S}[\phi]$. This action, up to corrections of order $\mathcal{O}(E/M)$, is obtained from the initial $S[\phi, \Phi]$ through omitting the terms of it containing the heavy fields Φ and replacing the original mass m and the light couplings g by new parameters $\widetilde{m}$ and $\widetilde{g}$. These new parameters will be functions of the high energy ones, i.e. $\widetilde{m}(m, g, M, \lambda)$ and $\widetilde{g}(m, g, M, \lambda)$.

The hypothesis the theorem is based on is that both the original action $S[\phi, \Phi]$ [10] and the low energy effective action $\widetilde{S}[\phi]$ [13] must be renormalizable. Thus, in our case with QCD for a number n_f of flavours at momenta $s \ll m_c^2 \sim (1.5 \text{ GeV})^2$ one may consider QCD with just the light quarks $u/d/s$, satisfying the Appelquist-Carazzone theorem since QCD is renormalizable for any number of flavours n_f.

However, in other cases when one of the theories –the original or the low energy

one– is not renormalizable the conditions of applicability of the theorem are not well known. Thus, later we will study a theory including heavy resonances ($M_R \sim 1$ GeV) and the light octet of pseudo-scalars and will compare the result with that expected from the decoupling theorem. Due to the non-renormalizability of both theories (they are renormalizable order by order) one may not ensure that when integrating out the resonance degrees of freedom there are not large contributions in the form of logarithms of the high scale over the light one. Something similar to this happens in the electroweak theory with the $SU(2)_L$ doublet (t, b) when trying to build an EFT for just the quark b. For the scales of the low energy theory, $m_b \sim 5$ GeV, there are large contributions from logarithms of the form $\ln(m_t/m_b)$ with $m_t \sim 150$ GeV, since the effective theory with just the quark b breaks the electroweak gauge symmetry, spoiling the renormalizability of the theory [13].

In QCD with just $u/d/s$ one realizes that all the information from the heavy quarks is within the couplings of the three-light-flavour QCD (together with the low energy constants of effective operators suppressed by the heavy quark masses).

Once the heavy degrees of freedom (d.o.f.) are removed from QCD one observes that, even so, the quarks and the gluons are not the suitable d.o.f. since their interactions become strong and perturbation theory fails.

In order to construct the EFT lagrangian one will consider the massless QCD lagrangian, adding the masses later as a perturbation.

The massless d.o.f. that appeared from the SχSB were associated to the generators of the chiral group that did not leave the vacuum invariant, the axial generators. Thus, when an infinitesimal axial transformation g_A acts over the vacuum it generates a NGB state π^a with the quantum numbers of the given generator Q_A^a:

$$g_A\,|0\rangle \;=\; \left\{ 1 + i\epsilon^a Q_A^a + \mathcal{O}(\epsilon^2) \right\} |0\rangle \;=\; |0\rangle + i\epsilon^a|\pi^a\rangle + |\mathcal{O}(\epsilon^2)\rangle \qquad (3.1)$$

where the axial charges Q_A^a are the generators of the transformations on the Fock space [58]. At this point one realizes that the definition of the NGB fields is not unique beyond infinitesimal transformations. This has nothing to do with QCD itself. Even in the simplest case of spontaneous symmetry breaking, with a complex field Φ and a quartic potential, the NGB can be realized either as $\Phi = \frac{1}{\sqrt{2}}(v + \phi + i\pi)$ or as $\Phi = \frac{1}{\sqrt{2}}(v + \phi)exp[i\pi/v]$, with v the vacuum expectation value of Φ. Only when computing the on-shell amplitudes all the realizations provide the same result.

Therefore we are going to parametrize –to map– all the possible NGB states. We will perform arbitrary chiral transformations $\Xi(x) \in G$ over the vacuum $|0\rangle$. This will characterize any possible state $|\phi(x)\rangle$ of the Fock space of Goldstone bosons:

$$|\Phi(x)\rangle \;=\; \Xi(x)\,|0\rangle. \qquad (3.2)$$

Notice that now the transformations are not local and are different for every point x. This set of general transformations $\Xi(x) = \Xi[\epsilon_A^a(x)Q_A^a, \epsilon_V^b(x)Q_V^b] \in G$ are not infinitesimal in general, but when taking the infinitesimal limit $\Xi(x) = 1 + \epsilon_A^a(x)Q_A^a +$

$\epsilon_V^b(x)Q_V^b + \mathcal{O}(\epsilon^2)$ they must reproduce the result in Eq. (3.1). Through this prescription one may characterise the Goldstone fields at the infinitesimal level by $\epsilon_A^a(x)Q_A^a |0\rangle = |\pi(x)\rangle$. Therefore one may replace the charges by the NGB fields when working in a concrete realization. Some extra factors may be left dividing or multiplying, in order to have their corresponding kinetic terms normalized and the scalar fields with their canonical dimension $[\pi] = E$.

The ϵ^a parameters of the transformations are now $\epsilon^a(x)$ but the action of the charges has not changed. Moreover, if a global group leaves the vacuum invariant, the same group with local transformations also leaves the vacuum unchanged. Therefore one has that for $g_h(x) = (h(x), h(x)) \in H$, then $g_h(x) |0\rangle = |0\rangle$. Thus our description of the states $|\Phi(x)\rangle$ is ambiguous since

$$\Xi(x) |0\rangle = (\Xi(x)g_h^\dagger(x)) g_h(x) |0\rangle = (\Xi(x)g_h^\dagger(x)) |0\rangle . \qquad (3.3)$$

The same state is then described by a set of equivalent transformation $\Xi(x)g_h(x)^\dagger$, for any $g_h(x) \in H$. The set of transformations is divided then in classes of equivalence $[\Xi(x)] = \{\Xi(x)g_h(x)^\dagger : g_h(x) \in H\}$. Therefore one must choose a representative of each class of equivalence, $\overline{\Xi}(x) = (\xi_L(x), \xi_R(x))$. Thise choice of representatives breaks the ambiguity and maps uniquely all the NGB states.

However, the fact of choosing a representative of the class modifies the transformation properties of the fields: When applying a chiral transformation $g = (g_L, g_R)$ over the NGB state $\overline{\Xi}(x) |0\rangle$, the new state may not be a representative of its class:

$$(\xi_L(\phi), \xi_R(\phi)) \quad \xrightarrow{G} \quad (\xi_L', \xi_R') = (g_L \xi_L(\phi), g_R \xi_R(\phi)) . \qquad (3.4)$$

Therefore, one has to apply a compensating transformation $g_h(g, \Xi(x))^\dagger$ on the right which depends on either the initial state and the chiral transformation:

$$g \cdot \Xi(x) \quad \xrightarrow{g_h^\dagger} \quad \overline{\Xi}'(x) = g \cdot \Xi(x) \cdot g_h(g, \Xi)^\dagger , \qquad (3.5)$$

which for each coordinate means

$$g_L \xi_L(x) \quad \xrightarrow{g_h^\dagger} \quad \xi_L'(x) = g_L \xi_L(x) h(g, \Xi)^\dagger ,$$

$$\qquad (3.6)$$

$$g_R \xi_R(x) \quad \xrightarrow{g_h^\dagger} \quad \xi_R'(x) = g_R \xi_R(x) h(g, \Xi)^\dagger ,$$

and in such a way that $\overline{\Xi}'(x)$ is again a representative of its class. Obviously the compensating transformation depends on our choice for the chiral group representation.

3.1.1   Different representations

There are many different options for this mapping but I will consider in this work just the two main ones used in the bibliography:

I) Representation $U(x)$:

This is the one used by Gasser and Leutwyler in their initial papers [8, 9]. Here one of the coordinates $\xi_{L,R}$ is set to unit (we will use $\xi_L = 1$). The coordinates are then expressed as elements of the chiral group with the form $(1, U(x))$, with $U(x) \in SU(n_f)$. In order to represent the NGB fields, one has to choose also how to map these $U(x)$ transformations in such a way that an infinitesimal transformation of the group reproduces what is expected from equation Eq. (3.1). In this work I will use a matrix representation of the NGB fields, through

$$\Phi \equiv \frac{\lambda^a}{\sqrt{2}}\phi^a = \begin{pmatrix} \frac{\pi^0}{\sqrt{2}} + \frac{\eta_8}{\sqrt{6}} & \pi^+ & K^+ \\ \pi^- & -\frac{\pi^0}{\sqrt{2}} + \frac{\eta_8}{\sqrt{6}} & K^0 \\ K^- & \overline{K}^0 & -\frac{2\eta_8}{\sqrt{6}} \end{pmatrix}, \tag{3.7}$$

in such a way that an infinitesimal transformation must be equal to

$$(\xi_L(x), \xi_R(x)) = \left\{ 1 + \frac{i}{F\sqrt{2}}\Phi(x) + \mathcal{O}(\Phi^2) \right\} \cdot g_h(x), \tag{3.8}$$

where the factor $\frac{1}{F\sqrt{2}}$ is not really relevant and normalizes the fields in the canonical way and to the standard scalar field dimensions. The vector component of the transformation, $g_h(x) \in SU(n_f)_{L+R} \subset SU(n_f)_L \otimes SU(n_f)_R$, would leave the vacuum unchanged: $g_h(x)|0\rangle = |0\rangle$.

For this representation it means that an infinitesimal $U(x)$ must be equal to $U(x) = 1 + \frac{i\sqrt{2}}{F}\Phi + \mathcal{O}(\Phi^2)$, with the remaining vector component being $g_h = \left(1 - \frac{i\sqrt{2}}{2F}\Phi + \mathcal{O}(\Phi^2), 1 - \frac{i\sqrt{2}}{2F}\Phi + \mathcal{O}(\Phi^2)\right)$. Even at this level there are many ways to map the matrix $U(x)$, and all of them are going to have the same chiral transformation properties.

The most usual choice of coordinates is the exponential realization:

$$U(x) = \exp\left\{ \frac{i\sqrt{2}}{F}\Phi(x) \right\}. \tag{3.9}$$

However there is an infinity of available realization. Another could be for instance, $U(x) = \left(1 - \frac{i}{\sqrt{2}F}\Phi\right)^{-1}\left(1 + \frac{i}{\sqrt{2}F}\Phi\right)$, with this $U(x)$ also belonging to $SU(n_f)$. Although all of them provide the same on-shell description, they generate different off-shell behaviours, pointing out the fact that the EFT is uniquely defined only for amplitudes with the fields of the external legs being on-shell.

The chiral transformation properties for this choice of coordinates will be:

$$(1, U(x)) \xrightarrow{G} (g_L, g_R U(x)) \xrightarrow{g_h^\dagger = (g_L^\dagger, g_L^\dagger)} (1, U'(x)) = (1, g_R U(x) g_L^\dagger), \tag{3.10}$$

where in this case the compensating transformation is just $g_h^\dagger = (g_L^\dagger, g_L^\dagger)$ and does not depend on the coordinates. The coordinates transform then as:

$$U(\phi) \xrightarrow{G} g_R\, U(\phi)\, g_L^\dagger\,. \tag{3.11}$$

Notice that the coordinate $U(x)$ transforms linearly under the chiral group but not so the NGB fields $\Phi(x)$ in it. For vector transformations, this is $g = (g_L, g_R) = (h, h)$, the compensating transformation is Φ-independent and values $g_h(g, \phi) = (h, h)$. In that situation, the NGB fields transform linearly as the coordinates, i.e., $\Phi \longrightarrow \Phi' = h\,\Phi\,h^\dagger$.

II) Representation $u(x)$:

An alternative representation of the chiral group, which is also employed later in the resonance EFT, is the Callan-Coleman-Wess-Zumino formalism in terms of $u(x)$. It simplifies the construction of chiral invariant operators and it is employed for instance in the $\mathcal{O}(p^6)$ χPT lagrangian [16]. It is also employed when building up the effective theory of Goldstones and resonances [19].

In this case the set of representatives has the form $\Xi(x) = (u(x)^\dagger, u(x))$, i.e., the corresponding left-right coordinates obey the relation $\xi_R(x) = \xi_L(x)^\dagger$.

The action of the chiral group is then given by a compensating transformation $g_h^\dagger$ which depends also on $\Xi(x)$

$$(u^\dagger\,,\, u) \quad \xrightarrow{G} \quad (g_L\, u^\dagger\,,\, g_R\, u) \quad \xrightarrow{g_h^\dagger} \quad (u'^\dagger\,,\, u') = (\, g_L\, u^\dagger h(g,u)^\dagger\,,\, g_R\, u\, h(g,u)^\dagger\,),$$
$$\tag{3.12}$$

with $h(g,u)$ such that $u'(x) = g_R\, u(x)\, h(g,u)^\dagger = h(g,u)\, u(x)\, g_L^\dagger$.

Similarly to the previous realization, when one has an infinitesimal transformation it reproduces the structure in Eq. (3.8). This contains an ambiguity in the realization of the non-infinitesimal transformations. In general the usual choice is the exponential:

$$u(\phi) = \exp\left[i\frac{\lambda^a}{2}\frac{\phi^a}{F}\right] = \exp\left[i\frac{\Phi}{\sqrt{2}F}\right] \in SU(3) \quad. \tag{3.13}$$

Again, in general the action of the chiral group over the NGB fields is not linear. However, it becomes so when it is the vector subgroup who acts. When one has a chiral element $g = (h, h^\dagger)$ from the vector subgroup the compensating transformation turns out to be independent of the state Φ and equal to $g_h[g, \phi] = (h, h)$. Then the $u(x)$ tensor and the NGB fields transform similarly: $u \longrightarrow u' = h\, u\, h^\dagger$ and $\Phi \longrightarrow \Phi' = h\,\Phi\,h^\dagger$.

Now that we have seen two alternative realizations of the NGB fields let us proceed to construct the most general chiral invariant lagrangian. However, before that, a last modification will be performed to the QCD lagrangian in order to reproduce some QCD properties in a straight-forward way and to compute some matrix elements.

3.2 QCD in the presence of external currents: Local chiral symmetry

When analysing the massless QCD lagrangian one observes that it is invariant under global chiral transformations. However it leaves several problems open: How to introduce the quark mass effect, how to compute the matrix elements of a quark current, and what is more important, the question about the validity of the Ward identities from QCD in the EFT.

The solution to all these problems is given by the external field method. With it we introduce some auxiliary fields (v^μ, a^μ, s, p) which, although external fields, they make the lagrangian invariant under local chiral transformation if they are transformed properly. These fields do not have any kinetic term and do not propagate; their unique purpose is to gauge the symmetry. Thanks to them, the chiral gauge symmetry ensures that the relations for the vector and axial current conservations, derived in QCD can be directly applied in the EFT [58]:

$$\langle \dots \partial_\mu \bar{q}_i \gamma^\mu q_j \dots \rangle^{EFT} = \langle \dots (m_{q_i} - m_{q_j}) \bar{q}_i q_j \dots \rangle^{EFT}, \tag{3.14}$$

evaluated for a given initial and final state, denoted by the bra-ket $\langle \dots \rangle$. It happens similarly for the other Ward identities.

Thus, we perform an extension of the QCD lagrangian such that

$$\begin{aligned}
\mathcal{L}_\chi &= \mathcal{L}^0_{QCD} + \overline{\Psi}\gamma^\mu(v_\mu + \gamma_5 a_\mu)\Psi - \overline{\Psi}(s - i\gamma_5 p)\Psi = \\
&= \mathcal{L}^0_{QCD} + \overline{\Psi}_L\gamma^\mu l_\mu \Psi_L + \overline{\Psi}_R\gamma^\mu r_\mu \Psi_R - \overline{\Psi}(s - i\gamma_5 p)\Psi,
\end{aligned} \tag{3.15}$$

with $r_\mu \equiv v_\mu + a_\mu$, $l_\mu \equiv v_\mu - a_\mu$. The external fields are put together into the $n_f \times n_f$ flavour matrices s, p, v^μ and a^μ. In order to have a hermitian lagrangian these external field matrices must be hermitian ($s = s^\dagger, \dots$). Likewise, since we are interested by now just on the $SU(n_f)$ transformations (non-singlet) the flavour matrices of the external fields will be traceless.

In order to make the action invariant under local chiral transformations these new fields must change in a proper way:

$$\begin{aligned}
\Psi_L &\xrightarrow{G^{local}} g_L(x)\,\Psi_L \quad, \\
\Psi_R &\xrightarrow{G^{local}} g_R(x)\,\Psi_R \quad, \\
l_\mu &\xrightarrow{G^{local}} g_L(x)\,l_\mu\,g_L(x)^\dagger + i\,g_L(x)\,\partial_\mu g_L(x)^\dagger \quad, \\
r_\mu &\xrightarrow{G^{local}} g_R(x)\,r_\mu\,g_R(x)^\dagger + i\,g_R(x)\,\partial_\mu g_R(x)^\dagger \quad, \\
(s + ip) &\xrightarrow{G^{local}} g_R(x)\,(s + ip)\,g_L(x)^\dagger \quad,
\end{aligned} \tag{3.16}$$

with $g_L(x) \in SU(N_f)^{local}_L$, $g_R(x) \in SU(N_f)^{local}_R$.

At this point one may recover the rest of the Standard Model through these external fields. One has to incorporate the quark mass terms and the electroweak

interactions. These terms lacking are nothing else but a particular choice of the chiral gauge. This is, one must break the chiral symmetry by setting this external fields to a given value. The essential point is that one may play the same game in the EFT: first constructing a chiral gauge invariant EFT lagrangian and afterwards fixing the same gauge as in the Standard Model. This gives:

$$
\begin{aligned}
r_\mu &= eQA_\mu \,, \\[2mm]
l_\mu &= eQA_\mu + \frac{e}{\sqrt{2}sin\theta_W}(W_\mu^\dagger T_+ + h.c.), \\[2mm]
s &= \mathcal{M} \,, \\[2mm]
p &= 0 \,,
\end{aligned}
\tag{3.17}
$$

where $\mathcal{Q} = \frac{1}{3}\mathrm{diag}(2,-1,-1)$ and $\mathcal{M} = \mathrm{diag}(m_u, m_d, m_s)$ denote the diagonal matrices of charge and quark mass respectively. The $n_f \times n_f$ matrix T_+ contains the Cabibo electroweak mixing angles,

$$
T_+ = \begin{pmatrix} 0 & V_{ud} & V_{us} \\ 0 & 0 & 0 \\ 0 & 0 & 0 \end{pmatrix} \,.
\tag{3.18}
$$

Thus, our effective lagrangian will contain not only the NGB fields but also the external fields, in all the possible forms that preserve the local chiral symmetry. The vector and axial-vector fields v^μ, a^μ will be related with the operators containing derivatives, since the local transformations may leave undesired extra pieces. They will enter through the covariant derivatives.

As we have now not only the SχSB but also the explicit symmetry breaking the NGB properties change slightly. They will gain masses due to the quark masses.

3.3   Effective lagrangian in the $U(x)$ formalism

As one knows that the massless QCD lagrangian is chiral invariant, the effective lagrangian for the NGB will contain all the possible terms containing these fields which preserve the invariance. In the $U(x)$ formalism the NGB are introduced through the chiral tensor $U(x)$. In addition, once the symmetry has been gauged, one must introduce as well the external fields $\{v^\mu, a^\mu, s, p\}$ in all the possible invariant ways. The symmetry will tell us the available structures for the operators but the values of the couplings in front have to be fixed by other means.

Then, one may construct a series of infinite terms preserving the chiral symmetry. In this set of terms there will be some kind of ordering depending on the importance of their contributions. Each term in the lagrangian will contain a given number of derivatives. In the chiral counting the external fields will scale as the momenta of

the Goldstones, providing at the end a consistent construction, as we will see. This ordering of the terms and the observables in powers of the NGB momenta is known as the chiral counting.

At low momenta the most important terms will be those with lower number of derivatives. However, when the energy increases all terms become equally important and we loose this ordering. The power of χPT is that in addition to this ordering, the chiral symmetry allows to relate an infinite number of low energy processes, since each operator containing $U(x)$ owns an infinite series of powers of NGB fields.

Our EFT will be then predictive just at low energies. When studying larger energies one will need to include terms of higher chiral orders to keep a given accuracy. Finally, when reaching energies around a characteristic chiral scale, $\Lambda_\chi \sim 4\pi F_\pi \sim$ 1.2 GeV, one looses all predictability since all the terms have the same size. By analysing the observables one realizes that the NLO calculation reaches momenta up to $E \lesssim 400$ MeV and that the NNLO calculation increases the range of validity not further than 500 MeV. Higher order calculations become terribly complicated so effectively this is the limit range of validity of χPT. Moreover, since we know that there is a vector multiplet with $M_V \sim 770$ MeV which has not been included in the EFT, this sets an extra limitation to the validity of χPT.

The external fields v_μ, a_μ, s, p have been introduced into the QCD action and we have to include them as well into the effective action. The extension of the global chiral group to gauge chiral transformations simplifies the obtention of the QCD Ward Identities in the effective picture [12, 14, 58].

We know how these fields transform under the chiral group and how the pNGB representative $U(\Phi)$ changes. It contains the Goldstone fields to build up the most general EFT with. Notice that in order to preserve the local invariance the gauge fields v_μ, a_μ may only appear either through the covariant derivative of the $U(x)$ tensor,

$$D_\mu U \;\; \equiv \;\; \partial_\mu U \; - \; ir_\mu U \; + \; iUl_\mu \;\; , \tag{3.19}$$

$$(D_\mu U)^\dagger \;\; \equiv \;\; \partial_\mu U^\dagger \; + \; iU^\dagger r_\mu \; - \; il_\mu U^\dagger \;\; , \tag{3.20}$$

or through the strength field tensors,

$$F_L^{\mu\nu} \;\; = \;\; \partial^\mu l^\nu - \partial^\nu l^\mu - i[l^\mu, l^\nu] \;\; , \tag{3.21}$$

$$F_R^{\mu\nu} \;\; = \;\; \partial^\mu r^\nu - \partial^\nu r^\mu - i[r^\mu, r^\nu] \;\; . \tag{3.22}$$

Since the external left-right fields are hermitian ($r_\mu = r_\mu^\dagger$, $l_\mu = l_\mu^\dagger$) and traceless in the $SU(n_f)$ scenario, one finds that $F_{L,R}^{\mu\nu} = F_{L,R}^{\mu\nu\,\dagger}$.

The scalar and pseudo-scalar external fields are usually put together in the chiral tensor $\chi \equiv 2B_0(s + ip)$, which transforms as $U(x)$. It has dimensions of $[\chi] = E^2$. The choice of the constant B_0 in the definition of χ (with dimensions $[B_0] = E$) is arbitrary, but it simplifies the construction of the χPT lagrangian. Actually it is nothing else but the constant that would arise in the simpler term that one could

Tensor	P	C	h.c.	χ order
Φ	$-\Phi$	Φ^T	Φ	~ 1
U	$U^\dagger$	U^T	$U^\dagger$	~ 1
$D_\mu U$	$(D^\mu U)^\dagger$	$(D_\mu U)^T$	$(D_\mu U)^\dagger$	$\sim p$
v_μ	v^μ	$-v_\mu^T$	v_μ	$\sim p$
a_μ	$-a^\mu$	a_μ^T	a_μ	$\sim p$
r_μ	l^μ	$-l_\mu^T$	r_μ	$\sim p$
l_μ	r^μ	$-r_\mu^T$	l_μ	$\sim p$
χ	$\chi^\dagger$	χ^T	$\chi^\dagger$	$\sim p^2$
$F_R^{\mu\nu}$	$F_{L\,\mu\nu}$	$-(F_L^{\mu\nu})^T$	$F_R^{\mu\nu}$	$\sim p^2$
$F_L^{\mu\nu}$	$F_{R\,\mu\nu}$	$-(F_L^{\mu\nu})^T$	$F_L^{\mu\nu}$	$\sim p^2$

Table 3.1: Transformation properties under C, P and hermitian conjugate of the tensors in the $U(x)$ formalism.

make with just one scalar field, in the $\mathcal{L}_{2\chi}$ lagrangian that we will see below. In this form the physical meaning of this constant becomes clearer. Hence, the combination in χ will scale as $\mathcal{O}(p^2)$ in the chiral counting, since it is essentially the square mass of the Goldstones.

The chiral tensors χ, $(D_\mu U)$ and $F_{R,L}^{\mu\nu}$ transform then covariantly as the coordinate $U(\phi)$ in Eq. (3.11).

3.3.1   LO lagrangian: Order $\mathcal{O}(p^2)$

Due to Lorentz invariance the number of derivatives must be even. The terms of the lagrangian with $U(x)$ and no other field or derivative just contribute adding a trivial constant term, since $U^\dagger U = U U^\dagger = \mathcal{I}$.

The first non-trivial term will be $\mathcal{O}(p^2)$:

$$\mathcal{L}_{2\chi} = \frac{F^2}{4} \langle\, D_\mu U^\dagger D^\mu U \;+\; U^\dagger \chi \;+\; \chi^\dagger U \,\rangle \quad , \tag{3.23}$$

with $\langle\,\ldots\,\rangle$ short for the trace in the flavour matrix space.

At this point one realizes the physical meaning of F and B_0, since the expansion of the lagrangian up to order Φ^2 is:

$$\mathcal{L}_{2\chi} = \frac{1}{2}\langle\, \partial_\mu\Phi\partial^\mu\Phi - 2B_0\mathcal{M}\Phi^2 \,\rangle \; + \; F^2\mathcal{O}\left(\frac{\Phi^3}{F^3}\right) \,, \tag{3.24}$$

where the external fields have been substituted by $v^\mu = a^\mu = p = 0$, $s = \mathcal{M}$, and then the square mass of the NGB fields is given by the matrix $2B_0\mathcal{M}$:

$$m_\pi^2 = 2B_0\hat{m}\,, \qquad m_K^2 = B_0(\hat{m} + m_s)\,, \qquad m_{\eta_8}^2 = 2B_0\left(\frac{\hat{m}}{3} + \frac{2m_s}{3}\right)\,, \tag{3.25}$$

where the isospin limit has been considered ($m_u = m_d = \hat{m}$).

The constants F and B_0 were at first introduced when defining $U(x)$ and χ in a very arbitrary way. One could even avoid introducing this constants, leaving the NGB fields with dimension $[\phi^a] = 1$ and with $[\chi] = E$. In that case, the NGB propagators would not have the canonical dimensions and would be $\Delta(p^2) \sim \frac{i}{F^2p^2}$, appearing F^2 in the lagrangian just as the constant in front of the $\mathcal{O}(p^2)$ chiral operators. In addition, the constant B_0 would appear in the constant term as an explicit parameter of $\mathcal{L}_{2\chi}$.

These are the unique terms preserving all desired properties: Lorentz, charge-conjugation, parity invariance and hermiticity of the lagrangian, and of course chiral symmetry.

The F coupling is obtained from the pion decay amplitude at LO in the chiral expansion. Its value is $F \simeq F_\pi = 92.4$ MeV and when calculating loops it is going to provide the characteristic chiral scale $\Lambda_\chi \sim 4\pi F \sim 1.2$ GeV from the chiral expansion in the radiative corrections.

3.3.2 NLO lagrangian: Order $\mathcal{O}(p^4)$

The terms allowed by the symmetry at NLO –$\mathcal{O}(p^4)$– are:

$$\begin{aligned}
\mathcal{L}_4 = \;& L_1\langle\, D_\mu U^\dagger D^\mu U \,\rangle^2 \; + \; L_2\langle\, D_\mu U^\dagger D_\nu U \,\rangle\langle\, D^\mu U^\dagger D^\nu U \,\rangle \\
& + \; L_3\langle\, D_\mu U^\dagger D^\mu U \; D_\nu U^\dagger D^\nu U \,\rangle \; + \; L_4\langle\, D_\mu U^\dagger D^\mu U \,\rangle\langle\, U^\dagger\chi + \chi^\dagger U \,\rangle \\
& + \; L_5\langle\, D_\mu U^\dagger D^\mu U(U^\dagger\chi + \chi^\dagger U) \,\rangle \; + \; L_6\langle\, U^\dagger\chi + \chi^\dagger U \,\rangle^2 \\
& + \; L_7\langle\, U^\dagger\chi - \chi^\dagger U \,\rangle^2 \; + \; L_8\langle\, U^\dagger\chi U^\dagger\chi + \chi^\dagger U\chi^\dagger U \,\rangle \\
& - \; iL_9\langle\, F_R^{\mu\nu}D^\mu U D^\nu U^\dagger + F_L^{\mu\nu}D^\mu U^\dagger D^\nu U \,\rangle \; + \; L_{10}\langle\, U^\dagger F_R^{\mu\nu}U F_{L\mu\nu} \,\rangle \\
& + \; H_1\langle\, F_{R\mu\nu}F_R^{\mu\nu} + F_{L\mu\nu}F_L^{\mu\nu} \,\rangle \; + \; H_2\langle\, \chi^\dagger\chi \,\rangle \,,
\end{aligned} \tag{3.26}$$

where the terms with H_1 and H_2 do not contain NGB fields and are not measurable in QCD. They just help to make some processes finite.

The symmetry allows to add a extra term as $\langle\, D_\mu U^\dagger D_\nu U D^\mu U^\dagger D^\nu U \,\rangle$ but through $SU(3)$ algebra relations (Appendix E) one can see that it can always be decomposed

in other operators already in the lagrangian:

$$\langle\, D_\mu U^\dagger D_\nu U D^\mu U^\dagger D^\nu U - D_\mu U^\dagger D_\nu U D^\nu U^\dagger D^\mu U \,\rangle \;=$$

$$-3\langle\, D_\mu U^\dagger D^\mu U D_\nu U^\dagger D^\nu U \,\rangle + \tfrac{1}{2}\langle\, D_\mu U^\dagger D^\mu U \,\rangle^2 + \langle\, D_\mu U^\dagger D_\nu U \,\rangle\langle\, D^\mu U^\dagger D^\nu U \,\rangle , \tag{3.27}$$

with them already in the former $\mathcal{O}(p^4)$ lagrangian.

In addition there are two more independent terms. Nonetheless, they vanish when employing the equations of motion (EOM) of the $\mathcal{O}(p^2)$ lagrangian $\mathcal{L}_{2\chi}$,

$$\mathcal{O}^{2\chi}_{EOM}(U) \;=\; (D^2 U)U^\dagger - U(D^2 U)^\dagger - \Big(\chi U^\dagger - U\chi^\dagger\Big) + \frac{1}{n_f}\langle\, \chi U^\dagger - U\chi^\dagger \,\rangle \;=\; 0 . \tag{3.28}$$

These extra terms are of the form

$$\mathcal{L}^{off-shell}_{4\chi} \;=\; L_{11}\langle\, \Big(\chi U^\dagger - U\chi^\dagger\Big)\, \mathcal{O}^{EOM}_{2\chi}(U) \,\rangle - L_{12}\langle\, \mathcal{O}^{EOM}_{2\chi}(U)\mathcal{O}^{EOM}_{2\chi}(U)^\dagger \,\rangle , \tag{3.29}$$

and they do not produce modifications in the NLO calculation. That is the reason why they are not usually considered. They are equivalent to field redefinitions and only become relevant at next-to-next-to-leading order.

Already at $\mathcal{O}(p^4)$ one realizes that the number of unknown extra couplings L_i are ten. These constants parametrize our lack of knowledge about low energy QCD. In principle all the effective constants stem from the QCD parameters. The L_i couplings do not depend on the quark masses –which may enter only through the chiral tensor χ– and therefore depend only on α_S. Nevertheless, since this derivation is still not possible one has to fix them through the low energy phenomenology. But once fixed, they relate many processes and their value are the same in all of them.

One technical detail when computing NLO computations is the fact that although $\mathcal{L}_{2\chi}$ provides a canonically normalized kinetic term, this is not so for $\mathcal{L}_{2\chi} + \mathcal{L}_{4\chi}$ or higher orders. They contain more terms quadratic on the NGB fields which require field redefinitions in order to have the kinetic term properly normalized. Similarly these higher order terms modify the relations between the NGB and the quark masses.

In the two flavour χPT one considers $m_s \gg m_u, m_d$ and the strange quark is integrated out of the theory. The available chiral invariant operators are now less numerous, as the number of low energy couplings. There are some structures from $SU(3)$ that still remain and the constants are renamed in the bibliography (the coupling L_9 from three flavours is changed by $-\ell_6/2$ in $SU(2)$). Some other structures vanish due to relations between 2×2 matrices. The $n_f = 2$ lagrangian is shown in Appendix D.

Comparing the lagrangians $\mathcal{L}_{2\chi}$ and $\mathcal{L}_{4\chi}$ one may perform an estimate for the size of the coupling constants L_i [6]. The radiative corrections at NLO due to the vertices from $\mathcal{L}_{2\chi}$ are of the order $\sim \frac{1}{(4\pi F)^2}p^4$ whereas those from $\mathcal{L}_{4\chi}$ are $\sim \frac{L_i}{F^2}p^4$. If the EFT has any sense the radiative corrections are of the same order as the

counterterms and therefore $L_i \sim \frac{1}{(4\pi)^2} \sim 5 \cdot 10^{-3}$. Observing the phenomenological values obtained from the experiments (Appendix D) one can see that this estimate is rather good.

Beyond $\mathcal{O}(p^4)$ the number of allowed terms increases considerably (57 new terms in $SU(2)$ and 94 in $SU(3)$). The calculations become more and more complex and the improvements in the accuracy are smaller and smaller. Due to this and the experimental uncertainties most of the $\mathcal{O}(p^6)$ couplings own large errors that only allow estimating the order of magnitude of the couplings.

An overview of the $\mathcal{O}(p^6)$ lagrangian is left for the last section of the chapter [16].

3.4   Effective lagrangian in the $u(x)$ formalism

The lagrangians from (3.23) and (3.26), expressed in the $U(x)$ formalism, can also be written in the formalism in terms of $u(x)$.

The chiral tensor $u(x)$ transforms now in a different way. The compensating transformation $h(g, \phi)$ appears now explicitly and one must join the pieces in the proper way to cancel it.

A very useful way to construct the lagrangian is through chiral tensors X [16, 19] which vary covariantly as

$$X \xrightarrow{g \in G} h(g, \phi)\, X\, h(g, \phi)^{\dagger} \quad . \tag{3.30}$$

Thus, the trace of a product of tensors of this kind would be chiral invariant.

Likewise, one wants to introduce partial derivatives of this operators, $\partial^{\mu} X$. The problem is that the partial derivative is not chiral invariant. One needs to construct a new covariant derivative ∇^{μ} for objects transforming as Eq. (3.30). Therefore we have to introduce a connection term $[\Gamma_{\mu}, \cdot]$:

$$\nabla_{\mu} X = \partial_{\mu} X + [\Gamma_{\mu}, X] \,, \tag{3.31}$$

with the connection

$$\Gamma_{\mu} = \frac{1}{2} \left\{ u^{\dagger}(\partial_{\mu} - ir_{\mu})u + u(\partial_{\mu} - il_{\mu})u^{\dagger} \right\} . \tag{3.32}$$

It is easy to check that $(\nabla_{\mu} X)^{\dagger} = \nabla_{\mu}\left(X^{\dagger}\right)$. Notice that Γ_{μ} does not transform covariantly as Eq. (3.30). It will be useful in the next chapter when introducing the chiral multiplets of resonances R, which transform in this way. With this connection one may also construct the covariant tensor

$$\Gamma_{\mu\nu} = \partial_{\mu}\Gamma_{\nu} - \partial_{\nu}\Gamma_{\mu} + [\Gamma_{\mu}, \Gamma_{\nu}], \tag{3.33}$$

which is antisymmetric under $\mu \leftrightarrow \nu$ and will be useful when studying relations among different chiral operators.

The simplest operators $-\mathcal{O}(p^2)-$ including the NGB tensor $u(x)$ and the external fields are:

$$
\begin{aligned}
u_\mu &= iu^\dagger D_\mu U u^\dagger = -iu D_\mu U^\dagger u = u_\mu^\dagger \quad, \\
u_\mu u_\nu &\quad, \\
h_{\mu\nu} &= \nabla_\mu u_\nu + \nabla_\nu u_\mu \quad, \\
u_{\mu\nu} &= iu^\dagger D_\mu D_\nu U u^\dagger \quad, \\
\chi_\pm &= u^\dagger \chi u^\dagger \pm u \chi^\dagger u \quad, \\
f_\pm^{\mu\nu} &= u F_L^{\mu\nu} u^\dagger \pm u^\dagger F_R^{\mu\nu} u \quad,
\end{aligned}
\tag{3.34}
$$

transforming all of them covariantly as in Eq. (3.30).

Some trace properties of these tensors in $SU(n_f)$ are:

$$
\begin{aligned}
\langle u_\mu \rangle &= 0\,, \\
\langle u_{\mu\nu} \rangle &= i\langle u_\mu u_\nu \rangle\,.
\end{aligned}
\tag{3.35}
$$

There are also some relations among them:

$$
\begin{aligned}
\nabla_\mu u_\nu &= u_{\mu\nu} + \tfrac{i}{2}\left[u_\mu u_\nu + u_\nu u_\mu \right]\,, \\
\nabla^\mu u^\nu - \nabla^\nu u^\mu &= -f_-^{\mu\nu}\,, \\
[\nabla^\mu, \nabla^\nu] X &= [\Gamma^{\mu\nu}, X]\,.
\end{aligned}
\tag{3.36}
$$

All these pieces and products of them transform as a singlet under the chiral group when taking the trace: $\langle u_\mu u_\nu \rangle$, $\langle \chi_\pm \rangle$...

The way how they transform under C, P and hermitian conjugation can be found in Table (3.2).

3.4.1   LO and NLO lagrangian in terms of $u(x)$

The $\mathcal{O}(p^2)$ lagrangian in terms of these tensors is:

$$
\mathcal{L}_{2\chi} = \frac{F^2}{4}\langle u_\mu u^\mu + \chi_+ \rangle \quad,
\tag{3.37}
$$

and at $\mathcal{O}(p^4)$ one has

$$
\begin{aligned}
\mathcal{L}_{4\chi} &= L_1 \langle u_\mu u^\mu \rangle^2 + L_2 \langle u_\mu u_\nu \rangle \langle u^\mu u^\nu \rangle + L_3 \langle u_\mu u^\mu u_\nu u^\nu \rangle \\[4pt]
&\quad + L_4 \langle u_\mu u^\mu \rangle \langle \chi_+ \rangle + L_5 \langle u_\mu u^\mu \chi_+ \rangle + L_6 \langle \chi_+ \rangle^2 + L_7 \langle \chi_- \rangle^2 \\[4pt]
&\quad + L_8 \tfrac{1}{2}\langle \chi_+^2 + \chi_-^2 \rangle - iL_9 \langle f_+^{\mu\nu} u_\mu u_\nu \rangle \\[4pt]
&\quad + L_{10}\tfrac{1}{4}\langle f_{+\mu\nu} f_+^{\mu\nu} - f_{-\mu\nu} f_-^{\mu\nu} \rangle \\[4pt]
&\quad + H_1 \tfrac{1}{2}\langle f_{+\mu\nu} f_+^{\mu\nu} + f_{-\mu\nu} f_-^{\mu\nu} \rangle + H_2 \tfrac{1}{4}\langle \chi_+^2 - \chi_-^2 \rangle \quad,
\end{aligned}
\tag{3.38}
$$

Tensor	P	C	h.c.	χ order
Φ	$-\Phi$	Φ^T	Φ	~ 1
u	$u^\dagger$	u^T	$u^\dagger$	~ 1
u_μ	$-u^\mu$	u_μ^T	u_μ	$\sim p$
Γ^μ	Γ_μ	$-\Gamma^{\mu\,T}$	$-\Gamma^\mu$	$\sim p$
$u_{\mu\nu}$	$-u^{\mu\nu\,\dagger}$	$u_{\mu\nu}^T$	$u_{\mu\nu}^\dagger$	$\sim p^2$
$\chi_\pm$	$\pm\chi_\pm$	$\chi_\pm^T$	$\pm\chi_\pm$	$\sim p^2$
$f_\pm^{\mu\nu}$	$\pm f_{\pm\,\mu\nu}$	$\mp f_\pm^{\mu\nu\,T}$	$f_\pm^{\mu\nu}$	$\sim p^2$
$\nabla_\mu u_\nu$	$-\nabla^\mu u^\nu$	$(\nabla_\mu u_\nu)^T$	$\nabla_\mu u_\nu$	$\sim p^2$

Table 3.2: Transformation properties under C, P and hermitian conjugate.

Now the EOM from $\mathcal{L}_{2\chi}$ is:

$$\mathcal{O}_{2\chi}^{EOM}(u) = \nabla_\mu u^\mu - \frac{i}{2}\left(\chi_- - \frac{1}{n_f}\langle\chi_-\rangle\right) = 0 . \tag{3.39}$$

These operator allows constructing two more invariant operator that however do not contribute to the on-shell matrix elements at this order:

$$\mathcal{L}_{4\chi}^{off-shell} = L_{11}\langle\chi_-\mathcal{O}_{2\chi}^{EOM}(u)\rangle - L_{12}\langle\mathcal{O}_{2\chi}^{EOM}(u)\mathcal{O}_{2\chi}^{EOM}(u)^\dagger\rangle . \tag{3.40}$$

At this point one realizes that if one takes the same exponential realization – either in the $U(x)$ or the $u(x)$ formalism– then both lagrangians are identical even off-shell.

3.5 Systematic chiral counting at the loop level

We have seen till now how the chiral symmetry helps us to build an effective lagrangian to describe the NGB interactions. A well defined ordering in powers of the momenta can be established when computing processes at tree-level. In this section I will show how to handle the chiral counting when computing quantum loops.

The loop integrals are functions of the external momenta and the pNGB masses (which in the chiral counting scale as the external momenta). The analytic part of

these integrals is an homogeneus function of this parameters and also its non-analytic part up to logarithmic factors of the type $\ln(p^2/\mu^2)$. A general diagram containing N_d vertices of dimension $\mathcal{O}(p^d)$ will be considered. By that it is meant a vertex with any number of outgoing Goldstone bosons with a power p^d of the momenta of the particles in the vertex. This diagram may contain L loops, with a number I of internal propagators and E of external particles. A dimensional analysis of the diagram shows that it scales as p^D, with D equal to:

$$D = 4L - 2I + \sum_{d=2}^{\infty} d\, N_d, \qquad (3.41)$$

where each loop introduces four powers of momenta from the integration $\int dk^4$ (a dimension-4 space has been assumed), each vertex of dimension d introduces this number of powers of the external momenta p, and each internal propagator scales as $\sim 1/p^2$. In addition, the number of internal lines is related to the number of loops and the number of vertices: $L = 1 + I - \sum_d N_d$, this is, $I = L - 1 + \sum_d N_d$. Thus the superficial degree of divergence becomes

$$D = 2L + 2 + \sum_{d=2}^{\infty} (d-2)\, N_d. \qquad (3.42)$$

This simple formula classifies the diagrams in a given order $\mathcal{O}(p^D)$. The loops are going to provide non-analytic structures (logs, dilogarithms...) multiplying to polynomial terms of the external momenta. The diagrams of lowest order $-\mathcal{O}(p^2)-$ will be those with $L = 0$ and all the vertices with $d = 2$ coming from the lagrangian $\mathcal{L}_{2\chi}$, i.e. they are provided by the leading lagrangian of χPT at tree-level. The next-to-leading order contributions $-\mathcal{O}(p^4)-$ is given by two kind of diagrams: a) diagrams with $L = 0$ containing just one vertex with $d = 4$ from $\mathcal{L}_{4\chi}$ (and any number from $\mathcal{L}_{2\chi}$); b)diagrams with $L = 1$ and just dimension $d = 2$ vertices.

In all the cases the increasing of the order of momenta through the loops is always compensated by the dimensionful constants of the vertices. For instance, the vertices of dimension $d = 2$ always provide the corresponding factors of F^2 dividing, in order to keep the dimensions of the observable unchanged. In addition, each loop introduces a phase-space factor $1/(4\pi)^2$. Thus, an observable $\mathcal{T}$ is given by the series of contributions coming from any number of loops:

$$\mathcal{T} \sim \sum_{L=0}^{\infty} p^2 \left(\frac{1}{(4\pi)^2} \frac{p^2}{F^2} \right)^L. \qquad (3.43)$$

Therefore at the loop level the characteristic expansion scale which provides the lagrangian $\mathcal{L}_{2\chi}$ is $\Lambda_\chi \sim 4\pi F$. If the effective theory is well defined one expects that this scale to be around the same size as the characteristic scale for the diagrams with vertices from $\mathcal{L}_{4\chi}$ and higher orders. This is well observed experimentally, where

the $\mathcal{O}(p^4)$ contributions from the couplings L_i are of the same order as the radiative corrections from the one loop diagrams.

When constructing the RχT lagrangian at the loop level the same kind of arguments will be employed. One will consider that the local counterterms are of the same order as the radiative corrections.

3.6   Overview of the $\mathcal{O}(p^6)$ Lagrangian

As it was said before, the number of independent structures that can be built at $\mathcal{O}(p^6)$ is huge. However, when analysing a given process the amount of relevant couplings is not that big.

In this work we are interested mostly in the pion vector form factor. In that case there are only two operators contributing at tree-level:

$$\mathcal{L}_{6\chi} \;=\; ... ic_{51} \langle \nabla^\rho f_+^{\mu\nu} [h_{\mu\rho}, u_\nu] \rangle \;+\; ic_{53} \langle \nabla_\mu f_+^{\mu\nu} [h_{\nu\rho}, u^\rho] \rangle . \tag{3.44}$$

These operators contribute both in the $SU(2)$ and in the $SU(3)$ cases [16]. Actually only the combination $r_{V2} \equiv 4F^2(c_{53} - c_{51})$ will be relevant in the pion vector form-factor that will be analysed later.

A more extended study of the construction and development of the $\mathcal{O}(p^6)$ lagrangian can be found in Ref. [16].

3.7 χPT and large N_C

Since χPT is the EFT of QCD at low energies one may analyse the dependence of its parameters on the number of colours N_C of QCD [5, 20, 46].

Let us make some previous considerations first. The two-current correlator $\langle J(x)J^\dagger(y) \rangle$, built with two bilinears of the form $J = \bar{q}\Gamma q$, is described in the large N_C limit by a single quark loop connecting both currents surrounded by a cloud of planar gluons. Thus, this correlator is proportional to the number of colours of the quarks that can run within the loop, i.e., $\langle J(x)J^\dagger(y) \rangle \sim \mathcal{O}(N_C)$. In this limit, the only intermediate hadronic states will be those $q\bar{q}$ mesons M_i with the proper quantum numbers, exchanged at tree-level. Therefore, Using the Optical Theorem one finds that $\mathrm{Im}\langle J(x)J^\dagger(y) \rangle \sim |\langle 0| J |M_i \rangle|^2$, so the form factor of a bilinear current into a meson is $\mathcal{O}(\sqrt{N_C})$.

At lowest order $-\mathcal{O}(p^2)-$ the chiral lagrangian contains only two parameters: F and B_0. The coupling F is the pion decay constant at LO, given by $\langle 0| J_A^\mu |\pi^-(p) \rangle = i\sqrt{2}Fp^\mu$. Since we saw that this matrix element is $\mathcal{O}(\sqrt{N_C})$ then one has that

$$F \;\sim\; \mathcal{O}(\sqrt{N_C}) \tag{3.45}$$

The constant B_0 is related to the quark condensate together with the coupling F through the LO equality $\langle 0| \bar{q}_i q_j |0\rangle = -F^2 B_0 \delta_{ij}$. This matrix element is proportional to N_C (the summation on the colour indices is assumed in $\bar{q}q$). Since F^2 is

also of that order one concludes that

$$B_0 \;\sim\; \mathcal{O}(N_C^0)\,. \tag{3.46}$$

For the NLO lagrangian $\mathcal{L}_{4\chi}$ in Eqs. (3.26) or (3.38) the dependences are something more complicated. The terms with one trace imply one quark loop and those with two traces have an extra quark loop. Thus, the operators with two flavour traces will be suppressed by $1/N_C$ with respect to those with just one. Through an analysis of the observables similar to the one at LO one finds that the two-trace couplings L_4, L_6, L_7 are order $\mathcal{O}(N_C^0)$, and those corresponding to the one-trace operators, L_3, L_5, L_8, L_9, L_{10}, are $\mathcal{O}(N_C)$.

The couplings L_1 and L_2 demand a further study. These two terms contain two traces so naively they are expected to be order $\mathcal{O}(N_C^0)$. To show that this not really so we will consider the 3×3 matrix relation shown before in Eq. (3.27). That operator $\langle\, D_\mu U \; D_\nu U^\dagger D^\mu U \; D^\nu U^\dagger \,\rangle$ could have appeared in the lagrangian $\mathcal{L}_{4\chi}$. It was omitted since it was not independent from the terms with L_1, L_2 y L_3. Thus, the symmetry allows this one-trace $\mathcal{O}(p^4)$ operator, with a coefficient C of order $\mathcal{O}(N_C)$. When decomposing this operator through Eq. (E.7) the other $\mathcal{L}_{4\chi}$ couplings would gain the contributions $\Delta L_1 = C/2$, $\Delta L_2 = C$ and $\Delta L_3 = -2C$, all of them order $\mathcal{O}(N_C)$. Since the information of the non-independent operator of C has been shuffled to $L_{1,2,3}$ then one has that L_1 and L_2 become order $\mathcal{O}(N_C)$ (that happened already with L_3). Nevertheless the combination $2L_1 - L_2$ is $\mathcal{O}(N_C^0)$ since the contribution from C is removed.

Summarising:

     * $\mathcal{O}(N_C)$: L_1, L_2, L_3, L_5, L_8, L_9 y L_{10}.

     * $\mathcal{O}(1)$: $2L_1 - L_2$, L_4, L_6 y L_7.

Chapter 4

Resonance Chiral Theory

Already in the 50's and 60's, when the first analyses of pion-nucleus scattering, it was discovered that there were peaks of probability in fixed channels around some values of the total momentum squared, e.g. two final pions with $I = J = 1$. These peaks were quickly associated and described with intermediate heavy meson states, formed by a $q\bar{q}$ pair, when the quark model was started.

Models with resonances included these fields to explain analogous features in the amplitudes when these intermediate states pop up on their mass-shell in the s-channel. These resonances, as they were named, had different parities, angular momenta and strangeness. They had masses of the order of $M_R \sim 1$ GeV and they were constituted by light quarks $u/d/s$ and gluons. In addition, they could be classified in $SU(3)$ flavour multiplets, as the NGB. Actually they accepted better a $U(3)$ classification, as will be stated under the large N_C limit in the next section.

With time, several works showed how it was possible to describe the pNGB interactions out of the resonance range through local interactions provided by χPT [83, 84, 8, 9]. It was understood that the resonance contribution could be integrated out providing contributions suppressed by the resonance masses to the χPT operators [8, 19, 41], with $\Lambda_\chi \sim M_R \sim 1$ GeV.

However, for momenta of the order of the resonance mass χPT breaks down and one has to design a quantum field theory including also the resonance fields. The chiral counting fails in this range of energies and an alternative procedure is required if one wants to provide an effective description. As it was introduced in a former chapter, the alternative procedure considered here is the $1/N_C$ counting. The large N_C limit together with the QCD short distance behaviour –provided by the operator product expansion (OPE)– and the QCD large distance energy region –provided by χPT– will help us to fix many of the parameters of the theory.

Some of the first steps were already walked when developing the χPT lagrangian. Knowing the transformation properties, Gasser and Leutwyler also built up in their $SU(2)$ analysis the most general lagrangian at $\mathcal{O}(p^2)$ being chiral invariant and including the vector resonance $\rho(770)$ [8]. Afterwards, it was generalized for three

flavour and adding also axial-vector, scalar and pseudo-scalar resonances [19, 83, 84]. This chiral invariant EFT was named Resonance Chiral Theory (RχT) and was remarkably successful at tree-level. In this chapter we will see how it is possible to establish a well defined perturbative counting and a systematic renormalization procedure.

4.1   Resonances in the large N_C limit

At large N_C the $q\bar{q}$ resonances get classified into chiral multiplets with one chiral-singlet field and $(n_f^2 - 1)$ chiral covariant resonances [5]. Also the pNGB get grouped in that way and for three flavours we have the nine lighter pseudo-scalars, (π, K, η_8, η_1).

In the $1/N_C$ framework the leading contributions to the amplitudes are given by tree-level diagrams whereas every loop must be suppressed by a power of $1/N_C$ [5]. In the next section I will show a lagrangian that obeys this kind of requirements. Actually, the effective lagrangian is not unique. The vector fields may be described by several different formalisms: antisymmetric tensors, Proca fields, and vectors considered as gauge fields. Beside this, for a given formalism the lagrangian is not unique. We will work under the chiral symmetry. This constrains the possible operators that one can have in the effective lagrangian. Nonetheless, the number of terms that one may construct is infinite, since one may add more and more powers of the momenta either to the Goldstones or to the resonance fields.

There are some points that I will consider in order to develop a reasonable effective field theory for the meson interactions at the quantum level:

1. **Chiral Symmetry:** The peculiar nature of the NGB fields yields that processes with different number of external pions are not independent. The axial transformations modify the vacuum and change the number of Goldstone bosons. The $\pi\pi$ scattering, for instance, is given in χPT by the same constant as the pion decay. The resonance fields, on the contrary, have a different origin than the Goldstones and the chiral transformations do not vary their number.

   The power of working under the chiral symmetry is that, –as it will be shown below– although the infinite number of unrelated QCD Green functions cannot be described by a finite number of effective couplings, the chiral symmetry establishes relations among observables with a different number of external Goldstones. This class of processes will be given by a finite number of couplings. The number of out-going resonances will not change under the chiral group but there will be an infinity of related diagrams. Moreover, the renormalization of one of the diagrams of the class ensures the renormalizability of the related ones. In addition, once the QCD constraints are imposed on a given amplitude and the matrix element obeys the right scaling $\sim p^D$ at high energies, then it is shuffled automatically to the rest of the processes of the class since the chiral transformations do not change the scaling in momenta.

2. **Effective description of a class of processes:** There is an infinite number
of possible Green functions in QCD; they can have an arbitrary number of
external legs. In perturbative QCD they are all related through one single
parameter, the strong coupling constant. However it is not possible to argue
that all the QCD information can be recovered through a finite number of
effective couplings. A lagrangian with a finite number of terms will be valid
to describe just a class of QCD Green functions and all the processes related
through chiral symmetry up to a given order in the $1/N_C$ counting. The
analysis of other observables and higher orders in $1/N_C$ requires the addition
of extra operators to the lagrangian. Thus, the study of Green functions with
more and more external currents and resonances requires a lagrangian more
and more complicated.

3. **High and low energy limits:** One of the strongest constraints to the EFT
of the meson interactions is given by the asymptotic behaviours of QCD both
at short and long distances. The EFT is expected to be dual to QCD and it
must be recovered in the limits where it is already known. At high energy the
EFT must match the OPE description and at low energies one must reproduce
χPT. Both limits must be reproduced at every single order in the $1/N_C$ expan-
sion. The requirement that the Green functions should follow the momentum
dependence of QCD in those regimes will be very useful to constrain the theory
and to fix many of the effective parameters. From the next analyses one real-
izes that the low energy behaviour is recovered not only at tree-level but also
at one-loop. Therefore, it seems quite likely that χPT can be automatically
recovered at low energies once the chiral symmetry is imposed on the effective
lagrangian with resonances. Although there is not a strict demostration prov-
ing this statement we will see in the next calculations that it is immediately
obeyed without any kind of tuning of the EFT couplings.

4. **Minimal Hadronical Ansatz:** The large N_C analysis of QCD predicts that
at LO the observables are given by the tree-level exchange of an infinite tower
of mesonic states. However, phenomenologically it is well known that the
operator product expansion (OPE) –QCD in the perturbative regime– starts
working at energies $\sqrt{s} \sim 2$ GeV. Beyond this point the resonant structure
(here, only resonances with $u/d/s$ content are considered) disappears and one
observes a continuum. Therefore, the finite number of active multiplets within
the non-perturbative range of QCD converge to OPE not at $\sqrt{s} \to \infty$ but
already around a finite value $\sqrt{s} \to \sqrt{s_{OPE}} \sim 2$ GeV. Thus, the EFT with
a finite number of resonances will approach asymptotically to the OPE de-
scription. The Minimal Hadronical Ansatz (MHA) states that one needs to
consider just a minimal number of resonances to fulfill the QCD short distance
constraints in addition to the low energy requirements [55]. The infinite pile of
resonance multiplets is then truncated, keeping just a finite number of them.
The information of the dropped states is assumed to be absorbed within the

effective couplings of our finite theory. In addition, the minimal number of multiplets required by MHA may vary from one class of processes to another, since they are given by different sets of terms of the lagrangian.

5. **Spectrum of the EFT:** Under the MHA the series of resonance multiplets become truncated but keeping a number enough to recover the low and high energy limits. Nevertheless, the intermediate region may contain more resonance multiplets which are not required to fulfill QCD. For instance, the vector form factor requires just one vector multiplet but there is more than one vector multiplet observed experimentally. When increasing the energy in the form factor it comes close to the second multiplet ρ' of vectors, whose influence was neglected for energies away of the ρ' pole. However, this degree of freedom must be included for momenta close to its mass-shell.

Summarising

At LO in $1/N_C$ our amplitudes will be given by tree-level diagrams. Depending on the range of energies to consider, the spectrum of the EFT will be extended to include the corresponding multiplets of mesons. However, the amplitudes must obey the short and long distance asymptotic behaviour of QCD. This requires the inclusion of at least a minimum number of resonance multiplets.

4.1.1   Lagrangian in the antisymmetric formalism

Now we will see the lagrangian that was put forward in Ref. [19]. This is the formalism and the lagrangian that will be employed to provide the LO in $1/N_C$ amplitudes in all the calculations performed in this work.

The present formalism describes the vector and axial-vector mesons as antisymmetric tensors $V^{\mu\nu}$ and $A^{\mu\nu}$. In the next sections other formalisms are also presented and compared.

The compensating transformation $h(g, \phi)$ defined when one chooses the chiral representation of the Goldstones in Eq. (3.12) is the ingredient required to describe the properties of the chiral transformations on the resonance fields. We will choose for the NGB the representation in terms of the tensor $u(x)$. The action of the chiral group over this tensor is:

$$u(\phi) \quad \xrightarrow{G} \quad g_R \ u(\phi) \ h^\dagger(g, \phi) \ = \ h(g, \phi) \ u(\phi) \ g_L^\dagger \quad , \tag{4.1}$$

where at LO in $1/N_C$ the axial anomaly vanishes and the eta singlet becomes the ninth NGB:

$$\Phi \equiv \frac{\lambda^a}{\sqrt{2}}\phi^a = \begin{pmatrix} \frac{\pi^0}{\sqrt{2}} + \frac{\eta_8}{\sqrt{6}} + \frac{\eta_1}{\sqrt{3}} & \pi^+ & K^+ \\ \pi^- & -\frac{\pi^0}{\sqrt{2}} + \frac{\eta_8}{\sqrt{6}} + \frac{\eta_0}{\sqrt{3}} & K^0 \\ K^- & \overline{K}^0 & -\frac{2\eta_8}{\sqrt{6}} + \frac{\eta_1}{\sqrt{3}} \end{pmatrix} . \tag{4.2}$$

We are going to describe resonances transforming as a $U(3)$ nonet. The multiplet is provided here by the matrix:

$$R \equiv \sum_{a=0}^{8} \frac{\lambda^a}{\sqrt{2}} R^a,$$

(4.3)

containing the fields transforming like an octet, $a = 1, 2...8$, and like a $SU(3)_V$ singlet, $a = 0$. For instance, the vector resonances in the antisymmetric tensor formalism are given by:

$$V_{\mu\nu} = \frac{\lambda^a}{\sqrt{2}} R^a =$$

$$= \begin{pmatrix} \frac{1}{\sqrt{2}}\rho^0 + \frac{1}{\sqrt{6}}\omega_8 + \frac{1}{\sqrt{3}}\omega_1 & \rho^+ & K^{*+} \\ \rho^- & -\frac{1}{\sqrt{2}}\rho^0 + \frac{1}{\sqrt{6}}\omega_8 + \frac{1}{\sqrt{3}}\omega_1 & K^{*0} \\ K^{*-} & \bar{K}^{*0} & -\frac{2}{\sqrt{6}}\omega_8 + \frac{1}{\sqrt{3}}\omega_1 \end{pmatrix}_{\mu\nu},$$

(4.4)

where it also usually employed the "ideal-mixing" combinations $\omega \equiv \sqrt{\frac{1}{3}}\omega_8 + \sqrt{\frac{2}{3}}\omega_1$, $\Phi \equiv -\sqrt{\frac{2}{3}}\omega_8 + \sqrt{\frac{1}{3}}\omega_1$.

The transformation properties of these resonance multiplets under an element of $U(3) \otimes U(3)$ is given by:

$$R \xrightarrow{G} h(\phi, g) \, R \, h(\phi, g)^\dagger.$$

(4.5)

In order to preserve the local chiral invariance one needs to define a covariant derivative for any tensor X transforming as Eq. (4.5). This covariant derivative $\nabla_\mu X$ was introduced before in Eq. (3.31). That definition ensures that the object $\nabla_\mu X$ transforms as X under the chiral group, being $X = R$ or any of the chiral tensors introduced in the $u(x)$ formalism of χPT (u^μ, χ_+...) transforming as in Eq. (4.5).

The resonance fields become then coupled to the Goldstone field through their covariant derivatives: The resonance kinetic term is going to provide interactions between Goldstones and two resonance fields.

The transformation properties of the resonance fields under C, P and hermitian conjugated can be observed in Table (4.1). With these ingredients and the NGB tensors it is possible to construct the most general chiral invariant lagrangian.

Therefore, the most general lagrangian linear in the resonance fields with an $\mathcal{O}(p^2)$ chiral tensor of Goldstones and including vectors (V), axial-vectors (A), scalars (S) and pseudo-scalar resonances (P) is:

$$\mathcal{L}_R = \sum_{R=V,A,S,P} \{\mathcal{L}_{\text{Kin}}(R) + \mathcal{L}_{2R}\},$$

(4.6)

with the kinetic terms

$$\mathcal{L}_{\text{Kin}}(R = V, A) = -\frac{1}{2}\langle \nabla^\lambda R_{\lambda\mu} \nabla_\nu R^{\nu\mu} - \frac{M_R^2}{2} R_{\mu\nu} R^{\mu\nu}\rangle,$$

$$\mathcal{L}_{\text{Kin}}(R = S, P) = \frac{1}{2}\langle \nabla^\mu R \nabla_\mu R - M_R^2 R^2\rangle.$$

(4.7)

Resonancia	P	C	h.c.
$V_{\mu\nu}$	$V^{\mu\nu}$	$-V_{\mu\nu}^T$	$V_{\mu\nu}$
$A_{\mu\nu}$	$-A^{\mu\nu}$	$A_{\mu\nu}^T$	$A_{\mu\nu}$
S	S	S^T	S
P	$-P$	P^T	P

Table 4.1: Transformation properties of the resonance fields under C and P.

The interaction terms with one resonance field and Goldstone fields are given by:

$$\begin{aligned}
\mathcal{L}_{2V} &= \frac{F_V}{2\sqrt{2}} \langle V_{\mu\nu} f_+^{\mu\nu} \rangle + \frac{iG_V}{2\sqrt{2}} \langle V_{\mu\nu}[u^\mu, u^\nu] \rangle\,, \\
\mathcal{L}_{2A} &= \frac{F_A}{2\sqrt{2}} \langle A_{\mu\nu} f_-^{\mu\nu} \rangle\,, \\
\mathcal{L}_{2S} &= c_d \langle S u_\mu u^\mu \rangle + c_m \langle S \chi_+ \rangle\,, \\
\mathcal{L}_{2P} &= i d_m \langle P \chi_- \rangle\,.
\end{aligned} \tag{4.8}$$

In the antisymmetric formalism the vector interactions are of order $\mathcal{O}(p^2)$ and it was proven that at LO in $1/N_C$ there are no local NGB interaction except that given by the $\mathcal{O}(p^2)$ term:

$$\mathcal{L}_{2\chi} = \frac{F^2}{4} \langle\, u^\mu u_\mu + \chi_+ \,\rangle\,. \tag{4.9}$$

For the former resonance lagrangian it was demostrated that the couplings for the $\mathcal{O}(p^4)$ chiral operators had to be zero at LO in $1/N_C$:

$$\widetilde{L}_i = 0\,, \tag{4.10}$$

where this are the couplings of the RχT lagrangian –the high energy theory– not the ones of χPT –the low energy theory–, which I denote as the usual L_i. At the end of the day both representations of the vector fields are equivalent and give the same descriptions at LO in $1/N_C$. Actually, the freedom is not so large once you require the amplitudes to behave in a given way at high and low energy.

Using the antisymmetry properties of $V^{\mu\nu}$ and $A^{\mu\nu}$ under $\mu \leftrightarrow \nu$ one finds that the singlet vectors and axial-vectors decouple from the Goldstones. Nevertheless, in the case of the scalars and pseudo-scalar resonances both octets and singlets interact with the NGB fields.

When going to low energies the resonances disappear from the theory and one observes local interactions between Goldstones instead of the exchange of a heavy resonance propagator. I will show that this feature happens not only at LO in $1/N_C$, i.e. at tree-level, but even at the one-loop level. A complete list of the contributions to L_i from the χPT low energy lagrangian $\mathcal{L}_{4\chi}$ can be found in Appendix D.

4.1.2 Proca field

At the same time that the antisymmetric formalism was developed, also the lagrangian in terms of the Proca field was studied [41, 42, 23]

For the local NGB interactions they considered not only the lowest chiral lagrangian but also the one at order $\mathcal{O}(p^4)$:

$$\mathcal{L}_\chi = \mathcal{L}_{2\chi} + \widetilde{\mathcal{L}}_{4\chi}, \tag{4.11}$$

where $\widetilde{\mathcal{L}}_{4\chi}$ contained the same operators as the usual χPT lagrangian $\mathcal{L}_{4\chi}$ but the couplings $\widetilde{L}_i$ were different since one was now in a theory with explicit resonance fields.

For the vector and axial resonances I use now the vector fields $\hat{V}_\mu$, $\hat{A}_\mu$ and its strength field tensors:

$$\hat{V}_{\mu\nu} = \nabla_\mu \hat{V}_\nu - \nabla_\nu \hat{V}_\mu, \qquad \hat{A}_{\mu\nu} = \nabla_\mu \hat{A}_\nu - \nabla_\nu \hat{A}_\mu, \tag{4.12}$$

with all of them transforming covariantly as

$$\begin{aligned} \hat{V}_\mu &\longrightarrow h\hat{V}_\mu h^\dagger, \\ \hat{A}_\mu &\longrightarrow h\hat{A}_\mu h^\dagger, \end{aligned} \tag{4.13}$$

and the covariant derivative defined as before.

The resonance lagrangian contains now a kinetic term:

$$\mathcal{L}^{Kin}[R = V, A] = -\frac{1}{4}\langle\, \hat{R}_{\mu\nu}\hat{R}^{\mu\nu} - 2M_R^2\hat{R}_\mu\hat{R}^\mu \,\rangle, \tag{4.14}$$

and the interaction terms

$$\begin{aligned} \mathcal{L}_{2V} &= -\frac{f_V}{2\sqrt{2}}\langle\, \hat{V}_{\mu\nu}f_+^{\mu\nu} \,\rangle - \frac{ig_V}{2\sqrt{2}}\langle\, \hat{V}_{\mu\nu}[u^\mu, u^\nu] \,\rangle, \\ \mathcal{L}_{2A} &= \frac{f_A}{2\sqrt{2}}\langle\, \hat{A}_{\mu\nu}f_-^{\mu\nu} \,\rangle. \end{aligned} \tag{4.15}$$

Although they show a structure similar to the one in the antisymmetric formalism these terms contain one more power of the momentum and therefore they produce a contribution to the amplitude which needs of the terms $\widetilde{\mathcal{L}}_{4\chi}$ to fulfill the QCD constraints.

4.1.3 Hidden local symmetry

The last analysis about how introducing the vector field has to do with a remnant symmetry of the effective lagrangian. It is based on the freedom that exists to choose the representatives of the coset G/H of the chiral group G over the vector subgroup [43].

Let us focus the attention on the chiral tensor $U(\phi(x))$ which contains the Goldstone fields and is given by the combination of coordinates of the chiral group

$U(x) = \xi_R(x)\,\xi_L(x)^\dagger$. One realizes that there occurs an extra symmetry –or ambiguity, as one could call it as well–. The tensors (ξ_L, ξ_R) get changed under a chiral transformation $g = (g_L, g_R)$ and modify $U(x)$ in the way shown before,

$$U \longrightarrow U' = g_R\,U\,g_L^\dagger \qquad \longrightarrow \begin{cases} \xi_L \longrightarrow \xi_L' = g_L\,\xi_L\,h(g,\phi)^\dagger\,, \\ \xi_R \longrightarrow \xi_R' = h(g,\phi)\,\xi_R\,g_R^\dagger\,, \end{cases} \qquad (4.16)$$

However, it contains an extra freedom. The compensating transformation $h(g, \phi(x)) \in SU(n_f)_V^{local}$ is provided by the chiral element g and by the value of the Goldstone field in each point $\phi(x)$. It takes the transformed element from (ξ_L, ξ_R) back to the coset space class representative. However, there is a freedom in the choice of the representative class element which is easily illustrated by the fact that we can compensate the chiral transformation either with $h(g, \phi(x))$ or with $g_{HLS}(x)\,h(g, \phi)$, being $g_{HLS}(x) \in SU(n_f)$, and recover exactly the same transformed tensor $U' = \xi'_R\,\xi'^\dagger_L$.

In the Hidden Local Symmetry model the vector mesons are considered as authentic gauge bosons of the former local symmetry. These gauge bosons transform therefore as

$$\bar{V}_\mu \qquad \longrightarrow \qquad h\,\bar{V}_\mu\,h^\dagger + \frac{i}{g}\,h\,\partial_\mu h^\dagger\,, \qquad (4.17)$$

where the mesons are described through a vector field $\bar{V}_\mu$ and g is the gauge coupling constant.

The kinetic term for the vector field must be chiral invariant so one uses the Maurer-Cartan 1-form Γ_μ –employing the nomenclature in Ref. [43]– which is the connection defined before in χPT [43, 23]:

$$\mathcal{L}_V^{Kin} = -\frac{1}{4}\langle\,\bar{V}_{\mu\nu}\bar{V}^{\mu\nu}\,\rangle + \frac{1}{2}M_V^2\langle\,\left[\bar{V}_\mu - \frac{i}{g}\Gamma_\mu\right]^2\,\rangle\,, \qquad (4.18)$$

with $\bar{V}_{\mu\nu}$ the strength field tensor of $\bar{V}_\mu$:

$$\bar{V}_{\mu\nu} = \partial_\mu\bar{V}_\nu - \partial_\nu\bar{V}_\mu - ig[\bar{V}_\mu, \bar{V}_\nu]\,. \qquad (4.19)$$

Notice the relation existing between this tensor and the one from the Proca formalism, $\hat{V}_\mu = \bar{V}_\mu - (i/g)\Gamma_\mu$, that gives $\bar{V}_{\mu\nu} = \hat{V}_{\mu\nu} - ig[\hat{V}_\mu, \hat{V}_\nu] + (i/4g)[u_\mu, u_\nu] + (1/2g)f_{+\,\mu\nu}$. This shows that the former kinetic term for the vector field is equivalent to the Proca lagrangian for mesons (up to $\mathcal{O}(\hat{V})$) for a precise value of the coupling constant, $f_V = 1/g\sqrt{2}$ and $g_V = 1/2g\sqrt{2}$.

To describe the axial-vector meson one employs a similar field $\hat{A}_\mu$. This fields do not transform as the vectors under a chiral transformation but as

$$\hat{A}_\mu \qquad \longrightarrow \qquad h\hat{A}_\mu h^\dagger\,. \qquad (4.20)$$

To build its kinetic lagrangian the other Maurer-Cartan 1-form u^μ is employed:

$$\mathcal{L}_A^{Kin} = -\frac{1}{4}\langle\,\hat{A}_{\mu\nu}\hat{A}^{\mu\nu}\,\rangle + \frac{1}{2}M_V^2\langle\,\left[\hat{A}_\mu + \frac{1}{g'}u_\mu\right]^2\,\rangle\,, \qquad (4.21)$$

where again the former structure of the Proca lagrangian is recovered once the mixing axial-Goldstone term is removed through a field redefinition.

For the NGB fields the Hidden Local Symmetry model provides just the same term as the antisymmetric formalism,

$$\mathcal{L}_{2\chi} \;=\; \frac{F^2}{4} \langle \, u^\mu u_\mu \, \rangle \,, \tag{4.22}$$

but adding also a scalar σ-partner multiplet $\sigma = \sum_a \sigma_a \lambda_a / \sqrt{2}$, to the pseudo-scalar multiplet of Goldstones when choosing the the representative of the G/H coset:

$$\xi_{L,R}(x) \;=\; \exp\left\{ \frac{i\sigma(x)}{F_\sigma} \right\} \exp\left\{ \pm \frac{i\pi(x)}{F_\pi} \right\}. \tag{4.23}$$

These $\sigma_a(x)$ are the Nambu-Goldstone bosons of the Hidden Local Symmetry which are eaten by the gauge vector bosons in a given gauge and provide the masses to the vectors. Thus, in that gauge the σ states disappear, the vectors gain the mass term shown before and the coset coordinates of G/H become the usual ones from χPT in the $u(x)$ formalism, $\xi_L(x) = u(x)^\dagger$ and $\xi_R(x) = u(x)$.

One of the advantages of the Hidden Local Symmetry model is that its lagrangian contains terms with just two power of the momenta, on the contrary to the Proca description which contained as well terms of order p^4. We will see later that when computing loops this becomes an important point since the diagrams behave badly at high energies and one needs more sophisticated cancellations to make the full amplitude behave asymptotically as QCD prescribes at short distances.

However, the gauge nature of the vector mesons is not a very clear explanation and it may introduce some artificial constraints. The number of parameters is smaller but in the worst case one might reach some inconsistency due to the over-constraint of the EFT. Anyway, the study of this model is still open and can provide some interesting information about the structure of the vector meson interactions.

4.2 QCD short distance constraints at LO in $1/N_C$

In this section the dependence of the resonance couplings on the number of colours is studied.

As it was shown in the former chapter, the matrix element of a bilinear quark current producing a meson, $\langle M_i | J | 0 \rangle$, is $\mathcal{O}(\sqrt{N_C})$ and is just given by the tree-level meson production. It easy to check that these processes are given by the couplings of the resonance lagrangian

$$F_V, \; F_A, \; c_m, \; d_m, \; \sim \; \mathcal{O}(\sqrt{N_C}) \quad . \tag{4.24}$$

The remaining couplings G_V and c_d will be obtained from the decay of a vector or a scalar into a pair of Goldstones. Through similar reasonings [5] one may prove that

the vertex functions with three external legs of mesons are of order $\mathcal{O}(1/\sqrt{N_C})$ [46, 5]. Thus, the computation of the vector decay shows that it is proportional to G_V/F^2. Since $F \sim \mathcal{O}(\sqrt{N_C})$, one has that

$$G_V \;\sim\; \mathcal{O}(\sqrt{N_C}) \quad . \tag{4.25}$$

For the scalar decay in the chiral limit –zero quark masses– (which is independent of the number of colours) the amplitude is proportional to c_d/F^2 and therefore

$$c_d \;\sim\; \mathcal{O}(\sqrt{N_C}) \quad . \tag{4.26}$$

The rest of parameters of the EFT, masses, momenta and external fields scale as $\mathcal{O}(N_C^0)$ in the $1/N_C$ counting.

Moreover one may go further than simply estimating the $1/N_C$ order. By imposing the QCD high energy behaviour to the amplitudes it is possible to fix all the parameters at LO in $1/N_C$ in terms of F [21, 22, 23].

From the analysis of the vector, axial-vector and scalar form factors [22, 23] one gets the relations:

$$1 \,-\, \sum_i \frac{F_{V_i} G_{V_i}}{F^2} \;=\; 0 \,,$$

$$\sum_i \frac{F_{V_i}^2 - 2 F_{V_i} G_{V_i}}{M_{V_i}^2} \;=\; 0 \,,$$

$$1 \,-\, \sum_i \frac{4 c_{d_i}^2}{F^2} \;=\; 0 \,, \tag{4.27}$$

$$c_{d_i} \;=\; c_{m_i} \,.$$

The requirement that the $\Pi_{LR}(s)$ current correlator vanishes faster than $1/s^2$ in the chiral limit provides the first and second Weinberg-sum-rules [48]:

$$F^2 \,-\, \sum_i \left(F_{V_i}^2 - F_{A_i}^2 \right) \;=\; 0 \,,$$

$$\sum_i \left(M_{V_i}^2 F_{V_i}^2 - M_{A_i}^2 F_{A_i}^2 \right) \;=\; 0 \,. \tag{4.28}$$

For massless quarks the two-scalar current correlator minus the two-pseudo-scalar one, $\Pi_{SS-PP}(s)$, vanishes as $1/s^2$ as $s \to \infty$ with a coefficient proportional to $\alpha_s \langle \bar{q}q \rangle^2 \sim \alpha_s B_0^2$. The EFT result diverges at first as s and provides two constraints when matching the OPE behaviour [49]:

$$\frac{F^2}{8} \,-\, \sum_i (c_{m_i}^2 - d_{m_i}^2) \;=\; 0$$

$$\sum_i (M_{S_i}^2 c_{m_i}^2 - M_{P_i}^2 d_{m_i}^2) \;=\; \frac{3\pi\alpha_s}{4} F^4 \,, \tag{4.29}$$

where in the $1/N_C$ counting the strong coupling constant scales as $\alpha_s \sim \mathcal{O}(N_C^{-1})$.

Observing every relation one realizes that they are consistent with the former estimations of the $1/N_C$ order and that all the terms are of the same order for a given equality. In addition, if just one multiplet is considered, they fully determine the value of the seven couplings for the interactions with the Goldstones,

$$\frac{F_V}{\sqrt{2}} = \sqrt{2}G_V = F_A = 2c_d = 2c_m = 2\sqrt{2}d_m = F \qquad \sim \qquad \mathcal{O}(\sqrt{N_C})\,, \quad (4.30)$$

and relate the different masses,

$$M_A^2 = 2M_V^2\,, \quad M_P^2 = 2M_S^2\,(1-\delta) \qquad \sim \qquad \mathcal{O}(N_C^0)\,, \qquad (4.31)$$

with the small order $\mathcal{O}(N_C^0)$ correction $\delta \approx 3\pi\alpha_s F^2/M_S^2 \sim 0.08\alpha_s$, which is numerically negligible.

Through them one gets the low energy χPT couplings at LO in $1/N_C$ in terms of just three parameters, M_V, M_S and F [21]:

$$2L_1 = L_2 = \tfrac{1}{4}L_9 = -\tfrac{1}{3}L_{10} = \frac{F^2}{8M_V^2}\,,$$

$$L_3 = -\frac{3F^2}{8M_V^2} + \frac{F^2}{8M_S^2}\,, \qquad L_5 = \tfrac{8}{3}L_8 = \frac{F^2}{4M_S^2}\,, \qquad L_4 = L_6 = 0\,, \qquad (4.32)$$

with all the non-zero L_i being of $\mathcal{O}(N_C)$. The coupling L_7 would have contributions from the pseudo-scalar resonances. However, one would have to consider the pseudo-scalar meson η_1. Being a NGB in the large N_C limit, it gains a large mass in physical QCD for $N_C = 3$ due to the axial anomaly and its exchange gives the main contribution to the χPT coupling, $L_7 = -F^2/(16M_{\eta_1}^2)$.

These relations will be employed in the following chapters when computing the vector and scalar form factors.

4.3 $1/N_C$ counting at the loop level

At this point one needs to control the order in $1/N_C$ of any diagram that one may construct, not only those at tree-level. If the idea is to construct an effective field theory at the quantum level one must be able to control the perturbative order of the diagrams beyond tree-level. In this way, it will be possible to estimate the size of the radiative corrections coming from the loops of the LO lagrangian. Assuming the fact that the counterterms must be of the same order as the radiative corrections this analysis will be very instructive about how these counterterms must be.

Consider any diagram constructed through the vertices from the LO lagrangian. The interacting terms of the resonances show the structure:

$$\mathcal{L}_{2R} \quad \sim \quad F_R\,R\,p^2 \sum_k \frac{\phi^k}{F^k}\,, \qquad (4.33)$$

where $F_R = F_V, G_V, c_d...$ are the different couplings of each resonance field R and all become proportional to the pion decay constant F in the large N_C limit ($F_V = F\sqrt{2}$, $G_V = F/\sqrt{2}$, $c_d = F/2...$), and therefore they scale as $F_R \sim F \sim N_C^{-1/2}$. The factor p^2 in Eq. (4.33) stands for any of the $\mathcal{O}(p^2)$ structures of derivatives, pNGB masses or external fields that one find in the lagrangian. Finally, the infinite series $\sum_k \frac{\phi^k}{F^k}$ takes into account the expansion of the chiral tensors in terms of the NGB fields ϕ. Taking into account that in the $1/N_C$ counting the NGB fields has the same scaling as the resonance fields, i.e. $R \sim \phi \sim \Psi$, then one has that the interacting terms are of the form

$$\mathcal{L}_{2R} \ \sim \ F^2 p^2 \sum_{k'} \frac{\Psi^{k'}}{F^{k'}}, \tag{4.34}$$

where Ψ denotes any meson field.

The interacting kinetic terms of the resonances show the same structure:

$$\mathcal{L}_R^{Kin} \ \sim \ p^2 R^2 \left(1 + \sum_k \frac{\phi^k}{F^k}\right) \ = \ F^2 p^2 \sum_{k'} \frac{\Psi^{k'}}{F^{k'}}, \tag{4.35}$$

where the series of NGB interactions come from the connection in the covariant derivative.

To end with, I demostrate that this structure appears also in the $\mathcal{O}(p^2)$ term from χPT lagrangian:

$$\mathcal{L}_{2\chi} \ \sim \ F^2 p^2 \sum_k \frac{\phi^k}{F^k} \ = \ F^2 p^2 \sum_k \frac{\Psi^k}{F^k}. \tag{4.36}$$

Let us now consider a vertex of the diagram, coming from the LO lagrangian, and with k external legs. This vertex will come from a term of the lagrangian with k powers of the fields Ψ. Therefore, that vertex will be proportional to $p^2 F^{2-k}$, keeping in mind that $p^2 \sim \mathcal{O}(N_C^0)$ and $F \sim \mathcal{O}(N_C^{\frac{1}{2}})$.

We will assume that the diagram contains N_k vertices with k legs. It will contain a number L of loops, I of internal propagators and E of external legs. Here one must be careful since there appear to kind of countings, the counting in momenta and the counting in $1/N_C$. The integration over the momenta of the loop does not modify the $1/N_C$ order of the diagram, since it is given by the couplings of the vertices. Then, it is easy to check that the amplitude $\mathcal{T}$ obeys the $1/N_C$ counting:

$$1/N_C \text{ order} \longrightarrow \quad \mathcal{T}_{(L)} \ \sim \ F^{\sum_k N_k(2-k)} \ \sim \ N_C^{\sum_k N_k(1-k/2)}. \tag{4.37}$$

It is equally simple to obtain the superficial divergence order p^D by an analysis similar to that in χPT:

$$p^D \text{ order} \longrightarrow \quad \mathcal{T}_{(L)} \ \sim \ p^{4L-2I+\sum_k 2N_k}, \tag{4.38}$$

where now all the vertices are $\mathcal{O}(p^2)$.

One may use the relations between the number of vertices, loops and external and internal lines: $\sum_k N_k k = E + 2I$ and $L = 1 + I - \sum_k N_k$. Therefore one may replace the exponents that depend on the number of vertices by the expressions $\sum_k N_k k/2 = E/2 + I$ and $\sum_k N_k = 1 + I - L$, getting:

$$
\begin{aligned}
1/N_C \text{ order} \longrightarrow \quad & \mathcal{T}_{(L)} \sim F^{2-E-2L} \sim N_C^{1-E/2-L}, \\
& \\
p^D \text{ order} \longrightarrow \quad & \mathcal{T}_{(L)} \sim p^{2+2L},
\end{aligned}
\tag{4.39}
$$

which can be put together into

$$
\mathcal{T}_{(L)} \sim p^2 F^{2-E} \cdot \left(\frac{1}{(4\pi)^2} \frac{p^2}{F^2} \right)^L \sim p^2 F^{2-E} \cdot N_C^{-L}, \tag{4.40}
$$

where one phase-space factor $\frac{1}{(4\pi)^2}$ appears from every loop.

These interesting results show many things. First of all, one can see that for a given process all the diagrams with the same number of loops are of the same order in the $1/N_C$ counting; the number of external legs does not change and the suppression in $1/N_C$ is given just by the number of loops as it was expected from qualitative arguments [5].

The formal $1/N_C$ expansion is given in the EFT by the powers $p^2/(4\pi F)^2$. More exactly the number of colours enters in the EFT through the dimensionful parameters, the meson masses $M^2 \equiv m_\phi^2$, $M_R^2 \sim \mathcal{O}(N_C^0)$ and $F_R^2 \sim F^2 \sim \mathcal{O}(N_C)$. However, the result in Eq. (4.40) shows that the dimensionless expansion parameter is $\varrho = \frac{M^2}{(4\pi F)^2}$. This ϱ is what one expects to become small in the large N_C limit. Thus the former expression Eq. (4.40) can be given in terms of ϱ and an order $\mathcal{O}(N_C^0)$ function $f_{(L)}\left(\frac{p_i}{M}\right)$ of the external momenta p_i and the meson masses:

$$
\mathcal{T}_{(L)} \sim p^2 F^{2-E} \cdot \varrho^L \cdot f_{(L)}\left(\frac{p_i}{M} \right). \tag{4.41}
$$

The real problem in all this argumentation is that the function $f_{(L)}\left(\frac{p_i}{M}\right)$ from every individual diagram behaves as a power series on momenta $f_{(L)}\left(\frac{p_i}{M}\right) = B_L(p^2)^L + B_{L-1}(p^2)^{L-1} + ...$, so the radiative corrections always become large above some energy. However, it is at this point where the matching with QCD short distance can save the convergence of the $1/N_C$ expansion. Assuming that the behaviour of the observable at LO in $1/N_C$ is the same as that for the whole observable, and also requiring that order by order $1/N_C$ the observable vanishes faster than a power of the momenta at short distances, then one finds that the function $f^{(L)}(p_i(M)$ can grow at most as a constant. This ensures that the subleading corrections do not grow indefinitely and follow the same power behaviour as the LO:

$$
\left| \mathcal{T}_{(L+1)} \right| \leq C_{(L+1)} \cdot \varrho \cdot \left| \mathcal{T}_{(L)} \right|, \tag{4.42}
$$

where the $\mathcal{O}(1)$ bound $C_{(L+1)}\,\varrho$ depends on the shape of $f_{(L)}\left(\frac{p_i}{M}\right)$. In order to preserve the convergence of the $1/N_C$ series this bound should be smaller than 1. However, there is no general argument that ensures this for all the amplitudes and Green-functions, only having demostrations for some observables. For instance, the imaginary part of the pion vector form factor ($\mathcal{F}(s)$) coming from the $\pi\pi$ cut obeys the relation $|\mathrm{Im}\{\mathcal{F}(s)\}| = |\sigma_\pi\,\mathcal{F}(s)^*\,T_{I,J}(s)| = \sigma_\pi\,|\mathcal{F}(s)|\,|T_{I,J}(s)| \le |\mathcal{F}(s)|$, with the (I,J) $\pi\pi \to \pi\pi$ partial wave $|T_{I,J}(s)| \le 1$. This at NLO in the perturbative level implies that $|\mathrm{Im}\{\mathcal{F}_{(1)}(s)\}| \le |\mathcal{F}_{(0)}(s)|$.

4.3.1   Ultraviolet divergences

At this point it is good to remind that p stands till now for either momenta, meson masses and external fields. The non-analytic structures that are going to arise from the loop calculation will be proportional to the corresponding power p^{2+2L} obtained before.

In addition, the ultraviolet divergences will be proportional to p^{2+2L}. At one loop, $L = 1$, one is going to find ultraviolet divergences of order p^4. The lagrangian developed at LO contains just $\mathcal{O}(p^2)$ vertices and therefore it is unable to provide the counterterms. Through this derivation it appears manifestly the necessity of introducing a NLO lagrangian with chiral tensors of $\mathcal{O}(p^4)$.

The structure of the divergences must obey precise rules. Since the Feynman integrals must be defined for any value of the parameters –external momenta p_i, meson masses M_i and external fields (v^μ, a^μ, s, p)– therefore they must be well defined when they are evaluated at zero. In order to have the amplitudes well defined for any value of the external parameters the divergences must not contain poles of of them: The divergent piece of the amplitude will be a $\mathcal{O}(p^{2+2L})$ polynomium of them.

Nevertheless, some of these higher order divergences are really proportional to masses of resonances (which are chiral invariant) and may be renormalized by lower order operators. But those of order p^{2+2L} containing genuine derivatives can be reabsorbed just by new operators with a larger number of derivatives, as it was said before.

There is only one detail missing here: The non-physical degrees of freedom of the vector mesons (the longitudinal ones in the Proca formalism). As it already happened in the Standard Model, the existence of massive vector fields gives some problems at high energies and when renormalizing. The Standard Model solved the problem providing the mass to the gauge bosons through the Higgs Mechanism of spontaneous symmetry breaking. Thus, the renormalizability properties were preserved at the same time that the vector bosons looked like massive for some choices of the gauge.

This is a typical problem in the Proca formalism R^μ. On the other hand, in the antisymmetric formalism $R^{\mu\nu}$ one does not have problems with the longitudinal modes of the field but with a given set of components of the tensor $R^{\mu\nu}$ –the Ω

projection of the field–. The operator $\Omega(\partial)$ is defined in Appendix B and will appear in a next chapter when performing the perturbative calculation.

In RχT the effect of the Ω–projection of the vector propagator (longitudinal modes in the Proca formalism) produces the presence of poles $1/M_{V,A}^2$ in the amplitudes for $M_{V,A} = 0$. In the NLO calculation of the vector form factor (Chapter 6) one observes the appearance of this kind of poles on M_V in the loop with a cut of two vectors (it is explained with more detail in Appendix C). In addition, although the expected scaling of the one-loop diagram would be $\mathcal{O}(p^4) \sim q^2(p_{\pi^+}^\mu - p_{\pi^-}^\mu)v(x)_\mu$, the actual momentum structure is $q^4/M_V^2(p_{\pi^+}^\mu - p_{\pi^-}^\mu)v(x)_\mu$, where $v(x)^\mu$ is the auxiliary vector field introduced before. Therefore the $1/N_C$ ordering of the diagrams turns out to be spoiled by these Ω–modes; the renormalization requires not only the $\mathcal{O}(p^4)$ operators but also some $\mathcal{O}(p^6)$ structures. However, these extra degrees of freedom (Ω or longitudinal modes, depending on the formalism) do not appear at high energies in perturbative QCD, which is a theory of massless states (once the quark masses are neglected).

This problem is much more dismaying than what it looks at first glance. One may think that it is just a problem of introducing new NLO operators in $1/N_C$. However one must also take into account the absorptive contributions. The non-analytic functions that arise at the loop level cannot be compensated with any local operator. Thus, returning to the latter example of the form factor, one finds that the Ω–components of the vector propagator produce not only a divergence of the form $q^4/M_V^2(p_{\pi^+}^\mu - p_{\pi^-}^\mu)v(x)_\mu$ but also the logarithm $q^4 \ln(-q^2)/M_V^2(p_{\pi^+}^\mu - p_{\pi^-}^\mu)v(x)_\mu$. The way how the extra modes disappear at high energy is something that remains out of the reach of this work but it is definitely something that will have to be analysed in future.

4.3.2   Short distance asymptotic behaviour

At this point one is ready to analyse the high energy behaviour of the quantum loops. The observables in perturbative QCD are functions of the number of colours and of the momenta. The OPE provides an expansion in powers of the momenta whose coefficients are functions of the number of colours and the strong coupling constant. Therefore it is reasonable to argue that every single OPE coefficient accepts an expansion in $1/N_C$ and that, therefore, the observable obeys the asymptotic behaviour order by order in $1/N_C$ independently. This means that the short distance cancellations must occur not only in the calculation at LO but also in the perturbative calculation at NLO, NNLO and so on.

In the EFT picture one would compute the one loop diagrams and the corresponding tree-level amplitudes including a NLO vertex. If the effective description has any sense the dependence in momenta of the NLO amplitude –once all the contributions are summed up– cannot become dominant compared with the LO one, i.e. it must not grow faster in the momenta. Otherwise we would be dropping out an infinity of higher orders with larger dependences on the energy and our perturbative
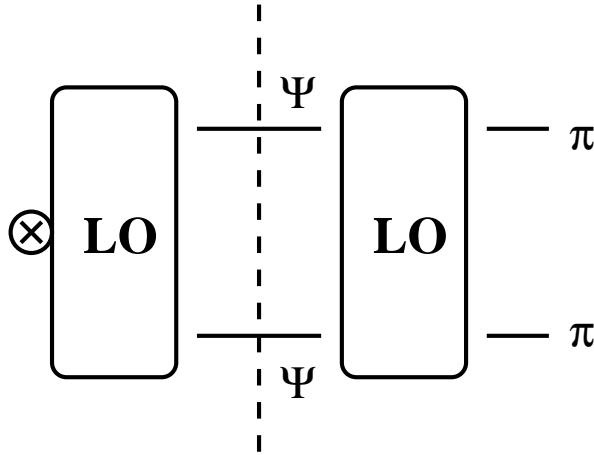
Figure 4.1: Absorptive cuts at one loop in the pion vector form factor.

calculation would turn meaningless.

Once it becomes clear that the comparison with the OPE behaviour must be done separately order by order, there arises the question about how the cancellations occur. Through the former analysis of the superficial degree of divergence one realises that every individual one-loop diagram has a power p^2 more than the tree-level amplitudes. Therefore, there must be subtle cancellations between diagrams in order to decrease this extra power of the momenta, in addition to those that already happened at LO in $1/N_C$; as it was shown before, the form-factors and correlators have been imposed to follow the QCD high energy behaviour at LO in $1/N_C$. Through them we could fix the values of the couplings in the lagrangian at LO in $1/N_C$. But, how do these cancellations occur at the loop level?

On the contrary to what at first it may seem, the problem is not in the analytic part of the loops, which can fixed by tuning the counterterms; moreover, the short distance constraints would fix the counterterms up to the considered order. The problem comes from the non-analytic part of the one-loop amplitude. It cannot be varied by any NLO term that one may introduce in the lagrangian. They are only ruled by the LO vertices. Thus, the high energy behaviour at one loop is ruled by the high energy behaviour of the diagrams at tree-level.

Consider now the one-loop amplitude. Take all the diagrams with a given absorptive cut X –e.g. an intermediate state with two resonances (actually at one loop there can be at most two particles in an intermediate state)–. The first part of the diagram is nothing else but the form factor to that mesonic state X at LO in $1/N_C$, and it must obey the scaling $\sim 1/q^2$ at short distances.

The second part of the cut diagram, which can be beheld in Fig. (4.1), would

correspond to the tree-level scattering of the intermediate state X –in the former example the two resonances– into a $\pi\pi$ pair. The superficial dimensional analysis shows that it behaves like $\sim p^2 F^{2-E}$, with E the number of external legs in the scattering. Therefore, assuming that the X–form factor behaves as $\sim 1/q^2$, a naive overview would tell us that the amplitude related to the absorptive cut X diverges as $\sim p^2 \sim (p^\mu_{\pi^+} - p^\mu_{\pi^-})v(x)_\mu$. This would mean that the one-loop form factor would go as a constant and would not vanish at infinite momentum transfer, even although if every form factor at LO in $1/N_C$ was well behaved.

There are two possible ways out to this riddle:

a) Either every channel $X \to \pi\pi$ suffer cancellations between diagrams so the summed up tree-level amplitude $\mathcal{T}(X \to \pi\pi)$ tends to a constant at short distances,

b) Or there is a more complicated cancellation between different channels once all are summed up.

Obviously, the second one seems to be a more complicated solution and not so clear once we go to analyse other observables. The first option looks more natural and solves at once the problems for any possible observable at one loop: All the tree-level amplitudes diverge as dimensionless constants at high momentum and then the non-analytic structures from the one-loop diagrams diverge also as a constant, keeping the same behaviour as the tree-level matrix elements.

A hint of the first choice as the right one comes from the $\pi\pi \to \pi\pi$ scattering behaviour. Let us assume that the partial wave of angular momentum J behaves as $T_J \sim s^D$ when $s \to \infty$. Unitarity provides the inequality

$$\text{Im } T_J \; \geq \; \sigma_\pi |T_J|^2 \, . \tag{4.43}$$

This implies that the imaginary part grows at least as fast as $\text{Im} T_J \gtrsim s^{2D}$, so therefore $D = 0$ and the partial wave amplitudes goes as $T_J \sim s^0$ at infinite momentum. At the perturbative level this is reflected as

$$\text{Im } T_J^{NLO} \; \geq \; \sigma_\pi |T_J^{LO}|^2 \, . \tag{4.44}$$

One can see that the saturation of the Froissart bound at LO in $1/N_C$ [54], i.e. $s \lesssim T_J^{LO} \lesssim s^2$, spoils the behaviour at NLO since $\text{Im} T_J^{NLO} \gtrsim s^2$. In general the requirement of perturbative unitarity demands that the asymptotic behaviour of the scattering amplitude at every order in $1/N_C$ is the same as the whole amplitude.

Using the same arguments of unitarity it is possible to demostrate that the scattering amplitude to any state must behave as a constant at high energies:

$$\text{Im } \langle \pi\pi |T| \pi\pi \rangle \; = \; \sum_X \int d\Phi_X \, |\langle X|T|\pi\pi \rangle|^2 \, , \tag{4.45}$$

where one has the summation on every available intermediate state X and integrating over its space-phase. The left-hand-side has been proven to go as a constant. Then each individual term –which is positive– must go at most as a constant. Therefore the amplitude of $\pi\pi \to X$ tends to $\langle X|T|\pi\pi \rangle \to const.$ when $s \to \infty$. The requirement of every order in $1/N_C$ to behave as the whole observable ensures the constant behaviour also at the perturbative level.

4.4   Construction of the NLO lagrangian in $1/N_C$

Following the steps commented in the former section we are going to build up to the NLO lagrangian required to renormalize the one-loop diagrams [106]. In this work the attention has been focused on the pion vector form factor and only the terms contributing to this process will be given. Nevertheless, the analysis of the scattering amplitudes and other form factors at one loop would provide the remaining NLO terms.

4.4.1   Subleading lagrangian

For the VFF we need to compute several types of 1PI Green functions. At one loop the Feynman integrals produce ultraviolet divergences which the former LO lagrangian is not able to renormalize. New divergent structures appear at NLO in $1/N_C$ demanding the inclusion of extra pieces in the lagrangian.

The LO lagrangian will be extended by the inclusion of just those pieces needed to renormalize the one loop diagrams. These new pieces will contain tensors of $\mathcal{O}(p^4)$, i.e. with four derivatives or equivalent, as it was derived in the analysis of the superficial degree of divergence. Higher order operator are supposed to be zero at NLO since the radiative corrections for those orders are zero and a counterterm much larger than the radiative corrections would not have any sense.

The only exception to what I have just referred comes from the loop with two vectors, as it was announced before. The Ω–modes of the massive vectors spoil the ordering and one has to introduce some $\mathcal{O}(p^6)$ operators.

Higher orders in χPT

We need to include new terms for the interactions among Goldstones. Since they must be chiral invariant they have the structure of the higher order χPT lagrangian but with different couplings because we are now in a different theory. The terms of the $\mathcal{O}(p^4)$ χPT lagrangian relevant for the tree-level vector form-factor are:

$$\widetilde{\mathcal{L}}_{4\chi} \;\; = \;\; \frac{i\widetilde{\ell}_6}{4}\langle\, f_+^{\mu\nu}\,[u_\mu, u_\nu]\,\rangle \;-\; \widetilde{\ell}_{12}\langle\, \mathcal{O}_{EOM}^{2\chi}\mathcal{O}_{EOM}^{2\chi}\,\rangle\,, \tag{4.46}$$

where the dots represent the remaining structures which do not contribute to the VFF at tree-level and $\mathcal{O}_{EOM}^{2\chi} = \nabla^\mu u_\mu - \frac{i}{2}\left(\chi_- - \frac{1}{n_f}\langle\,\chi_-\,\rangle\right)$, being $n_f = 2$ in the

$SU(2)$ theory. I also remind the different definitions of the couplings in the two– and three–flavour theories, $\ell_6 = -2L_9$.

We will use the tilde to refer the chiral couplings in the theory with explicit resonance fields, and without it to refer the parameters in standard χPT. These $\widetilde{\ell}_i$ are at most $\mathcal{O}(1)$ in the $1/N_C$ counting, i.e. NLO compared with the usual χPT ℓ_i in Ref. [8, 16], which are $\mathcal{O}(N_C)$. The last structure in Eq. (4.46) does not contribute to the VFF when it is included in a tree-level diagram with the external legs on-shell. However, it serves to renormalise the $\mathcal{O}(p^4)$ divergence in the pion self-energy.

Also a subleading lagrangian with the structures of the $\mathcal{O}(p^6)$ χPT lagrangian $\widetilde{\mathcal{L}}_6$ will be necessary but with NLO in $1/N_C$ couplings different to the usual ones in regular χPT [16]. For the process under analysis only a pair of terms contribute:

$$\widetilde{\mathcal{L}}_{6\chi} = i\widetilde{c}_{51}\langle \nabla^\rho f_+^{\mu\nu}[h_{\mu\rho}, u_\nu]\rangle + i\widetilde{c}_{53}\langle \nabla_\mu f_+^{\mu\nu}[h_{\nu\rho}, u^\rho]\rangle. \tag{4.47}$$

In fact, only the precise combination of the couplings $\widetilde{r}_{V_1} \equiv 4F^2(\widetilde{c}_{53} - \widetilde{c}_{51})$ is going to be relevant for the pion vector-form factor that will be computed in a next chapter.

Higher orders in the resonance Lagrangian

To renormalize some Green functions including resonances we are going to need new terms with higher derivatives: Pieces to renormalize the vector-vector Green function $(V^{\mu\nu}(x) - V^{\rho\sigma}(y))$,

$$\mathcal{L}_{4Z} = \frac{X_{Z_1}}{2}\langle \nabla^2 V^{\mu\nu}\{\nabla_\nu, \nabla^\sigma\}V_{\mu\sigma}\rangle + \frac{X_{Z_2}}{4}\langle\{\nabla_\nu, \nabla_\alpha\}V^{\mu\nu}\{\nabla^\sigma, \nabla^\alpha\}V_{\mu\sigma}\rangle$$

$$+ \frac{X_{Z_3}}{4}\langle\{\nabla^\sigma, \nabla^\alpha\}V^{\mu\nu}\{\nabla_\nu, \nabla_\alpha\}V_{\mu\sigma}\rangle + ..., \tag{4.48}$$

and we will define $X_Z \equiv X_{Z_1} + X_{Z_2} + X_{Z_3}$; pieces to renormalize the current-vector resonance Green function $(v(x)^\mu - V^{\rho\sigma}(y))$,

$$\mathcal{L}_{4F} = X_{F_1}\langle V_{\mu\nu}\nabla^2 f_+^{\mu\nu}\rangle + X_{F_2}\langle V_{\mu\nu}\{\nabla^\mu, \nabla_\alpha\}f_+^{\alpha\nu}\rangle + ..., \tag{4.49}$$

where we make the definition $X_F \equiv X_{F_1} + X_{F_2}$; and pieces to renormalize the vector-Goldstone-Goldstone Green function $(V^{\mu\nu}(x)\pi(y)\pi(z))$,

$$\mathcal{L}_{4G} = iX_{G_1}\langle\{\nabla^\alpha, \nabla_\mu\}V^{\mu\nu}[u_\nu, u_\alpha]\rangle + iX_{G_2}\langle V^{\mu\nu}[h_{\alpha\mu}, h_\nu^\alpha]\rangle + ..., \tag{4.50}$$

with the definition $X_G \equiv X_{G_2} - \frac{1}{2}X_{G_1}$. The ellipsis denotes more operators allowed by the symmetry but not entering in the VFF at this order in $1/N_C$. The dimensions of the couplings are $[X_Z] = E^{-2}$ and $[X_{F_i}] = [X_{G_i}] = E^{-1}$, and $X_{Z_i} = \mathcal{O}(1/N_C)$ and $X_{F_i}, X_{G_i} = \mathcal{O}(1/\sqrt{N_C})$ in the $1/N_C$ counting.

4.4.2   Equations of motion at LO in $1/N_C$

From the LO lagrangian one can derive the corresponding equations of motion (EOM), which are obeyed up to NLO in the tree level processes. The relevant EOM for the vector form factor are the ones corresponding to the vector fields:

$$\nabla^\mu \nabla_\rho V^{\rho\nu} - \nabla^\nu \nabla_\rho V^{\rho\mu} = -M_V^2 V^{\mu\nu} - \frac{F_V}{\sqrt{2}} f_+^{\mu\nu} - \frac{iG_V}{\sqrt{2}} [u^\mu, u^\nu] \; . \tag{4.51}$$

The derivation has been done for a single multiplet. For a series of vector multiplets without mixing terms one would have separate EOMs for every vector with the corresponding couplings for every case.

Analysing some processes (vector, axial-vector [23] and scalar [22] form factors) we obtained the large N_C relations for the resonance couplings from Eqs. (4.30) and (4.31). However, at one loop they suffer next-to-leading order deviations (NLO), as it was observed in Ref. [105]. Since our calculation is at one loop, the large N_C relations can be substituted in the one loop diagrams as the modifications would go to next-to-next to leading order. Only in the tree-level diagrams will be important to take into account the NLO value of the renormalized vector couplings, F_V^r, G_V^r and M_V^r.

At the order of the present calculation these terms only enter trough tree level diagrams (with the resonances only as internal lines). Thence, a great simplification can be made in the lagrangian: Through the EOM in Eq. (4.51) we get a new lagrangian completely equivalent to that up to NLO, $[\mathcal{L}_{2\chi} + \mathcal{L}_{2R}] + [\mathcal{L}_{4\chi,6\chi} + \mathcal{L}_{4R}]$, but now containing only $\mathcal{O}(p^2)$ interactions for the resonances. Also there arise operators with the structures of the $\mathcal{O}(p^4)\chi$PT lagrangian. We have now pieces from $\mathcal{L}_{4Z}$:

$$\mathcal{L}_{4Z}^{+EOM} = \frac{X_Z M_V^4}{2} \langle V^{\mu\nu} V_{\mu\nu} \rangle + \frac{X_Z M_V^2 F_V}{\sqrt{2}} \langle V_{\mu\nu} f_+^{\mu\nu} \rangle + \frac{i X_Z M_V^2 G_V}{\sqrt{2}} \langle V_{\mu\nu} [u^\mu, u^\nu] \rangle$$

$$+ \frac{i X_Z F_V G_V}{2} \langle f_+^{\mu\nu} [u_\mu, u_\nu] \rangle + ... \tag{4.52}$$

pieces for $v(x)^\mu - V^{\rho\sigma}(y)$,

$$\mathcal{L}_{4F}^{+EOM} = -X_F M_V^2 \langle V_{\mu\nu} f_+^{\mu\nu} \rangle - \frac{i X_F G_V}{\sqrt{2}} \langle f_+^{\mu\nu} [u_\mu, u_\nu] \rangle + ... \tag{4.53}$$

and pieces from the $V^{\mu\nu}(x)\pi(y)\pi(z)$ interaction,

$$\mathcal{L}_{4G}^{+EOM} = -2i X_G M_V^2 \langle V^{\alpha\nu} [u_\alpha, u_\nu] \rangle - i\sqrt{2} X_G F_V \langle f_+^{\mu\nu} [u_\mu, u_\nu] \rangle + ... \tag{4.54}$$

The dots denote other terms which are not relevant for the VFF at this order: other $\mathcal{O}(p^4)$ and $\mathcal{O}(p^6)$ χPT terms and extra vector-vector-NGB interactions.

One can easily observe that the higher-order-derivative resonance lagrangian in Eqs. (4.48), (4.49) and (4.50) is something spurious and that it is just equivalent

to a shift in the LO resonance couplings and the χPT couplings. The shifts in the relevant couplings for VFF are:

$$\tilde{\ell}_6^{eff} = \tilde{\ell}_6 + 2X_Z F_V G_V - 2\sqrt{2}X_F G_V - 4\sqrt{2}X_G F_V,$$

$$F_V^{eff} = F_V + 2X_Z M_V^2 F_V - 2\sqrt{2}X_F M_V^2,$$

$$G_V^{eff} = G_V + 2X_Z M_V^2 G_V - 4\sqrt{2}X_G M_V^2, \tag{4.55}$$

$$M_V^{eff\,2} = M_V^2 + 2X_Z M_V^4.$$

Notice that the modifications introduced by the EOM come at NLO, so in the one-loop diagrams one will have $F_V \sim F_V^r \sim F_V{}^{eff}$ (and similarly for G_V and M_V).

In chapter 6 we will make the renormalization of the vector form factor through the higher order lagrangian. Afterwards we will apply the EOM transformations to eliminate these spurious parameters. What phenomenology is going to fix is just the effective parameters. The relations (4.55) are valid also for the renormalized couplings. Therefore after the EOM transformation the new effective couplings own a different running due to the $X_{Z,F,G}^r(\mu)$ contributions.

Next steps in forthcoming works are the inclusion of higher multiplets of resonances and the renormalization of other interesting observables like the scalar form factor and the scattering amplitudes. However, the addition of extra resonances presents the problem of the mixing and other interesting features.

Chapter 5

Vector sector

The vector sector is one of the most worked out areas in the hadronic phenomenology. The fact that the interaction between leptons and hadrons are mediated by vector gauge bosons makes this channel one of the easiest to produce and analyse experimentally. A lot of information has been obtained either through tau decays or through e^+e^- collisions. The presence of maximums in the cross section for determined energies points out the presence of hadronic resonances with $J = 1$. Below the first vector resonance χPT provides a fair description of the amplitude [40]. RχT considers the resonance fields once the energy increases and it has provided many successful results describing the first multiple within a QFT framework [26, 27, 63, 105]. However a theoretical explanation for the hadronic spectral function between 1 and 2 GeV is still lacking although some works point out in that direction [44, 105]. Below the second multiplet of vectors the main channels are the two-Goldstone channel, and just $\pi\pi$ below the $K\overline{K}$ threshold. Multiparticle states are clearly suppressed kinematically.

In this chapter I will show several analysis that have done about one of the simplest matrix elements in hadron physics, the pion vector form factor. Nevertheless, in spite of its relative simplicity it has been shown to be one of the most fruitful and relevant observables, for instance, in the $g - 2$ determination.

Besides, its theoretical simplicity nowadays we own a large amount of experimental data either from tau decay or from e^+e^- colliders. Some experiments of this kind can be found in Refs. [65, 66, 67, 68, 69].

5.1 The vector form factor

Within the Standard Model the leptonic particles couple to the hadronic states just through the exchange of electroweak vector bosons ($W^\pm$, Z^0, γ). At leading order in the electroweak coupling the interaction is provided by the exchange of a single boson. This produces a quark-antiquark pair that hadronizes due to the non-perturbative action of the gluons. One of the typical examples of this is the

tau lepton decay (which is the only lepton heavy enough to decay into hadrons). It generates a tau neutrino beside some outgoing hadrons X_H. This hadronic state X_H carries the quantum numbers of the intermediate gauge boson, i.e., total angular momentum $J = 1$. In Fig. (5.1) one can observe a scheme of the tau decay.

Since the tau mass is $m_\tau = 1.777$ GeV and the neutrino one is negligible, the experiment yields information about the available hadronic states $X_H[J = 1]$ between the lowest threshold –the two-pion channel, with invariant square mass $4m_\pi^2 = (275$ MeV$)^2$– up to the tau mass.
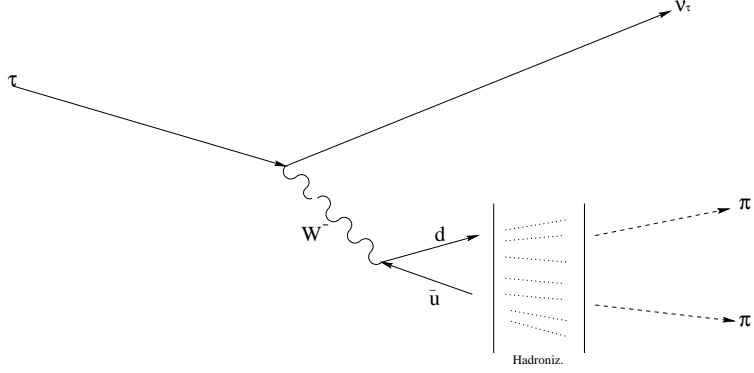

Figure 5.1: Decay $\tau^- \to \nu_\tau \pi^- \pi^0$.

The production of hadrons through a vector quark current is one of the cleanest ways to explore QCD due to the simplicity of the interaction. Once the $q\bar{q}$ pair is produced it evolves just due to the QCD action (neglecting the contributions from extra electroweak exchanges). Hence we have a clear initial state in terms of quarks and clear final states in terms of hadrons. It is essentially a perfect experiment to obtain information about the complex mechanisms of hadronization in QCD.

The absence of interaction between the quark and leptonic sectors allows a factorization of the amplitude into a electroweak and a strong interacting part. For instance, for the charged current present in the tau decay one has the amplitude:

$$\langle\, X_H(q),\, \nu_\tau(p_\nu) | \mathcal{T} | \tau(P_\tau)\,\rangle\ =$$

$$= \langle\, X_H(q) | J_L^\mu | 0\,\rangle \,\times\, \left[4ig_W^2 \cos\theta_C\, \Delta_{\mu\nu}^{(W^-)}\right] \,\times\, \langle\, \nu_\tau(p_\nu) | J_L^\nu | \tau(P_\tau)\,\rangle\ +\ \mathcal{O}(g_W^4)\,,$$

$$(5.1)$$

where $\Delta_{\mu\nu}^{(W^-)}$ is the W^- propagator, g_W is the weak gauge coupling and θ_C is the Cabbibo angle. The quark left current for the tau decay is $J_L^\mu = \frac{1}{2}\bar{d}\gamma^\mu(1-\gamma_5)u$ and contains a vector and an axial-vector component. The leptonic matrix element can be computed directly.

Since the energy we are considering ($\sqrt{s} < 2$ GeV) is much lighter than the weak boson mass ($M_W = 80$ GeV), its propagator becomes point-like and the matrix

element turns into

$$\langle\, X_H(q),\, \nu_\tau(p_\nu)|\mathcal{T}|\tau(P_\tau)\,\rangle \;=$$

$$= \langle\, X_H(q)|J_L^\mu|0\,\rangle \;\times\; \left[\sqrt{2}G_F\cos\theta_C\, g_{\mu\nu}\right] \times\; \bar{u}_{\nu_\tau}(p_\nu)\gamma^\nu(1-\gamma_5)u_\tau(P_\tau) \;+\; \mathcal{O}(g_W^4)\,,$$
$$(5.2)$$

with the Fermi constant $G_F = \sqrt{2}g_W^2/M_W^2$ and the leptonic matrix element already substituted.

Therefore the amplitude is given by a set of well known electroweak parameters together with the hadronic matrix element $\langle\, X_H(q)|J_L^\mu|0\,\rangle$. One of the main channels is the two-pion production. It only gains contributions from the vector part of the left current. The rest are going to be less relevant at low energy due to phase space suppression. However, at some energies one can generate a resonance in the s−channel with the proper quantum numbers being near its mass-shell. It then provides there the main contribution to the cross section. However, since the mesonic resonances own widths of hundreds of MeV they cannot be taken as asymptotic states for the energies treated in this thesis ($s \lesssim 1$ GeV). For the range of momenta studied here the only asymptotic states are the pNGB. Thus, we will take just pNGB as final states. As the momentum transfer increases more states are available and one has to perform a couple channel analysis.

The most general Lorentz structure for the production of two pNGB PP' –the PP' vector form factor (VFF)– is:

$$\langle\, P(p_1)P'(p_2)|J_V^\mu|0\,\rangle \;=\; (p_1-p_2)^\mu f_+(q^2) \;+\; (p_1+p_2)^\mu f_-(q^2)\,, \qquad (5.3)$$

where P and P' are the outgoing pseudo-scalars and the scalar functions $f_\pm(q^2)$ carry all the information. For the charged current we will have the $I = J = 1$ vector current $J_V^\mu = \bar{d}\gamma^\mu u$, whereas for the neutral case its corresponding $I = J = 1$ combination is $J_V^\mu = \frac{1}{\sqrt{2}}\left(\bar{u}\gamma^\mu u - \bar{d}\gamma^\mu d\right)$. One is just an isospin rotation of the other. For the isospin $I = 1$ charged channel the only available two-pseudoscalar states are $\pi^-\pi^0$ and K^-K^0.

In the isospin limit ($m_u - m_d = 0$ and $\alpha_{EM} \to 0$) the mass of the two outgoing pNGB is the same and therefore $f_-(q^2) = 0$. In addition, the conservation of the associated vector charge implies $f_+(0) = 1$ [39]. In order to accomplish this normalization condition the pNGB propagators must be renormalized in the on-shell scheme.

Therefore, the general form for the $I = 1$ VFF in the isospin limit is:

$$\langle\, P(p_1)P'(p_2)|J_V^\mu|0\,\rangle \;=\; \sqrt{2}(p_1-p_2)^\mu\, \mathcal{F}(q^2) \quad, \qquad (5.4)$$

with $q \equiv (p_1 + p_2)$ and J_V^μ being the charged or neutral current. For the neutral case $P(p_1)$ will correspond to the positive charged particle whereas for the charged current it will denote the negative charged meson.

When analysing the data from e^+e^- experiments one must remember that besides the $I = 1$ interaction the electromagnetic current contains also a $I = 0$ component. This fact does not occur in the tau decay. This gives an extra contribution to the VFF from the $I = 0$ channel. In general it is tiny but it becomes relevant near the $\rho(770)$ peak due to a large enhancement from the $I = 0$ vector resonance $\omega(782)$. This variation is easily described through mixing terms [46, 28] In addition, the process $e\pi \to e\pi$ allows us to obtain data for the $\pi\pi$ photo-production in the negative q^2 region [66].

5.2   VFF in perturbative QCD

Before more sophisticated EFT were developed to explain the low energy phenomenology lots of work had already be done to describe the pion VFF. Its asymptotic behaviour for $q^2 \equiv -Q^2 < 0$ was obtained through partonic analysis based on QCD. They showed that a infinite momentum transfer $Q^2 \equiv -q^2$ its behaviour –up to $\mathcal{O}(1/Q^2)$ and $\mathcal{O}(\alpha_s^2)$ corrections– was [50, 51]:

$$\mathcal{F}(Q^2) = \frac{16\pi\alpha_s(Q^2)F_\pi^2}{Q^2}, \qquad (5.5)$$

where $\alpha_S(Q^2)$ is the strong coupling constant at the scale $\mu^2 = Q^2$ and provides a logarithmic dependence. Actually the whole form factor would be given by the infinite series of subleading powers in $1/Q^2$:

$$\mathcal{F}(Q^2) = \sum_{n=1}^{\infty} \frac{C_{(n)}}{(Q^2)^n}, \qquad (5.6)$$

where the coefficients $C_{(n)}$ are functions of $\alpha_s(Q^2)$ which grow at most as a power of $\ln Q^2$. Actually, these coefficients accept an expansion in $1/N_C$ starting at order $\mathcal{O}(1)$ in this counting, since the VFF is $\mathcal{O}(1)$: $C_{(n)} = C_{(n)}^{[0]} + C_{(n)}^{[1]} + ...$, with $C_{(n)}^{[k]} \sim \mathcal{O}\left(\frac{1}{N_C^k}\right)$. Therefore the VFF from QCD can be expanded in an infinite series in $1/N_C$:

$$\mathcal{F}(Q^2) = \sum_{k=0}^{\infty} \left[\sum_{n=1}^{\infty} \frac{C_{(n)}^{[k]}}{(Q^2)^n} \right]. \qquad (5.7)$$

Thence, order at order in $1/N_C$ the form factor vanishes as q^2 tends to infinity. Therefore the asymptotic behaviour will be imposed not only to the whole VFF but also to every individual order in $1/N_C$.

Through analytic continuation one gets that in general the VFF vanishes at least as $\mathcal{F} \sim 1/q^2$ in the limit $|q^2| \to \infty$. This will be an essential result in our EFT constructions. Eventually the hadronic description must approach asymptotically to the perturbative QCD one. The large N_C analysis [5] showed the EFT requires

a pile of infinite resonances. However it is clear that resonant behaviour disappears for $\sqrt{s} \gtrsim \sqrt{s_{OPE}} \sim 2$ GeV and one observes just the perturbative QCD continuum (here I am talking just about light quark $u/d/s$ mesons).

Thus, the asymptotic QCD short distance conditions can be also applied to the truncated EFT that follows the behaviour not only at $s \to \infty$ but even above a finite value $\sqrt{s} \gtrsim \sqrt{s_{OPE}} \sim 2$ GeV. The uncertainty in the resulting relations are expected to be of the order $M_R^{EFT}/M_R^{negl.}$, where M_R^{EFT} are the masses of the resonances included in the EFT and $M_R^{negl.}$ the ones from the higher mass multiplets that had not been considered.

Therefore we will assume the Minimal Hadronic Approximation [55] (MHA). We will truncate the infinite pile of resonances but taking at least the minimum number of multiplets needed to fulfill the QCD short distance conditions. For the amplitudes studied here I will work with just the first multiplet of vector, scalar, axial-vector and pseudo-scalar resonances. A second multiplet will be only considered in order to estimate possible variations to the first multiplet parameters.

5.3 VFF in χPT

In χPT we have now an EFT expressed in terms of mesons. To solve the question about how to relate these fields with the quark currents one has to use the auxiliary fields v^μ, a^μ, s and p introduced in the QCD and χPT lagrangians. The essential assumption is that the QCD generating functional $W[v^\mu, a^\mu, s, p]^{QCD}$ is completely equivalent to the EFT one, $W[v^\mu, a^\mu, s, p]^{EFT}$.

To obtain a Green Function $\langle ...\bar{q}(x)\Gamma q(x)... \rangle$ with one bilinear quark current one has to functionally derive the QCD generating functional with respect to the corresponding auxiliary field. For instance, the vector current would be given by:

$$\langle ...\bar{q}_i(x)\gamma_\mu q_j(x)... \rangle = \frac{\delta}{\delta v_{ij}^\mu(x)}...W^{QCD} = \langle ...\frac{\delta S^{QCD}}{\delta v_{ij}^\mu(x)}... \rangle, \qquad (5.8)$$

where v_{ij}^μ is the (i,j) element of the $n_f \times n_f$ flavour matrix v^μ.

To get the current expressed in terms of hadrons one repeats the same procedure but over the effective action:

$$\langle ...\bar{q}_i(x)\gamma_\mu q_j(x)... \rangle = \frac{\delta}{\delta v_{ij}^\mu(x)}...W^{EFT} = \langle ...\frac{\delta S^{EFT}}{\delta v_{ij}^\mu(x)}... \rangle, \qquad (5.9)$$

where now the Green Function is given in terms of mesons, which can be contracted directly with the corresponding outgoing hadronic fields. This derivation does not depend on what EFT we are considering if it is equivalent to the QCD action, so it will be employed as well in the RχT calculation.

By similar procedures one can also compute the EFT picture for more complicated Green Functions containing a higher number of quark currents.

The χPT calculation has yielded precise descriptions for the processes among pNGB at low energies ($\sqrt{q^2} \lesssim 400$ MeV). The pion VFF up to $\mathcal{O}(p^4)$ in $SU(3)\,\chi$PT gives a good description of the experimental data within that range [40, 9]:

$$\mathcal{F}^{(2+4)}_{\chi PT}(q^2) \;=\; 1 \;+\; \frac{2L^r_9(\mu)}{F^2}q^2 \;-\; \frac{2q^2}{F^2}\left[\, B^{r,(\pi)}_{22} \;+\; \frac{1}{2}B^{r,(K)}_{22}\right], \qquad (5.10)$$

with the finite part of the Feynman integral

$$B^{r,(P)}_{22}(q^2) \;=\; \frac{1}{192\pi^2}\left[\frac{1}{3}+\ln\left(\frac{m_P^2}{\mu^2}\right)\right] - \frac{\sigma_P^2}{12}\overline{J}_{PP}(q^2) \;=$$

$$\qquad\qquad (5.11)$$

$$\;=\; \frac{1}{192\pi^2}\left[\ln\left(\frac{m_P^2}{\mu^2}\right) \;+\; \frac{8m_P^2}{q^2} \;-\; \frac{5}{3} \;+\; \sigma_P^3\ln\left(\frac{\sigma_P+1}{\sigma_P-1}\right)\right] \;,$$

with the phase-space factor $\sigma_P \equiv \sqrt{1-4m_P^2/q^2}$. The finite function $\overline{J}_{PP}(q^2) = \frac{1}{16\pi^2}\left(2-\sigma_P\ln\left(\frac{\sigma_P+1}{\sigma_P-1}\right)\right)$ is the scalar two-propagator Feynman integral $B_0(q^2; m_P^2, m_P^2)$ subtracted by $B_0(0; ,_P^2, m_P^2)$. Their relations with the divergent Feynman integrals can be found in Appendix A. The contribution from the one loop diagrams are given by this function and $F = 92.4$ MeV is the pion decay constant at LO in the chiral counting. The scale dependent parameter $L^r_9(\mu)$ is the coupling from the $\mathcal{O}(p^4)$ χPT lagrangian $\mathcal{L}^4_\chi$ renormalized in the $\overline{MS}-1$ scheme.

This coupling can be obtained through the measurement of the VFF at low energies. Expanding it in powers of q^2 one gets the pion electromagnetic charge radius, $\mathcal{F}(q^2) = 1 + \frac{1}{6}\langle r^2\rangle^\pi_V\,q^2 + \mathcal{O}(q^4)$. Its relation with the effective coupling is $L^r_9(\mu) = \frac{1}{3}F^2\langle r^2\rangle^\pi_V + \frac{1}{48\pi^2}\left(\ln\frac{m_\pi^2}{\mu^2}+\frac{1}{2}\ln\frac{m_K^2}{\mu^2}\right) + \frac{1}{32\pi^2}$. The experimental charge radius is $\langle r^2\rangle^\pi_V = (0.439\pm0.008)$ fm^2, which provides $L^r_9(M_\rho) = (6.9\pm0.7)10^{-3}$ [9].

Actually the importance of the strange flavour is not very high at low energies and sometimes the $SU(2)$ calculation is good enough [8]:

$$\mathcal{F}^{(2+4)}_{\chi PT}(q^2) \;=\; 1 + \frac{q^2}{96\pi^2 F^2}(\bar{\ell}_6 - \frac{1}{3}) + \frac{q^2\sigma_\pi^2}{6F^2}\overline{J}_{PP}(q^2) \;=$$

$$\qquad\qquad (5.12)$$

$$\;=\; 1 - \frac{\ell^r_6(\mu)}{F^2}\,q^2 \;-\; \frac{2q^2}{F^2}B^{r,(\pi)}_{22}(q^2)\,.$$

The parameter $\bar{\ell}_6$ is a scale independent combination of the renormalized coupling and the logarithm $\ln\frac{m_\pi^2}{\mu^2}$ which is given in Appendix B. The two flavour ($m_u, m_d \ll m_s$) and three flavour results are easy to relate through $\ell^r_6(\mu) = -2L^r_9(\mu) + \frac{1}{192\pi^2}(\ln\frac{m_K^2}{\mu^2}+1)$.

Moreover, may times the massless calculation is also very useful and carries the bulk of the form factor. The $n_f = 2$ VFF in this limit becomes

$$\mathcal{F}^{(2+4)}_{\chi PT}(q^2) \;=\; 1 \;-\; \frac{\ell^r_6(\mu)}{F^2}\,q^2 \;+\; \frac{q^2}{96\pi^2 F^2}\left[\frac{5}{3} - \ln\left(-\frac{q^2}{\mu^2}\right)\right]. \qquad (5.13)$$

The result for the $n_f = 3$ theory (in the $m_u = m_d = m_s = 0$ limit) is completely analogous but with $2L_9^r(\mu)$ instead of $(-\ell_6^r(\mu))$.

In order to improve the accuracy and to carry the description on to slightly higher energies ($q^2 \lesssim (500 \text{ MeV})^2$) one has to include the next chiral order, $\mathcal{O}(p^6)$. The contribution to VFF at this order in the $SU(2)$ theory [18, 17] is given by

$$\mathcal{F}_{\chi PT}^{(6)}(s) = \frac{m_\pi^4}{f^4}(P_V + U_V) \quad , \tag{5.14}$$

where the polynomial part of the amplitude is

$$\begin{aligned}
P_V &= x^2 \left[\tfrac{1}{12}k_1 - \tfrac{1}{24}k_2 + \tfrac{1}{24}k_6 + \tfrac{1}{9(4\pi)^2}(\ell_1^r - \tfrac{1}{2}\ell_2^r + \tfrac{1}{2}\ell_6^r - \tfrac{1}{12}H - \tfrac{1}{384} - \tfrac{47}{192(4\pi)^2}) \right. \\
&\quad \left. + r_{V2}^r \right] + x \left[-\tfrac{1}{2}k_1 + \tfrac{1}{4}k_2 - \tfrac{1}{12}k_4 + \tfrac{1}{2}k_6 - \ell_4^r(2\ell_6^r + \tfrac{1}{9(4\pi)^2}) \right. \\
&\quad \left. + \tfrac{23}{36(4\pi)^2}H + \tfrac{5}{576(4\pi)^2} + \tfrac{37}{864(4\pi)^4} + r_{V1}^r \right]
\end{aligned} \tag{5.15}$$

and the dispersive part is

$$\begin{aligned}
U_V &= \overline{B}_0(x) \left[\tfrac{1}{3}\ell_1^r(-x^2 + 4x) + \tfrac{1}{6}\ell_2^r(x^2 - 4x) + \tfrac{1}{3}\ell_4^r(x - 4) + \tfrac{1}{6}\ell_6^r(-x^2 + 4x) \right. \\
&\quad \left. - \tfrac{1}{36}H(x^2 + 8x - 48) + \tfrac{1}{(4\pi)^2}(\tfrac{7}{108}x^2 - \tfrac{97}{108}x + \tfrac{3}{4}) \right] \\
&\quad + \tfrac{1}{9}K_1(x) + \tfrac{1}{9}K_2(x)\left[\tfrac{1}{8}x^2 - x + 4\right] + \tfrac{1}{6}K_3(x)\left[x - \tfrac{1}{3}\right] - \tfrac{5}{3}K_4(x) \quad ,
\end{aligned} \tag{5.16}$$

being $x \equiv \frac{q^2}{m_\pi^2}$ and $H \equiv \frac{1}{(4\pi)^2}\ln\left(\frac{m_\pi^2}{\mu^2}\right)$. The $\mathcal{L}_{4\chi}$ couplings ℓ_i^r are also within the $\bar{\ell}_i$ and k_i definitions as given in Appendix B [17]. The $\mathcal{L}_{6\chi}$ couplings are encoded within the r_{Vi}^r parameters (other works consider alternative combinations of couplings f_i^r). The one-, two-, three- and four-propagator Feynman integrals are given by the functions $\overline{B}_0(x)$ and $K_i(x)$. Their definitions appear in Ref. [17].

5.4 VFF with resonances: LO in $1/N_C$

When introducing the resonance fields the chiral counting becomes inadequate. The introductions of heavy scales M_R spoils the chiral expansion. However at energies below the first multiplet one can recover χPT through an hybrid expansion either in the energy as $q^2/(4\pi F)^2$ and in q^2/M_R^2 (or in the pNGB masses). Thus the heavy propagators $\frac{1}{p^2 - M_R^2}$ turns out to be $-\frac{1}{M_R^2}\left(1 + \frac{p^2}{M_R^2} + ...\right)$ and gives contributions to all chiral orders.

Even at the loop level one recovers the χPT interaction at low energies if the resonance lagrangian is appropriately constructed preserving the chiral symmetry.
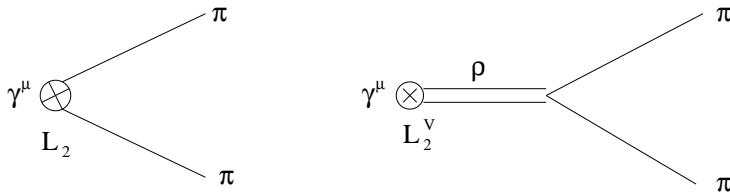
Figure 5.2: Two-pion production in the limit $N_C \to \infty$.

Since the chiral counting is not valid around the mass of the resonances we will consider an alternative counting, the $1/N_C$ counting. As it was told in the former chapters the LO will be provided by the tree level diagrams (which can also contain subleading contributions). The naive counting gives a $1/N_C$ suppression by each mesonic loop. We will see in the next section that this suppression is obeyed in the one loop calculation either formally and numerically.

QCD short distance analysis [23] have proved that at LO in $1/N_C$ the $\mathcal{O}(p^4)$ χPT low energy couplings are given just by the exchange of heavy resonances, when working in the antisymmetric formalism for the vector and axial resonances. This means that in the large N_C limit there are not $\mathcal{O}(p^4)$ pieces with χPT structure when working in a theory with active resonance fields, RχT. This does not mean that these terms do not exist in the lagrangian but that they are subleading in the $1/N_C$ counting. It is very important not to confuse the low energy couplings L_i from χPT with the analogous high energy couplings $\widetilde{L}_i$ from RχT.

The Proca formalism for the vectors and axials gives equivalent results but the low energy couplings are not fully saturated by the exchange of heavy resonances and the local interactions from $\widetilde{\mathcal{L}}_{4\chi}$ are necessary even at LO in $1/N_C$. From now on I will employ the antisymmetric formalism due to the simpler form of the lagrangian.

Focusing our attention on the observable we are now studying one can see that at LO in $1/N_C$ there are just two contributions (Fig. (5.2)): The direct production of the two pions through a vertex from $\mathcal{L}_{2\chi}$; and the production through an intermediate vector meson. Below 1 GeV the main contribution is given by the $\rho(770)$. The inclusion of higher multiplets introduces just small modifications for the region considered here and they will be neglected. Nonetheless, they become essential to describe the observables between 1 and 2 GeV [44].

The tree-level calculation yields:

$$\mathcal{F}(q^2) \;=\; 1 \;+\; \frac{F_V G_V}{F^2} \frac{q^2}{M_V^2 - q^2} \quad . \tag{5.17}$$

The couplings F_V and G_V characterize the strength of the interactions $\gamma \to \rho$ and $\rho \to \pi\pi$ respectively. Some phenomenological determinations on the $\rho(770)$ peak quote them as $F_V \simeq 154$ MeV (from $\Gamma_{exp}(\rho^0 \to e^+e^-)$) and $G_V \simeq 69$ MeV (from $\Gamma_{exp}(\rho \to \pi\pi)$).
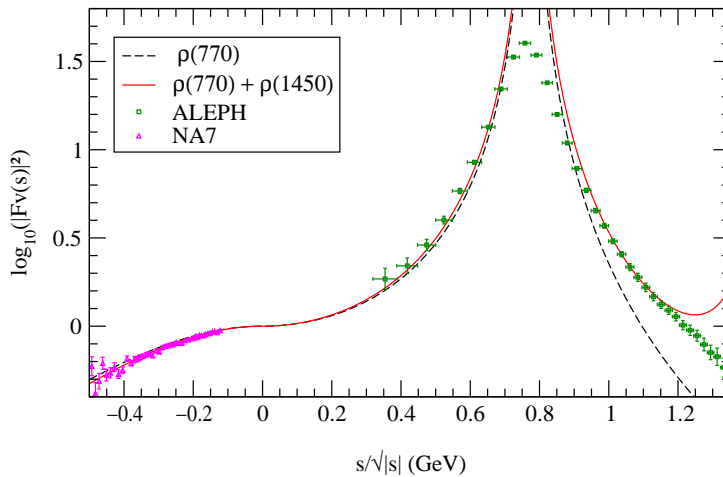
Figure 5.3: VFF at leading order in $1/N_C$ with one and two vector resonances. For the two-resonance case we have adopted the input parameters $M_{V_1} = 775$ MeV, $M_{V_2} = 1450$ MeV, $F_{V_1}G_{V_1}/F^2 = 1.1$ and $F_{V_2}G_{V_2}/F^2 = -0.1$. Data from ALEPH [65] and NA7 [66].

At this point one may argue that the asymptotic behaviour of QCD should be also obeyed at large momentum: the pion VFF at LO in $1/N_C$ should vanish in the limit $q^2 \to \infty$. This gives us the LO in $1/N_C$ constraint:

$$1 - \frac{F_V G_V}{F^2} = 0, \tag{5.18}$$

which together with other constraints on the axial form factor [23] fixes completely the values of the vector couplings at LO: $F_V = F\sqrt{2} = 2G_V$. For $F = 92.4$ MeV this means $F_V = 132$ MeV and $G_V = 66$ MeV, giving an relatively good agreement with the former experimental determinations.

When using this large N_C relations for just one multiplet of resonances Eq. (5.17) becomes the known monopole result for the Minimal Hadronic Approximation (MHA):

$$\mathcal{F}(s)|_{MHA} = \frac{M_V^2}{M_V^2 - s} \quad . \tag{5.19}$$

It is important to remark that this is a theoretical prediction of large N_C (MHA would be more accurate) and QCD short distance constraints. It does not contain any free parameter but the mass of the resonance. In Fig. (5.3) one can see the comparison between this theoretical prediction for $M_V = 770$ MeV and some experimental results. It also includes the $\mathcal{O}(p^4)$ χPT prediction, which agrees perfectly with both experiment and MHA at low energies.

The inclusion of higher multiplets in the EFT is completely straight forward. Assuming that the interaction with the pNGB has the same structure from $\mathcal{L}_{2V}$ but

owning different couplings F_{V_i}, G_{V_i}, then the tree-level VFF is:

$$\mathcal{F}(q^2) = 1 + \sum_i \frac{F_{V_i}G_{V_i}}{F^2}\frac{q^2}{M_{V_i}^2 - q^2}\,. \qquad (5.20)$$

The exigency of the QCD asymptotic behaviour in this extended theory gives a slightly modified relation for the LO in $1/N_C$:

$$1 - \sum_i \frac{F_{V_i}G_{V_i}}{F^2} = 0\,, \qquad (5.21)$$

where the couplings now do not become completely fixed but related among them. In Fig. (5.3) I plot the VFF at LO in $1/N_C$ for RχT with one and two vector multiplets.

5.5 VFF calculation near the resonance mass: Dyson-Schwinger resummation

5.5.1 The $\rho(770)$ width

In the former section the vector meson dominance expression (VMD) in Eq. (5.19) was obtained. As it can be observed in Fig. (5.3), it provides a good description of the VFF to higher energies than those reached by χPT, either at order $\mathcal{O}(p^4)$ or $\mathcal{O}(p^6)$.

Thus, VMD accurately describes the data up to $\sqrt{s} \lesssim 1$ GeV. However the result fails in the resonance peak, since one has the real pole $s = M_\rho^2$ in the tree-level vector propagator and the amplitude diverges. This obviously does not happen experimentally, where one observes a resonance with given non-zero width, instead of a real pole. In a recent work [72] it has been suggested the construction of soft-collinear effective field theories in order to describe the decays of a heavy meson (the rho meson) into light particles (the pions). In order to provide a rigorous description one should construct an effective field theory identifying the relevant degrees of freedom for that range of energies (the collinear modes). Eventually the effective couplings could be determined by a matching with the EFT away from the resonance peak. In this work I just make a simplified analysis by resumming the important contributions to resonance pole with the RχT lagrangian introduced in the former chapter.

The difficulties in Eq. (5.19) are given because one has included only the LO contributions in $1/N_C$. If we were able to do an all order calculation our real pole would be modified by a contribution from the self-energy. This would shift the real tree-level pole M_ρ^2 to a complex value in an unphysical Rienman sheet, $s_\rho^{pole} = (M_\rho^{pole} - i\Gamma_\rho^{pole}/2)^2$. Thus, when varying our value of q^2 throughout the real axis the VFF would a peak in the amplitude in the nearest point to the complex pole.

The resonance becomes narrower and more pronounced as the value of the width Γ_ρ^{pole} is smaller and smaller. It is good to notice at this point that the bibliography employs usually two different definitions of the resonance mass. Here it is used even a third one, M_V, which will be the parameter of the lagrangian, renormalization scale dependent, and will be related with the other two scale independent definitions. One of the definitions is the latter, pole mass and width, M_ρ^{pole} and Γ_ρ^{pole}. The other is the Breit-Wigner definition, defined through the point $q^2 = M_{BW}^2$ where the phase-shift of the scattering amplitude in that channel crosses $90°$. In the case of the form factor that we will compute later only the denominator of the VFF, $D(q^2)$, contains imaginary pieces. The Breit-Wigner mass will be given by the value where $D(q^2)$ becomes purely imaginary. In the same way it is often given a Breit-Wigner definition for the width coming from the slope of the scattering phase-shift [29], and which at first order is given also by the value of the denominator at the Breit-Wigner mass: $-iM_{BW}\Gamma_{BW} = D(q^2 = M_{BW}^2)$. All the definitions are equally physical –they provide the same information for the VFF– and they can be related one each other. Actually, at LO in the perturbative parameter of interaction, all choices take the same value, i.e. $M_V \simeq M_\rho^{pole} \simeq M_{BW}$ and $\Gamma_{BW} \simeq \Gamma_\rho^{pole}$. In this work I will also called as off-shell width to that provided by the imaginary part $\text{Im}\{D(q^2)\} = -M_V\Gamma_V(q^2)$ for real q^2.

In Ref. [26] some important information about the denominator $D(q^2)$ was obtained. The ultraviolet divergences from the loops –which are real– go to the real part of $D(q^2)$, what points out a renormalization problem that will be studied in the next chapter. However, one observes from Ref. [26] that the width of the resummed expression denominator gets a finite value.

When performing the resummation I will employ not the chiral counting but the counting in $1/N_C$, which means also a counting in the number of loops. One must also remember that at LO in $1/N_C$ the couplings take the values $F_V = 2G_V = \sqrt{2}F \sim \mathcal{O}(\sqrt{N_C})$.

The VFF is mainly given by the tree-level production of the two pions, either directly through the vertex form $\mathcal{L}_{2\chi}$ or through an intermediate vector meson. In order to build up our resummation one must think first of a way to systematize the construction of the diagrams and of avoiding the double counting. At the same time it is convenient to have present which are the important contributions and which are suppressed. Since this analysis is focused on the width calculation, the important ones will be those with absorptive cuts; the tadpoles will be neglected.

What available intermediate states are there in this channel? The initial vector current selects only those with that quantum numbers. The simplest are those with one intermediate vector mesons and those with two intermediate mesons with total $I = J = 1$. In the analysis of the VFF in the momentum range $s \sim M_\rho^2$ only the two-pNGB cut is considered. Other cuts will be suppressed by $1/N_C$ and phase-space. Thus, I will not consider four-pNGB cuts, two resonances, one resonance and two Goldstones... They only become relevant away from the rho peak.

The self-energy arises at NLO and therefore the width of the resonances is zero.

The standard way to regularize the propagators near their mass shell is through a Dyson-Schwinger summation of self-energies. This procedure allows obtaining the value of the resonance width in the neighbourhood of its mass-shell beyond the leading order. Nonetheless, the $1/N_C$ counting introduces very important modifications that produces variations in the momentum dependence of the off-shell width. The usual Dyson-Schwinger summation sums a series of one particle irreducible blocks (1PI) linked by free propagators. When considering the $1/N_C$ counting the re-scattering through a tree-level resonance propagator is of the same order as a local scattering vertex. Thus, one finds that this local-vertex re-scatterings produces a similar series that modifies the resonance propagator at the same order as the usual self-energy.

This can be computed in many ways, since there are many ways to order and classify the diagrams and to perform the summation. Working out the LO lagrangian form RχT one realizes that the LO scattering vertices can be combined into a simple effective vertex, and similarly with the LO vertices connecting a current and two pions [26, 105]. These calculations performed a re-summation of the main contributions to the propagator, the $\pi\pi$ loop. However when computing the whole calculation one finds also other more complicate diagrams that needs a more general systematic of classification. Let us first analyse the standard way to compute the NLO calculations, in order to realize where the modifications occur.

5.6   One-vertex irreducible sub-diagrams

In a usual QFT calculation, the one-particle irreducible sub-diagrams (1PI) are defined as those that cannot be split just by cutting one internal propagator. This provides a general classification and decomposition of any complex diagrams in terms of 1PI blocks linked by propagators which do not run within a loop.

Nonetheless, there exists a further decomposition of the 1PI blocks which shows that the local interactions may produce a shift into the resonance pole. Some of this 1PI diagrams are composed by two independent blocks joined just by a local vertex. The momentum structure of the linking vertex may be more or less complicated depending on the incoming and outgoing particles and the perturbative order in the counting. However, the locality of this vertices requires that they are analytic functions of these momenta, i.e., they are polynomials and therefore the contribution of each monomial to the loops in one block does not interfere the loops in the other. The general result is given by the summation of the contributions from every monomial of the intermediate vertex. This means that the amplitude is equal to a summation of terms, being each one a product of a Feynman integral from the loops in the first block times another function from the loops in the second block.

This procedure can be repeated for the 1PI diagrams built by three blocks linked by a pair of intermediate local vertices. Again the amplitude can be decomposed in a sum of products of three independent Feynman integrals. In general I will
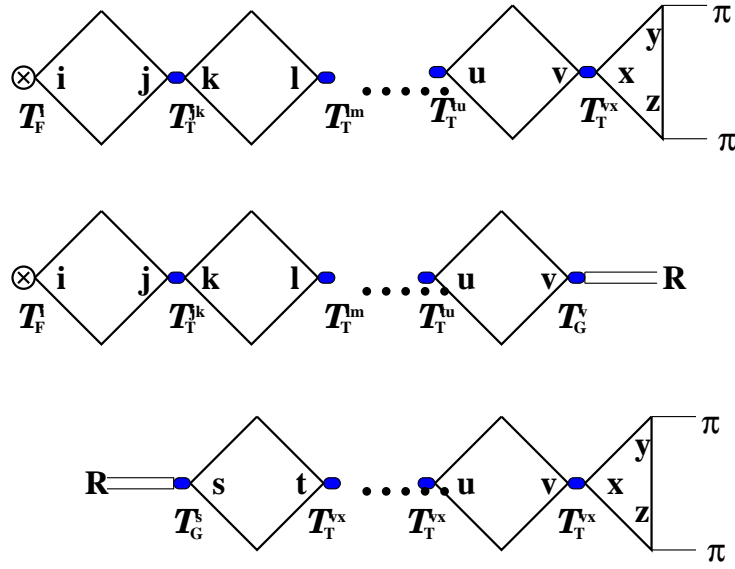
Figure 5.4: Geometrical series in the 1PI Green functions. Their summation to all orders generates a pole structure that modifies the resonance mass and width.

call each of these blocks –linked in a series one each other by just a local vertex– one-vertex irreducible blocks (1VI). Thus, a 1PI amplitude has contribution from diagrams with just one 1VI block, with two 1VI blocks, three and so on.

When analysing some specific channel –defined isospin or angular momentum– the intermediate vertices get simplified. In the simplest cases the part of the vertices contributing in that given channel turns out to be just a monomial, a product of some tensor depending on the incoming momenta times another tensor depending just on the outgoing momenta. Then, a 1PI amplitude $\mathcal{M}(q)$ with a decomposition in two 1VI blocks becomes equal to two independent calculations $\mathcal{M}(q) = S_1(q) \cdot S_2(q)$, where the appropriate Lorentz structures are assumed in the product. The diagrams composed by a larger series of 1VI blocks generate a similar structure of products. It is easy to realize that in these cases the summation of 1VI blocks for a number $N = 1, 2...$ of 1VI blocks produces a result completely analogous to the one in the Dyson-Schwinger summation.

These decompositions depend on many details and turn more and more compli- cated as the order of the calculation increases and the available intermediate 1VI blocks can be more and more complex. At lowest order in $1/N_C$ the 1VI blocks must

contain the lower number of loops. This gives as result that the LO contribution to the 1VI blocks is given by the one loop diagrams with two propagators linking one intermediate vertex and the next one. More complicated structures (crossed channels...) only may occur at two loops.

Therefore one can see that the calculation of the resonance width is a highly non-trivial problem. The 1PI topologies accept a geometrical series resummation already before performing the Dyson-Schwinger resummation of self-energies. It is possible to do this 1VI resummation for each 1PI topology relevant for the VFF: the external current to two pions, the external current two a vector resonance, and the vector resonance to two pions (in addition to the pion and vector self-energies). However, for practical purposes, for the $\pi\pi$ and $K\overline{K}$ absorptive contributions studied in the next section, it will be simpler to perform the 1VI resummation and the vector self-energy resummation at the same time, introducing effective scattering vertices in the fashion developed in Ref. [26].

This work analyses the width at energies much lower than the two-resonance threshold and at first approximation these channels may be neglected. The attention is focused then on the loops of two pNGB. The only intermediate local vertex is then $\pi\pi \to \pi\pi$ from the $\mathcal{L}_{2\chi}$ lagrangian in $SU(2)$. In the three-flavour theory one has also $\pi\pi \to K\overline{K}$, $K\overline{K} \to \pi\pi$ and $K\overline{K} \to K\overline{K}$. Nevertheless, afterwards it is shown how the resummation can be also generalised to 1VI blocks with a bigger number of loops. We will see also how to take into account the intermediate vertices with resonances and their influence below their production threshold.

5.6.1   The effective vertex resummation

At leading order in $1/N_C$, the vector form factor $\mathcal{F}_0^{(P)}(q^2)$ is easily computed through the diagrams shown in Fig. 5.5(a). The label (P) denotes the pair of pseudo-scalars which are produced in the final state, either $\pi^-\pi^0$ or K^-K^0.

The two form factors $\mathcal{F}_0^{(P)}(q^2)$ are put together within the vector

$$\vec{\mathcal{F}}_0(q^2) \equiv \left(\begin{array}{c} \mathcal{F}_0^{(\pi)}(q^2) \\ \mathcal{F}_0^{(K)}(q^2) \end{array} \right) = \left\{ 1 + \sum_i \frac{F_{V_i} G_{V_i}}{F^2} \frac{q^2}{M_{V_i}^2 - q^2} \right\} \left(\begin{array}{c} 1 \\ -\frac{1}{\sqrt{2}} \end{array} \right). \quad (5.22)$$

For the one multiplet situation, the short-distance QCD constraints yield $F_{V_1} = 2\,G_{V_1} = \sqrt{2}\,F$ at the large–N_C limit [23]. However, since we are going to work at higher orders in $1/N_C$, we will leave these couplings free. Their deviations of the experimental values from the large–N_C predictions will be tested afterwards *a posteriori*. We will see that they are small and within the expected order of fluctuation in $1/N_C$.

At energies close to the mass of a resonance we need to know the denominator of the resonance propagator beyond the leading, bare, order in $1/N_C$. What is usually done is a Dyson-Schwinger summation, as for instance in the QED photon polarization. That is, summing diagrams composed by a series of propagator, 1PI
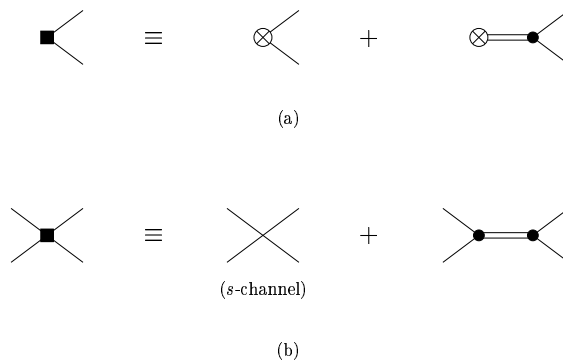
(a)

(b)

Figure 5.5: Effective vertices for the vector current insertion producing two pseudo-scalars (a) and for the two pseudo-scalar scattering (b). The first terms come from $\mathcal{L}_{\chi\mathrm{PT}}^{(2)}$ and the second ones from the interaction via an intermediate resonance due to the $\mathcal{L}_{\mathrm{R}\chi\mathrm{T}}^{V}$ lagrangian.

block, propagator, ..., and so on. This summation regularizes the pole of the bare propagator. It gives a self-energy with its corresponding absorptive part, up to the perturbative order employed for the 1PI block. In RχT, however, at the same order as the resonance-exchange contribution there is also a local interaction from the $\mathcal{L}_{2\chi}$ lagrangian. The Dyson-Schwinger summation must be then slightly modified. One constructs effective current vertices and effective scattering vertices [26], by adding the contribution from intermediate resonance exchanges in the s–channel to the local χPT interaction $\mathcal{L}_{2\chi}$. Both contributions are of the same order in the $1/N_C$ counting. These effective vertices, shown in Fig. 5.5, are independent of the explicit formulation adopted for the spin–1 fields [23, 26]. With the Proca formulation one would have to take into account the local interaction from the $\mathcal{O}(p^4)$ χPT lagrangian as it is described in Ref. [23]. The re-scattering through local vertices is not important on the resonance peak but it turns out to be relevant when separating away from it.

For the moment, we are only interested in the imaginary part of the self-energy. Therefore, we will concentrate ourselves on the summation over diagrams with absorptive cuts. For the range of energies we are interested, the most relevant contributions come from intermediate states with two pseudo-scalars; states with a higher number of particles being suppressed by phase space and $1/N_C$ counting. Thus, we are going to sum diagrams[1] constructed with an initial effective current insertion connected to an effective scattering vertex through a two-pseudoscalar loop. The pair of outgoing pseudo-scalars from the scattering vertex are again connected to another effective scattering vertex through another two-pseudoscalar loop, and so on, as it can be seen in Fig. 5.6.

---

[1]This diagrammatic construction solves the Bethe-Salpeter equation [31] in an iterative way. The effective vertices provide the corresponding "potentials" at LO in $1/N_C$.
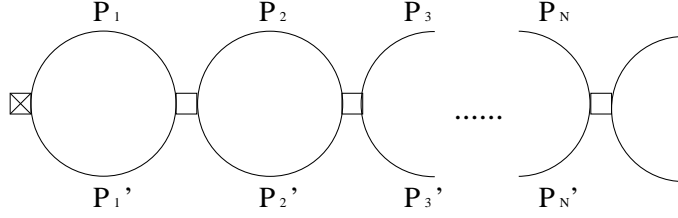
Figure 5.6: Diagrammatic summation at N loops.

The off-shell effective current vertex shows the momentum structure

$$\vec{V}_0^\mu \;=\; \sqrt{2}\,\left[\,\vec{\mathcal{F}}_0\,P_T^{\mu\nu}\;+\;\vec{\mathcal{F}}'_0\,P_L^{\mu\nu}\,\right]\,(p_1 - p_2)^\nu\,, \tag{5.23}$$

with $P_T^{\mu\nu} = g^{\mu\nu} - \frac{q^\mu q^\nu}{q^2}$ and $P_L^{\mu\nu} = \frac{q^\mu q^\nu}{q^2}$ the usual transverse and longitudinal Lorentz projectors. The vector $\vec{\mathcal{F}}_0$ is the on-shell VFF at tree-level from Eq. (5.22). In the isospin limit, the momentum structure with the second term $\vec{\mathcal{F}}'_0$ vanishes when the outgoing pseudo-scalars are both on-shell. Notice that this off-shell function depends on the adopted parameterization of the fields, but the final on-shell amplitude does not depend on it. They have the values:

$$\vec{\mathcal{F}}_0 \;=\; \left\{1 + \sum_i \frac{F_{V_i}G_{V_i}}{F^2}\frac{q^2}{M_{V_i}^2 - q^2}\right\}\left(\begin{array}{c} 1 \\ -\frac{1}{\sqrt{2}} \end{array}\right)\,,$$

$$\vec{\mathcal{F}}'_0 \;=\; -\,\sum_i \frac{F_{V_i}G_{V_i}}{F^2}\frac{q^2}{M_{V_i}^2 - q^2}\left(\begin{array}{c} 1 \\ -\frac{1}{\sqrt{2}} \end{array}\right)\,. \tag{5.24}$$

When the current insertion $\vec{V}_0^\mu$ is connected to a successive number of loops and effective scattering vertices one gets the amplitude $\vec{V}_N^\mu = \sqrt{2}\left[\vec{\mathcal{F}}_N P_T^{\mu\nu} + \vec{\mathcal{F}}'_N P_L^{\mu\nu}\right](p_1 - p_2)^\nu$, where N points out the number of intermediate loops in the diagrammatic chain shown in Fig. 5.6. In can be proved iteratively that the momentum structure remains. Inductively, one has the linear recurrence from N to $N+1$ loops, $\mathcal{F}_{N+1}^{(i)} = \sum_j \mathcal{M}^{ij}\,\mathcal{F}_N^{(j)}$, where the label $i = 1$ stands for $\pi\pi$ and $i = 2$ for $K\overline{K}$. This feature can be expressed in the matrix form

$$\vec{\mathcal{F}}_{N+1} \;=\; \mathcal{M}\,\vec{\mathcal{F}}_N \;=\; \mathcal{M}^2\,\vec{\mathcal{F}}_{N-1} \;=\; \cdots \;=\; \mathcal{M}^{N+1}\,\vec{\mathcal{F}}_0\,, \tag{5.25}$$

with $\vec{\mathcal{F}}_N$ the on-shell vector form factor at N loops. The 2×2 recurrence matrix takes the form

$$\mathcal{M} \;=\; -\,\Sigma^{-1}\,T_{\mathrm{LO}}^s\,\Sigma^{-1}\,(192\,\pi\,B_{22})\,, \tag{5.26}$$

with the diagonal matrix $\Sigma = \mathrm{diag}\,(\sigma_\pi,\ \sigma_K)$, being $\sigma_P = \sqrt{1 - 4\,m_P^2/q^2}$. The matrix

$$T_{\mathrm{LO}}^s \;=\; \frac{q^2}{96\pi F^2}\left\{1 + \sum_i \frac{2\,G_{V_i}^2}{F^2}\,\frac{q^2}{M_{V_1}^2 - q^2}\right\}\,\Sigma\begin{pmatrix} 1 & -\frac{1}{\sqrt{2}} \\ -\frac{1}{\sqrt{2}} & \frac{1}{2} \end{pmatrix}\Sigma\,, \quad (5.27)$$

is the s–channel partial-wave scattering amplitude with $I = J = 1$, at LO in $1/N_C$ [Fig. 5.5(b)]. The diagrams with resonances in the crossed channels produce a tiny contribution in this range of energies and will be analysed later. In Eq. (5.26) there is as well the diagonal matrix $B_{22} = \mathrm{diag}\left(B_{22}^{(\pi)},\ B_{22}^{(K)}\right)$, with the two-propagator Feynman integral $B_{22}^{(P)}$ given in Appendix A.

Since the on-shell VFF at $N + 1$ loops, $\vec{\mathcal{F}}_{N+1}$, do not depend on the off-shell form factor at N loops, $\vec{\mathcal{F}}_N'$, then the initial off-shell parameter $\vec{\mathcal{F}}_0'$ do not influence the on-shell VFF. Therefore it will not be considered any longer.

Summing the result in Eq. (5.25) for any number of loops, one gets a geometrical series which can be resummed:

$$\vec{\mathcal{F}} \;=\; \sum_{N=0}^{\infty}\vec{\mathcal{F}}_N \;=\; \left(\sum_{N=0}^{\infty}\mathcal{M}^N\right)\vec{\mathcal{F}}_0 \;=\; (1 - \mathcal{M})^{-1}\,\vec{\mathcal{F}}_0 \;=\; \frac{1}{1 - \mathrm{Tr}(\mathcal{M})}\,\vec{\mathcal{F}}_0\,. \quad (5.28)$$

The last identity is not trivial and stems from some properties of the matrices $\Sigma^{-1}T_{LO}^s\Sigma^{-1}$ and $\vec{\mathcal{F}}_0$. The $\Sigma^{-1}T_{\mathrm{LO}}^s\Sigma^{-1}$ matrix is proportional to a dimension-one projector and $\vec{\mathcal{F}}_0$ is precisely an eigenvector of this projector. Thus, $\mathcal{M}^N$ acting over $\vec{\mathcal{F}}_0$ reproduces again the vector $\vec{\mathcal{F}}_0$ times a number. The mathematical details can be found in Appendix B:

$$\mathcal{M}\vec{\mathcal{F}}_0 \;=\; \mathrm{Tr}(\mathcal{M})\,\vec{\mathcal{F}}_0 \;=\; -\frac{2q^2}{F^2}\left[1 + \sum_i \frac{2G_{V_i}^2}{F^2}\frac{q^2}{M_{V_i}^2 - q^2}\right]\left\{B_{22}^{(\pi)} + \frac{1}{2}B_{22}^{(K)}\right\}\vec{\mathcal{F}}_0\,, \quad (5.29)$$

where $\mathrm{Tr}(...)$ stands for the trace of the 2×2 matrix.

The interest of this resummation is to compute the LO contributions to the width. Therefore, only the absorptive diagrams have been included and only the imaginary part is under control. The factor $\frac{1}{1-\mathrm{Tr}(\mathcal{M})}$ from the all order summation, together with the tree-level pole in $\vec{\mathcal{F}}_0$, generates a complex denominator. In the single resonance case it takes the usual self-energy structure $M_{V_1}^2 - q^2 - \xi(q^2)$. This denominator contains a non-controlled real part plus a finite imaginary term, given by

$$\mathrm{Im}\,\xi(q^2) \;=\; \mathrm{Im}\,\xi_\pi(q^2) + \mathrm{Im}\,\xi_K(q^2)\,, \quad (5.30)$$

coming from the two-pseudoscalar loop summation. This provides separated contributions from the $\pi\pi$ and the $K\overline{K}$ channels. The corresponding partial widths are:

$$\mathrm{Im}\,\xi_P(q^2) \;=\; C_P\left(M_{V_1}^2 - q^2 + \frac{2\,G_{V_1}^2}{f^2}\,q^2\right)\frac{q^2\sigma_P^3}{96\,\pi\,f^2}\,\theta(q^2 - 4m_P^2)\,, \quad (5.31)$$

with $C_\pi = 1$ and $C_K = \frac{1}{2}$. When we substitute the coupling at LO in $1/N_C$, $G_{V_1} = F/\sqrt{2}$, these imaginary terms Im $\xi_P(q^2)$ agree with the partial widths $M_\rho \Gamma_\rho^{(P)}(q^2)$ obtained in Refs. [27, 26] from a simplified single-channel analysis. This energy dependence for the width was long ago considered by Gounaris and Sakurai from general arguments [29]. As well, they had exactly the same logarithm in their work as the one which naturally appears in our calculation of the absorptive contribution through the Feynman integral $B_{22}^{(P)}$.

The correlator of two vector currents and the $I = J = 1$ partial-wave scattering amplitude, can be computed in a similar way. For the correlator we begin with a current effective vertex, like for the form factor, and connect it to a N-loop final-state interaction, which ends into another current effective vertex. For the scattering amplitude we start from a scattering effective vertex and go on connecting loops and scattering vertices in the same way. A similar re-scattering effect appears in the three quantities. The resulting (s–channel) $I = J = 1$ scattering amplitude takes the form:

$$T \;=\; \Sigma \left(\sum_{N=0}^{\infty} \mathcal{M}^N \right) \Sigma^{-1}\, T_{\text{LO}}^s \;=\; \Sigma\,(1 - \mathcal{M})^{-1}\, \Sigma^{-1}\, T_{\text{LO}}^s \;=\; \frac{1}{1 - \text{Tr}\{\mathcal{M}\}}\; T_{\text{LO}}^s\,. \tag{5.32}$$

The matrix structure $(1 - \mathcal{M})^{-1}$ only depends on the scattering effective vertex and on the two-intermediate particle loop. As these are identical for the three quantities (VFF, correlator and scattering), the final-state interaction dresses the bare resonance pole in a universal way, providing the same complex pole for all processes.

5.6.2   Low-Energy Matching Conditions

All the former calculations must reproduce the QCD low-energy behaviour provided by the χPT framework. This allows to fix the polynomial ambiguities at a given order in the chiral expansion. The procedure to handle this ambiguities will be to consider the divergences λ_∞ from the infinite Feynman integrals B_{22} as a constant parameter which needs to be fixed. This is really what one does when renormalizing a process in QFT, although in a more careful and rigorous way. The aim of this subsection will be to provide this "unknown constant" with the proper value in order to reproduce adequately the low energy dynamics of QCD, which is χPT.

Therefore, the resummed VFF from Eq. (5.28) is expanded in powers of the momenta up to order $\mathcal{O}(E^4)$ (notice that for the form factor this means two powers less of the momenta, i.e. $\mathcal{O}(q^2)$, since one power is in the external current and other in the Lorentz structure):

$$\mathcal{F} \;=\; 1 \;+\; \sum_i \frac{F_{V_i} G_{V_i}}{F^2} \frac{q^2}{M_{V_i}^2} \;-\; \frac{2q^2}{F^2} \left\{ B_{22}^{(\pi)} + \frac{1}{2} B_{22}^{(K)} \right\} \;+\; \mathcal{O}(q^4)\,. \tag{5.33}$$

It is then compared with the standard $\mathcal{O}(E^4)$ result from the χPT calculation. We will take the ordinary $\overline{MS} - 1$ renormalization scheme [40]:

$$\mathcal{F} = 1 + \frac{2L_9^r(\mu)q^2}{F^2} - \frac{2q^2}{F^2}\left\{B_{22}^{(\pi)}(\mu)_{\overline{MS}-1} + \frac{1}{2}B_{22}^{(K)}(\mu)_{\overline{MS}-1}\right\} + \mathcal{O}(q^4)\,, \quad (5.34)$$

where the divergence λ_∞ has been subtracted in $B_{22}^{(P)}(\mu)_{\overline{MS}-1}$, which now depends in the renormalization scale μ. However, it is exactly canceled out with the μ–dependence in the low energy coupling $L_9^r(\mu)$.

At leading order in $1/N_C$, we have the well-known saturation [19, 21]:

$$L_9\big|_{N_C\to\infty} = \sum_i \frac{F_{V_i}G_{V_i}}{2\,M_{V_i}^2}\,, \quad (5.35)$$

with F_{V_i}, G_{V_i} and M_{V_i} the LO parameters in the RχT lagrangian. Therefore the full renormalized constant contains a fixed LO contribution plus an unknown term NLO in $1/NC$:

$$L_9^r(\mu) = L_9\big|_{N_C\to\infty} + \Delta L_9(\mu) = \sum_i \frac{F_{V_i}G_{V_i}}{2\,M_{V_i}^2} + \Delta L_9(\mu)\,, \quad (5.36)$$

where the whole μ dependence of $L_9^r(\mu)$ is in $\Delta L_9(\mu)$.

Through this relation one may match both form factors –Eq. (5.33) and Eq. (5.34)– and determine the finite values which the Feynman integrals $B_{22}^{(P)}$ must take. Hence this Feynman integrals become finite and are denoted as $B_{22}^{r,(P)}$ and, up to the chiral order of the matching, they are equal to [27, 26, 63]

$$B_{22}^{r,(P)} = B_{22}^{(P)}(\mu)_{\overline{MS}-1} - \frac{2}{3}\Delta L_9(\mu) =$$

$$= \frac{1}{192\pi^2}\left[\sigma_P^3\,\ln\left(\frac{\sigma_P+1}{\sigma_P-1}\right) + \ln\left(\frac{m_P^2}{\mu^2}\right) - \frac{5}{3} + \frac{8\,m_P^2}{q^2}\right] - \frac{2}{3}\Delta L_9(\mu)\,,$$
$$(5.37)$$

The renormalization scale dependence of the $\mathcal{O}(E^4)$ χPT coupling $L_9^r(\mu)$ –provided by $\Delta L_9(\mu)$– cancels out with the explicit logarithm $\ln\left(m_P^2/\mu^2\right)$ in the Feynman integral. Therefore $B_{22}^r[\Delta L_9(\mu),\mu]$ depends on $\Delta L_9(\mu)$ but it is really a scale independent quantity.

The resulting vector form factor from (5.28) takes then the form

$$\vec{\mathcal{F}} = \frac{1 + \sum_i \frac{F_{V_i}G_{V_i}}{F^2}\frac{q^2}{M_{V_i}^2 - q^2}}{1 + \left(1 + \sum_i \frac{2G_{V_i}^2}{F^2}\frac{q^2}{M_{V_i}^2 - q^2}\right)\frac{2q^2}{F^2}\left[B_{22}^{r,(\pi)} + \frac{1}{2}B_{22}^{r,(K)}\right]}\begin{pmatrix} 1 \\ -\frac{1}{\sqrt{2}} \end{pmatrix}.$$
$$(5.38)$$

With the information obtained from the VFF we obtain as well the (s–channel) $I = J = 1$ partial-wave scattering amplitude,

$$
T \;=\; \frac{\dfrac{q^2}{96\pi f^2}\left(1 + \sum_i \dfrac{2G_{V_i}^2}{F^2}\dfrac{q^2}{M_{V_i}^2 - q^2}\right)}{1 + \left(1 + \sum_i \dfrac{2G_{V_i}^2}{F^2}\dfrac{q^2}{M_{V_i}^2 - q^2}\right)\dfrac{2q^2}{F^2}\left[B_{22}^{r,(\pi)} + \dfrac{1}{2}B_{22}^{r,(K)}\right]} \left(\begin{array}{cc} \sigma_\pi^2 & -\dfrac{\sigma_\pi\sigma_K}{\sqrt{2}} \\[2ex] -\dfrac{\sigma_\pi\sigma_K}{\sqrt{2}} & \dfrac{\sigma_K^2}{2} \end{array}\right),
$$

$$
(5.39)
$$

with $B_{22}^{r,(P)}$ being the same as in the VFF due to the optical theorem.

5.6.3   Scale Running

When the low-energy matching was performed, the term $\Delta L_9(\mu)$ was left as a free parameter. It appeared as an extra constant in $B_{22}^{r,(P)}$. This also pointed out an ambiguity in the election of the scale and in the renormalization scheme, usually $\overline{MS} - 1$ but not the unique one.

For simplicity we will analyze this feature in the single resonance case and with the leading values in $1/N_C$ of the couplings, $F_{V_1} = \sqrt{2}F = 2G_{V_1}$.

In this situation the VFF becomes

$$
\vec{\mathcal{F}} = \frac{M_{V_1}^2}{M_{V_1}^2 - q^2 + \dfrac{2M_{V_1}^2 q^2}{f^2}\left(B_{22}^{r,(\pi)} + \dfrac{1}{2}B_{22}^{r,(K)}\right)} \left(\begin{array}{c} 1 \\[1ex] -\dfrac{1}{\sqrt{2}} \end{array}\right)
$$

$$
= \frac{M_{V_1}^2(\mu)}{M_{V_1}^2(\mu) - q^2 + \dfrac{2M_{V_1}^2(\mu)q^2}{f^2}\left(B_{22}^{r,(\pi)} + \dfrac{1}{2}B_{22}^{r,(K)}\right)\Big|_{\overline{MS}-1} + \mathcal{O}\left(\dfrac{1}{N_C^2}\right)} \left(\begin{array}{c} 1 \\[1ex] -\dfrac{1}{\sqrt{2}} \end{array}\right),
$$

$$
(5.40)
$$

where

$$
M_{V_1}^2(\mu) = M_{V_1}^2\left[1 - \frac{2\,\Delta L_9^r(\mu)}{F^2}M_{V_1}^2\right). \tag{5.41}
$$

The terms order $1/N_C^2$ in the denominator of the second line of Eq. (5.40) must be dropped out since our calculation included just the one loop contribution, i.e. $\mathcal{O}(1/N_C)$. In addition, this second line is easily obtained by multiplying the numerator and denominator of the first line by the factor $\left[1 - \frac{2\,\Delta L_9(\mu)}{F^2}M_{V_1}^2\right]$. After this operation $\Delta L_9(\mu)$ shuffles from $B_{22}^{r,(P)}$ to the combination of parameters given in $M_{V_1}^2(\mu)$. Thus instead of two independent constants, $\Delta L_9(\mu)$ and $M_{V_1}^2$, one only has the combination $M_{V_1}^2(\mu)$ replacing everywhere the parameter $M_{V_1}^2$. The term $\Delta L_9(\mu)$ disappears from $B_{22}^{r,(P)}$, hence leaving in the regularized Feynman integral an explicit dependence on μ.

Moreover, the use of the effective parameter $M_{V_1}^2(\mu)$ in (5.35) allows us to recover the whole value of the χPT running coupling:

$$L_9^r(\mu) \;\; = \;\; L_9^r\big|_{N_C \to \infty} + \Delta L_9^r(\mu) \;\; = \;\; \frac{F_{V_1} G_{V_1}}{2\, M_{V_1}^2(\mu)} \;+\; \mathcal{O}\left(\frac{1}{N_C}\right) \;\; , \qquad (5.42)$$

Therefore the parameter $M_{V_1}^2(\mu)$ captures the right dependence of $L_9^r(\mu)$ on the renormalization scale, up to the considered order in $1/N_C$ of the calculation (this order lays even beyond the order $\mathcal{O}(E^4)$ in χPT). In the phenomenological analysis, we will adopt the usual reference value $\mu = 770$ MeV. Later on, a numerical study at different scales μ will be performed, examining the corresponding values of $L_9^r(\mu)$ derived through (5.42). We will see that the neglected NNLO in $1/N_C$ corrections are indeed tiny and that the results are compatible with χPT for any scale. The prescription of eliminating $\Delta L_9(\mu)$ from $B_{22}^{r,(P)}$ is assumed in the following.

When studying the experimental data, we will observe that the couplings F_{V_1} and G_{V_1} are not exactly the ones provided by the large–N_C limit, but they own small deviations. These parameters suffer also slight variations when more than one resonance is taken into account. In that case, the scale dependence does not go in such a straightforward way to the parameter $M_{V_1}(\mu)$ as we have seen in (5.41), although the relation is still obeyed within a given accuracy. The other parameters are going to suffer very tiny modifications with the scale but, at the precision of our study, they remain like constants.

5.6.4   Phenomenology

We are going to analyze the experimental data for the vector form factor, which is much cleaner than the one from $\pi\pi$ scattering. The vector form factor can be experimentally tested in the photo-production of pseudo-scalars from $e^+ e^-$ annihilation or in τ decay. Although there are many data from $e^+ e^-$ [66, 67], we have decided not to consider them, as we have not taken into account the ω–ρ mixing. We have studied the $\tau \to \nu_\tau 2\pi$ data from ALEPH [65], which provides a covariance matrix to account for experimental error correlations. Similar data from CLEO [68] and OPAL [69] are also available.

The range of validity up to which we will extend our fit is at most $\sqrt{q^2} \le 1.2$ GeV. Beyond this energy, multiparticle channels become important. First we perform a fit to the modulus of the VFF (ALEPH data) with the $\rho(770)$ resonance only. This yields the parameter $M_{V_1}(\mu)$ and the couplings F_{V_1} and G_{V_1}. We choose as matching scale $\mu_0 = 770$ MeV, take the pion decay constant $F = F_\pi = 92.4$ MeV as an input, and fit the region $2\, m_\pi \le \sqrt{s} \le \Lambda_{\max} = 1.2$ GeV. We obtain the values shown in Table 5.1, with a $\chi^2/\mathrm{dof} = 24.8/25$. The corresponding VFF is shown in Fig. 5.7. In order to estimate the systematic errors, we have varied the chiral parameter F in the interval $F = 92.4 \pm 1.0$ MeV and the final point of the fit $\Lambda_{\max}$ between 1.0 and 1.2 GeV. All these effects yield a more conservative result with a broader error.

Chiral Coupling	$\rho(770)$	$\rho(770)\ +\ \rho(1450)$
$M_{V_1}(\mu_0)$	$845.4 \pm 1.1\,^{+0.8}_{-2.8}$ MeV	$839.4 \pm 1.4\,^{+0.9}_{-2.3}$ MeV
$\lvert F_{V_1}/F \rvert$	$1.696 \pm 0.008\,^{+0.010}_{-0.028}$	$1.669 \pm 0.008 \pm 0.017$
$\lvert G_{V_1}/F \rvert$	$0.695 \pm 0.004\,^{+0.011}_{-0.019}$	$0.670 \pm 0.005\,^{+0.012}_{-0.016}$
$F_{V_1} G_{V_1}/F^2$	$1.178 \pm 0.010\,^{+0.009}_{-0.004}$	$1.119 \pm 0.012\,^{+0.008}_{-0.018}$
$L_9^r(\mu_0) = \sum_i \frac{F_{V_i} G_{V_i}}{2 M_{V_i}^2(\mu_0)}$	$(7.04 \pm 0.05\,^{+0.19}_{-0.27}) \cdot 10^{-3}$	$(6.79 \pm 0.09\,^{+0.19}_{-0.27}) \cdot 10^{-3}$
M_{BW}	$776.0 \pm 1.6\,^{+0.3}_{-0.7}$ MeV	$773.9 \pm 2.0\,^{+0.3}_{-1.0}$ MeV
Γ_{BW}	$156.2 \pm 1.6\,^{+0.3}_{-3.0}$ MeV	$150.2 \pm 2.0\,^{+0.7}_{-1.6}$ MeV
M_ρ^{pole}	$764.1 \pm 2.7\,^{+4.0}_{-2.5}$ MeV	$770 \pm 3 \pm 3$ MeV
$\Gamma_\rho^{\text{pole}}$	$148.2 \pm 1.9\,^{+1.7}_{-5.0}$ MeV	$137.3 \pm 2.6 \pm 2.6$ MeV

Table 5.1: Determination of some RχT and χPT couplings, at the scale $\mu_0 = 770$ MeV, from the VFF fit. The parameters F_{V_1}/F and G_{V_1}/F have the same sign since $F_{V_1} G_{V_1}/F^2 > 0$.

The first error in Table 5.1 is the one provided by MINUIT [70], while the second is our estimated systematic uncertainty.

Besides the lagrangian parameter $M_{V_1}(\mu)$, we can determine the more usual "physical" masses: the Breit-Wigner mass M_{BW} and the pole mass M_ρ^{pole}. The energy where the phase-shift $\phi_{\pi\pi} = \frac{\pi}{2}$ defines the Breit-Wigner mass M_{BW} and the corresponding width is given by $1/\Gamma_{BW} = M_{BW} \left.\frac{d\phi_{\pi\pi}}{ds}\right|_{s=M_{BW}^2}$ [29]. The complex pole of the observables in the second Riemann sheet, $s_\rho^{\text{pole}} = (M_\rho^{\text{pole}} - i\,\Gamma_\rho^{\text{pole}}/2)^2$, defines the alternative pole parameters. In Table 5.1 we have written the resulting values for these two different mass and width definitions. In order to derive those numbers, we have taken into account the correlations among the fitted parameters $M_{V_1}(\mu_0)$, F_{V_1} and G_{V_1}. Owing to the off-shell q^2 behaviour of the denominator, the pole mass turns out to be lower than the Breit-Wigner mass, in agreement with former works [71]. The opposite behaviour would have been obtained from a constant Breit-Wigner width parameterization.

In Fig. 5.8 we plot the phase-shift $\phi_{\pi\pi}$. In the low-energy region $\sqrt{s} \lesssim 0.7$ GeV, the experimental data appears to be slightly above the predicted values. The same behaviour can be observed in previous theoretical studies [27, 28, 30, 32, 63]. The experimental errors are probably underestimated in this region, although higher-order chiral corrections could induce small variations to our predictions. Other studies [71] seem to have a better control of the region closer to the $\pi\pi$ threshold
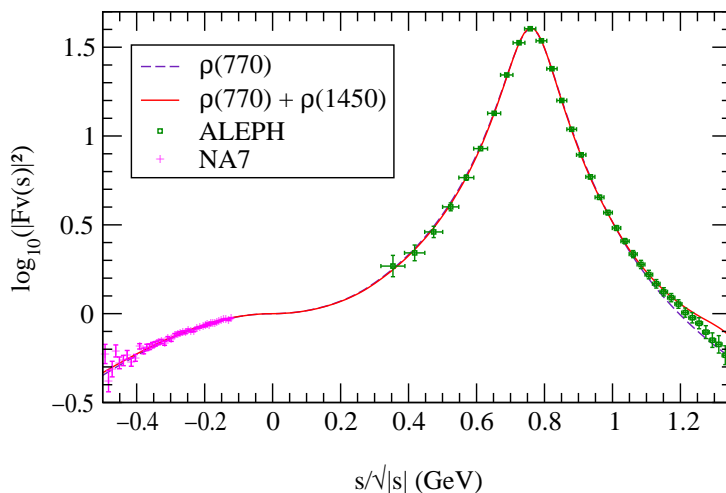
Figure 5.7: VFF fits for $\sqrt{s} < 1.2$ GeV to the $\tau \to \nu_\tau 2\pi$ ALEPH data [65], with one and two ρ resonances. $e^+e^- \to 2\pi$ data points from NA7 [66] are also shown.

and dominated by the χPT constraints. Beyond this region the agreement of our one-resonance analysis with the scattering data is good up to $\sqrt{q^2} \leq 1$ GeV. Above this point the prediction for the scattering amplitude begins to fail.

In order to better study the region around $\sqrt{s} \sim 1$ GeV, we include a second vector multiplet with the $\rho(1450)$. The effect of the tail of the $\rho(1450)$ can modify slightly the distribution in this region, where still the $\rho(770)$ dominates. Nonetheless, we cannot study energies much higher than $\sqrt{s} \sim 1.2$ GeV, since some not well-known strong inelasticities do arise (the experimental phase-shift data does not seem to pass through $3\pi/2$ at the $\rho(1450)$ mass [99]). Clearly, the two-pseudoscalar loops cannot incorporate all the inelasticity needed to describe the $\rho(1450)$ region. Other multiparticle intermediate states may be responsible for this large effect.

We have fitted our theoretical determination of the scattering amplitude with two resonances to the experimental phase-shift in the region 0.7 GeV$\leq \sqrt{s} \leq 1.2$ GeV. The fit is not very sensitive to the $\rho(1450)$ mass, allowing a wide range of values. Nevertheless, it requires that $M_{V_2}(\mu_0) \gtrsim 1550$ MeV. Taking $M_{V_2}(\mu_0) = 1550$ MeV, the fit to the phase-shift gives $M_{V_1}(\mu_0) = 841.8 \pm 0.6$ MeV, $G_{V_1}/F = 0.6631 \pm 0.0027$ and $G_{V_2}/F = 0.373 \pm 0.028$, with $\chi^2/\text{dof} = 18.8/22$. The fitted value of G_{V_2}/F increases for larger masses of the $\rho(1450)$ resonance; the central value grows to 0.57 for $M_{V_2}(\mu_0) = 2000$ MeV. The precision of G_{V_1}/F is improved, as expected, because the phase-shift has a larger sensitivity to this parameter. The differences between the analyses of $\phi_{\pi\pi}$ with one and two resonances are tiny for $\sqrt{s} \lesssim 1$ GeV. Beyond $\sqrt{s} \simeq 1.2$ GeV, the description breaks down because the pathological $\frac{\pi}{2}(2n+1)$ behaviour of the phase-shift in the neighbourhood of the $\rho(1450)$ still remains [see
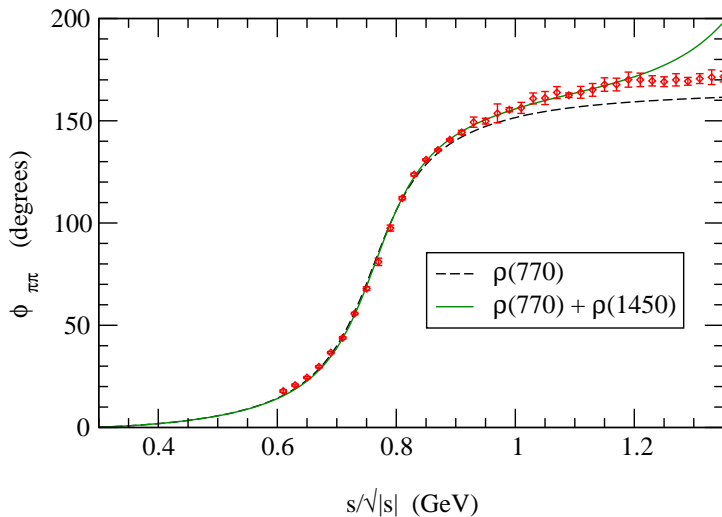
Figure 5.8: Phase-shift $\phi_{\pi\pi}$ of the $\pi\pi$ scattering amplitude. The parameters employed for the one-resonance graph are the same as in Fig. 5.7. The curve with two resonances takes the values from the fit to the scattering amplitude, with the inputs $M_{V_2}(\mu_0) = 1550$ MeV and $F = 92.4$ MeV.

Fig. 5.8].

We have performed next another fit to the VFF ALEPH data, with two vector multiplets and taking $\Lambda_{\max} = 1.2$ GeV. Since in this region the data have very small sensitivity to the $\rho(1450)$ mass and the coupling G_{V_2}, we introduce as an input the value of $M_{V_2}(\mu_0)$ and the corresponding coupling G_{V_2} obtained from the phase-shift fit. The results of this VFF fit, given in Table 5.1, have a $\chi^2/\mathrm{dof}= 14.7/24$. The systematic errors have been estimated varying the pion decay constant in the interval $F = 92.4 \pm 1.0$ MeV and the value of $M_{V_2}(\mu_0)$ in the range[2] from 1550 to 2000 MeV, which implies $G_{V_2}/F = 0.37 \pm 0.03\,{}^{+0.2}_{-0.0}$. In this analysis we have recovered as well the Breit-Wigner and pole masses and widths for the $\rho(770)$ meson. We have not tried to determine the $\rho(1450)$ pole, because it would lie in a region which is not well described. We also give in Table 5.1 the χPT coupling $L_9^r(\mu_0)$ at the matching scale $\mu_0 = 770$ MeV.

The VFF fit is sensitive to the product of couplings $F_{V_2}G_{V_2}/F^2$. One gets,

$$F_{V_2}G_{V_2}/F^2 = 0.007 \pm 0.024\,{}^{+0.000}_{-0.050}\,. \tag{5.43}$$

For the range of G_{V_2}/F values quoted before, this implies $F_{V_2}/F = 0.02 \pm 0.06\,{}^{+0.00}_{-0.08}$.

---

[2]Notice that the one-resonance results indicate that $M_V(\mu_0)$ is around 100 MeV larger than M_{BW} or M^{pole}. The experimental situation of the $\rho(1450)$ is rather unclear and it might be possible that it has an even higher mass or that a strong interference of two vectors, $\rho(1450)$ and $\rho(1700)$, is needed to properly describe the data [82]
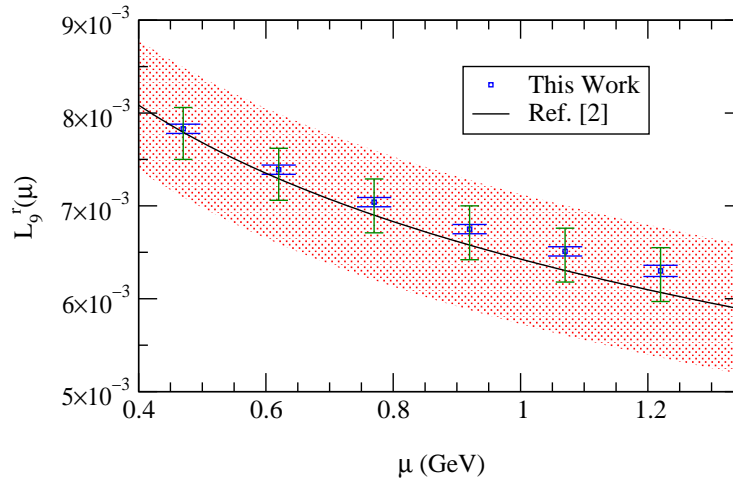
Figure 5.9: Comparison between the usually quoted value of the chiral coupling $L_9^r(\mu)$ [6] (shadowed band) and some determinations from the fit at several matching scales: $L_9^r(\mu) = \sum_i \frac{F_{V_i} G_{V_i}}{2 M_{V_i}^2(\mu)}$. The smaller error intervals are the statistical uncertainties given by MINUIT, the larger ones indicate the total errors including systematic contributions.

Modifications of the $\rho(1450)$ inputs produce sizable variations on the $\rho(770)$ couplings. Thus, a better knowledge of the $\rho(1450)$ is needed to get more accurate values of the $\rho(770)$ parameters from a two-resonance fit. The results are consistent with the more precise determinations from the fit with only one resonance, which we take as our best estimates. Notice, that although the two resonance fit has a slightly better χ^2, it leads to a worse behaviour at higher values of s outside the fitted region ($s > 1.2$ GeV).

5.6.5 Running of $L_9^r(\mu)$

We have seen in Section 4, from a simplified theoretical analysis, that the parameter $M_{V_1}(\mu)$ depends on the χPT renormalization scale adopted in the loop function $B_{22}^{r,(P)}$, in such a way that the physically measurable VFF is scale independent as it should. The dependence of $M_{V_1}(\mu)$ with the scale was given by the equation

$$M_{V_1}^2(\mu_2) - M_{V_1}^2(\mu_1) = \frac{M_{V_1}^2}{64\pi^2 F^2} \ln\left(\frac{\mu_2^2}{\mu_1^2}\right), \qquad (5.44)$$

as $L_9^r(\mu_2) - L_9^r(\mu_1) = \Delta L_9(\mu_2) - \Delta L_9(\mu_1) = -\frac{1}{128\pi^2} \ln\left(\frac{\mu_2^2}{\mu_1^2}\right)$. The theoretical running of $M_{V_1}^2(\mu)$ induces a scale dependence on the predicted value of $L_9^r(\mu)$ in Eq. (5.42). Notice that this relations are true just up to NLO in $1/N_C$. In fact, in the right-hand-side of Eq. (5.44) one finds the factor $M_{V_1}^2/64\pi^2 F^2$ without specifying the scale
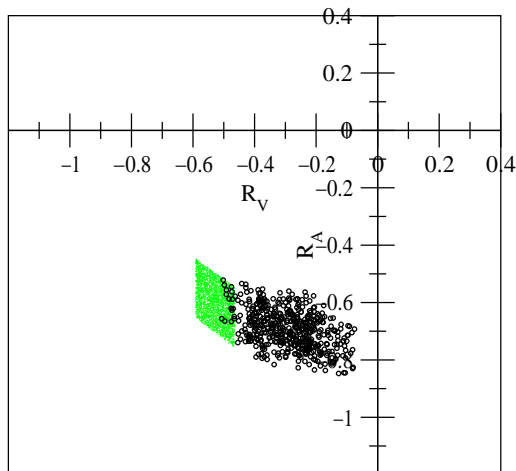
Figure 5.10: Allowed region in the (R_V, R_A) plane. The shaded zone on the left corresponds to the one-resonance study, while the dotted zone results from the analysis with two resonances.

for M_{V_1} since its variations contribute at NNLO in $1/N_C$.

When the phenomenological fit is performed at different values of μ, the parameter $M_{V_1}(\mu)$ increases with μ. The other parameters of the fit remain essentially unaffected, this is, they suffer modifications much smaller than their errors. Varying the scale μ in the wide range between 0.5 GeV and 1.2 GeV, the χ^2 varies less than 2%.

The fits provide a full table of values for the parameters, similar to Tab. (5.1), for every scale μ. From them one may derive the corresponding low energy constant $L_9^r(\mu)$ –through the expression of Eq. (5.42)–. These results are compared in Fig. 5.9 to the usually quoted values from χPT [6]. At the standard reference scale $\mu_0 = 770$ MeV, one obtains from the resummed expression

$$L_9^r(\mu_0) = (7.04 \pm 0.05\,{}^{+0.19}_{-0.27}) \cdot 10^{-3}\,, \tag{5.45}$$

which improves considerably previous determinations [6, 100]. The systematic errors would increase to ${}^{+0.19}_{-0.50}$ if we would have considered the fit with two resonances. The lack of knowledge about the second multiplet parameters introduces an extra uncertainty of the same order as the one we have with only one resonance.

5.6.6   Large–N_C relations

As we work at higher orders in $1/N_C$, our experimental results have next-to-leading deviations from the LO values provided by the two short-distance QCD

relations from the vector and axial form factors at LO in $1/N_C$:

$$r_V \equiv 1 - \sum_i \frac{F_{V_i} G_{V_i}}{F^2} = 0 \quad , \qquad r_A \equiv \sum_i \frac{2F_{V_i} G_{V_i} - F_{V_i}^2}{M_{V_i}^2} = 0 \,. \qquad (5.46)$$

We are going to test now how well they are satisfied. One must be careful. At LO in $1/N_C$ one has in the former relations a set of non-zero terms which cancel out when summing up. However at NLO one expects deviations of order $1/N_C$ in each term which make the relations be not fully fulfilled. However, it is possible to estimate the deviation as roughly $1/N_C$ times each term, with $N_C = 3$ in physical QCD. The largest contribution in the summations are given by the first multiplet parameters. In the first relation the contribution from the $\rho(770)$ is $F_{V_1} G_{V_1}/F^2 \simeq 1$ and the expected deviation is $\Delta r_V^{th} = 1 \times 1/N_C$. For the axial form factor relation The deviation in the axial form factor constraint should be of $\Delta r_A^{th} = 3{\cdot}10^{-2} \times 1/N_C$, because its larger term is $2F_{V_1} G_{V_1}/M_{V_1}^2 \simeq 4L_9 \simeq 3 \cdot 10^{-2}$. In Fig. 5.10, the variables (R_V, R_A) have been plotted employing our phenomenological determination:

$$R_V \equiv \frac{r_V}{\Delta r_V^{th}} \quad , \qquad R_A \equiv \frac{r_A}{\Delta r_A^{th}} \,, \qquad (5.47)$$

where r_V and r_A have been conveniently normalized with the appropriate factors Δr_V^{th} and Δr_A^{th}, such that the expected deviations from zero are $\mathcal{O}(1)$. A scanning of the range of values has been performed in the graph, using the RχT couplings obtained from the VFF fits. One can see in the figure that the separation from the large–N_C QCD relations is indeed of the expected order for both types of fits (with one or two resonances). Thus, the short-distance relations in Eq. (5.46) are well satisfied, within the given accuracy.

A simpler check can be done just by analysing the experimental determination for F_V and G_V with the expected results at LO in $1/N_C$ for the single resonance case ($F_V = 2G_V = F\sqrt{2}$):

$$\frac{F_V}{F_V|_{N_C \to \infty}} - 1 = \frac{F_V}{F\sqrt{2}} - 1 = 0.199 \pm 0.006^{+0.007}_{-0.020} \quad ,$$

$$\frac{G_V}{G_V|_{N_C \to \infty}} - 1 = \frac{G_V}{F/\sqrt{2}} - 1 = -0.017 \pm 0.006^{+0.016}_{-0.027} \,, \qquad (5.48)$$

which, as expected, deviates from the theoretical prediction within a range of the $1/N_C = 33\%$.

5.6.7   Uncertainties from Higher-Order Corrections

There exist many more diagrammatic contributions which have not been included in the former results. I show now that, when the production of multiparticle states is neglected, it is possible to define a generalized summation of Feynman diagrams with two-body topologies. It makes use of a kernel function $\mathcal{K}$, associated with the

two-body scattering amplitude, which incorporates those contributions not included in our effective s–channel vertex of Fig. 5.5(b). The resulting VFF can be formally written in a very compact form, given in Eq. (5.58). Making a $1/N_C$ expansion of the kernel $\mathcal{K}$, one can easily check that our s–channel result in Eq. (5.28) corresponds to the leading-order approximation. The first correction originates from a single resonance exchange in the t–channel, which induces a subleading contribution of $\mathcal{O}(1/N_C)$ to the kernel $\mathcal{K}$. The exchange of n meson fields contributes to the kernel at $\mathcal{O}(1/N_C^n)$.

Summation of general two-pNGB absorptive cuts

The Dyson-Schwinger summation performed before incorporates the dominant s-channel contributions. Moreover, the adopted matching procedure to the low-energy χPT results takes care of tadpoles and local contributions, to the considered order in the momentum expansion. There are, however, many more diagrammatic topologies which have not been considered yet. Neglecting the small corrections at these energies coming from multi-particle intermediate states, it is possible to define a generalized summation of Feynman diagrams with two-body topologies.

As we saw before, the effective vertex in Fig. 5.5(a) for the vector current insertion producing a $P\bar{P}$ pair of pseudo-scalars shows the momentum structure:

$$\vec{V}_0^\mu \;=\; (p_1 - p_2)^\nu \left[\vec{\mathcal{F}}_0(s)\, P_T{}_\nu^\mu \;+\; \vec{\mathcal{F}}'_0(s)\, P_L{}_\nu^\mu \right] \sqrt{2} \,, \qquad (5.49)$$

with $P_T^{\mu\nu} = g^{\mu\nu} - \frac{q^\mu q^\nu}{q^2}$ and $P_L^{\mu\nu} = \frac{q^\mu q^\nu}{q^2}$ the usual transverse and longitudinal Lorentz projectors. In a similar way, the effective vertex in Fig. 5.5(b) describing the s–channel scattering of two pseudo-scalars, when projected on the P-wave ($I = J = 1$), takes the form:

$$\mathcal{T}_0 \;=$$

$$(p_1 - p_2)^\beta \left[\Sigma^{-1} T_{\text{LO}}^s(s)\, \Sigma^{-1}\, P_T{}_\beta^\alpha \;+\; \Sigma^{-1} T'^{\,s}_{\text{LO}}(s)\, \Sigma^{-1}\, P_L{}_\beta^\alpha \right] \left(-\frac{48\pi i}{q^2} \right)\, (k_1 - k_2)_\alpha \,,$$
$$(5.50)$$

with p_1, p_2 (k_1, k_2) the outgoing (incoming) momenta. The matrix T_{LO}^s is the corresponding $I = J = 1$ partial-wave scattering amplitude.

Let us define a general kernel $\mathcal{K}^{(m,n)}(k_1, k_2, p_1, p_2)$ associated with the two-body scattering amplitude from (n)–type pseudo-scalars to (m)–type pseudo-scalars. This kernel, shown in Fig. 5.11(c), contains the identity operator (no scattering) plus all interaction diagrams without intermediate effective vertices (5.50).

Now let us connect the effective vector current insertion $\vec{V}_0^\mu$ to the kernel $\mathcal{K}^{(m,n)}$, as shown in Fig. 5.11(a). The outgoing pseudo-scalars from the kernel are joined
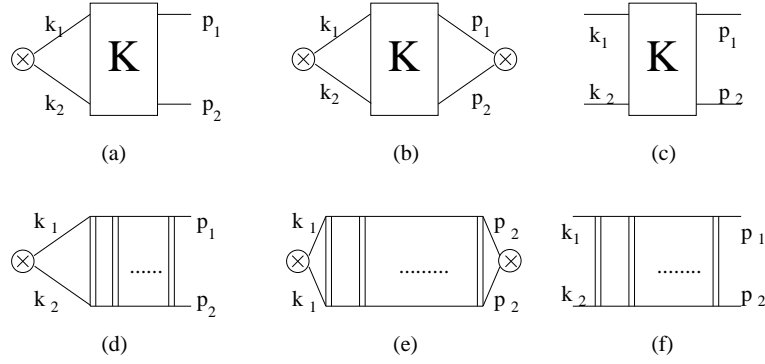
Figure 5.11: Basic pieces of the general summation of two-body topologies. The first row shows the general kernel $\mathcal{K}$ while the second one only includes the contributions from ladder diagrams.

again into an effective scattering vertex (5.50). This generates the dressed structure:

$$
\begin{aligned}
\vec{V}_1^\mu &= (p_1 - p_2)^\beta \left[\Sigma^{-1} T_{\mathrm{L0}}^s(s)\, \Sigma^{-1}\, P_{T\,\beta}^\alpha + \Sigma^{-1} T'^s_{\mathrm{L0}}(s)\, \Sigma^{-1}\, P_{L\,\beta}^\alpha \right] \times \\
&\quad \times \left[\Pi(s)\, P_{T\,\alpha}^\nu + \Pi'(s)\, P_{L\,\alpha}^\nu \right] \left[\vec{\mathcal{F}}_0(s)\, P_{T\,\nu}^\mu + \vec{\mathcal{F}}'_0(s)\, P_{L\,\nu}^\mu \right] \sqrt{2},
\end{aligned}
\tag{5.51}
$$

with the matrices $\Pi(s)$ and $\Pi'(s)$ defined from the kernel integral

$$
\Pi^{(m,n)}(s)\, P_{T\,\alpha}^\nu + \Pi'^{(m,n)}(s)\, P_{L\,\alpha}^\nu = \left(-\frac{48\pi i}{q^2} \right) \times
$$

$$
\times \int \frac{dk'^d}{(2\pi)^d} \frac{dk^d}{(2\pi)^d} \left\{ (k'_1 - k'_2)_\alpha \Delta^{(m)}(k'^2_1) \Delta^{(m)}(k'^2_2) \right.
$$

$$
\left. \mathcal{K}^{(m,n)}(k'_1, k'_2, k_1, k_2) \Delta^{(n)}(k_1^2) \Delta^{(n)}(k_2^2)(k_1 - k_2)^\nu \right\},
\tag{5.52}
$$

where $\Delta^{(m)}(k^2)$ is the propagator of a (m)–type pseudo-scalar. Performing the trivial products of Lorentz projectors, the vector current matrix element with one intermediate kernel and ending into an effective scattering vertex takes the form:

$$
\vec{V}_1^\mu =
$$

$$
(p_1 - p_2)^\nu \left[\Sigma^{-1} T_{\mathrm{LO}}^s(s) \Sigma^{-1} \Pi(s)\, \vec{\mathcal{F}}_0(s) P_{T\,\nu}^\mu + \Sigma^{-1} T'^s_{\mathrm{LO}}(s) \Sigma^{-1} \Pi'(s)\, \vec{\mathcal{F}}'_0(s) P_{L\,\nu}^\mu \right] \sqrt{2}.
\tag{5.53}
$$

When the outgoing pseudo-scalars are both on the mass shell the longitudinal term becomes zero.

We can easily iterate this algebraic procedure and consider a series of N intermediate kernels and effective scattering vertices, attached to the current insertion. The

first kernel is connected directly to $\vec{V}_0^\mu$; then it comes an effective scattering vertex $\mathcal{T}_0$, followed by another kernel, and so on. The outgoing pseudo-scalars are attached to the final effective vertex. The resulting contribution to the VFF is expressed as:

$$\vec{V}_N^\mu \ = \ (p_1 - p_2)^\nu \left[\ (\Sigma^{-1} T_{\mathrm{LO}}^s \Sigma^{-1} \Pi)^N \ \vec{\mathcal{F}}_0 \ P_T{}_\nu^\mu \ + \ (\Sigma^{-1} T_{\mathrm{LO}}'^s \Sigma^{-1} \Pi')^N \ \vec{\mathcal{F}}'_0 \ P_L{}_\nu^\mu \ \right] \sqrt{2} \, . \tag{5.54}$$

Thus, the summation from $N = 0$ to infinity becomes:

$$\vec{V}^\mu =$$

$$(p_1 - p_2)^\nu \left[(1 - \Sigma^{-1} T_{\mathrm{LO}}^s \Sigma^{-1} \Pi)^{-1} \ \vec{\mathcal{F}}_0 P_T{}_\nu^\mu + (1 - \Sigma^{-1} T_{\mathrm{LO}}'^s \Sigma^{-1} \Pi')^{-1} \vec{\mathcal{F}}'_0 P_L{}_\nu^\mu \right] \sqrt{2} \, . \tag{5.55}$$

This sums all diagrams ending in an effective scattering vertex. Finally, we add the diagrams where the last effective vertex is connected to the outgoing pseudo-scalars through the kernel. This extra contribution is given by the form factor $\mathcal{G}^\nu$ of the factorized element $(p_1 - p_2)^\nu$,

$$\mathcal{G}_{(m,n)}^\nu \ = \ (p_1 - p_2)^\beta \left[\mathcal{G}^{(m,n)} P_T{}_\beta^\nu + \mathcal{G}'^{(m,n)} P_L{}_\beta^\nu \right] \ =$$

$$\int \frac{dk^d}{(2\pi)^d} \ \mathcal{K}^{(m,n)}(k_1, k_2, p_1, p_2) \ \Delta^{(n)}(k_1^2) \ \Delta^{(n)}(k_2^2) \ (k_1 - k_2)^\nu \, , \tag{5.56}$$

shown in Fig. 5.11(a), which we have separated into transverse and longitudinal parts. The summation of all types of diagrams gives then,

$$\vec{V}^\mu = (p_1 - p_2)^\nu \left[\mathcal{G} \left(1 - \Sigma^{-1} T_{\mathrm{LO}}^s \Sigma^{-1} \Pi \right)^{-1} \ \vec{\mathcal{F}}_0 \ P_T{}_\nu^\mu \right.$$

$$\left. + \ \mathcal{G}' \left(1 - \Sigma^{-1} T_{\mathrm{LO}}'^s \Sigma^{-1} \Pi' \right)^{-1} \ \vec{\mathcal{F}}'_0 \ P_L{}_\nu^\mu \right] \sqrt{2} \, . \tag{5.57}$$

With the outgoing pseudo-scalars being on-shell, the resulting VFF takes the compact form:

$$\vec{\mathcal{F}} \ = \ \mathcal{G} \cdot \left(1 - \Sigma^{-1} T_{\mathrm{LO}}^s \, \Sigma^{-1} \Pi \right)^{-1} \cdot \vec{\mathcal{F}}_0 \, . \tag{5.58}$$

The simplest kernel is the trivial direct connection of the incoming and outgoing pseudo-scalars $(\mathcal{K} \doteq I)$. In that case, the integral (5.52) reduces to the usual two-propagator loop, $\Pi = -192\pi \, B_{22}$, and $\mathcal{G} = I$. One recovers then the expression (5.28), obtained through a Dyson-Schwinger summation of s-channel scattering vertices. Eq. (5.58) provides a systematic way of improving the result, with the use of more complex kernels. The calculation could be organized with the use of a $1/N_C$ expansion of the kernel $\mathcal{K}$; the trivial identity operator corresponding to the lowest-order approximation in this expansion. The first correction comes from a single resonance-exchange in the t channel, which induces a contribution of $\mathcal{O}(1/N_C)$ to the kernel. The exchange of n meson fields would contribute at $\mathcal{O}(1/N_C^n)$.

Ladder Diagrams

The calculation of higher-order diagrams with an arbitrary number of resonances exchanged in the t channel turns out to be a very complicated problem as each loop is connected to others. However the optical theorem relates the form factor diagrams Fig. 5.11(d) with the scattering amplitude through ladder diagrams, Fig. 5.11(f), in the familiar way [28, 30, 32]:

$$\text{Im } T^t = T^t \cdot \Sigma_\theta \cdot T^{t\,*}, \tag{5.59}$$

$$\text{Im } \mathcal{G}^t = \Sigma^{-1} T^t \Sigma^{-1} \cdot \Sigma_\theta^3 \cdot \mathcal{G}^{t\,*}, \tag{5.60}$$

implying

$$T^t = \left[T_{\text{LO}}^{t\,-1} + \mathcal{O}(1) - i\,\Sigma_\theta \right]^{-1}, \tag{5.61}$$

$$\mathcal{G}^t = \left[1 + \mathcal{O}(1/N_C) - i \left(\Sigma^{-1} T_{\text{LO}}^t \Sigma^{-1} + \mathcal{O}(1/N_C^2) \right) \Sigma_\theta^3 \right]^{-1}, \tag{5.62}$$

where the terms $\mathcal{O}(1)$, $\mathcal{O}(1/N_C)$ and $\mathcal{O}(1/N_C^2)$ correspond to NLO contributions in $1/N_C$, all of them real in the physical region when multi-particle channels are neglected. The matrix T_{LO}^t is the tree-level scattering amplitude through a crossed resonance and the diagonal matrix Σ_θ is just the phase-space matrix but with each σ_P multiplied by a threshold factor $\theta(q^2 - 4m_P^2)$.

The basic behaviour of these quantities is driven by the tree-level term, as the crossed scattering amplitude is tiny at the energies we are considering. It turns to be important at very high energy, where the t–channel becomes the dominant amplitude. Thus, the matching of $\mathcal{G}^t$ to the lowest-order contribution plus the diagrams with only one t–channel resonance exchange is a suitable assumption:

$$\mathcal{G}^t \simeq \left[1 - \mathcal{G}_{1R}^t \right]^{-1}, \tag{5.63}$$

with $\text{Im } \mathcal{G}_{1R}^t = \Sigma^{-1} T_{\text{LO}}^t \Sigma^{-1} \cdot \Sigma_\theta^3$.

The general calculation of those higher-order corrections is a formidable task. We know, however, that in the energy region we are studying the tree-level scattering in the t–channel is much smaller than the one coming from the s–channel, what seems to imply that they contribute as a small perturbation. To estimate the size of those corrections, we have analyzed the leading contribution from t–channel resonance exchange between the final pions. According to the result for the kernel resummation, it induces a multiplicative correction into the VFF:

$$\vec{\mathcal{F}} \approx \left[1 - \mathcal{G}_{1R}^t \right]^{-1} \left[1 + \Sigma^{-1} T_{\text{LO}}^s \Sigma^{-1} (192\pi B_{22}^r) \right]^{-1} \vec{\mathcal{F}}_0, \tag{5.64}$$

where $\mathcal{G}_{1R}^t$ is the contribution from a single t–channel exchange.

The complete calculation of $\mathcal{G}_{1R}^t$ is rather involved, since it makes necessary to address the renormalization of RχT. This is a very interesting issue, which is

analysed in the next chapter, where a full next-to-leading order in $1/N_C$ calculation of the VFF will be performed. By now, we are only interested in the numerical impact on the results presented in the previous sections. For simplicity, we will study $\mathcal{G}^t_{1R}$ in the SU(2) theory; i.e. we neglect the tiny contributions from diagrams with kaons in the intermediate loop or in the final state ($\mathcal{G}^{t\,(\pi,K)}_{1R} = \mathcal{G}^{t\,(K,\pi)}_{1R} = \mathcal{G}^{t\,(K,K)}_{1R} = 0$). Moreover, we will work in the chiral limit ($m_\pi = 0$).

Although there are several Feynman diagrams contributing, we only need to consider the dominant one where the current vertex ($k_1^\mu - k_2^\mu$) produces a $\pi^-(k_1)\pi^0(k_2)$ pair, which is re-scattered through a t–channel resonance. This diagram generates the interesting non-analytic contributions, plus a divergent local correction which should combine with the local contributions from the other diagrams to provide a physical finite result. Since we are interested in the region $\sqrt{s} \ll 2M_V$ (i.e. we work below the two-resonance cut), there are no additional sources of non-analytic terms. The local ambiguity can be fixed to $\mathcal{O}(E^4)$ by matching Eq. (5.64) with the known χPT result. This requires $\mathcal{G}^t_{1R} \sim \mathcal{O}(E^4)$. The exchange of a vector resonance can be easily computed in this way. One gets:

$$
\mathcal{G}^{t\,(\pi,\pi)}_{1V} = \frac{G^2_{V_1} M^2_{V_1}}{(4\pi)^2 f^4} \left\{ \left[\mathrm{Li}_2\left(1 + \frac{q^2}{M^2_{V_1}}\right) - \mathrm{Li}_2(1) \right] \left(2 \frac{M^4_{V_1}}{q^4} + 5 \frac{M^2_{V_1}}{q^2} + 2\right) \right.
$$

$$
\left. + \ln\left(-\frac{q^2}{M^2_{V_1}}\right)\left(2\frac{M^2_{V_1}}{q^2} + 4 + \frac{1}{6}\frac{q^2}{M^2_{V_1}}\right) - 2\frac{M^2_{V_1}}{q^2} - \frac{9}{2} - \frac{35}{36}\frac{q^2}{M^2_{V_1}} \right\} \,.
$$

$$(5.65)$$

Since $\mathcal{G}^{t\,(\pi,\pi)}_{1V} \sim q^4/M^2_V$, we can neglect the exchange of higher-mass vector resonances. However, we will also consider the t–channel exchange of scalar resonances from the lightest multiplet, with a mass $M_S \simeq 1$ GeV [19, 82] and couplings $c_d, c_m \simeq F/2$ [22]. It provides the contribution:

$$
\mathcal{G}^{t\,(\pi,\pi)}_{1S} = \frac{2\,c^2_d\,M^2_S}{(4\pi)^2 f^4} \left\{ \left[\mathrm{Li}_2\left(1 + \frac{q^2}{M^2_S}\right) - \mathrm{Li}_2(1) \right] \left(2\frac{M^4_S}{q^4} + \frac{M^2_S}{q^2}\right) \right.
$$

$$
\left. + \ln\left(-\frac{q^2}{M^2_S}\right)\left(2\frac{M^2_S}{q^2} + \frac{1}{6}\frac{q^2}{M^2_S}\right) - 2\frac{M^2_S}{q^2} - \frac{1}{2} + \frac{1}{36}\frac{q^2}{M^2_S} \right\} \,.
$$

$$(5.66)$$

This result includes contributions from the singlet and the octet scalars.

At energies below and around the $\rho(770)$ peak, these t–channel diagrams give a correction smaller than 5%, which is within the uncertainties of the numerical analyses performed in the previous section. However, above $E \sim 1.2$ GeV the vector contribution becomes larger than 10% and these topologies cannot be neglected any more. This kind of diagrams turn out to be very important at high energies.

We have repeated our previous fits to the VFF ALEPH data, including the correction induced by $\mathcal{G}^{t\,(\pi,\pi)}_{1R} = \mathcal{G}^{t\,(\pi,\pi)}_{1V} + \mathcal{G}^{t\,(\pi,\pi)}_{1S}$. The results of these fits are

compatible with the ones obtained before, showing that our former studies neglecting crossed channels provide a good description within the given precision.

5.6.8   Summary of the Dyson-Schwinger summation

A quantum field theory description of strong interactions at energies around the hadronization scale, $E \sim 1$ GeV, requires appropriate non-perturbative tools. While a fundamental understanding of the confinement region of QCD is still lacking, substantial phenomenological progress can be achieved through effective field theories incorporating the relevant symmetries and dynamical degrees of freedom.

Using an effective chiral lagrangian which includes pseudo-scalars and explicit resonance fields, we have investigated the VFF and related $I = J = 1$ observables in the interesting $E \sim 1$ GeV energy range. The heavy particles make the standard chiral counting in powers of momenta useless, because their masses are of the same order as the chiral symmetry breaking scale. Therefore, we have adopted instead the more convenient large–N_C expansion, which provides a powerful tool to organize the calculation.

At the leading order in $1/N_C$, one gets an excellent description of the VFF, far away from the resonance singularities. A proper understanding of the zone close to the $\rho(770)$ pole, requires the inclusion of next-to-leading contributions providing the non-zero width of the unstable meson. The dressed propagator can be calculated through a Dyson-Schwinger summation of the dominant s–channel re-scattering corrections, constructed from effective Goldstone vertices containing both the local χPT interaction and the resonance-exchange contributions [27, 21, 26, 63].

We have extended the Dyson-Schwinger summation of effective vertices to handle problems with coupled channels in a systematic way, through the recurrence matrix $\mathcal{M}$. The inverse matrix $(1 - \mathcal{M})^{-1}$, generated by final-state interactions, provides the right unitarity structure of the observables [28, 30, 32]. Moreover, with an $SU(3)$–symmetric dynamics (the vertices contain only derivatives and no quark masses), $(1 - \mathcal{M})^{-1}$ acts just like a pure number $[1 - \text{tr}\{\mathcal{M}\}]^{-1}$. Hence, there is no mixing among loops and the total decay width is simply given by a sum of separate contributions from the different channels, which correspond to the partial decay widths. An improved diagrammatic summation of more general two-body topologies has been also given. It includes the smaller t–channel corrections, through the $1/N_C$ expansion of a non-trivial interaction kernel $\mathcal{K}$ associated with the two-pseudoscalar scattering amplitude.

The Feynman loops fully determine the non-analytic contributions, which are dictated by unitarity and chiral symmetry. The local corrections, however, are functions of the theoretically unknown couplings of the effective lagrangian. They incorporate the short-distance dynamics and take care of the regularization and renormalization prescriptions adopted in the calculation. A significant reduction on the number of free parameters is obtained, requiring the different amplitudes to satisfy the appropriate QCD constraints at large momentum transfer [19, 23]. In fact,

a very successful prediction of the most relevant $O(E^4)$ χPT couplings is obtained, under the reasonable assumption that the lightest resonance multiplets give the dominant effects at low energies [21]. We have resolved the local ambiguities of the VFF, imposing the QCD short-distance constraints and performing a low-energy matching with the known $\mathcal{O}(E^4)$ χPT result.

Working within the single-resonance approximation [21], we have obtained a good fit to the ALEPH $\tau \to \nu_\tau 2\pi$ data [65], in the range $2m_\pi \leq \sqrt{q^2} \leq 1.2$ GeV. At the chiral renormalization scale $\mu_0 = 770$ MeV, the fit gives the values shown in Table 5.1 for the main ρ parameters. The corresponding resonance pole $s^{\mathrm{pole}} = (M_\rho^{\mathrm{pole}} - i\,\Gamma_\rho^{\mathrm{pole}}/2)^2$ in the second Riemann sheet is found to be at:

$$M_\rho^{\mathrm{pole}} = 764.1 \pm 2.7\,^{+4.0}_{-2.5}\ \mathrm{MeV}\,, \qquad\qquad \Gamma_\rho^{\mathrm{pole}} = 148.2 \pm 1.9\,^{+1.7}_{-5.0}\ \mathrm{MeV}\,. \qquad (5.67)$$

We have achieved an improved determination of the χPT coupling

$$L_9^r(\mu_0) = (7.04 \pm 0.05\,^{+0.19}_{-0.27}) \cdot 10^{-3}\,, \qquad\qquad\qquad (5.68)$$

at $\mu_0 = 770$ MeV. Performing the phenomenological fit at several scales μ, ones obtains the proper running of $L_9^r(\mu)$ as prescribed by χPT.

To test the convergence of the $1/N_C$ expansion, we have analyzed the deviations between the fitted parameters and the corresponding theoretical large–N_C predictions [23]. The differences are found to be of the expected $\mathcal{O}(1/N_C)$ size, showing that the limit $N_C \to \infty$ provides indeed an excellent description of the local chiral couplings.

We have also investigated the corrections induced by the tail of the $\rho(1450)$ vector resonance at the higher side of our energy range. The effects are sizable, but the sensitivity is not good enough to make a precise determination of its parameters or to disentangle the existence of several higher-mass states. In order to do that, one would need to study higher energies where other multi-particle final states, beyond the two-body modes that we have analyzed, become relevant. Moreover, a better calculation of t–channel contributions would be needed, because they are no longer small above 1.2 GeV.

To summarize, we have performed a detailed analysis of the $\rho(770)$ region, imposing all known theoretical constraints. The main ρ parameters and the χPT coupling $L_9^r(\mu)$ have been determined with rather good precision. More work is needed to extend the results at higher energies. It would also be very interesting to investigate in a similar way the scalar sector, specially the pathological $I = J = 0$ observables. We plan to address these issues in forthcoming works.

Chapter 6

Perturbative calculation of the VFF

6.1 The next-to-leading order VFF

It is generally accepted from the analysis of several strong interacting observables that the LO in $1/N_C$ diagrams provide the main contribution [6, 19, 21, 107]. Nonetheless the LO is not always accurate enough and it is not able to accommodate the experimental data. Moreover, since the $1/N_C$ counting is not an expansion on a parameter of the lagrangian, it is important to estimate the size of the NLO terms. The $1/N_C \simeq 33\%$ variation may be a rough bound and further studies should explore deeper the basis of the $1/N_C$ expansion. In this section I show the NLO calculation for the pion VFF [47, 106]. We will see how the parameters vary due to radiative corrections within the expected $1/N_C$ margin, as expected.

In this chapter I will study the VFF at NLO in $1/N_C$, this is, up to one loop. The detailed contribution from each diagram has been relegated to the appendix C. In the next sections I will show just the summation of all the diagrams for each 1PI topology. First I show the renormalized self-energies up to NLO in $1/N_C$ of the particles involved in the LO diagrams. Afterwards I renormalize the remaining 1PI topologies which are relevant for the VFF up to NLO.

Since we are just interested in the renormalization of the ultraviolet divergences we will consider the massless quark limit. This eliminates the contribution from all the possible pNGB tadpoles. We have made the calculation for both $n_f = 2$ and $n_f = 3$ theories in the massless quark limit. The results are completely equivalent except that for three flavours one has the constant in front of the operator is called $2L_9$ instead of the definition $(-\ell_6)$ in the $n_f = 2$ theory.

The renormalization procedure will be the following: First of all we will compute the renormalized propagators $\Delta_\phi^r(x,y) = \langle T\{\phi^r(x)\phi^r(y)\}\rangle$ of the particles relevant in this calculation. After that we will compute the renormalized 1PI Green functions $\langle ...\phi^r(x)\phi^r(y)\phi^r(z)...\rangle$. Actually we will obtain the amputated Green functions

$\Gamma^r(...u, v, w...)$, defined through

$$\langle\, T\{...\phi^r(x)\phi^r(y)\phi^r(z)...\}\,\rangle \ =$$

$$= \int ...du\, dv\, dw...\Delta^r_\phi(x, u)\Delta^r_\phi(y, v)\Delta^r_\phi(z, w)...\Gamma^r(...u, v, w...)\,. \tag{6.1}$$

The amplitudes can then always be expressed as a set of finite renormalised 1PI topologies $\Gamma^r(...u, v, w...)$ linked by finite renormalised propagators $\Delta^r_\phi(x, y)$ (here I mean the full propagator, not the free one).

For the VFF with physical (renormalized) pions there are only two possible decompositions in 1PI sub-topologies. They are shown in Fig. (6.1). The first possibility is the production of the renormalized pions without any intermediate tree-level propagators. The second possibility is given by the diagram with an intermediate renormalized vector propagator. Therefore the only propagator that we can put at tree-level is the vector one in the second option. Any other internal propagator will be within a loop in the 1PI blocks. Through this decomposition one has a general classification for any possible Feynman diagram.

The matrix element will be then given by the summation of both contributions:

$$\sqrt{2}\,\mathcal{F}(q^2)\,(p_1^\mu - p_2)^\mu \ = \ \sqrt{2}\,\mathcal{F}_\chi(q^2)\,(p_1^\mu - p_2)^\mu \ + \ i\Phi^r(q)^\mu_{\alpha\beta}\cdot\Delta^r_V(q)^{\alpha\beta,\rho\sigma}\cdot i\Gamma^r(p_1, p_2)_{\rho\sigma}\,, \tag{6.2}$$

where $\mathcal{F}_\chi(q^2)$ contains the contributions from the first type of diagrams, $i\Phi^r(q)^\mu_{\alpha\beta}$ is the amputated renormalized Green function *vector current* $\to$ *vector resonance*, $\Delta^r_V(q)^{\alpha\beta,\rho\sigma}$ is the propagator of the renormalized vector field, and $i\Gamma^r(p_1, p_2)_{\rho\sigma}$ is the amputated renormalized Green function $V \to \pi\pi$. Each of these elements is finite and will be computed in the next subsections.

To end with, just remind that in the case of more than one vector multiplet, one may also have topologies as the ones in the second option but with a renormalized propagator from each different multiplet in the intermediate state. This case requires a further study and it is not considered here.

6.1.1   Chiral singlet mesons

In real QCD, with $N_C = 3$, the $U(1)_A$ symmetry generator breaks down at the loop level. Thus the Goldstones turn out to be an $SU(n_f)$ multiplet instead of a $U(n_f)$ one.

However this axial anomaly is proportional to $1/N_C$ and thence in the large N_C limit the symmetry gets restored. This provides a clear explanation of the $U(n_f)$ classification of the resonance multiplets instead of the naively expected $SU(n_f)$ [5]. Moreover, there arises an extra Goldstone boson, singlet under the chiral group, which must be put together with the remaining $n_f^2 - 1$ mesons from the spontaneously chiral symmetry breaking.

When studying phenomenology one should also consider that this Goldstone singlet, η_1, gains mass both from quark masses and a contribution proportional to
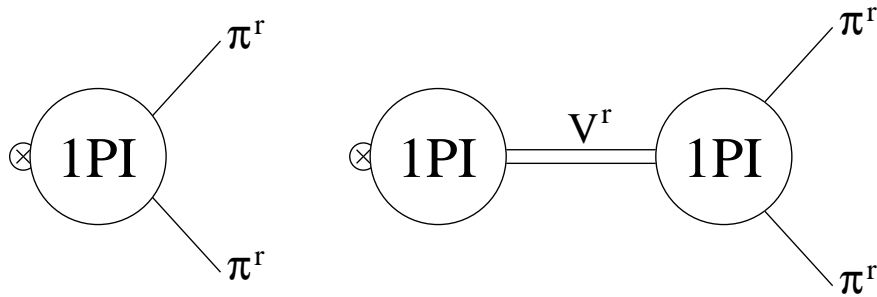
Figure 6.1: General 1PI decomposition in terms of renormalized fields. .

$1/N_C$ from the axial anomaly. Nevertheless in our $n_f = 2$ calculation the part coming from the u and d quarks will be small. At first one should consider also the η_0 mass proportional to $1/N_C$ but since the η's only occur at the one loop level, the mass effects come at the NNLO in our counting. Thus we expect the massless limit to provide a fair initial estimation.

Not considering this singlet produces large asymmetries between the $n_f = 2$ and $n_f = 3$ cases. If the η_0 is not included one obtains large renormalizations for two flavours which become small for three. Once all the mesons, Goldstone bosons and resonances, are classified in $U(n_f)$ multiplets this queer effects disappear. To obtain the renormalizations for $n_f = 3$, in the chiral limit, one just has to multiply by a factor $3/2$.

The meaning of the η meson in $U(2)$ may seem something more obscure than in $U(3)$. In $U(3)$ one actually has two η's with a contribution to their masses proportional to the mass of the strange quark. When going to $U(2)$ m_s is taken to infinity and one combination of the η's decouples whereas the orthogonal combination (with mass just proportional to $1/N_C$ from the axial anomaly) remains as an η singlet in $U(2)$. Thus this "light" degree of freedom gets a mass proportional to $1/N_C$. Since at this level of calculation the η's do not appear in the absorptive cuts of the VFF, the amplitude is analytic on the η mass. Thus, being it already $1/N_C$ and occurring the η just at the one loop level, one can fairly assume that the NNLO corrections from the η mass are small.

6.1.2 Pion self-energy

The first step in any quantum calculation is to make the two-point Green function finite. Here, I will refer to the charged pion though the neutral case is completely equivalent. Since we are working in the chiral limit this renormalization is identical for every pNGB.

The free propagator for the bare field is the usual

$$\Delta_\pi^{(B)}(x,y)\Big|_F = \langle T\{\pi_{(B)}^+(x)\pi_{(B)}^-(y)\}\rangle_F = \int \frac{d^4q}{(2\pi)^4} e^{-iq(x-y)} \Delta_\pi^{(B)}(q^2)\Big|_F , \quad (6.3)$$

with its representation in the momentum space,

$$\Delta_\pi^{(B)}(q^2)\Big|_F = \frac{i}{q^2+i\epsilon} . \quad (6.4)$$

Nevertheless when computing loops this Green function can be decomposed in a set of 1PI sub-diagrams linked by free propagators of the bare particle:

$$\langle T\{\pi_{(B)}^+(x)\pi_{(B)}^-(y)\}\rangle = \langle T\{\pi_{(B)}^+(x)\pi_{(B)}^-(y)\}\rangle_F +$$

$$+ \int d^4u\, d^4v\, \langle T\{\pi_{(B)}^+(x)\pi_{(B)}^-(u)\}\rangle_F\, (-i\Sigma^{(B)}(u,v))\, \langle T\{\pi_{(B)}^+(v)\pi_{(B)}^-(y)\}\rangle_F\ + ...$$
$$(6.5)$$

and thus following the geometric series of the Dyson summation. This can be easily expressed in the momentum space:

$$\Delta_\pi^{(B)}(q^2) = \quad \Delta_\pi^{(B)}(q^2)\Big|_F + \Delta_\pi^{(B)}(q^2)\Big|_F\ (-i\Sigma_\pi^{(B)}(q^2))\ \Delta_\pi^{(B)}(q^2)\Big|_F + ... =$$

$$= \frac{i}{q^2 - \Sigma_\pi^{(B)}(q^2)} .$$
$$(6.6)$$

The propagator of the bare fields is not physical due to the ultraviolet divergence which lies within the bare self-energy $-i\Sigma^{(B)}(x,y)$. To make it finite one has to perform a wave-function renormalization, $\pi_{(B)}^\pm = (1+\delta Z_\pi)^{\frac{1}{2}}\pi_r^\pm$. As we will see below in the explicit calculation, there is an extra divergence which can be removed either through a field redefinition or through extra counterterms in the lagrangian proportional to the EOM. Both procedures are equivalent but none of them physical: At NLO order, the observables are not dependent on this higher order renormalization.

Hence one has the finite propagator of the renormalized fields,

$$\Delta_\pi^r(x,y) = \langle T\{\pi_r^+(x)\pi_r^-(y)\}\rangle = Z_\pi^{-1}\langle T\{\pi_{(B)}^+(x)\pi_{(B)}^-(y)\}\rangle = Z_\pi^{-1}\Delta_\pi^{(B)}(x,y) ,$$
$$(6.7)$$

which again admits the decomposition in 1PI blocks linked by renormalized free propagators in terms of the renormalized mass:

$$\langle T\{\pi^r(x)\pi^r(y)\}\rangle = \langle T\{\pi^r(x)\pi^r(y)\}\rangle_F +$$

$$(6.8)$$

$$+ \int d^4u\, d^4v\, \langle T\{\pi^r(x)\pi^r(u)\}\rangle_F\, (-i\Sigma^r(u,v))\, \langle T\{\pi^r(v)\pi^r(y)\}\rangle_F\ + ...$$

Figure 6.2: Pion self-energy at NLO in $1/N_C$.

and in the momentum space:

$$
\Delta_\pi^r(q^2) = \left.\Delta_\pi^r(q^2)\right|_F + \left.\Delta_\pi^r(q^2)\right|_F \left(-i\Sigma_\pi^r(q^2)\right) \left.\Delta_\pi^r(q^2)\right|_F + \dots =
$$

$$
= \frac{i}{q^2 - \Sigma_\pi^r(q^2)} \, .
$$

(6.9)

And this defines the renormalized self-energy that is computed in this work. The pion self-energy will be renormalized in the on-shell scheme –i.e., the expansion in q^2 of the renormalized self-energy $-i\Sigma_\pi^r(p^2)$ starts at $\mathcal{O}(p^4)$–. Nevertheless, the usual $\overline{MS} - 1$ subtraction scheme will be employed for the remaining Green functions.

The diagrams that contribute to the pion self-energy at this order can be seen in Fig. (6.2). It receives contributions from vector and scalar resonances.

The one loop amplitude in Fig. (6.2) yields

$$
-i\Sigma_\pi^{loop}(p^2) = \; i\,\frac{2G_V^2}{F^4}\,\frac{n_f}{2}\left\{ A_0(M_V^2)\left[-3p^2 + \frac{p^4}{M_V^2}\right] + (p^2 - M_V^2)^2\,\overline{J}(q^2;0,M_V^2)\right\} +
$$

$$
+\,i\,\frac{4c_d^2}{F^2}\,\frac{n_f}{2}\left\{ A_0(M_S^2)\left[p^2 + \frac{p^4}{M_S^2}\right] + (p^2 - M_S^2)^2\,\overline{J}(q^2;0,M_S^2)\right\} =
$$

$$
= \; i\,p^2\,\frac{n_f}{2}\left\{ \frac{2G_V^2}{F^2}\,\frac{M_V^2}{F^2}\left[\frac{3\lambda_\infty}{16\pi^2} + \frac{3}{16\pi^2}\ln\frac{M_V^2}{\mu^2} + \frac{1}{32\pi^2}\right] + \right.
$$

$$
\left. + \frac{4c_d^2}{F^2}\,\frac{M_S^2}{F^2}\left[-\frac{\lambda_\infty}{16\pi^2} - \frac{1}{16\pi^2}\ln\frac{M_S^2}{\mu^2} + \frac{1}{32\pi^2}\right]\right\}
$$

$$
-i\,\frac{p^4}{16\pi^2 F^2}\,\frac{n_f}{2}\left\{ \left(\frac{2G_V^2}{F^2} + \frac{4c_d^2}{F^2}\right)\lambda_\infty + \right.
$$

$$
+ \frac{2\,G_V^2}{F^2}\left[\ln\frac{M_V^2}{\mu^2} + \phi\left(\frac{p^2}{M_V^2}\right)\right]
$$

$$
\left. + \frac{4c_d^2}{F^2}\left[\ln\frac{M_S^2}{\mu^2} + \phi\left(\frac{p^2}{M_S^2}\right)\right]\right\} \, ,
$$

(6.10)

which contains ultraviolet divergences which need to be renormalized. The function $\phi(x)$ which appears in the $\mathcal{O}(p^4)$ term is defined by:

$$-p^4\phi\left(\frac{p^2}{M^2}\right) =$$

$$= (p^2 - M^2)^2\,\overline{J}(p^2; 0, M^2) \;-\; p^2\frac{d}{dp^2}\left[(p^2 - M^2)^2\,\overline{J}(p^2; 0, M^2)\right]_{p^2=0} = \qquad (6.11)$$

$$= (p^2 - M^2)^2\,\overline{J}(p^2; 0, M^2) \;-\; p^2\,\frac{M^2}{32\pi^2}\,,$$

being $\phi(0) = -1/6$.

The counterterms from the LO lagrangian come from the pion kinetic term,

$$\mathcal{L}_\pi^{Kin}[\pi_{(B)}^\pm] \;=\; \partial_\mu\pi_{(B)}^+\partial^\mu\pi_{(B)}^-\,, \qquad (6.12)$$

through the wave-function renormalization $\pi_{(B)} = (1 + \delta Z_\pi)^{\frac{1}{2}}\pi_r$:

$$\mathcal{L}_\pi^{Kin}[\pi_{(B)}^\pm] \;=\; \mathcal{L}_\pi^{Kin}[\pi_r^\pm] \;+\; \delta Z_\pi\,\partial_\mu\pi_r^+\partial^\mu\pi_r^-\,. \qquad (6.13)$$

The wave-function redefinition δZ_π can be tuned to cancel out the $\mathcal{O}(p^2)$ divergences.

However, some extra terms with the $\mathcal{O}(p^4)$ χPT structure are required to remove the $\mathcal{O}(p^4)$ infinities:

$$\widetilde{\mathcal{L}}_{4\chi} \;=\; ... + i\widetilde{\ell}_{11}\langle\,\chi_-\,\mathcal{O}_{2\chi}^{EOM}(u)\,\rangle \;-\; \widetilde{\ell}_{12}\langle\,\mathcal{O}_{2\chi}^{EOM}(u)\,\mathcal{O}_{2\chi}^{EOM}(u)\,\rangle\,, \qquad (6.14)$$

where the hermitian operator $\mathcal{O}_{2\chi}^{EOM}(u)$ vanish when the equations of motion from the $\mathcal{L}_{2\chi}$ lagrangian are applied, as given in Eq. (3.39) and it is hermitian. In the massless case only $\widetilde{\ell}_{12}$ is needed. Actually at this level the parameters $\widetilde{\ell}_{11}$, $\widetilde{\ell}_{12}$ are not physical and are equivalent to pNGB field redefinitions. However I include them here for completeness.

Therefore one has the counterterm contribution to the pion self-energy:

$$-i\Sigma_\pi^{ct}(p^2) \;=\; i\delta Z_\pi\,p^2 \;-\; \frac{4i\widetilde{\ell}_{12}(\mu)}{F^2}\,p^4\,, \qquad (6.15)$$

which for the renormalizations

$$\delta Z_\pi \;=\; -\frac{2\,G_V^2}{F^2}\,\frac{3\,M_V^2}{16\pi^2 F^2}\,\frac{n_f}{2}\left\{\lambda_\infty + \ln\frac{M_V^2}{\mu^2} + \frac{1}{6}\right\} +$$

$$+\frac{4\,c_d^2}{F^2}\,\frac{M_S^2}{16\pi^2 F^2}\,\frac{n_f}{2}\left\{\lambda_\infty + \ln\frac{M_S^2}{\mu^2} - \frac{1}{2}\right\}\,, \qquad (6.16)$$

and

$$\widetilde{\ell}_{12} \equiv \widetilde{\ell}_{12}^r(\mu) + \delta\widetilde{\ell}_{12}(\mu) \qquad ; \qquad \delta\widetilde{\ell}_{12}(\mu) \;=\; -\frac{n_f}{2}\frac{2\,G_V^2 + 4\,c_d^2}{F^2}\,\frac{\lambda_\infty}{64\pi^2}\,. \qquad (6.17)$$

eliminates the divergences in $-i\Sigma_\pi^{loop}$.

Summing the counterterms to the one-loop diagrams the renormalized pion self-energy starts now at order $\mathcal{O}(p^4)$:

$$-i\,\Sigma_\pi^r(p^2) \;=\; -i\,\frac{p^4}{16\pi^2 F^2}\left\{64\pi^2\,\widetilde{\ell}_{12}^{\,r}(\mu) \,+\, \frac{2\,G_V^2}{F^2}\frac{n_f}{2}\left[\ln\frac{M_V^2}{\mu^2} + \phi\left(\frac{p^2}{M_V^2}\right)\right]\right.$$

$$\left. +\; \frac{4c_d^2}{F^2}\frac{n_f}{2}\left[\ln\frac{M_S^2}{\mu^2} + \phi\left(\frac{p^2}{M_S^2}\right)\right]\right\}. \tag{6.18}$$

At NLO in $1/N_C$ the only contribution to the VFF comes through the wave-function renormalization δZ_π of the Goldstone fields and the VFF is independent of $\widetilde{\ell}_{12}$.

LO evaluation: $F_V = 2G_V = 2\sqrt{2}c_d = F\sqrt{2}$

Since we are working at the NLO level one can substitute the value of the resonance couplings at LO in $1/N_C$. These were obtained through some QCD short distance analysis on a set of form factors, Green functions and scattering amplitudes [23, 22, 21]. This gives:

$$\delta Z_\pi \;=\; \frac{n_f}{2}\frac{(M_S^2 - 3M_V^2)}{16\pi^2 F^2}\lambda_\infty - \frac{n_f}{2}\frac{3\,M_V^2}{16\pi^2 F^2}\left\{\ln\frac{M_V^2}{\mu^2} + \frac{1}{6}\right\} +$$

$$+\; \frac{n_f}{2}\frac{M_S^2}{16\pi^2 F^2}\left\{\ln\frac{M_S^2}{\mu^2} - \frac{1}{2}\right\}, \tag{6.19}$$

$$\delta\widetilde{\ell}_{12}(\mu) \;=\; -\frac{n_f}{2}\frac{\lambda_\infty}{32\pi^2}.$$

6.1.3 ρ self-energy

We will renormalize the ρ^0 field which is the relevant one in the neutral current matrix element. However, in the chiral and large N_C limits all vector self-energies are identical.

The free propagator for the vector field in the antisymmetric formalism is:

$$\Delta_V^{\mu\nu,\rho\sigma}(x,y)\big|_F \;=\; \langle T\{V^{\mu\nu}(x)\,V^{\rho\sigma}(y)\}\rangle \;=\; \int\frac{d^4q}{(2\pi)^4}\,\Delta_V^{\mu\nu,\rho\sigma}(q)\big|_F\,, \tag{6.20}$$

being the free propagator in the momentum space

$$\Delta_V^{\mu\nu,\rho\sigma}(q) \;=\; \frac{2i}{M_V^2 - q^2}\,\mathcal{A}(q) \,+\, \frac{2i}{M_V^2}\Omega(q)\,, \tag{6.21}$$

with the projectors

$$\mathcal{A}(q)_{\mu\nu,\rho\sigma} = \frac{1}{2q^2} \left(g_{\mu\rho}q_\nu q_\sigma - g_{\rho\nu}q_\mu q_\sigma - (\rho \leftrightarrow \sigma) \right),$$

$$\Omega(q)_{\mu\nu,\rho\sigma} = -\frac{1}{2q^2} \left(g_{\mu\rho}q_\nu q_\sigma - g_{\rho\nu}q_\mu q_\sigma - q^2 g_{\mu\rho}g_{\nu\sigma} - (\rho \leftrightarrow \sigma) \right),$$

(6.22)

Some properties of these projectors and the free propagator can be found in the Appendix B.

In quantum field theory a massive spin $S = 1$ field can be expressed either by a 4-vector $\hat{V}^\mu$ (Proca formalism) or by an antisymmetric tensor $V^{\mu\nu}$ of order two. In this second formalism the tensor actually contains six degrees of freedom; it describes not one but two vector states. The operators $\mathcal{A}(q)^{\mu\nu}_{\rho\sigma}$ and $\Omega(q)^{\mu\nu}_{\rho\sigma}$ project over each of the two vector particles. Since RχT for the lightest resonance multiplets contains just one vector multiplet with a pole at $q^2 = M_V^2$ the second state (the one related to the Ω-projection) must not propagate. Its propagator does not contain poles (it is constant) and its degrees of freedom are frozen.

When the vector field interacts the free propagator gets modified. However, it can be still decomposed in a set of 1PI blocks connected by free propagators. The renormalized self-energy $-i\Sigma_{ab,cd}(u,v)$ of a vector field is finite and is defined from the two-point Green function of the renormalized fields, as it was for the pion field:

$$\langle T\{V^{\mu\nu}(x) V^{\rho\sigma}(y)\} \rangle = \langle T\{V^{\mu\nu}V^{\rho\sigma}\} \rangle_F +$$

$$\int d^4u\, d^4v\, \langle T\{V^{\mu\nu}(x) V^{ab}(u)\} \rangle_F \left(-i\Sigma^V_{ab,cd}(u,v)\right) \langle T\{V^{cd}(v) V^{\rho\sigma}(y)\} \rangle_F + \dots$$

(6.23)

with the self-energy $-i\Sigma^V_{ab,cd}(u,v)$. It obeys the symmetry properties

$$\Delta_V^{\mu\nu,\rho\sigma}(x,y) = -\Delta_V^{\nu\mu,\rho\sigma}(x,y) = -\Delta_V^{\mu\nu,\sigma\rho}(x,y) = \Delta_V^{\rho\sigma,\mu\nu}(x,y).$$

(6.24)

Due to this antisymmetry of the vector fields $V^{\alpha\beta}$ the self-energy definition is ambiguous. However, at the end of the day the only part contributing is the one obeying the antisymmetric properties of the tree-level propagator. A general review of its properties can be found in Appendix B.

In the momentum space the full propagator would be

$$\Delta_V^{\mu\nu,\rho\sigma}(q) = \Delta_V^{\mu\nu,\rho\sigma}(q)\big|_F + \Delta_V^{\mu\nu,ab}(q)\big|_F \left(-i\Sigma^V_{ab,cd}(q)\right) \Delta_V^{cd,\rho\sigma}(q)\big|_F + \dots =$$

$$= \left\{ \mathcal{I}^{\mu\nu,cd} - \Delta_V^{\mu\nu,ab}(q)\big|_F \left(-i\Sigma^V_{ab,cd}(q)\right) \right\}^{-1} \Delta_V^{cd,\rho\sigma}(q)\big|_F,$$

(6.25)

with the antisymmetric identity operator,

$$\mathcal{I}_{\mu\nu,\rho\sigma} = \frac{1}{2} \left(g_{\mu\rho}g_{\nu\sigma} - g_{\mu\sigma}g_{\nu\rho} \right),$$

(6.26)
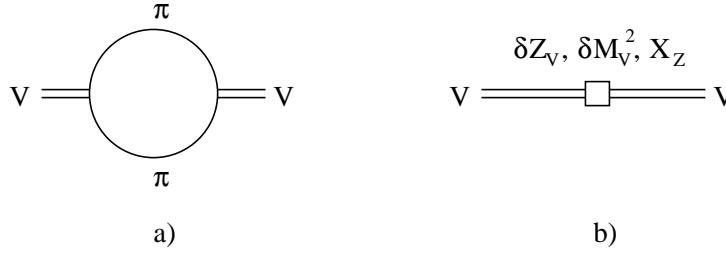
Figure 6.3: ρ self-energy at NLO in $1/N_C$.

Moreover, the self-energy can be decomposed in the two Lorentz structures

$$-i\Sigma^V_{ab,cd}(q) = -\frac{1}{2}i\Sigma^A_V(q^2)\mathcal{A}(q)_{ab,cd} - \frac{1}{2}i\Sigma^\Omega_V(q^2)\Omega(q)_{ab,cd}\,, \qquad (6.27)$$

where the factor $\frac{1}{2}$ is introduced in order to recover the usual scalar self-energy convention. The full propagator gets then simplified:

$$\Delta^{\mu\nu,\rho\sigma}_V(q) \;=\; \frac{2i}{M^2_V - q^2 - \Sigma^A_V(q^2)}\,\mathcal{A}(q)^{\mu\nu,\rho\sigma} \;+\; \frac{2i}{M^2_V - \Sigma^\Omega_V(q^2)}\,\Omega(q)^{\mu\nu,\rho\sigma}\,. \quad (6.28)$$

Notice that once one goes to the quantum loop level the propagator of the second vector state (the Ω-projection) might gain some contribution and one may naively think that a spurious pole can be generated. However, the vector self-energy at leading order is proportional to $\mathcal{A}(q)$ preventing that, although nothing is known yet about higher orders.

Moreover, even being a non propagating state, the Ω-projection gives a non-vanishing contribution to the $v(x)^\mu - \pi\pi$ Green function. This contribution is responsible of the obtention of q^4/F^2 terms and of its bad asymptotic behaviour at large momentum.

The diagrams contributing to the renormalized rho self-energy up to NLO in $1/N_C$ can be seen in Fig. (6.3). The part coming from the one-loop diagrams is

$$-i\Sigma^{loop}_V(q)^{\mu\nu,\rho\sigma} \;=$$

$$= -\frac{i}{2}\mathcal{A}(q)^{\mu\nu,\rho\sigma}\,\left[q^4\,\frac{n_f}{2}\,\frac{2G^2_V}{F^4}\,\left\{-\frac{\lambda_\infty}{96\pi^2} + \frac{\hat{B}(q^2/\mu^2)}{6} + \frac{1}{144\pi^2}\right\}\right]\,. \qquad (6.29)$$

Hence, the factor between the brackets [...] is the projection Σ^A_V defined before and at this order one finds $\Sigma^\Omega_V = 0$.

The redefinitions of the bare vector mass and the vector wave-function renormalization in the RχT lagrangian yield:

$$\mathcal{L}_V^{Kin}[V^{(B)}] = \mathcal{L}_V^{Kin}[V^r] +$$

$$+ \frac{\delta M_V^2}{4} \langle V_{\mu\nu}^r V_r^{\mu\nu} \rangle + \delta Z_V \langle -\frac{1}{2} \nabla^\lambda V_{\lambda\mu}^r \nabla_\nu V_r^{\nu\mu} + \frac{M_{r,V}^2}{4} V_{\mu\nu}^r V_r^{\mu\nu} \rangle , \tag{6.30}$$

where $V_{(B)}^{\mu\nu} = (1 + \delta Z_\rho)^{\frac{1}{2}} V_r^{\mu\nu}$ and $M_{(B)\,V}^2 = M_V^{r\,2} + \delta M_V^2$ cannot renormalise the $\mathcal{O}(q^4)$ one-loop divergence. An operator with four derivatives is required. Chiral symmetry allows us to construct the most general chiral invariant terms containing four derivatives and two vector fields [47, 106]. These operators are not in the LO lagrangian and their couplings are subleading in $1/N_C$. Not all contribute to the self energy but just three pieces:

$$\mathcal{L}_{4Z} = \frac{X_{Z_1}}{2} \langle \nabla^2 V^{\mu\nu} \{\nabla_\nu, \nabla^\sigma\} V_{\mu\sigma} \rangle + \frac{X_{Z_2}}{4} \langle \{\nabla_\nu, \nabla_\alpha\} V^{\mu\nu} \{\nabla^\sigma, \nabla^\alpha\} V_{\mu\sigma} \rangle$$

$$+ \frac{X_{Z_3}}{4} \langle \{\nabla^\sigma, \nabla^\alpha\} V^{\mu\nu} \{\nabla_\nu, \nabla_\alpha\} V_{\mu\sigma} \rangle . \tag{6.31}$$

Actually the self-energy depends only on a precise combination $X_Z = X_{Z_1} + X_{Z_2} + X_{Z_3}$ of them.

These counterterms from $\mathcal{L}_V^{Kin} + \mathcal{L}_{4Z}$ contain an infinite part which kills the divergences from the loops:

$$-i\Sigma^{ct}(q)^{\mu\nu,\rho\sigma} = i\frac{\delta M_V^2}{2} \mathcal{I}^{\mu\nu,\rho\sigma} - \delta Z_V \, \Delta_V^{-1\,\mu\nu,\rho\sigma}\Big|_F + \frac{i}{2}\mathcal{A}(q)^{\mu\nu,\rho\sigma} \, 2\delta X_Z(\mu) q^4 =$$

$$= \mathcal{A}(q)^{\mu\nu,\rho\sigma} \left[i\frac{\delta M_V^2}{2} + i\frac{\delta Z_V}{2}(M_V^2 - q^2) + i\delta X_Z(\mu)q^4\right] +$$

$$+ \Omega(q)^{\mu\nu,\rho\sigma} \left[i\frac{\delta M_V^2}{2} + i\frac{\delta Z_V}{2} M_V^2\right] , \tag{6.32}$$

through the values

$$\begin{aligned}
\delta M_V^2 &= 0 , \\
\delta Z_V &= 0 , \\
\delta X_Z(\mu) &= -\frac{2G_V^2}{F^2} \frac{n_f}{2} \frac{\lambda_\infty}{192\pi^2 F^2} .
\end{aligned} \tag{6.33}$$

Summing up everything the renormalized self-energy becomes:

$$-i\Sigma_V^r(q)^{\mu\nu,\rho\sigma} = -i\frac{1}{2}\mathcal{A}(q)^{\mu\nu,\rho\sigma} \Sigma_V^{\mathcal{A}}(q^2) , \tag{6.34}$$

with the renormalized $\mathcal{A}$-projection,

$$\Sigma_V^{\mathcal{A}}(q^2) = q^4 \left\{-2X_Z^r(\mu) + \frac{2G_V^2}{F^4} \frac{n_f}{2} \left[\frac{\hat{B}_0(q^2/\mu^2)}{6} + \frac{1}{144\pi^2}\right]\right\} . \tag{6.35}$$
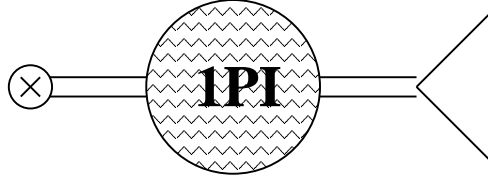
Figure 6.4: Perturbative contribution at NLO in $1/N_C$ to the VFF from the ρ self-energy.

The finite function $\hat{B}_0(q^2/\mu^2)$ is the massless Feynman integral $B_0(q^2; 0, 0)$ with its divergence subtracted in the $\overline{MS} - 1$ scheme (Appendix B).

At the perturbative level this one-loop self-energy gives a contribution to the VFF in the way shown in Fig. (6.4):

$$\Delta \mathcal{F}_Z = \frac{F_V^r(\mu) G_V^r(\mu)}{F^2} \frac{q^2}{M_V^r(\mu)^2 - q^2 - \Sigma_V^{\mathcal{A}}(q^2)} =$$

$$= \frac{F_V^r(\mu) G_V^r(\mu)}{F^2} \frac{q^2}{M_V^r(\mu)^2 - q^2} + \frac{F_V G_V}{F^2} \frac{q^2}{M_V^2 - q^2} \frac{\Sigma_V^{\mathcal{A}}(q^2)}{M_V^2 - q^2} + \mathcal{O}\left(\frac{1}{N_C^2}\right),$$
$$(6.36)$$

where the first term in the second line is the tree-level production and the second one is the diagram with one intermediate self-energy.

The perturbative description however fails when $s \sim M_V^2$ and one has to perform a whole order resummation. The usual Dyson-Schwinger self-energy resummation is the first step to regularize the real pole. Thus, when computing the physical VFF one must replace the free propagator $\Delta_V(q)^{\mu\nu,\rho\sigma}|_F$ for the dressed one $\Delta_V^r(q)^{\mu\nu,\rho\sigma}$ in Eq. (6.2). This expression showed the contribution from each 1PI topology to the VFF. However, as it was shown in the former chapter, this resummation is incomplete since there are other diagrams that also modify the pole at the same order as the self-energy and are not resummed.

LO evaluation: $F_V = 2 G_V = 2\sqrt{2} c_d = F\sqrt{2}$

Evaluating the results for the values of the couplings at leading order in $1/N_C$, one obtains the renormalizations

$$\begin{aligned}
\delta M_V^2 &= 0, \\
\delta Z_V &= 0 \\
\delta X_Z(\mu) &= -\frac{n_f}{2} \frac{\lambda_\infty}{192\pi^2 F^2},
\end{aligned} \qquad (6.37)$$

and the renormalized self-energy $\mathcal{A}$-projection becomes

$$\Sigma_V^{\mathcal{A}}(q^2) = q^4 \left\{ -2 X_Z^r(\mu) + \frac{1}{F^2} \frac{n_f}{2} \left[\frac{\hat{B}_0(q^2/\mu^2)}{6} + \frac{1}{144\pi^2} \right] \right\}. \qquad (6.38)$$

The insertion of the vector self-energy in the VFF would give the perturbative contribution:

$$\Delta\mathcal{F}_Z = \frac{q^2}{M_V^2 - q^2 - \Sigma_V^{\mathcal{A}}(q^2)} =$$

$$= \frac{F_V^r(\mu)G_V^r(\mu)}{F^2} \frac{q^2}{M_V^r(\mu)^2 - q^2} + \frac{q^2}{M_V^2 - q^2} \frac{\Sigma_V^{\mathcal{A}}(q^2)}{M_V^2 - q^2} + \mathcal{O}\left(\frac{1}{N_C^2}\right),$$

$$(6.39)$$

with the value of $\Sigma_V^{\mathcal{A}}(q^2)$ given in Eq. (6.38).

6.2 $V^{\mu\nu} \to \pi\pi$ vertex

Now I am going to start the calculation of more complicated Green functions. But first I will make some remarks on the computation procedure that is adopted in this work. The EFT provides us an effective lagrangian in terms of a set of bare fields and couplings. When performing loops the Green functions of the bare fields become in general infinite:

$$\langle\, T\{...\phi^{(B)}(x)\phi^{(B)}(y)\phi^{(B)}(z)...\}\,\rangle \;\sim\; \lambda_\infty\,. \qquad (6.40)$$

However, through a proper field redefinition $\phi^{(B)} = (1+\delta Z_\phi)^{\frac{1}{2}}\phi^r$, the Green function of a number n of renormalized fields ϕ^r becomes now finite:

$$\langle\, T\{...\phi^r(x)\phi^r(y)\phi^r(z)...\}\,\rangle \;=$$

$$(6.41)$$

$$Z_\phi^{-n/2}\langle\, T\{...\phi^{(B)}(x)\phi^{(B)}(y)\phi^{(B)}(z)...\}\,\rangle \;\sim\; finite\,.$$

At this point one may describe the amplitudes in terms of the renormalized fields ϕ^r. Those can be decomposed in finite renormalized 1PI sub-diagrams connected by renormalized propagators, as it is shown in Fig. (6.5). These renormalized propagators are the free propagator plus corrections due to the interactions.

The Green function to renormalize in this section is the three point function $V\pi\pi$:

$$\langle\, T\{\rho_r^0(x)^{\mu\nu}\, \pi_r^+(y)\, \pi_r^-(z)\}\,\rangle \;=$$

$$(6.42)$$

$$= \int d^4u\, d^4v\, d^4w\; \Delta_V^r(x,u)^{\mu\nu,\rho\sigma}\, \Delta_\pi^r(y,v)\, \Delta_\pi^r(z,w)\; i\Gamma(u,v,w)^{\rho\sigma}\,,$$

which in the momentum space is represented by $i\Gamma(p_1,p_2)^{\mu\nu}$. We will drop the symmetric part of $i\Gamma(p_1,p_2)^{\mu\nu}$ which gives a zero contribution and will just keep its antisymmetric part.
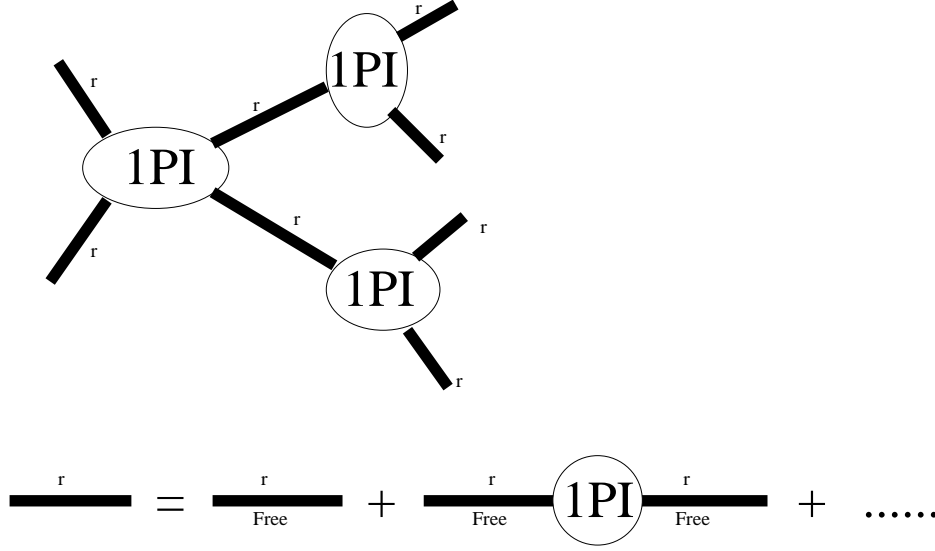
Figure 6.5: General decomposition of the Green functions for renormalized fields.

The one loop diagrams for the 1PI amputated Green function of the renormalized fields $V^r_{\mu\nu}$ and π^r contain the divergent terms

$$i\Gamma^{loop}(p_1, p_2)^{\mu\nu} = \quad finite +$$

$$+ \mathcal{A}(q)^{\mu\nu}_{\rho\sigma} q^\rho (p_1 - p_2)^\sigma \; \frac{G_V}{F^4} \, \frac{n_f}{2} \; \left\{ \frac{q^2}{192\pi^2} \left[\frac{2G_V^2}{F^2} + \frac{4c_d^2}{F^2} - 2 \right] + \left[\frac{3M_V^2}{32\pi^2} \right] \right\} \lambda_\infty \;,$$
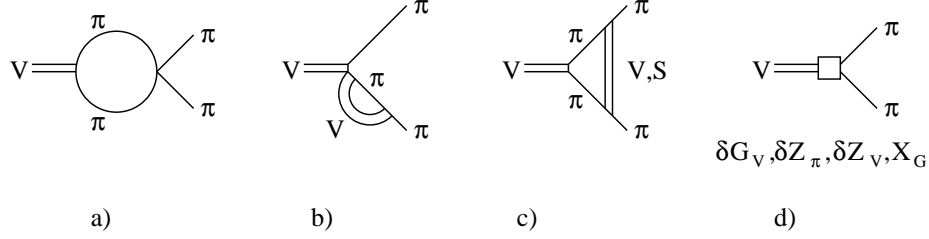
$$(6.43)$$

and the finite part

$$i\Gamma^{loop}(p_1, p_2)^{\mu\nu} = \quad (div. \propto \lambda_\infty) \; +$$

$$+ \frac{G_V}{F^4} \, \frac{n_f}{2} \left\{ \frac{2G_V^2}{F^2} \left[C_0(q^2, 0, 0, M_V^2) \left(-\frac{M_V^6}{q^2} - \frac{5M_V^4}{2} - q^2 M_V^2 \right) + \right. \right.$$

$$+ \hat{B}_0(q^2, 0, 0) \left(-\frac{M_V^4}{q^2} - 2M_V^2 - \frac{q^2}{12} \right)$$

$$\left. - \frac{M_V^2}{16\pi^2} \ln\left(\frac{M_V^2}{\mu^2} \right) \left(\frac{M_V^2}{q^2} + 2 \right) - \frac{M_V^2}{64\pi^2} - \frac{q^2}{288\pi^2} \right] +$$

$$+ \frac{4c_d^2}{F^2} \left[C_0(q^2, 0, 0, M_S^2) \left(-\frac{M_S^2}{q^2} - \frac{M_S^4}{2} \right) + \right.$$

Figure 6.6: $V\pi\pi$ vertex at NLO in $1/N_C$.

$$+\hat{B}_0(q^2,0,0)\left(-\frac{M_S^4}{q^2}-\frac{q^2}{12}\right)+$$

$$-\frac{M_S^2}{16\pi^2}\ln\left(\frac{M_S^2}{\mu^2}\right)\left(\frac{M_S^2}{q^2}\right)-\frac{M_S^2}{64\pi^2}-\frac{q^2}{288\pi^2}\right]+$$

$$+\left[\frac{q^2}{6}\hat{B}_0(q^2,0,0)+\frac{q^2}{144\pi^2}\right]+ \tag{6.44}$$

$$+\left[\frac{M_V^2}{64\pi^2}+\frac{3M_V^2}{32\pi^2}\ln\left(\frac{M_V^2}{\mu^2}\right)\right]\right\}\mathcal{A}^{\mu\nu}_{\alpha\beta}q^\alpha(p_1-p_2)^\beta.$$

In the renormalized Green function the latter divergences are killed by the re-definitions of the parameters in the lagrangian. The wave function renormalizations δZ_V and δZ_π were fixed before by the two point Green functions. However one has still the freedom to renormalize the coupling $G_V^{(B)}$. The piece in the lagrangian which contributes to the $V\pi\pi$ Green function is:

$$\mathcal{L}_{2V}[V^{\mu\nu}_{(B)},\Phi^{(B)}] \quad = \quad \dots \quad + \quad i\frac{G_V^{(B)}\sqrt{2}}{F^2}\langle V^{\mu\nu}_{(B)}\partial_\mu\Phi^{(B)}\partial_\nu\Phi^{(B)}\rangle \quad =$$

$$\overset{\substack{V^{\mu\nu}_{(B)}=(1+\delta Z_V)^{\frac{1}{2}}V_r^{\mu\nu}\\ \Phi^{(B)}=(1+\delta Z_\pi)^{\frac{1}{2}}\Phi^r}}{=} \quad i\frac{G_V^{(B)}\sqrt{2}}{F^2}\langle V_r^{\mu\nu}\partial_\mu\Phi^r\partial_\nu\Phi^r\rangle+$$

$$+i\left[\frac{1}{2}\delta Z_V+\delta Z_\pi\right]\frac{G_V^{(B)}\sqrt{2}}{F^2}\langle V_r^{\mu\nu}\partial_\mu\Phi^r\partial_\nu\Phi^r\rangle \quad = \tag{6.45}$$

$$\overset{G_V^{(B)}=G_V^r+\delta G_V}{=} \quad i\frac{G_V^r\sqrt{2}}{F^2}\langle V_r^{\mu\nu}\partial_\mu\Phi^r\partial_\nu\Phi^r\rangle+$$

$$+i\left[\delta G_V+G_V\left(\frac{1}{2}\delta Z_V+\delta Z_\pi\right)\right]\frac{\sqrt{2}}{F^2}\langle V_r^{\mu\nu}\partial_\mu\Phi^r\partial_\nu\Phi^r\rangle.$$

Nonetheless the Green function contains again divergences which cannot be removed just by the renormalization of the LO lagrangian. The $\mathcal{O}(p^4)$ divergence in Eq. (6.43) requires new pieces with one vector field and four derivatives. The terms allowed by the symmetry that contribute to this Green function at NLO in $1/N_C$ are: (V-GG),

$$\mathcal{L}_{4G} = iX_{G_1}\langle \{\nabla^\alpha, \nabla_\mu\} V^{\mu\nu} [u_\nu, u_\alpha]\rangle + iX_{G_2}\langle V^{\mu\nu} [h_{\alpha\mu}, h^\alpha_\nu]\rangle \qquad (6.46)$$

where this Green function depends only on the combination $X_G \equiv X_{G_2} - \frac{1}{2}X_{G_1}$.

All these counterterms remove the divergences in Eq. (6.43) through the infinite contribution

$$i\Gamma^{ct}(p_1, p_2)^{\mu\nu} = \left[\frac{\delta G_V}{F^2} + \frac{1}{2}\delta Z_V \frac{G_V}{F^2} + \delta Z_\pi \frac{G_V}{F^2} - \frac{4\sqrt{2}\delta X_G(\mu)q^2}{F^2}\right] \mathcal{I}^{\mu\nu}_{\alpha\beta} q^\alpha (p_1 - p_2)^\beta .$$

$$= \mathcal{A}^{\mu\nu}_{\alpha\beta} q^\alpha (p_1 - p_2)^\beta \left[\frac{\delta G_V}{F^2} + \frac{1}{2}\delta Z_V \frac{G_V}{F^2} + \delta Z_\pi \frac{G_V}{F^2} - \frac{4\sqrt{2}\delta X_G(\mu)q^2}{F^2}\right],$$

$$(6.47)$$

with the renormalizations

$$\delta X^r_G(\mu) = \frac{\sqrt{2}G_V}{F^2} \frac{n_f}{2} \left[\frac{2G_V^2}{F^2} + \frac{4c_d^2}{F^2} - 2\right] \frac{\lambda_\infty}{1536\pi^2},$$

$$\delta G_V(\mu) = G_V \frac{n_f}{2} \left[\frac{3M_V^2}{F^2} \left(\frac{2G_V^2}{F^2} - \frac{1}{2}\right) - \frac{M_S^2}{F^2} \frac{4c_d^2}{F^2}\right] \frac{\lambda_\infty}{16\pi^2}.$$

$$(6.48)$$

The summation of all the contributions up to NLO becomes finite:

$$i\Gamma^r_{\mu\nu}(p_1, p_2) = \mathcal{A}^{\alpha\beta}_{\mu\nu} q_\alpha (p_1 - p_2)_\beta \frac{1}{F^2} \left\{G^r_V(\mu) \left[1 - \frac{\Delta\Gamma(q^2)}{F^2}\right] - 4\sqrt{2}X^r_G(\mu) q^2\right\},$$
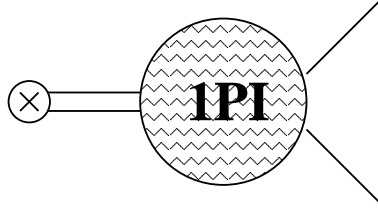
$$(6.49)$$

Figure 6.7: Perturbative contribution to the VFF.

with the subleading contribution

$$
\Delta\Gamma(q^2) = -\left\{ \frac{2G_V^2}{F^2} C_0(q^2,0,0,M_V^2) \left[-\frac{M_V^6}{q^2} - \frac{5M_V^4}{2} - q^2 M_V^2 \right] + \right.
$$

$$
+ \frac{4c_d^2}{F^2} C_0(q^2,0,0,M_S^2) \left[-\frac{M_S^6}{q^2} - \frac{M_S^4}{2} \right] +
$$

$$
+ \hat{B}_0(q^2) \left[\frac{2G_V^2}{F^2} \left(-\frac{M_V^4}{q^2} - 2M_V^2 - \frac{q^2}{12} \right) + \frac{4c_d^2}{F^2} \left(-\frac{M_S^4}{q^2} - \frac{q^2}{12} \right) + \frac{q^2}{6} \right] +
$$

$$
+ \frac{M_V^2}{16\pi^2} \log\frac{M_V^2}{\mu^2} \left[\frac{2G_V^2}{F^2} \left(-\frac{M_V^2}{q^2} - 5 \right) + \frac{3}{2} \right] + \frac{M_S^2}{16\pi^2} \log\frac{M_S^2}{\mu^2} \left[\frac{4c_d^2}{F^2} \left(-\frac{M_S^2}{q^2} + 1 \right) \right] +
$$

$$
\left. + \frac{M_V^2}{64\pi^2} \left[1 - 3\frac{2G_V^2}{F^2} \right] - \frac{3M_S^2}{64\pi^2}\frac{4c_d^2}{F^2} + \frac{q^2}{288\pi^2} \left[2 - \frac{2G_V^2}{F^2} - \frac{4c_d^2}{F^2} \right] \right\}.
$$

$$
(6.50)
$$

The perturbative contribution to the VFF up to NLO from this kind of topology would be:

$$
\Delta\mathcal{F}(q^2) = \left\{ \frac{F_V^r(\mu)G_V^r(\mu)}{F^2} \left[1 - \frac{\Delta\Gamma(q^2)}{F^2} \right] - \frac{4\sqrt{2}F_V X_G^r(\mu)}{F^2} q^2 \right\} \frac{q^2}{M_V^r(\mu)^2 - q^2}.
$$

$$
(6.51)
$$

This contribution is shown in Fig. (6.7)

LO evaluation: $F_V = 2G_V = 2\sqrt{2}c_d = F\sqrt{2}$

The renormalization becomes

$$
\delta X_G^r(\mu) = 0,
$$

$$
\delta G_V(\mu) = \frac{F}{\sqrt{2}} \frac{n_f}{2} \left[\frac{3M_V^2}{32\pi^2 F^2} - \frac{M_S^2}{16\pi^2 F^2} \right] \lambda_\infty,
$$

$$
(6.52)
$$

with the subleading contribution

$$
\begin{aligned}
\Delta\Gamma(q^2) \;=\; & -\Bigg\{ C_0(q^2,0,0,M_V^2)\left[-\frac{M_V^6}{q^2}-\frac{5M_V^4}{2}-q^2M_V^2\right] + \\[2mm]
& + C_0(q^2,0,0,M_S^2)\left[-\frac{M_S^6}{q^2}-\frac{M_S^4}{2}\right] + \\[2mm]
& + \hat{B}_0(q^2)\left[\left(-\frac{M_V^4}{q^2}-2M_V^2-\frac{q^2}{12}\right)+\left(-\frac{M_S^4}{q^2}-\frac{q^2}{12}\right)+\frac{q^2}{6}\right] + \\[2mm]
& + \frac{M_V^2}{16\pi^2}\log\frac{M_V^2}{\mu^2}\left[\left(-\frac{M_V^2}{q^2}-5\right)+\frac{3}{2}\right]+\frac{M_S^2}{16\pi^2}\log\frac{M_S^2}{\mu^2}\left[\left(-\frac{M_S^2}{q^2}+1\right)\right] + \\[2mm]
& - \frac{M_V^2}{32\pi^2}-\frac{3M_S^2}{64\pi^2}\Bigg\}\,.
\end{aligned}
\tag{6.53}
$$

6.3 $v^\mu(x) \to V^{\rho\sigma}$ **Green function**

I will study now the remaining Green function with a vector in an external leg, the one connecting the external vector field $v^\mu(x)$ with renormalized vector $V_r^{\mu\nu}(y)$. We will compute again the amputated Green function $i\Phi^r(x,u)_{\rho\sigma}^\mu$:

$$
\langle\, T\{v^\mu(x)\,V_r^{\alpha\beta}(y)\}\,\rangle \;=\; \int d^4u\, i\Phi^r(x,u)_{\rho\sigma}^\mu\,\Delta_V^r(u,y)^{\rho\sigma,\alpha\beta}\,.
\tag{6.54}
$$

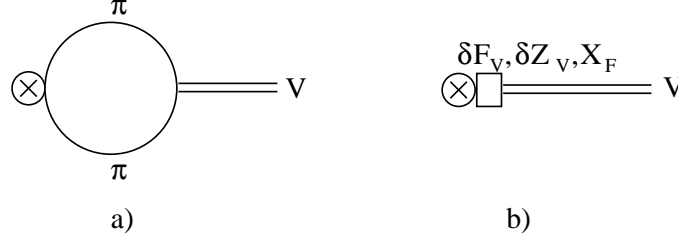We will use its representation in the momentum space, $i\Phi^r(q)_{\rho\sigma}^\mu$:

$$
i\Phi^r(x,u)_{\rho\sigma}^\mu \;=\; \int\frac{d^4q}{(2\pi)^4}\,e^{-iq(x-u)}\,i\Phi^r(q)_{\rho\sigma}^\mu\,.
\tag{6.55}
$$

This amputated Green function has the same ambiguity as the ρ self-energy. Since it is defined through the amputation of the outgoing vector propagators, the combinations symmetric on the second Lorentz indices $\{\rho\sigma\}$ do not contribute. Therefore here only the antisymmetric part is shown.

This Green function has been calculated for the neutral I=1 current $\frac{1}{\sqrt{2}}\bar{u}\gamma^\mu u - \frac{1}{\sqrt{2}}\bar{d}\gamma^\mu d$ producing a ρ^0 meson. The rest of currents are just $SU(3)$ chiral rotations.

The contribution from the one loop diagrams is:

$$
\begin{aligned}
i\Phi(q)^{\mu,\rho\sigma} \;=\; & i\sqrt{2}\,\frac{2G_V}{F^2}\frac{n_f}{2}\,\frac{q^\rho g^{\mu\sigma}q^2}{2}\left\{-\frac{B_0(q^2,0,0)}{6}-\frac{1}{144\pi^2}\right\}-(\rho\leftrightarrow\sigma) \;= \\[2mm]
\;=\; & i\sqrt{2}\,q^\alpha g^{\mu\beta}\,\mathcal{A}(q)_{\alpha\beta}^{\rho\sigma}\,q^2\,\frac{2G_V}{F^2}\frac{n_f}{2}\left\{\frac{\lambda_\infty}{96\pi^2}-\frac{\hat{B}_0(q^2)}{6}-\frac{1}{144\pi^2}\right\}\,.
\end{aligned}
\tag{6.56}
$$

Figure 6.8: $v^\mu(x) \to V_r^{\alpha\beta}$ Green function at NLO in $1/N_C$.

The RχT lagrangian contains a set of counterterms that remove the divergences in the one loop contribution. One comes from the vector wave-function renormalization δZ_V, which is fixed by the self-energy renormalization. Other comes from the renormalization of the coupling $F_V^{(B)} = F_V^r + \delta F_V$:

$$\mathcal{L}_{2V}[V_{(B)}^{\mu\nu}] = \ldots - \sqrt{2}F_V^{(B)}\langle v_\nu \partial_\mu V_{(B)}^{\mu\nu}\rangle =$$

$$\overset{V_{(B)}^{\mu\nu} = (1+\delta Z_V)^{\frac{1}{2}}V_r^{\mu\nu}}{=} \quad - \sqrt{2}F_V^{(B)}\langle v_\nu \partial_\mu V_r^{\mu\nu}\rangle - \frac{1}{2}\delta Z_V\sqrt{2}F_V^{(B)}\langle v_\nu \partial_\mu V_r^{\mu\nu}\rangle = \qquad (6.57)$$

$$\overset{F_V^{(B)} = F_V^r + \delta F_V}{=} \quad - \sqrt{2}F_V^r\langle v_\nu \partial_\mu V_r^{\mu\nu}\rangle - \sqrt{2}\left(\delta F_V + \frac{1}{2}\delta Z_V F_V\right)\langle v^\nu \partial^\mu V_{\mu\nu}^{(R)}\rangle\,,$$

Once more these counterterms are not enough to kill all the divergences from the one loop diagrams. Again there arises $\mathcal{O}(p^4)$ infinities which require terms with one vector field and four derivatives, which must be subleading in our $1/N_C$ counting. The operators allowed by the chiral symmetry and contributing to this Green function are:

$$\mathcal{L}_{4F} = X_{F_1}\langle V_{\mu\nu}\nabla^2 f_+^{\mu\nu}\rangle + X_{F_2}\langle V_{\mu\nu}\{\nabla^\mu, \nabla_\alpha\} f_+^{\alpha\nu}\rangle\,, \qquad (6.58)$$

where our Green function depends just on the combination $X_F \equiv X_{F_1} + X_{F_2}$.

All these counterterms yield an infinite contribution

$$i\Phi_{ct}^{\mu,\rho\sigma}(q) = -i\sqrt{2}\left(\delta F_V + \frac{1}{2}\delta Z_V F_V - 2\sqrt{2}\delta X_F(\mu)\, q^2\right)\mathcal{A}_{\alpha\beta}^{\rho\sigma}q^\alpha g^{\mu\beta}\,, \qquad (6.59)$$

which makes the whole Green function finite through the redefinitions

$$\delta X_F(\mu) = - \frac{n_f}{2}\frac{\sqrt{2}G_V}{F^2}\frac{\lambda_\infty}{192\pi^2}\,,$$
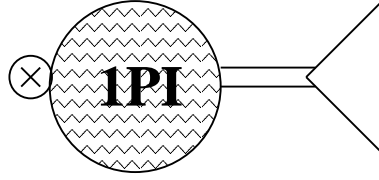
$$\delta F_V = 0\,. \qquad (6.60)$$

Figure 6.9: Perturbative contribution to the VFF.

Notice that F_V is not renormalized so $F_V^r = F_V$.

Summing up everything together the renormalized Green function is given by

$$i\Phi^r(q)^{\mu,\rho\sigma} = -i\sqrt{2} \, \mathcal{A}_{\alpha\beta}^{\rho\sigma}(q) \, q^\alpha g^{\mu\beta} \left\{ F_V^r(\mu) \left[1 - \frac{\Delta\Phi(q^2)}{F^2} \right] - 2\sqrt{2} X_F^r(\mu) q^2 \right\} ,$$
$$(6.61)$$

with

$$\Delta\Phi(q^2) = -q^2 \frac{2G_V}{F_V} \frac{n_f}{2} \left\{ \frac{\hat{B}_0(q^2)}{6} + \frac{1}{144\pi^2} \right\} . \qquad (6.62)$$

LO evaluation: $F_V = 2G_V = 2\sqrt{2}c_d = F\sqrt{2}$

The renormalization becomes

$$\delta X_F(\mu) = -\frac{n_f}{2} \frac{\lambda_\infty}{192\pi^2 F} ,$$
$$(6.63)$$
$$\delta F_V = 0 ,$$

producing the finite renormalized Green function in Eq. (6.59), with

$$\Delta\Phi(q^2) = -q^2 \frac{n_f}{2} \left\{ \frac{\hat{B}_0(q^2)}{6} + \frac{1}{144\pi^2} \right\} . \qquad (6.64)$$

6.4 1PI Green function for $v^\mu(x) \to \pi\pi$

This three-point Green function is defined by:

$$\langle\, T\{v^\mu(x)\, \pi_r^+(y)\, \pi_r^-(z)\}\,\rangle =$$
$$(6.65)$$
$$= \int d^4v\, d^4w\, \Delta_\pi^r(y,v)\, \Delta_\pi^r(z,w)\, \sqrt{2}\mathcal{F}^\chi(x,v,w) ,$$

which in the momentum space is represented by $\sqrt{2}\mathcal{F}^\chi(q^2)\, (p_1^\mu - p_2^\mu)$. This momentum dependence arises when putting the outgoing pions on their mass-shell.
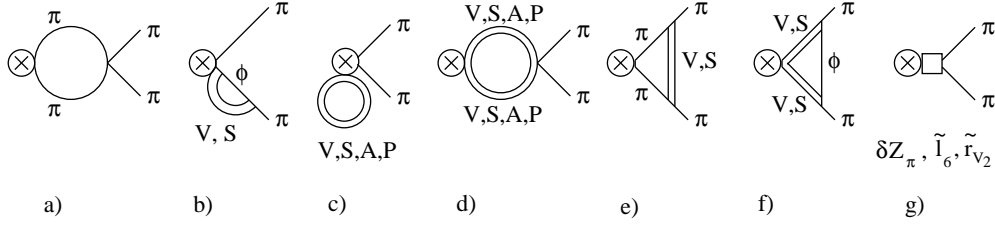
Figure 6.10: $v^\mu(x) \to \pi^r \pi^r$ Green function at NLO in $1/N_C$.

In Fig. (6.10) one may see the diagrams that contribute to this Green function at NLO. The one loop contribution to the renormalized Green function is quite complex and it has been divided in several parts. The first loop in the figure contains vertices from just the pNGB lagrangian $\mathcal{L}_{2\chi}$; the second graph carries vectors and scalars; in the third and fourth ones there can be any kind of resonance (vector, scalar, axial-vector and pseudo-scalar); and in the fifth and sixth loop in the figure we may have vector and scalar resonances. The last plotted contribution is the one coming from the counterterms.

The one loop contribution to $\mathcal{F}^\chi(q^2)$ from the diagrams with vertices just from $\mathcal{L}_{2\chi}$ has a finite piece:

$$\mathcal{F}^\chi_{\mathcal{L}_{2\chi}}(q^2) \quad = \quad \frac{q^2}{F^2}\, \frac{n_f}{2}\, \left\{ \frac{1}{6}\hat{B}_0(q^2/\mu^2) + \frac{1}{144\pi^2} \right\}. \tag{6.66}$$

The renormalized contribution from the loops with vectors is:

$$
\begin{aligned}
\mathcal{F}^\chi_V(q^2) \quad = \quad & \frac{n_f}{2}\, \frac{2G_V^2}{F^4}\, \left\{ -3\hat{A}_0(M_V^2) + \frac{M_V^2}{32\pi^2} \right\} + \\
& + \frac{n_f}{2}\, \frac{1}{F^2}\, \left\{ \frac{3}{2}\hat{A}_0(M_V^2) - \frac{M_V^2}{64\pi^2} \right\} + \\
& + \frac{n_f}{2}\, \frac{1}{F^2}\, \left\{ \hat{B}_0(q^2, M_V^2, M_V^2) \left[-2M_V^2 - \frac{q^2}{6} + \frac{q^4}{6M_V^2} \right] \right. \\
& \left. + \hat{A}_0(M_V^2) \left[\frac{1}{2} - \frac{q^2}{3M_V^2} \right] - \frac{7M_V^2}{64\pi^2} + \frac{q^2}{48\pi^2} - \frac{q^4}{288\pi^2 M_V^2} \right\} + \\
& + \frac{n_f}{2}\, \frac{2G_V^2}{F^4}\, \left\{ \hat{C}_0(q^2, 0, 0, M_V^2) \left[-\frac{M_V^6}{q^2} - \frac{5M_V^4}{2} - q^2 M_V^2 \right] \right. \\
& \left. + \hat{B}_0(q^2, 0, 0) \left[-\frac{M_V^4}{q^2} - 2M_V^2 - \frac{q^2}{12} \right] + \hat{A}_0(M_V^2) \left[\frac{M_V^2}{q^2} + 2 \right] \right.
\end{aligned}
$$

$$-\frac{M_V^2}{64\pi^2} - \frac{q^2}{288\pi^2}\bigg\} +$$

$$+\frac{n_f}{2}\frac{2G_V^2}{F^4}\bigg\{\hat{C}_0(q^2, M_V^2, M_V^2, 0)\left[\frac{M_V^6}{q^2} + \frac{M_V^4}{2}\right]$$

$$+\hat{B}_0(q^2, M_V^2, M_V^2)\left[-\frac{M_V^4}{q^2} - \frac{2M_V^2}{3} + \frac{5q^2}{12}\right] + \hat{A}_0(M_V^2)\left[\frac{M_V^2}{q^2} + \frac{2}{3}\right]$$

$$+\frac{M_V^2}{192\pi^2} - \frac{q^2}{288\pi^2}\bigg\} . \tag{6.67}$$

The scalar loops produce:

$$\mathcal{F}_S^\chi(q^2) = \frac{n_f}{2}\frac{4c_d^2}{F^4}\bigg\{\hat{A}_0(M_S^2) + \frac{M_S^2}{32\pi^2}\bigg\} +$$

$$+\frac{n_f}{2}\frac{1}{F^2}\bigg\{\hat{A}_0(M_S^2)\bigg\} +$$

$$+\frac{n_f}{2}\frac{1}{F^2}\bigg\{\hat{B}_0(q^2, M_S^2, M_S^2)\left[-\frac{2M_S^2}{3} + \frac{q^2}{6}\right]$$

$$+\hat{A}_0(M_S^2)\left[-\frac{1}{3}\right] - \frac{M_S^2}{24\pi^2} + \frac{q^2}{144\pi^2}\bigg\} +$$

$$+\frac{n_f}{2}\frac{4c_d^2}{F^4}\bigg\{\hat{C}_0(q^2, 0, 0, M_S^2)\left[-\frac{M_S^6}{q^2} - \frac{M_S^4}{2}\right]$$

$$+\hat{B}_0(q^2, 0, 0)\left[-\frac{M_S^4}{q^2} - \frac{q^2}{12}\right] + \hat{A}_0(M_V^2)\left[\frac{M_S^2}{q^2}\right]$$

$$-\frac{M_S^2}{64\pi^2} - \frac{q^2}{288\pi^2}\bigg\} +$$

$$+\frac{n_f}{2}\frac{4c_d^2}{F^4}\bigg\{C_0(q^2; M_S^2, M_S^2, 0)\left[\frac{M_S^6}{q^2} - \frac{M_S^4}{2}\right]$$

$$+\hat{B}_0(q^2, M_S^2, M_S^2)\left[-\frac{M_S^4}{q^2} + \frac{M_S^2}{3} - \frac{q^2}{12}\right] + \hat{A}_0(M_S^2)\left[\frac{M_S^2}{q^2} - \frac{1}{3}\right]$$

$$+\frac{M_S^2}{192\pi^2} - \frac{q^2}{288\pi^2}\bigg\} , \tag{6.68}$$

and from the axial-vector loops,

$$
\mathcal{F}_A^\chi(q^2) \;=\; \frac{n_f}{2}\,\frac{1}{F^2}\left\{\frac{3}{2}\hat{A}_0(M_A^2) - \frac{M_A^2}{64\pi^2}\right\}
$$

$$
\frac{n_f}{2}\,\frac{1}{F^2}\left\{\hat{B}_0(q^2, M_A^2, M_A^2)\left[-2M_A^2 - \frac{q^2}{6} + \frac{q^4}{6M_A^2}\right]\right.
$$
$$
\left. + \hat{A}_0(M_A^2)\left[\frac{1}{2} - \frac{q^2}{3M_A^2}\right] - \frac{7M_A^2}{64\pi^2} + \frac{q^2}{48\pi^2} - \frac{q^4}{288\pi^2 M_A^2}\right\}\,,
$$

(6.69)

and finally from the pseudo-scalar resonance loops,

$$
\mathcal{F}_P^\chi(q^2) \;=\; \frac{n_f}{2}\,\frac{1}{F^2}\left\{\hat{A}_0(M_P^2)\right\} +
$$

$$
+\frac{n_f}{2}\,\frac{1}{F^2}\left\{\hat{B}_0(q^2, M_P^2, M_P^2)\left[-\frac{2M_P^2}{3} + \frac{q^2}{6}\right]\right.
$$
$$
\left. + \hat{A}_0(M_P^2)\left[-\frac{1}{3}\right] - \frac{M_P^2}{24\pi^2} + \frac{q^2}{144\pi^2}\right\}\,.
$$

(6.70)

The divergences from the just-pNGB, vector, scalar, axial-vector and pseudo-scalar resonance loops are:

$$
\mathcal{F}^\chi(q^2)^{loop} \;=\; finite + \frac{n_f}{2}\,\frac{1}{F^2}\left\{-\frac{q^2}{96\pi^2}\right\}\lambda_\infty \;+
$$

$$
+\frac{n_f}{2}\,\frac{1}{F^2}\left\{\frac{3M_V^2}{16\pi^2}\frac{2G_V^2}{F^2} + \frac{q^2}{48\pi^2}\left[1 - \frac{2G_V^2}{F^2}\right] - \frac{q^4}{96\pi^2 M_V^2}\right\}\lambda_\infty
$$

$$
+\frac{n_f}{2}\,\frac{4c_d^2}{F^4}\left\{-\frac{M_S^2}{16\pi^2}\right\}\lambda_\infty + \frac{q^2}{576\pi^2 F^2}\left\{7\frac{4c_d^2}{F^2} - 9\right\}\lambda_\infty +
$$

(6.71)

$$
+\frac{n_f}{2}\,\frac{1}{F^2}\left\{\frac{q^2}{32\pi^2} - \frac{q^4}{96\pi^2 M_A^2}\right\}\lambda_\infty +
$$

$$
+\frac{n_f}{2}\,\frac{1}{F^2}\left\{-\frac{q^2}{96\pi^2}\right\}\lambda_\infty\,.
$$

These infinities are partially cancelled out by the ones in the counterterms coming form the LO lagrangian $\mathcal{L}_{2\chi}$:

$$
\mathcal{L}_{2\chi}[\Phi_{(B)}] \;=\; \ldots \;+\; i\langle v^\mu\left(\partial_\mu\Phi_{(B)}\Phi_{(B)} - \Phi_{(B)}\partial_\mu\Phi_{(B)}\right)\rangle =
$$

$$
\stackrel{\Phi_{(B)} = (1+\delta Z_\pi)^{\frac{1}{2}}\Phi_r}{=} \quad i\langle v^\mu\left(\partial_\mu\Phi_r\Phi_r - \Phi_r\partial_\mu\Phi_r\right)\rangle \;+\; \delta Z_\pi i\langle v^\mu\left(\partial_\mu\Phi_r\Phi_r - \Phi_r\partial_\mu\Phi_r\right)\rangle\,.
$$

(6.72)

The contribution from this counterterm was fixed before by the pion self-energy renormalization. It cancels the constant terms in the VFF and ensures the proper

normalization at zero momentum transfer. However, again there are divergences with higher order derivatives. In order to renormalize them one needs chiral invariant terms of that order. However, although the structures are the same as in χPT the couplings are now different. The pieces relevant for this process are:

$$\widetilde{\mathcal{L}}_{4\chi} = \frac{i\,\widetilde{\ell}_6}{4} \langle\, f_+^{\mu\nu}\,[u_\mu, u_\nu]\,\rangle - \widetilde{\ell}_{12} \langle\, \nabla^\mu u_\mu \nabla^\nu u_\nu \,\rangle\,, \tag{6.73}$$

$$\widetilde{\mathcal{L}}_{6\chi} = i\,\widetilde{c}_{51} \langle\, \nabla^\rho f_+^{\mu\nu}[h_{\mu\rho}, u_\nu]\,\rangle + i\,\widetilde{c}_{53} \langle\, \nabla_\mu f_+^{\mu\nu}[h_{\nu\rho}, u^\rho]\,\rangle\,. \tag{6.74}$$

The relevant combination for the on-shell pion VFF will be $\widetilde{r}_{V_2} \equiv 4F^2(\widetilde{c}_{53} - \widetilde{c}_{51})$. All these counterterms provide:

$$\begin{aligned}
\Delta\mathcal{F}_{ct}^\chi &= -\frac{2G_V^2}{F^2}\,\frac{n_f}{2}\,\frac{M_V^2}{16\pi^2 F^2}\left\{3\lambda_\infty + 3\,\ln\frac{M_V^2}{\mu^2} + \frac{1}{2}\right\} + \\
&\quad + \frac{4c_d^2}{F^2}\,\frac{n_f}{2}\,\frac{M_S^2}{16\pi^2 F^2}\left\{\lambda_\infty + \ln\frac{M_S^2}{\mu^2} - \frac{1}{2}\right\} \\
&\quad - \frac{\delta\widetilde{\ell}_6(\mu)q^2}{F^2} + \frac{\delta\widetilde{r}_{V2}(\mu)q^4}{F^4} - \frac{\widetilde{\ell}_6^r(\mu)q^2}{F^2} + \frac{\widetilde{r}_{V2}^r(\mu)q^4}{F^4}\,, \tag{6.75}
\end{aligned}$$

where the first line comes from δZ_π. The physical contribution in $\mathcal{F}_\chi^{ct}$ is given by the finite parts after removing the λ_∞ terms, $\delta\widetilde{\ell}_6(\mu)$ and $\delta\widetilde{r}_{V2}(\mu)$. All the divergences from the one loops calculation in Eq. (6.71) are cancelled by these divergent terms through the renormalizations:

$$\widetilde{\ell}_6 \equiv \widetilde{\ell}_6^r(\mu) + \delta\widetilde{\ell}_6(\mu) \quad;\quad \delta\widetilde{\ell}_6(\mu) = \left\{3 - 2\frac{2G_V^2}{F^2} + \frac{4c_d^2}{F^2}\right\}\frac{n_f}{2}\,\frac{\lambda_\infty}{96\pi^2}\,, \tag{6.76}$$

$$\widetilde{r}_{V2} \equiv \widetilde{r}_{V2}^r(\mu) + \delta\widetilde{r}_{V2}(\mu) \quad;\quad \delta\widetilde{r}_{V2}(\mu) = \frac{F^2\,\lambda_\infty}{96\pi^2}\,\frac{n_f}{2}\left\{\frac{1}{M_V^2} + \frac{1}{M_A^2}\right\}\,. \tag{6.77}$$

These chiral couplings of the high energy theory must be subleading in the $1/N_C$ counting in order to $\widetilde{L}_9/F^2 \to 0$ and $\widetilde{r}_{V2}/F^4 \to 0$ as $N_C \to \infty$. Therefore one has:

$$\begin{aligned}
\widetilde{\ell}_6 &= \mathcal{O}(1)\,, \\
\widetilde{r}_{V2} &= \mathcal{O}(N_C)\,. \tag{6.78}
\end{aligned}$$

The total contribution to the VFF form this topology is:

$$\mathcal{F}^\chi = \mathcal{F}_{\mathcal{L}_2}^\chi + \mathcal{F}_V^\chi + \mathcal{F}_S^\chi + \mathcal{F}_A^\chi + \mathcal{F}_P^\chi + \mathcal{F}_{ct}^\chi \tag{6.79}$$
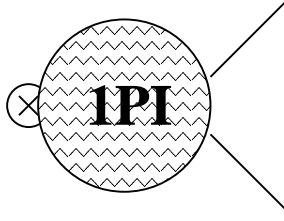
Figure 6.11: Perturbative contribution to the VFF up to $1/N_C$.

LO evaluation: $F_V = 2G_V = 2\sqrt{2}c_d = F\sqrt{2}$

There is a finite contribution which comes from the loops with only the vertices from ChPT lagrangian $\mathcal{L}_2$,

$$\mathcal{F}_{\mathcal{L}_{2\chi}}^{\chi}(q^2) = \frac{q^2}{F^2}\frac{n_f}{2}\left\{\frac{1}{6}\hat{B}_0(q^2/\mu^2) + \frac{1}{144\pi^2}\right\} . \tag{6.80}$$

and the finite contribution to the VFF from the vector loops,

$$\begin{aligned}
\mathcal{F}_V^{\chi}(q^2) = & \ \frac{n_f}{2}\frac{1}{F^2}\left\{-3\hat{A}_0(M_V^2) + \frac{M_V^2}{32\pi^2}\right\} + \\[1em]
& + \frac{n_f}{2}\frac{1}{F^2}\left\{\frac{3}{2}\hat{A}_0(M_V^2) - \frac{M_V^2}{64\pi^2}\right\} + \\[1em]
& + \frac{n_f}{2}\frac{1}{F^2}\left\{\hat{B}_0(q^2, M_V^2, M_V^2)\left[-2M_V^2 - \frac{q^2}{6} + \frac{q^4}{6M_V^2}\right]\right.\\
& \left.\quad + \hat{A}_0(M_V^2)\left[\frac{1}{2} - \frac{q^2}{3M_V^2}\right] - \frac{7M_V^2}{64\pi^2} + \frac{q^2}{48\pi^2} - \frac{q^4}{288\pi^2 M_V^2}\right\} + \\[1em]
& + \frac{n_f}{2}\frac{1}{F^2}\left\{\hat{C}_0(q^2, 0, 0, M_V^2)\left[-\frac{M_V^6}{q^2} - \frac{5M_V^4}{2} - q^2 M_V^2\right]\right.\\
& \quad + \hat{B}_0(q^2, 0, 0)\left[-\frac{M_V^4}{q^2} - 2M_V^2 - \frac{q^2}{12}\right] + \hat{A}_0(M_V^2)\left[\frac{M_V^2}{q^2} + 2\right] \\
& \left.\quad - \frac{M_V^2}{64\pi^2} - \frac{q^2}{288\pi^2}\right\} + \\[1em]
& + \frac{n_f}{2}\frac{1}{F^2}\left\{\hat{C}_0(q^2, M_V^2, M_V^2, 0)\left[\frac{M_V^6}{q^2} + \frac{M_V^4}{2}\right]\right.\\
& \quad + \hat{B}_0(q^2, M_V^2, M_V^2)\left[-\frac{M_V^4}{q^2} - \frac{2M_V^2}{3} + \frac{5q^2}{12}\right] + \hat{A}_0(M_V^2)\left[\frac{M_V^2}{q^2} + \frac{2}{3}\right] \\
& \left.\quad + \frac{M_V^2}{192\pi^2} - \frac{q^2}{288\pi^2}\right\} .
\end{aligned}$$

$$\tag{6.81}$$

and from the scalar

$$
\begin{aligned}
\mathcal{F}_S^\chi(q^2) \;=\;& \frac{n_f}{2}\frac{1}{F^2}\left\{\hat{A}_0(M_S^2) + \frac{M_S^2}{32\pi^2}\right\} + \\
&+\frac{n_f}{2}\frac{1}{F^2}\left\{\hat{A}_0(M_S^2)\right\} + \\
&+\frac{n_f}{2}\frac{1}{F^2}\left\{\hat{B}_0(q^2,M_S^2,M_S^2)\left[-\frac{2M_S^2}{3}+\frac{q^2}{6}\right]\right. \\
&\left.+ \hat{A}_0(M_S^2)\left[-\frac{1}{3}\right] - \frac{M_S^2}{24\pi^2} + \frac{q^2}{144\pi^2}\right\} + \\
&+\frac{n_f}{2}\frac{1}{F^2}\left\{\hat{C}_0(q^2,0,0,M_S^2)\left[-\frac{M_S^6}{q^2}-\frac{M_S^4}{2}\right]\right. \\
&+ \hat{B}_0(q^2,0,0)\left[-\frac{M_S^4}{q^2}-\frac{q^2}{12}\right] + \hat{A}_0(M_V^2)\left[\frac{M_S^2}{q^2}\right] \\
&\left.-\frac{M_S^2}{64\pi^2}-\frac{q^2}{288\pi^2}\right\} + \\
&+\frac{n_f}{2}\frac{1}{F^2}\left\{C_0(q^2,M_S^2,M_S^2,0)\left[\frac{M_S^6}{q^2}-\frac{M_S^4}{2}\right]\right. \\
&+ \hat{B}_0(q^2,M_S^2,M_S^2)\left[-\frac{M_S^4}{q^2}+\frac{M_S^2}{3}-\frac{q^2}{12}\right] + \hat{A}_0(M_S^2)\left[\frac{M_S^2}{q^2}-\frac{1}{3}\right] \\
&\left.+\frac{M_S^2}{192\pi^2}-\frac{q^2}{288\pi^2}\right\} ,
\end{aligned}
$$

$\qquad$ (6.82)

$\qquad$ (6.83)

and from the axial loops,

$$
\begin{aligned}
\mathcal{F}_A^\chi(q^2) \;=\;& \frac{n_f}{2}\frac{1}{F^2}\left\{\frac{3}{2}\hat{A}_0(M_A^2) - \frac{M_A^2}{64\pi^2}\right\} \\
&\frac{n_f}{2}\frac{1}{F^2}\left\{\hat{B}_0(q^2,M_A^2,M_A^2)\left[-2M_A^2-\frac{q^2}{6}+\frac{q^4}{6M_A^2}\right]\right. \\
&\left.+ \hat{A}_0(M_A^2)\left[\frac{1}{2}-\frac{q^2}{3M_A^2}\right] - \frac{7M_A^2}{64\pi^2}+\frac{q^2}{48\pi^2}-\frac{q^4}{288\pi^2 M_A^2}\right\} ,
\end{aligned}
$$

$\qquad$ (6.84)

and finally from the pseudo-scalar resonance loops,

$$
\begin{aligned}
\mathcal{F}_P^\chi(q^2) \;=\;& \frac{n_f}{2}\frac{1}{F^2}\left\{\hat{A}_0(M_P^2)\right\} + \\
&+\frac{n_f}{2}\frac{1}{F^2}\left\{\hat{B}_0(q^2,M_P^2,M_P^2)\left[-\frac{2M_P^2}{3}+\frac{q^2}{6}\right]\right. \\
&\left.+ \hat{A}_0(M_P^2)\left[-\frac{1}{3}\right] - \frac{M_P^2}{24\pi^2} + \frac{q^2}{144\pi^2}\right\} .
\end{aligned}
$$

$\qquad$ (6.85)

The finite contribution form the counterterms is:

$$\Delta\mathcal{F}_{ct}^{\chi} = -\frac{n_f}{2}\frac{M_V^2}{16\pi^2 F^2}\left\{3\ln\frac{M_V^2}{\mu^2}+\frac{1}{2}\right\} + \frac{n_f}{2}\frac{M_S^2}{16\pi^2 F^2}\left\{+\ln\frac{M_S^2}{\mu^2}-\frac{1}{2}\right\}$$

$$-\frac{\widetilde{\ell}_6^r(\mu)q^2}{F^2} + \frac{2\widetilde{f}_1^r(\mu)q^4}{F^2}\,, \tag{6.86}$$

with the renormalizations

$$\widetilde{\ell}_6 \equiv \widetilde{\ell}_6^r(\mu) + \delta\widetilde{\ell}_6(\mu) \qquad ; \qquad \delta\widetilde{\ell}_6(\mu) = \frac{n_f}{2}\frac{\lambda_\infty}{48\pi^2}\,, \tag{6.87}$$

$$\widetilde{r}_{V2} \equiv \widetilde{r}_{V2}^r(\mu) + \delta\widetilde{r}_{V2}(\mu) \qquad ; \qquad \delta\widetilde{r}_{V2}(\mu) = \frac{F^2\,\lambda_\infty}{96\pi^2}\frac{n_f}{2}\left\{\frac{1}{M_V^2}+\frac{1}{M_A^2}\right\}. \tag{6.88}$$

6.5   Effective couplings

In Chapter 4 we could see that not all the terms of the NLO lagrangian where really independent. Some of them could be transformed into others already existing by the use of the EOM from the LO lagrangian. Only some combinations of the couplings were really physical.

In addition, the EOM may be not fully applied to each term X_I, but to a fraction η_I of it. Thus one may select the operator in which to put the physical information and which others to remove:

$$\begin{aligned}
X_Z^{eff} &= (1-\eta_Z)\,X_Z\,,\\
X_F^{eff} &= (1-\eta_F)\,X_F\,,\\
X_G^{eff} &= (1-\eta_G)\,X_G\,,\\
\widetilde{\ell}_6^{eff} &= \widetilde{\ell}_6 + 2\eta_Z X_Z F_V G_V - 2\sqrt{2}\eta_F X_F G_V - 4\sqrt{2}\eta_G X_G F_V\,,\\
\widetilde{r}_{V2}^{eff} &= \widetilde{r}_{V2}\,,\\
F_V^{eff} &= F_V + 2\eta_Z X_Z M_V^2 F_V - 2\sqrt{2}\eta_F X_F M_V^2\,,\\
G_V^{eff} &= G_V + 2\eta_Z X_Z M_V^2 G_V - 4\sqrt{2}\eta_G M_V^2 X_G\,,\\
M_V^{2\,eff} &= M_V^2 + 2\eta_Z X_Z M_V^4\,.
\end{aligned} \tag{6.89}$$

We saw that the $\mathcal{O}(p^4)$ couplings for the vector can be converted into the LO $\mathcal{O}(p^2)$ operators and a contribution to the $\mathcal{O}(p^4)$ χPT operator by choosing $\eta_Z = \eta_F = \eta_G = 1$:

$$\begin{aligned}
X_Z^{eff} &= 0\,,\\
X_F^{eff} &= 0\,,\\
X_G^{eff} &= 0\,,\\
\widetilde{\ell}_6^{eff} &= \widetilde{\ell}_6 + 2X_Z F_V G_V - 2\sqrt{2}X_F G_V - 4\sqrt{2}X_G F_V\,,\\
\widetilde{r}_{V2}^{eff} &= \widetilde{r}_{V2}\,,\\
F_V^{eff} &= F_V + 2X_Z M_V^2 F_V - 2\sqrt{2}X_F M_V^2\,,\\
G_V^{eff} &= G_V + 2X_Z M_V^2 G_V - 4\sqrt{2}M_V^2 X_G\\
M_V^{2\,eff} &= M_V^2 + 2X_Z M_V^4\,.
\end{aligned} \tag{6.90}$$

This choice makes the observable depend just on the couplings M_V^{eff}, F_V^{eff} and G_V^{eff} of the LO lagrangian –which have been shifted at NLO to an effective value– and two effective couplings $\tilde{\ell}_6^{eff}$ and $\tilde{r}_{V2}$ of the χPT operators of the NLO lagrangian. This is the choice that shows the information of the coupling constants more clearly and the one employed in the next sections.

Nevertheless, up to the NLO all the other choices are completely equivalent. Thus, one could prefer removing the couplings $\tilde{\ell}_6$, X_F and X_G, leaving just the operators bilinear in the vector fields corresponding to X_Z (The coupling $\tilde{r}_{V2}$ is not affected by the EOM). This would be obtained through the values

$$\eta_F \; = \; \eta_G \; = \; 1\,, \qquad\qquad \eta_Z \; = \; \frac{1}{2X_Z F_V G_V} \left[-\tilde{\ell}_6 + 2\sqrt{2}G_V X_F + 4\sqrt{2}F_V X_G \right]\,, \tag{6.91}$$

producing the effective couplings

$$
\begin{aligned}
X_Z^{eff} \; &= \; \frac{1}{2X_Z F_V G_V} \left[\tilde{\ell}_6 + 2X_Z F_V G_V - 2\sqrt{2}G_V X_F - 4\sqrt{2}F_V X_G \right] X_Z\,, \\
X_F^{eff} \; &= \; 0\,, \\
X_G^{eff} \; &= \; 0\,, \\
\tilde{\ell}_6^{eff} \; &= \; 0\,, \\
\tilde{r}_{V2}^{eff} \; &= \; \tilde{r}_{V2}\,, \\
F_V^{eff} \; &= \; F_V + \left[-\tilde{\ell}_6 + 2\sqrt{2}G_V X_F + 4\sqrt{2}F_V X_G \right] \frac{M_V^2}{G_V} - 2\sqrt{2}X_F M_V^2\,, \\
G_V^{eff} \; &= \; G_V + \left[-\tilde{\ell}_6 + 2\sqrt{2}G_V X_F + 4\sqrt{2}F_V X_G \right] \frac{M_V^2}{F_V} - 4\sqrt{2}M_V^2 X_G \\
M_V^{2\,eff} \; &= \; M_V^2 + \left[-\tilde{\ell}_6 + 2\sqrt{2}G_V X_F + 4\sqrt{2}F_V X_G \right] \frac{M_V^4}{F_V G_V}\,.
\end{aligned}
\tag{6.92}
$$

Thus, it is possible to convert all the new NLO couplings (except $\tilde{r}_{V2}$, which has a different origin –it is introduced to renormalized the $\mathcal{O}(p^6)$ divergence– but will be studied later) into just one parameter. In this alternative choice the NLO informations are encoded into the coupling of operators bilinear in the vector fields. One can calculate the exact contribution of this kind of operators to all orders, since they would be part of the tree-level vector propagator. Thus, this choice might be more convenient for studies on the resonances peak based on this perturbative calculation since it allows to resum at all orders the contributions from the NLO couplings.

6.6   Renormalized VFF

Putting the results for each 1PI topologies up to NLO into the VFF expression from Eq. (6.2) one finds the result:

$$\mathcal{F}(q^2) \; = \; \mathcal{F}_\chi(q^2) \; +$$

$$+ \left\{ F_V^r(\mu) \left[1 - \frac{\Delta\Phi(q^2)}{F^2} \right] - 2\sqrt{2}X_F^r(\mu)q^2 \right\} \times \frac{q^2}{M_V^r(\mu)^2 - q^2 - \Sigma_V^{\mathcal{A}}(q^2)} \times$$

$$\times \left\{ \frac{G_V^r(\mu)}{F^2} \left[1 - \frac{\Delta\Gamma(q^2)}{F^2} \right] - \frac{4\sqrt{2}X_G^r(\mu)q^2}{F^2} \right\} =$$

$$= \mathcal{F}_\chi(q^2) + \frac{F_V^r(\mu)G_V^r(\mu)}{F^2} \frac{q^2}{M_V^r(\mu)^2 - q^2} +$$

$$+ \frac{q^2}{M_V^2 - q^2} \left\{ \frac{F_V G_V}{F^2} \left[\frac{\Sigma_V^{\mathcal{A}}(q^2)}{M_V^2 - q^2} - \frac{\Delta\Phi(q^2)}{F^2} - \frac{\Delta\Gamma(q^2)}{F^2} \right] \right. \tag{6.93}$$

$$\left. - \frac{2\sqrt{2}X_F^r(\mu)G_V}{F^2}q^2 - \frac{4\sqrt{2}F_V X_G^r(\mu)}{F^2}q^2 \right\} \quad + \mathcal{O}\left(\frac{1}{N_C^2} \right) .$$

The perturbative expression expanded up to NLO in Eq. (6.93) is quite clarifying. There one finds that before using the equations of motion, the NLO couplings ℓ_6 (from $\mathcal{F}_\chi$), X_Z (from $\Sigma_V^{\mathcal{A}}$), X_F and X_G (given explicitly) yield similar dependences in q^2 when summed up and only some combinations of them (which one realizes that are just the effective couplings from Chapter 4) can be fixed by comparison with the experiment.

The perturbative expression of the VFF and the result with the Dyson summation (first two lines) are completely equivalent at the perturbative level. They give similar descriptions away from the vector pole. However, near the mass-shell of the ρ it is more convenient the resummed expression which is regular. Nevertheless one must remember that this expression only resums part of the absorptive contributions to the pole, the re-scattering through intermediate vector mesons. These are the most important ones just on the ρ peak, providing for the mass-less pion limit and $n_f = 2$ the on-shell width:

$$\text{Im}\{\Sigma_V^{\mathcal{A}}(q^2)\}|_{q^2=M_V^2} = M_V \Gamma_V(q^2)|_{q^2=M_V^2} , \tag{6.94}$$

with

$$\Gamma_V(q^2) = \frac{q^4}{96\pi M_V F^2} \theta(q^2) , \tag{6.95}$$

in complete agreement with the width obtained in several former works [27, 26, 29, 105] when the vector is on its mass-shell,

$$\Gamma_V(q^2) = \frac{M_V q^2 \sigma_\pi^3}{96\pi F^2} \theta(q^2 - 4m_\pi^2) . \tag{6.96}$$

Nevertheless, the VFF in Eq. (6.93) does not resum the re-scatterings through local vertices of Goldstones and thus there are variations of order $\sim \mathcal{O}(q^2 - M_V^2)$ when
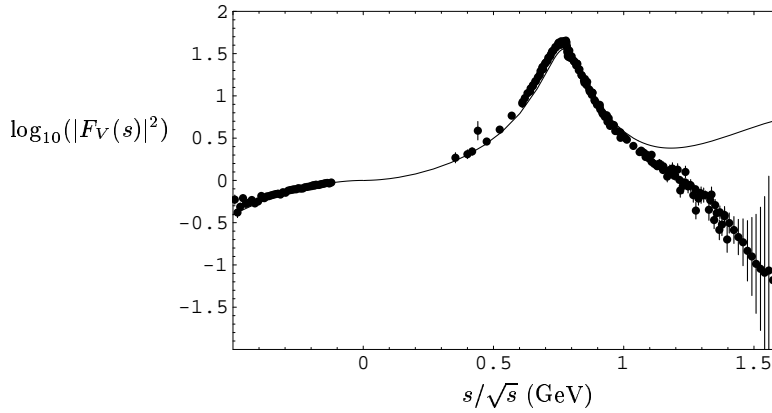
Figure 6.12: Comparison of the one loop VFF including a multiplet of resonances and the ALEPH [65] and NA7 [66] data.

moving away from the peak: The simple Dyson-Schwinger resummation does not fully provide the $\rho(770)$ off-shell width.

In addition one must remember that although the massless pion limit is suitable, the influence of the pion mass is not completely negligible, being the on-shell widths $\Gamma_V^{on-shell}(m_\pi = 0) \simeq 177$ MeV and $\Gamma_V^{on-shell}(m_\pi = m_\pi^{phys}) \simeq 144$ (taking $M_V \simeq 770$ MeV), this is, a 23 % modification in the width! However, this is just the width at LO in $1/N_C$. The value of the parameter M_V of the lagrangian may vary from $M_V \simeq 770$ MeV at LO in $1/N_C$ to $M_V(\mu) \simeq 850$ MeV taking a NLO result [105], i.e., a 10 % variation. This uncertainty would be the error due to the truncation of the $1/N_C$ expansion at LO.

Thus, the Dyson-resummed VFF in the massless limit is just a formal analysis and an estimate of the VFF. In Fig. (6.12) I have plotted the Dyson expression taking for the coupling of the LO lagrangian the values obtained in a former work [105], $F_V^{eff}(\mu)G_V^{eff}(\mu)/F^2 = 1.178$, $2G_V^{eff}(\mu)^2/F^2 = 0.966$ and $M_V^{eff}(\mu) = 845.4$ MeV for $\mu = 770$ MeV. The rest of resonance parameters only appears at NLO so one can employ it value at LO in $1/N_C$, $c_d = F/2$, $M_A^2 = 2M_V^2$ and the estimate $M_P^2 \simeq 2M_S^2$. About the RχT chiral couplings $\widetilde{\ell}_6^{eff}(\mu)$ and $\widetilde{r}_{V2}^{eff}(\mu)$ nothing is known by now but that their contributions must be suppressed by $1/N_C$. Therefore, I have taken $\widetilde{r}_{V2}^{eff}(\mu) = 0$ for that μ. The RχT coupling $\widetilde{\ell}_6^{eff}(\mu)$ will be estimated in Section 6.9 from the measured low energy coupling $\ell_6^{\chi PT}$, obtaining the value $\widetilde{\ell}_6^{eff}(\mu) \simeq -3.5 \cdot 10^{-3}$ for $\mu = 770$ MeV. What we have here , shown in Fig. (6.12), is just an estimate of the VFF, a check that ensures that the NLO loops do not produce huge variations when they are added to the VFF at LO in $1/N_C$.

6.7   Scale dependence of the couplings

In this section I am going to analyse how the different couplings vary with the renormalization scale. I will show first the couplings that have been renormalized in the 1PI analysis. However, the observable is not really dependent on all these constants but only on a precise combination of them. Thus, they can be reduced to effective couplings of the χPT terms, $\widetilde{\ell}_6^{eff}$ and $\widetilde{r}_{V2}^{eff}$, and of the LO vector lagrangian, M_V^{eff}, F_V^{eff} and G_V^{eff}. In the following and so on I will use the effective combinations from Eq. (4.55) in Chapter 4. These are really the physical parameters. We will see that their modifications with the scale are really suppressed and that the perturbative $1/N_C$ expansion converges thus properly.

In addition the underlying QCD dynamics appears here in an explicit way. In the large N_C analysis of QCD [5] one finds that the closed loops have a formal suppression in $1/N_C$. On the other hand, they also have an enhancement proportional to n_f, since all the n_f flavours can be equally produced within closed loop in QCD. From the calculations in $U(2)$ and $U(3)$ one finds that this factor appears explicitly in the renormalizations and in the radiative corrections which are shown below.

6.7.1 $\widetilde{\ell}_6$ scale dependence

The scale dependence of the chiral coupling $\widetilde{\ell}_6^r(\mu)$ is provided by the value that the counterterm $\delta\widetilde{\ell}_6(\mu)$ takes to reabsorb the corresponding ultraviolet divergence:

$$\delta\widetilde{\ell}_6(\mu) \; = \; \frac{n_f}{2} \frac{\lambda_\infty(\mu)}{96\pi^2} \left(3 + \frac{4c_d^2}{F^2} - 2\frac{2G_V^2}{F^2} \right) , \tag{6.97}$$

where one has the ultraviolet divergence $\lambda_\infty(\mu) = \frac{2\mu^{d-4}}{d-4} + \gamma_E - \ln 4\pi - 1 = \frac{1}{d-4} + \gamma_E - \ln 4\pi - 1 + \ln(\mu^2)$. At this order one can substitute the LO values for the resonance couplings, $F_V = 2G_V = 2\sqrt{2}c_d = \sqrt{2}F$:

$$\delta\widetilde{\ell}_6(\mu) \; = \; \frac{n_f}{2} \frac{\lambda_\infty(\mu)}{48\pi^2} , \tag{6.98}$$

and therefore the variation with the scale is

$$\widetilde{\ell}_6(\mu_1) - \widetilde{\ell}_6(\mu_2) = \delta\widetilde{\ell}_6(\mu_2) - \delta\widetilde{\ell}_6(\mu_1) = \frac{n_f}{2} \frac{1}{96\pi^2} \left(3 + \frac{4c_d^2}{F^2} - 2\frac{2G_V^2}{F^2} \right) \ln\left(\frac{\mu_2^2}{\mu_1^2}\right) , \tag{6.99}$$

which for the LO values of the resonance couplings is

$$\widetilde{\ell}_6(\mu_1) - \widetilde{\ell}_6(\mu_2) = \frac{\widetilde{\gamma}_6}{32\pi^2} \ln\left(\frac{\mu_2^2}{\mu_1^2}\right) = \frac{n_f}{2} \frac{1}{48\pi^2} \ln\left(\frac{\mu_2^2}{\mu_1^2}\right) \sim 2 \cdot 10^{-3} \times \frac{n_f}{2} \ln\left(\frac{\mu_2^2}{\mu_1^2}\right) , \tag{6.100}$$

whence one observes that the running for this coupling in RχT –ruled by $\widetilde{\gamma}_6 = \frac{n_f}{2}\frac{2}{3}$– does not coincide with that at low energies for χPT, where one has $\gamma_6^{\chi PT} = -\frac{n_f}{2}\frac{1}{3}$.

The effective combination for this coupling, once the NLO couplings $X_{Z,F,G}$ are removed, gives the renormalization:

$$\delta\widetilde{\ell}_6^{eff}(\mu) = \delta\widetilde{\ell}_6(\mu) + 2F_V G_V \delta X_Z(\mu) - 2\sqrt{2}G_V \delta X_F(\mu) - 4\sqrt{2}F_V \delta X_G(\mu) =$$

$$= \frac{n_f}{2}\frac{\lambda_\infty(\mu)}{96\pi^2}\left\{\left(3 + \frac{4c_d^2}{F^2} - 2\frac{2G_V^2}{F^2}\right) + \frac{2G_V^2}{F^2}\left(1 - \frac{F_V G_V}{F^2}\right) + \right.$$

$$\left. + \frac{F_V G_V}{F^2}\left(1 - \frac{G_V^2}{F^2} - \frac{2c_d^2}{F^2}\right)\right\},$$

$$(6.101)$$

which for the LO values gives

$$\delta\widetilde{\ell}_6^{eff}(\mu) = \frac{n_f}{2}\frac{\lambda_\infty(\mu)}{48\pi^2}, \qquad (6.102)$$

that is, in this case both the initial and the effective couplings have the same running, given before in Eq. (6.100)

The coupling $\widetilde{\ell}_6$ is assumed to be of NLO in $1/N_C$ and therefore suppressed. Its variation with the scale is also of NLO and thus the coupling up to NLO is expected to be of similar size as the numerical value of the coupling at LO. In addition, one also expects the RχT coupling $\widetilde{\ell}_6$ –order $\mathcal{O}(N_C^0)$– to be suppressed with respect to the χPT coupling $\ell_6^{\chi PT}$ –order $\mathcal{O}(N_C)$–. We will see in a later analysis of these couplings that this suppression is indeed observed phenomenologically.

6.7.2 M_V scale dependence

The renormalization of the vector self-energy yields

$$M_V^{r\,2}(\mu_1) - M_V^{r\,2}(\mu_2) = \delta M_V^2(\mu_2) - \delta M_V^2(\mu_1) = 0, \qquad (6.103)$$

since $\delta M_V^2 = 0$.

However, when removing $X_{Z,F,G}$ one gets the effective counterterm

$$\delta M_V^{2\,eff}(\mu) = \delta M_V^2(\mu) + 2M_V^4 \delta X_Z(\mu) = -\frac{n_f}{2}\frac{M_V^4}{96\pi^2 F^2}\frac{2G_V^2}{F^2}\lambda_\infty(\mu), \quad (6.104)$$

and for the LO values of the resonance couplings yields

$$\frac{\delta M_V^{2\,eff}(\mu)}{M_V^2} = -\frac{n_f}{2}\frac{M_V^2}{96\pi^2 F^2}\lambda_\infty(\mu), \qquad (6.105)$$

which produces the relative variation with the scale

$$\frac{M_V^{2\,eff}(\mu_1) - M_V^{2\,eff}(\mu_2)}{M_V^2} = -\frac{n_f}{2}\frac{M_V^2}{96\pi^2 F^2}\ln\left(\frac{\mu_2^2}{\mu_1^2}\right) \sim -7\% \times \frac{n_f}{2}\ln\left(\frac{\mu_2^2}{\mu_1^2}\right),$$

$$(6.106)$$

taking for the the vector mass the LO value $M_V = 770$ MeV. One can see that the corrections are really tiny and that the loops produce just subleading modifications.

6.7.3 F_V scale dependence

As it happened before with the vector mass, the calculation shows that this parameter is not renormalized:

$$F_V^r(\mu_1) - F_V^r(\mu_2) = \delta F_V(\mu_2) - \delta F_V(\mu_1) = 0 \,, \qquad (6.107)$$

since $\delta F_V = 0$.

The effective counterterm for this coupling is

$$\delta F_V^{eff}(\mu) = \delta F_V(\mu) + 2F_V M_V^2 \delta X_Z(\mu) - 2\sqrt{2} M_V^2 \delta X_F(\mu) =$$

$$= \frac{n_f}{2} F_V \frac{M_V^2}{96\pi^2 F^2} \left(\frac{2G_V}{F_V} - 1\right) \lambda_\infty(\mu) \,, \qquad (6.108)$$

which for the LO values $F_V = 2G_V$ yields

$$\delta F_V^{eff} = 0 \,, \qquad (6.109)$$

this is,

$$\frac{F_V^{eff}(\mu_1) - F_V^{eff}(\mu_2)}{F_V} = 0 \,. \qquad (6.110)$$

Therefore, neither the effective combination varies with the scale and the LO coupling do not suffer radiative corrections.

6.7.4 G_V scale dependence

The variation of the renormalized coupling G_V^r with the scale is non-zero in this case:

$$G_V^r(\mu_1) - G_V^r(\mu_2) = \delta G_V(\mu_2) - \delta G_V(\mu_1) =$$

$$= G_V \left\{ \frac{3M_V^2}{32\pi^2 F^2} \left(2\frac{2G_V^2}{F^2} - 1\right) - \frac{4c_d^2}{F^2} \frac{M_S^2}{16\pi^2 F^2} \right\} \frac{n_f}{2} \ln\left(\frac{\mu_2^2}{\mu_1^2}\right) \,, \qquad (6.111)$$

which for the LO values $F_V = 2G_V = 2\sqrt{2}c_d = \sqrt{2}F$ yields the relative variation,

$$\frac{G_V^r(\mu_1) - G_V^r(\mu_2)}{G_V} = \left\{ \frac{3M_V^2}{32\pi^2 F^2} - \frac{4c_d^2}{F^2} \frac{M_S^2}{16\pi^2 F^2} \right\} \frac{n_f}{2} \ln\left(\frac{\mu_2^2}{\mu_1^2}\right) \sim$$

$$\sim (66\% - 74\%) \frac{n_f}{2} \ln\left(\frac{\mu_2^2}{\mu_1^2}\right) \,, \qquad (6.112)$$

where the last result has been obtained employing the values $M_V = 770$ MeV and $M_S = 1$ GeV. One realizes that in this case the good convergence of the $1/N_C$ radiative corrections is not so trivial. The separate contributions from vectors and

scalars are huge and only through a cancellation between them one recovers again a tiny variation with the scale of order 8%.

For the effective combination of this coupling will occur exactly the same. Only the interplay between vector and scalars loops makes the radiative corrections small. The counterterm for the effective coupling is:

$$
\delta G_V^{eff}(\mu) = \delta G_V(\mu) + 2G_V M_V^2 \delta X_Z(\mu) - 4\sqrt{2} M_V^2 \delta X_G(\mu) =
$$

$$
= G_V \left\{ \frac{M_V^2}{192\pi^2 F^2} \left(33\frac{2G_V^2}{F^2} - 16 - \frac{4c_d^2}{F^2} \right) - \frac{4c_d^2}{F^2}\frac{M_S^2}{16\pi^2 F^2} \right\} \frac{n_f}{2} \lambda_\infty(\mu) ,
$$
(6.113)

which for the LO values of the couplings yields,

$$
\frac{\delta G_V^{eff}(\mu)}{G_V} = \left\{ \frac{M_V^2}{12\pi^2 F^2} - \frac{M_S^2}{16\pi^2 F^2} \right\} \frac{n_f}{2} \lambda_\infty(\mu) ,
$$
(6.114)

generating the relative variation with the scale,

$$
\frac{G_V^{eff}(\mu_1) - G_V^{eff}(\mu_2)}{G_V} = \left\{ \frac{M_V^2}{12\pi^2 F^2} - \frac{M_S^2}{16\pi^2 F^2} \right\} \frac{n_f}{2} \ln\left(\frac{\mu_2^2}{\mu_1^2} \right) \sim
$$

$$
\sim (59\% - 74\%) \frac{n_f}{2} \ln\left(\frac{\mu_2^2}{\mu_1^2} \right) ,
$$
(6.115)

with the same values for the masses as before.

As it happened for the initial coupling, the variations with the scale remain small –of the order of the 15%– due to big cancellations between the vector and scalar loops.

6.8 Low energy limit: $q^2 \to 0$

Now one would like to check how the RχT result connects with the VFF computed in the low energy theory, χPT, which is known up to two loops. Our result up to NLO in $1/N_C$ will be expanded in powers of q^2. This will produce powers of q^2/M_R^2 and $q^2/(4\pi F)^2$. At the considered order one can take for the physical masses of the scalar, axial-vector and pseudo-scalar resonances their LO values in $1/N_C$, $M_S^{r\,2} = M_S^2$, $M_A^{r\,2} = M_A^2$ and $M_P^{r\,2} = M_P^2$, which are scale independent. For the vector mass however we will have to employ its NLO expression $M_V^r(\mu)$ considered at a given reference scale μ.

The expansion of the RχT result yields:

$$
\begin{aligned}
\mathcal{F}(q^2) = \quad & 1 - \frac{q^2}{F^2} \left\{ \widetilde{\ell}_6^{eff}(\mu) - \frac{F_V^{eff}(\mu) G_V^{eff}(\mu)}{M_V^{eff}(\mu)^2} \right\} \\[2mm]
& - \frac{n_f}{2} \frac{q^2}{F^2} \left\{ \frac{1}{576\pi^2} \left[\frac{9 F_V G_V}{F^2} \left(2\frac{2G_V^2}{F^2} - 1 + 2\frac{4c_d^2}{F^2}\frac{M_S^2}{M_V^2} \right) + \right. \right. \\[2mm]
& \left. +11\frac{2G_V^2}{F^2} + 2\frac{4c_d^2}{F^2} \right] + \\[2mm]
& + \frac{1}{96\pi^2} \ln\left(\frac{M_V^2}{\mu^2} \right) \left[\frac{9 F_V G_V}{F^2} \left(2\frac{2G_V^2}{F^2} - 1 \right) + 2\frac{2G_V^2}{F^2} - 3 \right] + \\[2mm]
& + \frac{1}{96\pi^2} \ln\left(\frac{M_S^2}{\mu^2} \right) \left[1 - \frac{4c_d^2}{F^2} - 6\frac{F_V G_V}{F^2} \frac{4c_d^2}{F^2}\frac{M_S^2}{M_V^2} \right] \\[2mm]
& \left. - \frac{1}{32\pi^2} \ln\left(\frac{M_A^2}{\mu^2} \right) + \frac{1}{96\pi^2} \ln\left(\frac{M_P^2}{\mu^2} \right) \right\} + \\[2mm]
& + \frac{n_f}{2} \frac{5q^2}{288\pi^2 F^2} - \frac{n_f}{2} \frac{q^2}{96\pi^2 F^2} \ln\left(-\frac{q^2}{\mu^2} \right) \quad + \quad \mathcal{O}\left(\frac{q^4}{\Lambda_\chi^4} \right).
\end{aligned}
$$

$$ (6.116) $$

This expressions can be easily compared with that from χPT [17]:

$$
\begin{aligned}
\mathcal{F}^{\chi PT}(q^2) = \quad & 1 - \frac{\ell_6^r(\mu)\, q^2}{F^2} + \frac{n_f}{2} \frac{5q^2}{288\pi^2 F^2} - \frac{n_f}{2} \frac{q^2}{96\pi^2 F^2} \ln\left(-\frac{q^2}{\mu^2} \right) + \\[2mm]
& + \left[\frac{r_{V2}^r(\mu) q^4}{F^4} - \frac{n_f}{2} \frac{5q^4}{288\pi^2 F^4} \left(2\ell_1 - \ell_2 + 2\ell_6 \right) + \right. \\[2mm]
& \left. + \frac{n_f}{2} \frac{q^4}{96\pi^2 F^4} \left(2\ell_1 - \ell_2 + 2\ell_6 \right) \ln\left(-\frac{q^2}{\mu^2} \right) + \mathcal{O}\left(\frac{1}{N_C^2} \right) \right] \\[2mm]
& + \quad \mathcal{O}\left(q^6 \right),
\end{aligned}
$$

$$ (6.117) $$

where $\ell_6^r(\mu)$ and $r_{V2}^r(\mu)$ are the low energy couplings from χPT.

It is possible therefore to fix complete the value of the low energy coupling $\ell_6^r(\mu)$

in terms of the renormalized RχT parameters:

$$
\begin{aligned}
\ell_6^r(\mu) = & \ \widetilde{\ell}_6^{eff}(\mu) - \frac{F_V^{eff}(\mu)G_V^{eff}(\mu)}{M_V^{eff}(\mu)^2} + \\
& + \frac{n_f}{2}\left\{ \frac{1}{576\pi^2}\left[\frac{9F_V G_V}{F^2}\left(2\frac{2G_V^2}{F^2} - 1 + 2\frac{4c_d^2}{F^2}\frac{M_S^2}{M_V^2} \right) + \right.\right. \\
& \left. +11\frac{2G_V^2}{F^2} + 2\frac{4c_d^2}{F^2} \right] + \\
& + \frac{1}{96\pi^2}\ln\left(\frac{M_V^2}{\mu^2} \right)\left[\frac{9F_V G_V}{F^2}\left(2\frac{2G_V^2}{F^2} - 1 \right) + 2\frac{2G_V^2}{F^2} - 3 \right] + \\
& + \frac{1}{96\pi^2}\ln\left(\frac{M_S^2}{\mu^2} \right)\left[1 - \frac{4c_d^2}{F^2} - 6\frac{F_V G_V}{F^2}\frac{4c_d^2}{F^2}\frac{M_S^2}{M_V^2} \right] \\
& \left. - \frac{1}{32\pi^2}\ln\left(\frac{M_A^2}{\mu^2} \right) + \frac{1}{96\pi^2}\ln\left(\frac{M_P^2}{\mu^2} \right) \right\} .
\end{aligned}
$$
(6.118)

The coincidence of the logarithm $q^2\ln(-q^2)$ shows that the one-loop calculation in RχT recovers fully the one-loop result in χPT. Therefore, the running of the χPT coupling is exactly recovered. Likewise, the saturation does not occur just for a particular renormalization scale. The vector mass and couplings, and the rest of RχT parameters, run exactly in the correct way to recover the χPT coupling at any scale μ.

Through this relations one can recover the RχT coupling $\widetilde{\ell}_6$ from the one in χPT. Thus, taking $\ell_6^r(\mu) = -13.8 \cdot 10^{-3}$ at $\mu = 770$ MeV and the same values for the resonance masses and couplings as in Fig. (6.12) one gets the RχT coupling $\widetilde{\ell}_6^{eff}(\mu) = -3.5 \cdot 10^{-3}$ at that same scale. In addition, one can make these couplings run since their precise renormalizations are well known in both theories. The result of this comparison is shown in Fig. (6.13). The largest uncertainty is given by the lack of knowledge of the scalar resonance mass, which varies in the range $M_S = 1.0 \to 1.4$ GeV. In spite of this one can see that the RχT coupling is much more suppressed than the one from χPT. This is observed phenomenologically independently of the value of the renormalization scale, which has been varied in a wide range $\mu = 0.5 \to 1.2$ GeV. In addition the variations with the scale of $\widetilde{\ell}_6^{eff}(\mu)$ are of the same order as its size. Thus, the phenomenology provides the chiral couplings with the expected sizes from the naive $1/N_C$ analysis: The χPT coupling $\ell_6^r(\mu)$ is "large" and of order $\mathcal{O}(N_C^1)$, with "small" scale variations $\mathcal{O}(N_C^0)$; the RχT coupling $\widetilde{\ell}_6^{eff}(\mu)$ is "small" and of order $\mathcal{O}(N_C^0)$, with "small" variations the same order $\mathcal{O}(N_C^0)$.

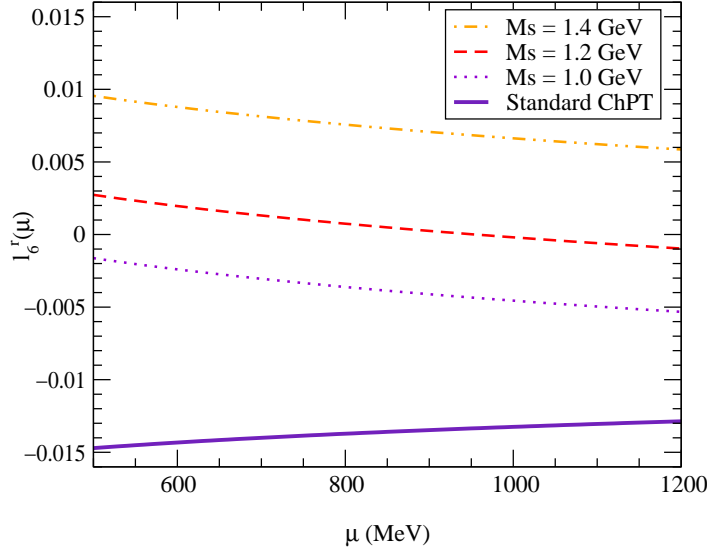It is also possible to give an estimate of the main contributions to the $\mathcal{O}(p^6)$

Figure 6.13: Comparison of the RχT and χPT couplings $\widetilde{\ell}_6^{eff}(\mu)$ and $\ell_6^r(\mu)$.

χPT coupling:

$$
\begin{aligned}
r_{V2}^r(\mu) = \quad & \frac{F^2\, F_V^{eff}(\mu)\, G_V^{eff}(\mu)}{M_V^{eff}(\mu)^4} \;+\; \widetilde{r}_{V2}^r(\mu) \;+ \\[2mm]
& + \frac{n_f}{2}\,\frac{F^2}{5760\pi^2}\Bigg\{ \left[\frac{F_V G_V}{F^2}\left(90 - 55\frac{4c_d^2}{F^2} - 55\frac{2G_V^2}{F^2} \right) \right. \\[2mm]
& \hspace{4cm} \left. - 45\frac{2G_V^2}{F^2} - 102 \right]\frac{1}{M_V^2} \\[2mm]
& - 180\frac{4c_d^2}{F^2}\frac{F_V G_V}{F^2}\frac{M_S^2}{M_V^4} + \left[6 + 45\frac{4c_d^2}{F^2} \right]\frac{1}{M_S^2} + \frac{6}{M_P^2} - \frac{102}{M_A^2} + \\[2mm]
& + \left[\frac{F_V G_V}{F^2}\left(540 - 1050\frac{2G_V^2}{F^2} \right) + 30\frac{2G_V^2}{F^2} - 60 \right]\ln\left(\frac{M_V^2}{\mu^2} \right) + \\[2mm]
& + 30\frac{4c_d^2}{F^2}\left[12\frac{F_V G_V}{F^2}\frac{M_S^2}{M_V^2} + \frac{F_V G_V}{F^2} - \frac{M_V^2}{M_S^2} \right]\ln\left(\frac{M_S^2}{\mu^2} \right) \\[2mm]
& - \frac{60M_V^2}{M_A^2}\ln\left(\frac{M_A^2}{\mu^2} \right) \Bigg\} \quad + \quad \mathcal{O}\left(\frac{1}{N_C} \right),
\end{aligned}
\tag{6.119}
$$

where, up to the considered order, we employed the LO in $1/N_C$ relation

$$\frac{q^4}{96\pi^2 F^4}\left(2\ell_1 - \ell_2 + \ell_6\right) = \frac{q^4}{96\pi^2 F^4}\left(\frac{2c_d^2}{M_S^2} - \frac{3G_V^2 + F_V G_V}{M_V^2}\right), \tag{6.120}$$

and likewise recovering the coefficient in front of the $q^4 \ln\left(-q^2\right)$ term and the exact running of $r_{V2}^r(\mu)$ in χPT up to the considered order in $1/N_C$. The missing NNLO contributions from two-loop diagrams are NNLO in $1/N_C$ and are expected to be small.

Resonance couplings at LO in $1/N_C$: $F_V = 2G_V = 2\sqrt{2}c_d = \sqrt{2}F$

One may substitute the LO values of the resonance couplings in the term which are already NLO in $1/N_C$. Thus, the relations between the low and high energy couplings become quite simplified:

$$\ell_6^r(\mu) = \widetilde{\ell}_6^{eff}(\mu) - \frac{F_V^{eff}(\mu) G_V^{eff}(\mu)}{M_V^{eff}(\mu)^2} + \frac{n_f}{2}\left\{\frac{11}{288\pi^2} + \frac{M_S^2}{32\pi^2 M_V^2} + \right.$$

$$\left. + \frac{1}{12\pi^2}\ln\left(\frac{M_V^2}{\mu^2}\right) - \frac{M_S^2}{16\pi^2 M_V^2}\ln\left(\frac{M_S^2}{\mu^2}\right) - \frac{1}{32\pi^2}\ln\left(\frac{M_A^2}{\mu^2}\right) + \frac{1}{96\pi^2}\ln\left(\frac{M_P^2}{\mu^2}\right)\right\}, \tag{6.121}$$

and the $\mathcal{O}(p^6)$ χPT coupling becomes:

$$r_{V2}^r(\mu) = \frac{F^2 F_V^{eff}(\mu) G_V^{eff}(\mu)}{M_V^{eff}(\mu)^4} + \widetilde{r}_{V2}^r(\mu) +$$

$$+ \frac{n_f}{2}\frac{F^2}{96\pi^2}\left\{\left(6\frac{M_S^2}{M_V^4} + \frac{1}{2M_V^2} - \frac{1}{2M_S^2}\right)\ln\frac{M_S^2}{\mu^2} - \frac{9}{M_V^2}\ln\frac{M_V^2}{\mu^2} - \frac{1}{M_A^2}\ln\frac{M_A^2}{\mu^2}\right.$$

$$\left. - \frac{167}{60M_V^2} - \frac{17}{10M_A^2} - \frac{3M_S^2}{M_V^4} + \frac{51}{60M_S^2} + \frac{1}{10M_P^2}\right\} + \mathcal{O}(N_C^0). \tag{6.122}$$

6.9   High energy limit: $q^2 \to \infty$

Now we are going to compare our one-loop calculation with the result expected in perturbative QCD [50]. Assuming that order by order the $1/N_C$ expansion follows the asymptotic behaviour of the full form factor at $q^2 \to \infty$, one would expect that our perturbative calculation up to NLO vanishes as the total momentum goes to infinity. Here one must expand the perturbative result. It is not legal to perform Dyson resummations because through the all order summation one converts the perturbative series $(1+a+\mathcal{O}(a^2))$ into the denominator $(1-a)^{-1}$. They are identical up to NLO but they may have completely different asymptotic behaviour. If one

had $a \sim q^2$, then in the resummed case the asymptotic behaviour of the amplitude would be ruled by the infinity of subleading orders ($\sim a^2$, $\sim a^3$...) resummed to build up the denominator. Thus, the $1/N_C$ expansion would not have any sense.

The behaviour at high energy of the VFF up to NLO in $1/N_C$ is:

$$
\begin{aligned}
\mathcal{F}(q^2) \;\overset{q^2 \to \infty}{\cong}\; & \frac{\widetilde{r}_{V2}^{eff}(\mu)\, q^4}{F^4} + \frac{n_f\, q^4}{96\pi^2 F^2}\left(\frac{1}{M_V^2} + \frac{1}{M_A^2}\right)\left[\frac{2}{3} - \ln\left(-\frac{q^2}{\mu^2}\right)\right] \\
& - \frac{\widetilde{\ell}_6^{eff}(\mu) q^2}{F^2} + \\
& + \frac{n_f\, q^2}{96\pi^2 F^2}\left[\frac{5}{6}\frac{4c_d^2}{F^2}\left(\frac{F_V G_V}{F^2} - 2\right) + \right. \\
& \qquad + \frac{5}{6}\frac{F_V G_V}{F^2}\left(3\frac{2G_V^2}{F^2} - 2\right) - \frac{1}{3}\frac{2G_V^2}{F^2} + \\
& \qquad + \left\{\frac{1}{2}\frac{4c_d^2}{F^2}\left(2 - \frac{F_V G_V}{F^2}\right) + \right. \\
& \qquad \left.\left. + \frac{1}{2}\frac{F_V G_V}{F^2}\left(2 - 3\frac{2G_V^2}{F^2}\right) - \frac{2G_V^2}{F^2} + 3\right\}\ln\left(-\frac{q^2}{\mu^2}\right)\right] + \\
& + 1 - \frac{F_V^{eff}(\mu) G_V^{eff}(\mu)}{F^2} + \frac{n_f\, M_A^2}{96\pi^2 F^2}\left[12\ln\left(-\frac{q^2}{M_A^2}\right) - 27\right] + \\
& \qquad + \frac{n_f\, M_P^2}{96\pi^2 F^2}\left[6\ln\left(-\frac{q^2}{M_P^2}\right) - 6\right] + \\
& + \frac{n_f\, M_S^2}{96\pi^2 F^2}\left[\frac{9}{2}\frac{4c_d^2}{F^2}\frac{F_V G_V}{F^2} - 6 + \right. \\
& \qquad \left. + \left\{6 - 3\frac{4c_d^2}{F^2}\right\}\ln\left(-\frac{q^2}{M_S^2}\right) - 6\frac{4c_d^2}{F^2}\frac{F_V G_V}{F^2}\ln\left(\frac{M_S^2}{\mu^2}\right)\right] + \\
& + \frac{n_f\, M_V^2}{96\pi^2 F^2}\left[\frac{5}{6}\frac{4c_d^2}{F^2}\frac{F_V G_V}{F^2} - \frac{19}{6}\frac{F_V G_V}{F^2} + \frac{62}{3}\frac{F_V G_V}{F^2}\frac{2G_V^2}{F^2}\right. \\
& \qquad - \frac{41}{3}\frac{2G_V^2}{F^2} + \pi^2\frac{2G_V^2}{F^2}\left(1 - \frac{F_V G_V}{F^2}\right) - 27 + \\
& \qquad \left. + 3\frac{2G_V^2}{F^2}\left(1 - \frac{F_V G_V}{F^2}\right)\ln\left(\frac{q^2}{M_V^2}\right)\left\{\ln\left(\frac{q^2}{\mu^2}\right) - \ln\left(-\frac{q^2}{M_V^2}\right)\right\}\right] +
\end{aligned}
$$

$$+ \left\{ -\frac{1}{2}\frac{4c_d^2}{F^2}\frac{F_V G_V}{F^2} + \frac{F_V G_V}{F^2} - \frac{29}{2}\frac{F_V G_V}{F^2}\frac{2G_V^2}{F^2} + \right.$$

$$\left. +22\frac{2G_V^2}{F^2} + 12 \right\} \ln\left(-\frac{q^2}{M_V^2}\right)$$

$$+ \left\{ -8\frac{F_V G_V}{F^2} + \frac{31}{2}\frac{F_V G_V}{F^2}\frac{2G_V^2}{F^2} + \frac{2G_V^2}{F^2} \right.$$

$$\left. -\frac{1}{2}\frac{4c_d^2}{F^2}\frac{F_V G_V}{F^2} \right\} \ln\left(\frac{M_V^2}{\mu^2}\right) \right] \quad + \quad \mathcal{O}\left(\frac{M_R^4}{q^2 F^2}\right), \qquad (6.123)$$

that for the LO values $F_V = 2G_V = 2\sqrt{2}c_d = \sqrt{2}F$ becomes

$$\mathcal{F}(q^2) \overset{q^2 \to \infty}{=} \frac{\widetilde{r}_{V2}^{eff}(\mu)\, q^4}{F^4} + \frac{n_f\, q^4}{96\pi^2 F^2}\left(\frac{1}{M_V^2} + \frac{1}{M_A^2}\right)\left[\frac{2}{3} - \ln\left(-\frac{q^2}{\mu^2}\right)\right]$$

$$-\frac{\widetilde{\ell}_6^{eff}(\mu)q^2}{F^2} + \frac{n_f\, q^2}{96\pi^2 F^2}\left[\frac{32}{3} + 2\ln\left(-\frac{q^2}{\mu^2}\right)\right] +$$

$$+1 - \frac{F_V^{eff}(\mu)G_V^{eff}(\mu)}{F^2} + \frac{n_f\, M_A^2}{96\pi^2 F^2}\left[12\ln\left(-\frac{q^2}{M_A^2}\right) - 27\right] +$$

$$+\frac{n_f\, M_P^2}{96\pi^2 F^2}\left[6\ln\left(-\frac{q^2}{M_P^2}\right) - 6\right] +$$

$$+\frac{n_f\, M_S^2}{96\pi^2 F^2}\left[\frac{3}{2} + 3\ln\left(-\frac{q^2}{M_S^2}\right) - 6\ln\left(\frac{M_V^2}{\mu^2}\right)\right] +$$

$$+\frac{n_f\, M_V^2}{96\pi^2 F^2}\left[-\frac{67}{3} + 20\ln\left(-\frac{q^2}{M_V^2}\right) + 8\ln\left(\frac{M_V^2}{\mu^2}\right)\right] +$$

$$+ \quad \mathcal{O}\left(\frac{M_R^4}{q^2 F^2}\right).$$

$$(6.124)$$

Observing this result one may understand some of the theoretical arguments developed when constructing the Resonance Chiral Theory in Chapter 4. Before going further one must remember that the amplitude is not just the form factor but also the Lorentz momentum structure $(p_{\pi^+} - p_{\pi^-})^\mu$ and the auxiliary vector field field $v(x)^\mu$, scaling each one as a power of the momentum $\sim p$. Therefore, a constant term in the VFF comes from an $\mathcal{O}(p^2)$ lagrangian, an order $\mathcal{O}(q^2)$ term corresponds to an $\mathcal{O}(p^4)$ operator in the lagrangian and so on.

Thus, it was demostrated that the tree-level contributions to the amplitude are $\sim p^2$, which for the VFF means a $\Delta\mathcal{F}(q^2) \sim const.$ contribution. The analysis of the

superficial degree of divergence tells us that the one loop amplitudes are $\sim p^4/F^2$, which means $\Delta \mathcal{F}(q^2) \sim q^2/F^2$ for the VFF.

What is the origin then for the $\Delta \mathcal{F}(q^2) \sim q^4/M_V^2 F^2$ term in Eq. (6.124)? This contribution comes from just a type of diagram: The loop of two vector (and axial-vector) propagators that can be seen in the fourth graph of Fig. (6.10) (diagrams V7 and A2 in Appendix C). In it one finds that the non-physical modes of one of the massive vector propagators (Ω–projection in the antisymmetric formalism) give a non-zero contribution. There appears then one more power of the momenta $\sim k^\mu k^\nu$ in the numerator, compensated by an extra power $M_{V,A}^2$ in the denominator. The way these extra degrees of freedom disappear in the high energy limit is not yet clear but it must be so if one wants to match with pQCD, a theory of massless particles.

The analytic terms in the VFF as $\Delta \mathcal{F}(q^2) \sim const.$ and as $\Delta \mathcal{F}(q^2) \sim q^2/F^2$ were the already expected contributions from tree-level and one loop amplitudes. By a second let us ignore the existence of the logarithmic terms $\ln\left(-q^2/\mu^2\right)$ and $\ln\left(-q^2/M_R^2\right)$. Thus, by imposing the VFF to behave as $\Delta \mathcal{F}(q^2) \sim 1/q^2$ one obtains constraints up to NLO in $1/N_C$ for the couplings:

$$\widetilde{r}_{V2}^{eff}(\mu) \;\overset{?}{=}\; -\frac{n_f}{2}\frac{F^2}{144\pi^2}\left(\frac{1}{M_V^2}+\frac{1}{M_A^2}\right),$$

$$\widetilde{\ell}_6^{eff}(\mu) \;\overset{?}{=}\; \frac{n_f}{2}\frac{1}{9\pi^2},$$

$$F_V^{eff}(\mu)G_V^{eff}(\mu) \;\overset{?}{=}\; 1 \;+\; \frac{n_f}{2}\frac{M_A^2}{96\pi^2}\left[-27\right] + \frac{n_f}{2}\frac{M_P^2}{96\pi^2}\left[-6\right] + \tag{6.125}$$

$$+\; \frac{n_f}{2}\frac{M_S^2}{96\pi^2}\left[\frac{3}{2}-6\ln\left(\frac{M_V^2}{\mu^2}\right)\right] +$$

$$+\; \frac{n_f}{2}\frac{M_V^2}{96\pi^2}\left[-\frac{67}{3}+8\ln\left(\frac{M_V^2}{\mu^2}\right)\right].$$

If there would not be any other non-analytic structure this would be a great result, since it would be possible to kill the growing of the amplitude at large momenta. Therefore the NLO contributions would be really suppressed not only in the formal counting but also numerically in the high energy analysis. Moreover, the QCD short distance constraints would fix again the value of the coupling constants leaving the vector mass as the only free parameter.

However, the expressions in Eq. (6.125) do not have the same running in the left and in the right-hand-side. This is because there are also logarithms $\ln\left(-\frac{q^2}{\mu^2}\right)$ with the same power behaviour as the couplings. Thus, it is not possible to remove the q^4, q^2 and q^0 terms from the VFF: The logarithms $\ln(-q^2)$ diverge at high momentum and cannot be killed by local counterterms, which are analytical. These logs come from absorptive two-particle cuts, which is the only possible type of absorptive cut at one loop. The imaginary parts of these non-analytic pieces are essentially the

tree level form-factors to a $\psi\psi$ intermediate state of two mesons, times the tree-level scattering amplitude $\psi\psi \to \pi\pi$ in the corresponding channel $I = J = 1$. Thus, the one-loop logarithms become fixed by the asymptotic behaviour of the two-particle vector form-factors and the $\psi\psi \to \pi\pi$ scattering amplitudes.

Although the way to work with final resonance states is not fully clear, it is reasonable to think that the two-meson vector form factors must also vanish at infinite momentum transfer [50]. This behaviour is obeyed by the pion VFF and the good asymptotic behaviour of the imaginary part of the two-point correlators seems to require the same kind of cancellation for the infinity of remaining intermediate cuts, as each one provides a positive contribution. In addition, due to unitarity requirements, the scattering amplitudes must remain finite at high energies. Therefore, the tree-level scatterings –LO in $1/N_C$– must go to a constant value if one demands them to behave as the full observable. Hence, the fulfillment of the proper behaviours for the tree-level form-factors and scatterings would automatically ensure the good behaviour of the non-analytic terms at one-loop.

The problem here is that although the tree-level pion VFF behaves properly, this is not true for the rest of channels. The two-resonance production is given just by the kinetic term through the chiral connection Γ^μ. This produces constant form-factors which do not vanish at high energies. The solution of this problem looks quite straight forward: The analysis of these form-factors and the inclusion of new vector-resonance-resonance vertices in the lagrangian to recover the familiar monopole structure $\frac{M_V^2}{M_V^2 - q^2}$.

The situation with the scattering amplitudes is a bit more complicated since they are ill-behaved even for the familiar $\pi\pi \to \pi\pi$ partial wave for this channel, $I = J = 1$. The sum of the contributions from the local $\mathcal{O}(p^2)$ χPT term and the s-channel exchange of a vector resonance gives a constant behaviour at $s \to \infty$. However, the exchange of mesons in the t-channel spoils completely the amplitude at high momentum. It spoils even our control over the needed spectrum of the EFT. It is very easy to control the particles produced in the s-channel, since they must have the proper quantum numbers; moreover, one may assume that the main contributions come from the first multiplets of the spectrum and neglect higher ones. However, in the t-channel one can insert all the possible quantum numbers without any kind of restriction. For instance, our RχT lagrangian implies that the contribution from the t-exchange of a vector is equal to that from the t-exchange of a scalar, and both of the same size at $s \to \infty$ as the s-channel diagram.

6.10 Summary

The one-loop analysis of the VFF has shown a series of interesting features. As expected, loop diagrams with massive resonance states in the internal lines generate ultraviolet divergences, which require additional higher-dimensional counterterms in the RχT lagrangian. Since these counterterms give rise to tree-level contributions

which grow too fast at large momenta, their corresponding couplings should be zero at leading order in the large–N_C expansion. Thus, one can establish a well defined counting in powers of $1/N_C$ to organize the calculation.

The formal renormalization is completely straightforward at one loop. One can easily determine the μ dependence of all relevant renormalized couplings. Moreover, the final result is only sensitive to some combinations of the chiral couplings. In fact, using the lowest-order equations of motion, one can eliminate most of the higher-order couplings. Their effects get then reabsorbed into redefinitions of the lowest-order parameters.

Expanding the result in powers of q^2/M_R^2, one recovers the usual χPT expression at low momenta. This relates the low-energy chiral couplings ℓ_6 and r_{V2} with their corresponding RχT counterparts $\widetilde{\ell}_6$ and $\widetilde{r}_{V2}$. The rigorous control of the renormalization scale dependences has allowed us to investigate the successful resonance saturation approximation at the next-to-leading order in $1/N_C$ at any scale μ.

At high energies, we have identified a problematic behaviour which originates in the two-resonance cuts: they generate an unphysical increase of the VFF at large values of momentum transfer. This is not surprising, since there are additional contributions generated by interaction terms with several resonances, which have not been included in the minimal RχT lagrangian. These new chiral structures should be taken into account to achieve a physical description of the VFF above the two-resonance thresholds. The short-distance QCD constraints can be used to determine their corresponding couplings as it has been analysed in Ref. [106].

This calculation represents a first step towards a systematic procedure to evaluate next-to-leading order contributions in the $1/N_C$ counting. However, more work in this direction is definitely necessary and already in progress.

Chapter 7

Scalar sector

In the last chapter, the creation of a $J = I = 1$ pion pair from a vector quark current was studied. In the next pages I treat the production of this $\pi\pi$ state but with $J = I = 0$ quantum numbers.

On the contrary to the vector case, the Standard Model lagrangian does not contain terms with scalar quark currents $q\bar{q}$. At first, there are not experimental processes with this kind of interaction[1].

Nevertheless, although there are no direct vertices, some more involved matrix elements accept decompositions in terms of smaller pieces, for instance, in terms of products of scalar quark currents. The theoretical control of the final state interactions (FSI) in this channel $-I = J = 0-$ is quite important since they have been shown to be larger than expected. Moreover, the scalar form factor (SFF) is closely related with several other observables through unitarity. In the elastic limit the $I = J = 0$ partial wave scattering phase is the same as the complex phase of the SFF. It is also relevant in electroweak physics since this channel is between the most important ones among the possible final states (for instance the neutral kaon decay into $\pi\pi$ [61]). A better knowledge of the SFF could improve the analysis of this kind of experiments.

Thus, there are no direct experimental data providing the amplitude of the SFF. Nonetheless, through the Watson theorem (unitarity and analyticity) the SFF phase can be known. It coincides –within the elastic region– with the phase of the $\pi\pi$-scattering amplitude in the $I = J = 0$ channel. The SFF modulus can be reconstructed from this phase-shift through the Omnés solution (analyticity). The study can be taken further, including the exact influence from $K\overline{K}$–channel through the extended Omnès-Muskhelishvili solution [56, 57].

---

[1]Actually, these vertices do exist: The interaction between the Higgs and all the fermions. Till now no process of this kind has been clearly detected. Moreover, these processes would be at energies far beyond the chiral theory range. However, before LEP ruled out a light Higgs of a few GeV, several scalar form factor analyses were performed in order to describe its possible hadronic decays [77, 78].

7.1   SFF in χPT

In order to obtain the scalar quark current $\bar{q}_i q_j$ we will employ the external fields introduced in the QCD lagrangian in Eq. (3.15). One has then to functionally derive the generating functional $W[s]^{QCD} = W[s]^{EFT}$, as it was done for the VFF:

$$\langle ...\bar{q}_i(x)q_j(x)...\rangle \;\; = \;\; -\langle ...\frac{\delta S_{QCD}}{\delta s(x)^{ij}}...\rangle \;\; = \;\; -\frac{\delta}{\delta s(x)^{ij}}...W[s]^{QCD} \;, \qquad (7.1)$$

which should be equal to the equivalent matrix in the EFT picture,

$$\langle ...\bar{q}_i(x)q_j(x)...\rangle \;\; = \;\; -\langle ...\frac{\delta S_{EFT}}{\delta s(x)^{ij}}...\rangle \;\; = \;\; -\frac{\delta}{\delta s(x)^{ij}}...W[s]^{EFT} \;, \qquad (7.2)$$

where S_{QCD} and S_{eff} are respectively the QCD and the EFT actions. The external fields $s(x)^{ij}$ were introduced in the χPT construction, in Eq. (3.15).

In this work only two scalar currents are studied: An octet scalar current $\sqrt{3}\ \overline{\Psi}\lambda^8\Psi = (\bar{u}u + \bar{d}d - 2\bar{s}s)$, and a singlet scalar current $\overline{\Psi}\Psi = (\bar{u}u + \bar{d}d + \bar{s}s)$. These are the $J = I = 0$ currents studied by Gasser and Leutwyler in their work on two-pNGB form factors [40]. When the outgoing pseudo-scalars are set on their mass shell the form-factors can be described by a single scalar function of the total momentum square q^2:

$$
\begin{aligned}
\langle\, P(p_1)\, \overline{P}'(p_2)|\bar{u}u + \bar{d}d - 2\bar{s}s\,|0\rangle &= \delta^{PP'}\mathcal{F}^{(8)}_{PP}(q^2) \quad, \\
\langle\, P(p_1)\, \overline{P}'(p_2)|\bar{u}u + \bar{d}d + \bar{s}s\,|0\rangle &= \delta^{PP'}\mathcal{F}^{(0)}_{PP}(q^2) \quad,
\end{aligned}
\qquad (7.3)
$$

with $q = p_1 + p_2$ and $P\overline{P}'$ stands for a pair of Goldstones which in $SU(3)$ may be $\pi\pi \equiv \pi^+\pi^-, \pi^0\pi^0$, $K\overline{K} \equiv K^+K^-, K^0\overline{K}^0$ and $\eta_8\eta_8$.

The value of $\mathcal{F}^{(n)}_{PP}(q^2)$ at $q^2 = 0$ can be factorized out and the SFF dynamics is provided by the functions $f(s)$ and $\widetilde{f}(s)$:

$$
\begin{aligned}
\mathcal{F}^{(8)}_{PP}(s) &= \mathcal{F}^{(8)}_{PP}(0)[1 + f(s)_{PP}] \quad, \\
\mathcal{F}^{(0)}_{PP}(s) &= \mathcal{F}^{(0)}_{PP}(0)[1 + f(s)_{PP} + \widetilde{f}(s)_{PP}] \quad.
\end{aligned}
\qquad (7.4)
$$

The function $\widetilde{f}(s)$ points out the difference between the octet and the singlet SFF and vanishes in the large-N_C and $SU(3)$ limits.

The normalization $\mathcal{F}(0)$ does not really carry information about the dynamics of the SFF, since it depends on the pseudo-scalar mass and it is given by the Feynman-Hellman theorem [89]. As a result of this, the expectation value for a mass eigenstate of the derivative of the hamiltonian is equal to the the derivative of the expectation value of the hamiltonian. In the SFF case one has:

$$\frac{\partial m_P^2}{\partial m_i} = \langle\, P|\bar{q}_i q_i|P\,\rangle \quad, \qquad (7.5)$$

Being $|P\rangle$ any pseudo-scalar state on its mass-shell. This means that for the octet and singlet components the normalizations are:

$$\mathcal{F}^{(8)}_{PP}(0) \;=\; \langle P|\bar{u}u + \bar{d}d - 2\bar{s}s|P\rangle \;=\; \left(\frac{\partial}{\partial m_u} + \frac{\partial}{\partial m_d} - 2\frac{\partial}{\partial m_s}\right) m_P^2 \quad, \quad (7.6)$$

$$\mathcal{F}^{(0)}_{PP}(0) \;=\; \langle P|\bar{u}u + \bar{d}d + \bar{s}s|P\rangle \;=\; \left(\frac{\partial}{\partial m_u} + \frac{\partial}{\partial m_d} + \frac{\partial}{\partial m_s}\right) m_P^2 \quad. \quad (7.7)$$

7.2 Pion SFF in χPT

At the lowest order in the chiral counting $-\mathcal{O}(p^2)-$ both form-factors coincide and are merely a constant:

$$\mathcal{F}^{(8)}_{\pi\pi}(q^2) \;=\; \mathcal{F}^{(0)}_{\pi\pi}(q^2) \;=\; 2B_0 \,. \tag{7.8}$$

In the $SU(3)$ case, at the NLO $-\mathcal{O}(p^4)-$, the matrix elements for these currents become a bit more complex [40]:

$$
\begin{aligned}
f(s)_{\pi\pi} \;&=\; \frac{1}{2F^2}(2s - m_\pi^2)\bar{J}_{\pi\pi}(s) - \frac{s}{4F^2}\bar{J}_{KK}(s) - \frac{m_\pi^2}{6F^2}\bar{J}_{\eta\eta}(s) \\
&\quad + \frac{4s}{F^2}\left\{ L_5^r(\mu) - \frac{1}{256\pi^2}\left(4\ln\frac{m_\pi^2}{\mu^2} - \ln\frac{m_K^2}{\mu^2} + 3\right)\right\} \quad,
\end{aligned}
$$

$$
\tilde{f}(s)_{\pi\pi} \;=\; \frac{3s}{4F^2}\bar{J}_{KK}(s) + \frac{m_\pi^2}{3F^2}\bar{J}_{\eta\eta}(s) + \frac{12s}{F^2}\left\{ L_4^r(\mu) - \frac{1}{256\pi^2}\left(\ln\frac{m_K^2}{\mu^2} + 1\right)\right\} \quad.
\tag{7.9}
$$

The value of the SFF at $q^2 = 0$ was factorized out.

In the $SU(2)$ case there is only one current with $I = 0$, $(\bar{u}u + \bar{d}d)$, and the SFF takes a simpler form:

$$
\begin{aligned}
\mathcal{F}(s)_{\pi\pi} \;&=\; \mathcal{F}(0)_{\pi\pi}\left[1 + \frac{1}{2F^2}(2s - m_\pi^2)\bar{J}_{\pi\pi}(s) + \frac{s}{16\pi^2 F^2}(\bar{\ell}_4 - 1)\right] \;= \\
&=\; \mathcal{F}(0)_{\pi\pi}\left[1 + \frac{1}{2F^2}(2s - m_\pi^2)\bar{J}_{\pi\pi}(s) + \frac{\ell_4^r(\mu)\, s}{F^2} - \frac{s}{16\pi^2 F^2}\left(\ln\frac{m_\pi^2}{\mu^2} + 1\right)\right] \quad,
\end{aligned}
\tag{7.10}
$$

with $\bar{\ell}_4 = 16\pi^2 \ell_4^r(\mu) - \ln\frac{m_\pi^2}{\mu^2}$ and the normalization at $s = 0$,

$$\mathcal{F}(0)_{\pi\pi} \;=\; 2B_0\left[1 - \frac{m_\pi^2}{16\pi^2 F^2}(\bar{\ell}_3 - \frac{1}{2})\right] \quad. \tag{7.11}$$

These results may be related with the $SU(3)$ one in the $m_u, m_d \ll m_s$ limit through the relations $\ell_4^r(\mu) = 4L_4^r(\mu) + 4L_5^r(\mu) - \frac{1}{64\pi^2}(\ln(\overline{m}_K^2/\mu^2) + 1)$ [9] [Appendix D], with $\overline{m}_K^2 = B_0 m_s$. In addition it is possible to compute the massless limit, getting

$$\mathcal{F}(q^2)_{\pi\pi} \;=\; \mathcal{F}(0)_{\pi\pi}\left[1 + \frac{\ell_4^r(\mu)\, q^2}{F^2} + \frac{q^2}{16\pi^2 F^2}\left\{1 - \ln\left(-\frac{q^2}{\mu^2}\right)\right\}\right] \quad. \tag{7.12}$$

When going to the next order in the chiral expansion $-\mathcal{O}(p^6)-$ the expression becomes more and more complicated and contains new low energy constants. The result for $SU(2)$ is [17]:

$$
\begin{aligned}
\mathcal{F}(x)_{\pi\pi} \;=\;& \mathcal{F}(0)_{\pi\pi} \left\{ 1 + \left(\tfrac{m_\pi^2}{F^2}\right) \left(\tfrac{1}{2}(2x-1)\bar{J}(x) + x(\ell_4^r - H - \tfrac{1}{N})\right) \right. \\
& \left. + \left(\tfrac{m_\pi^2}{F^2}\right)^2 \left(P_S(x) + U_S(x)\right) \right\} \quad ,
\end{aligned}
\tag{7.13}
$$

where $x \equiv q^2/m_\pi^2$ and the $\mathcal{O}(p^6)$ contributions are in the terms $P_S(x) + U_S(x)$, and in the normalization at $q^2 = 0$. The polynomial part is:

$$
\begin{aligned}
P_S(x) \;=\;& x^2 \left[-\tfrac{11}{12}k_1 - \tfrac{7}{12}k_2 - \tfrac{1}{4}k_4 \right. \\
& \left. + \tfrac{1}{N}\left(\tfrac{7}{1728} - \tfrac{32}{9}\ell_1^r - \tfrac{19}{9}\ell_2^r - \ell_4^r + \tfrac{85}{36}H\right) + \tfrac{1817}{1296}\tfrac{1}{N^2} + r_{S3}^r \right] \\
& + x\left[\tfrac{31}{6}k_1 + \tfrac{17}{6}k_2 - k_4 + \tfrac{1}{N}\left(-\tfrac{11}{864} + \tfrac{110}{9}\ell_1^r + \tfrac{40}{9}\ell_2^r - 2\ell_4^r + \tfrac{11}{9}H\right) \right. \\
& \left. - \tfrac{20}{81}\tfrac{1}{N^2} + 2(\ell_4^r)^2 - 4\ell_3^r\ell_4^r + r_{S2}^r \right] \quad ,
\end{aligned}
\tag{7.14}
$$

an the $\mathcal{O}(p^6)$ dispersive contribution is

$$
\begin{aligned}
U_S(x) \;=\;& \bar{J}(x)\left[\tfrac{1}{3}\ell_1^r\left(11x^2 - 40x + 44\right) + \tfrac{1}{3}\ell_2^r\left(7x^2 - 20x + 28\right) \right. \\
& + 5\ell_3^r + \ell_4^r\left(x^2 + \tfrac{3}{2}x - 1\right) + \tfrac{1}{18}H\left(-43x^2 + 53x - \tfrac{119}{2}\right) \\
& \left. + \tfrac{1}{N}\left(\tfrac{29}{12}x^2 - \tfrac{61}{9}x + \tfrac{391}{36}\right) \right] + \tfrac{3}{4}K_1(x) + K_2(x)\left(\tfrac{43}{36}x^2 - \tfrac{4}{3}x + \tfrac{1}{4}\right) \\
& + K_3(x)\left(\tfrac{1}{3}x - \tfrac{25}{18}\right) \quad ,
\end{aligned}
\tag{7.15}
$$

with the same definitions as those given for the VFF calculation in χPT at $\mathcal{O}(p^6)$.

χPT yields a suitable description at low energies but stops being reliable for $\sqrt{s} \gtrsim 600$ MeV. Actually the convergence in the scalar channel is much worse and the range of validity of χPT is even smaller.

In order to study the region beyond the range of validity of χPT one has to consider a different counting and to handle some new possible degrees of freedom, as scalar resonances.

7.3   Pion SFF in RχT: Limit $N_C \to \infty$

There are still many open questions and controversies about the scalar channel. Although a complete analysis of the scalar sector $\mathcal{L}_{2\chi} + \mathcal{L}_S$ in the RχT lagrangian

has not yet been performed –as it was done for the vector sector–, former analyses have shown that it provides fair results and that one fulfills the QCD short distance constraints for the SFF at LO in $1/N_C$ [22]. The necessity of extra terms for other matrix elements has not yet been studied.

The starting point will be again the RχT lagrangian at LO in $1/N_C$ which was developed in Chapter 4.

The high energy behaviour of the pion SFF is the same as the VFF; it vanishes at $q^2 \to \infty$, obeying an unsubtracted dispersion relation [50]. As it was done before for the vector sector analysis we will not handle the chiral counting any longer and the $1/N_C$ counting will be the considered one.

At LO in $1/N_C$ the relevant diagrams are the tree-level ones. These diagrams are the same as those in Fig. (5.2), but with a scalar resonance (octet or singlet) instead of the $\rho(770)$:

$$\mathcal{F}_{\pi\pi}^{(8)}(q^2) \quad = \mathcal{F}_{\pi\pi}^{(0)}(q^2) = \quad 2B_0 \left[1 + \frac{4c_m}{f^2} \frac{[c_d q^2 + 2(c_m - c_d)m_\pi^2]}{M_S^2 - q^2} \right] \quad . \tag{7.16}$$

One may factor out the normalization at $q^2 = 0$:

$$\mathcal{F}(q^2)_{\pi\pi} \quad = \quad \mathcal{F}(0)_{\pi\pi} \frac{M_S^2}{M_S^2 - q^2} \left[1 + q^2 \frac{\dfrac{4c_d c_m}{F^2} - 1}{M_S^2 + \dfrac{8c_m(c_m - c_d)}{F^2} m_\pi^2} \right] \quad , \tag{7.17}$$

with

$$\mathcal{F}(0)_{\pi\pi} \quad = \quad 2B_0 \left(1 + \frac{8c_m(c_m - c_d)}{F^2} \frac{m_\pi^2}{M_S^2} \right) \quad , \tag{7.18}$$

where the singlet and octet couplings coincide, this is, $\widetilde{c}_d = c_d/\sqrt{3}$, $\widetilde{c}_m = c_m/\sqrt{3}$ and $M_S = M_{S_1}$ in the notation of Ref. [19]. As it was expected, the octet and singlet form factors are equal in the large N_C limit.

When requiring that these expressions fulfill the QCD short distance constraints $\mathcal{F}(q^2) \stackrel{q^2 \to \infty}{\longrightarrow} 0$, a relation between the couplings arises in the limit $N_C \to \infty$:

$$1 - \frac{4c_m c_d}{F^2} \quad = \quad 0 \,, \tag{7.19}$$

completely analogous to the relation $1 - F_V G_V/F^2 = 0$ in the VFF case.

Thus, in the large N_C limit the SFF takes the familiar monopolar expression from vector meson dominance:

$$\mathcal{F}(q^2)_{\pi\pi} \quad = \quad \mathcal{F}(0)_{\pi\pi} \frac{M_S^2}{M_S^2 - q^2} \quad . \tag{7.20}$$

At this point one must consider one more contribution that has not been included till now, the scalar tadpole. A deeper inspection of the RχT lagrangian

shows that the chiral symmetry allows a linear term in the scalar field and it is proportional to the external fields in χ. When evaluating χ, one can see that this tadpole is proportional to the quark masses. It becomes relevant in the analysis of the strangeness-changing SFF to $K\pi$ and $K\eta_8$ [22]. The short distance behaviour gets modified and a new relation appears at LO in $1/N_C$:

$$c_d = c_m \xrightarrow{\;\frac{4c_d c_m}{F^2} = 1\;} c_d = c_m = F/2 \simeq 46.2 \text{ MeV} . \qquad (7.21)$$

This theoretical prediction agrees well with the experimental result $c_d = c_m \simeq 45.4$ MeV [76], obtained from a fit to $K\pi$ data under the restriction $c_d = c_m$. That work studied the channel with $(I = \frac{1}{2}, J = 0)$, getting for the corresponding scalar resonance $K_0^*(1430)$ the mass $M_{K_0^*} = 1.4$ GeV. This resonance is the lightest one with that quantum numbers and it is part of a scalar nonet with masses of that order. Nonetheless, in the last years there have been some works about the possible existence of a very broad and light resonance with those quantum numbers, the resonance κ. This point is still not clear at all and it is as controversial as it happens with the existence of the σ resonance.

In general the scalar tadpole influence is small at energies around the mass of the resonances since its contribution is proportional to the squared pNGB mass divided the squared scalar resonance mass. Nevertheless, in a next section I will study how it can provide sizable effects and how it explains the dependence of the pion decay constant on the quark masses observed in the Lattice simulations [101]. In that analysis one will also see that when expanding in powers of the pNGB mass this tadpole provides the $\mathcal{O}(p^4)$ modification to the pNGB mass.

When the energy of the processes decreases one expects to recover χPT. From the former calculation at LO in $1/N_C$ given in Eq. (7.16) (and particularized for given couplings in Eq. (7.20)) one recovers the LO in $1/N_C$ result in χPT, which is provided by the tree-level processes. Thus, the heavy resonance exchange is going to yield the bulk of the χPT low energy couplings when expanding in powers of the momenta:

$$\mathcal{F}(q^2)_{\pi\pi} = \mathcal{F}(0)_{\pi\pi} \left\{ 1 + \frac{4c_d c_m}{F^2} \frac{q^2}{M_S^2} + \mathcal{O}\left(\frac{q^4}{M_S^4}, \frac{q^2 m_\pi^2}{M_S^4} \right) \right\} , \qquad (7.22)$$

which compared with the LO in $1/N_C$ expression for χPT,

$$\mathcal{F}_{\pi\pi}^{(8)}(q^2) = \mathcal{F}_{\pi\pi}^{(8)}(0) \left\{ 1 + \frac{4L_5 q^2}{F^2} + \mathcal{O}\left(\frac{q^4}{F^4}, \frac{q^2 m_\pi^2}{M_S^4} \right) \right\} ,$$

$$\mathcal{F}_{\pi\pi}^{(0)}(q^2) = \mathcal{F}_{\pi\pi}^{(0)}(0) \left\{ 1 + \frac{(4L_5 + 12L_4)q^2}{F^2} + \mathcal{O}\left(\frac{q^4}{F^4}, \frac{q^2 m_\pi^2}{M_S^4} \right) \right\} , \qquad (7.23)$$

provides for the low energy couplings the LO in $1/N_C$ values

$$L_5 = \frac{c_d c_m}{M_S^2} = \frac{F^2}{4M_S^2} , \qquad\qquad L_4 = 0 , \qquad (7.24)$$

where the QCD short distance constraints have been employed in the third term, i.e., $c_d = c_m = F/2$. When taking the pion decay constant $F \simeq F_\pi = 92.4$ MeV and the mass $M_S = 1$ GeV one gets the theoretical predictions

$$L_5 = 2.1 \cdot 10^{-3} + \mathcal{O}\left(\frac{1}{N_C}\right), \qquad L_4 = 0 + \mathcal{O}\left(\frac{1}{N_C}\right). \qquad (7.25)$$

Notice that at LO in $1/N_C$ the observables are given by tree level processes and there is no renormalization scale. The running on μ would be a next-to-leading order effect and would provide subleading corrections to the L_i couplings, naively of the order $\sim \frac{1}{N_C} \times L_i$.

One can compare this prediction of RχT with the experimental results from χPT. In Appendix D it is possible to find a summary of the experimental values of the χPT couplings. The values of L_4 and L_5 are obtained from the pion and kaon decay constants:

$$F_\pi = F\left\{1 - 2\mu_\pi - \mu_K + \frac{4m_\pi^2}{F^2}L_5^r(\mu) + \frac{(8m_K^2 + 4m_\pi^2)}{F^2}L_4^r(\mu) + \mathcal{O}\left(\frac{m_P^4}{F^4}\right)\right\},$$

$$F_K = F\left\{1 - \frac{3}{4}\mu_\pi - \frac{3}{2}\mu_K - \frac{3}{4}\mu_{\eta 8} + \frac{4m_K^2}{F^2}L_5^r(\mu) + \frac{(8m_K^2 + 4m_\pi^2)}{F^2}L_4^r(\mu) + \right.$$
$$\left. + \mathcal{O}\left(\frac{m_P^4}{F^4}\right)\right\},$$

$$(7.26)$$

with $\mu_P \equiv \frac{m_P^2}{16\pi^2}\ln\frac{m_P^2}{\mu^2}$. This provides the experimental values [6]:

$$L_5^r(\mu) = (1.4 \pm 0.5) \cdot 10^{-3}, \qquad L_4^r(\mu) = (-0.3 \pm 0.5) \cdot 10^{-3}, \qquad (7.27)$$

for $\mu = 770$ MeV, and showing a great agreement with the theoretical predictions from RχT. The largest uncertainty comes from the scalar mass. Although the spectrum of the first multiplet of scalars is not clear yet, there are many hints pointing out that it must have a mass around the order $M_S \simeq 1$ GeV [32, 22, 104]. However, a slight larger mass of $M_S = 1.2$ GeV, would decrease the prediction for L_5 to $L_5 = 1.5 \cdot 10^{-3}$. In addition one must also have into account the subleading in $1/N_C$ scale corrections. Since the numerical value of L_5 is relatively small compared to other χPT couplings, as the vector channel coupling $L_9 \sim 7 \cdot 10^{-3}$ of the VFF, the radiative corrections seem to be larger in this case.

Thus, the RχT expression at LO in $1/N_C$, from Eq. (7.20), seems to give the proper description at low energies matching with the one prescribed by χPT. However, it is phenomenologically well known that the final state interactions are very important in the scalar channel [35, 62]. The radiative corrections are now much bigger than in the vector case. Therefore the bare scalar propagator suffers larger corrections and there appears a resonance structure with a broad width. Hence, one must perform a Dyson-Schwinger summation similar to the one made in the VFF.

7.4   Effective vertices resummation: Scalar resonance width

In order to obtain the shift on the pole of the scalar resonance due to the re-scattering, we will follow the same procedure as in the VFF analysis near the resonance peak.

At LO in $1/N_C$ the SFF has a real pole at $q^2 = M_S^2$. The pions are produced at tree-level either by direct production from a $\mathcal{L}_{2\chi}$ vertex or through an intermediate resonance. The next step is to compute the diagrams resulting from adding a 1PI block containing as many loops as needed for a given order in the self-energy. At LO this would be a 1PI block with just one-loop diagrams. This will provide the shift of the resonance pole at that order. This 1PI block is closed again into an effective scattering vertex as the one in Fig. (5.5). This effective vertex contains not only the re-scattering through an intermediate resonance but also through a local scattering vertex form $\mathcal{L}_{2\chi}$. For the scalar $I = 0$ case one must consider as well that there are two resonances, the octet and the singlet one, to construct the effective scattering vertex.

After that one would add one more 1PI block and an effective scattering vertex. Repeating the process for any number of 1PI block insertions one would obtain a geometrical series that can be resummed and which finally is going to modify the resonance propagator.

The $I = 0$ case has a peculiarity that was not present in the $I = 1$ analysis done for the vectors. Since the $U(3)$ anomaly is not only broken at the NLO in $1/N_C$ but explicitly through the quark masses, there is going to be a mixing between the octet and the singlet channels. Suppose that for instance the octet SFF is analysed. At tree level just the octet resonance can be generated. However when computing the NLO correction one has 1PI block insertions. Thus, the octet resonance can generate a pair of pNGB that joins again to produce a singlet resonance. In the next calculation we will see that this flip is proportional to the explicit $U(3)_V$ symmetry breaking parameter $\Delta_{K\pi} \equiv (m_K^2 - m_\pi^2)$. In the limit of $N_C \to \infty$ and $\Delta_{K\pi} \to 0$, this interference disappears.

In the $m_u = m_d$ isospin limit the effective current vertices show the momentum structure

$$S_0^{(P)}(q^2) \;=\; \mathcal{F}_0^{(P)}(q^2) \;+\; \mathcal{B}_0^{(P)}(q^2)\,\{p_1 p_2 - q^2/2 + m_P^2\}\,, \tag{7.28}$$

where m_P is the outgoing pseudo-scalar mass, p_1 and p_2 the pNGB momenta and $\mathcal{F}_0^{(P)}(q^2)$ is the on-shell tree-level SFF. The superscript (P) stands here for the type of pNGB produced. Similarly to the vector sector, here the second term, with $\mathcal{B}_0^{(P)}(q^2)$ vanishes when both outgoing pseudo-scalars become on-shell due to the inverse propagator structure $p_1 p_2 - \frac{q^2}{2} + m_P^2 \;=\; -\frac{1}{2}[p_1^2 - m_P^2] - \frac{1}{2}[p_2^2 - m_P^2]$. The three available channels of two pNGB with $I = 0$ $-\pi\pi$, $K\overline{K}$, $\eta_8\eta_8-$ may be put together in that ordering within the three-vector $\vec{S}$, $\vec{\mathcal{F}}_0$ and $\vec{\mathcal{B}}_0$.

Thus, the RχT lagrangian yields the values:

$$\vec{\mathcal{F}}_0^{(8)}(q^2)^{I,J} = 2B_0 \left\{1 + \frac{q^2}{M_8^2 - q^2}\right\} \begin{pmatrix} \sqrt{3} \\ -1 \\ -1 \end{pmatrix} + 2B_0 \frac{8\Delta_{K\pi}/3}{M_8^2 - q^2} \begin{pmatrix} 0 \\ 0 \\ -1 \end{pmatrix},$$

$$\vec{\mathcal{B}}_0^{(8)}(q^2)^{I,J} = 2B_0 \frac{2}{M_8^2 - q^2} \begin{pmatrix} \sqrt{3} \\ -1 \\ -1 \end{pmatrix},$$

$$(7.29)$$

for the octet current, with $\Delta_{K\pi} \equiv (m_K^2 - m_\pi^2)$, and

$$\vec{\mathcal{F}}_0^{(1)}(q^2)^{I,J} = 2B_0 \left\{1 + \frac{q^2}{M_1^2 - q^2}\right\} \begin{pmatrix} \sqrt{3} \\ 2 \\ 1 \end{pmatrix},$$

$$\vec{\mathcal{B}}_0^{(1)}(q^2)^{I,J} = 2B_0 \frac{2}{M_1^2 - q^2} \begin{pmatrix} \sqrt{3} \\ 2 \\ 1 \end{pmatrix},$$

$$(7.30)$$

for the singlet. In addition, the on-shell and off-shell components may be put to-gether in the vector $\vec{S}_0 \equiv \begin{pmatrix} \vec{\mathcal{F}}_0 \\ \vec{\mathcal{B}}_0 \end{pmatrix}$. The superscript I, J will be attached to the form-factor functions when the final states have definite isospin. In this case the isospin basis for the states has been preferred to the usual charge basis since the interference between the octet and the singlet state appears in a clearer and more crystal way. Thus, for $U(3)$ there are three $I = J = 0$ states [97]:

$$|\mathbf{8_1}\rangle^{0(0)} = \sqrt{\frac{3}{5}}|\pi\pi\rangle^{0(0)} - \sqrt{\frac{1}{5}}|K\overline{K}\rangle^{0(0)} - \sqrt{\frac{1}{5}}|\eta\eta\rangle^{0(0)} = \frac{1}{\sqrt{5}}\begin{pmatrix} \sqrt{3} \\ -1 \\ -1 \end{pmatrix},$$

$$|\mathbf{1}\rangle^{0(0)} = \sqrt{\frac{3}{8}}|\pi\pi\rangle^{0(0)} + \sqrt{\frac{1}{2}}|K\overline{K}\rangle^{0(0)} + \sqrt{\frac{1}{8}}|\eta\eta\rangle^{0(0)} = \frac{1}{\sqrt{8}}\begin{pmatrix} \sqrt{3} \\ 2 \\ 1 \end{pmatrix},$$

$$|\mathbf{27}\rangle^{0(0)} = \sqrt{\frac{3}{120}}|\pi\pi\rangle^{0(0)} - \frac{6}{\sqrt{120}}|K\overline{K}\rangle^{0(0)} + \frac{9}{\sqrt{120}}|\eta\eta\rangle^{0(0)} = \frac{1}{\sqrt{120}}\begin{pmatrix} \sqrt{3} \\ -6 \\ 9 \end{pmatrix},$$

$$(7.31)$$

with the $|P(p_1)\,\overline{P}(p_2)\,\rangle^{0(0)}$ isospin states related to the charge basis states through

$$|\pi\pi\,\rangle^{0(0)} \quad = \frac{1}{\sqrt{3}}\left\{|\pi^+\pi^-\,\rangle + |\pi^-\pi^+\,\rangle + |\pi^0\pi^0\,\rangle\right\},$$

$$|K\overline{K}\,\rangle^{0(0)} \quad = \frac{1}{2}\left\{|K^0\overline{K}^0\,\rangle + |\overline{K}^0 K^0\,\rangle + |K^+K^-\,\rangle + |K^-K^+\,\rangle\right\}, \qquad (7.32)$$

$$|\eta\eta\,\rangle^{0(0)} \quad = |\eta\eta\,\rangle,$$

where in the right-hand-side terms the first and second particles have momentum p_1 and p_2 respectively. One may easily transform the form-factor in the $U(3)$ basis, $\vec{\mathcal{F}}(q^2)^{I,J}$, into that in the charge basis, $\vec{\mathcal{F}}(q^2)$:

$$\begin{pmatrix} \mathcal{F}(q^2)_{\pi\pi} \\[2mm] \mathcal{F}(q^2)_{K\overline{K}} \\[2mm] \mathcal{F}(q^2)_{\eta_8\eta_8} \end{pmatrix} = \begin{pmatrix} \frac{1}{\sqrt{3}} & 0 & 0 \\[2mm] 0 & \frac{1}{2} & 0 \\[2mm] 0 & 0 & 1 \end{pmatrix} \begin{pmatrix} \mathcal{F}(q^2)^{I,J}_{\pi\pi} \\[2mm] \mathcal{F}(q^2)^{I,J}_{K\overline{K}} \\[2mm] \mathcal{F}(q^2)^{I,J}_{\eta_8\eta_8} \end{pmatrix}. \qquad (7.33)$$

One can demonstrate by induction that when a successive number of N two-pseudo-scalar loops and effective scattering vertices are connected, the momentum structure in the effective current vertex $S_0(q^2)$ still remains:

$$\vec{S}_N(q^2) \;=\; \vec{\mathcal{F}}_N(q^2) \;+\; \vec{\mathcal{B}}_N(q^2)\,\{p_1 p_2 - q^2/2 + m_P^2\}. \qquad (7.34)$$

However the recurrence from N to $N+1$ couples the on-shell and the off-shell parts, such that $\mathcal{F}^{(i)}_{N+1} = \sum_j \mathcal{M}^{ij}_A \mathcal{F}^{(j)}_n + \sum_j \mathcal{M}^{ij}_B \mathcal{B}^{(j)}_N$ and also that $\mathcal{B}^{(i)}_{N+1} = \sum_j \mathcal{M}^{ij}_C \mathcal{F}^{(j)}_N + \sum_j \mathcal{M}^{ij}_D \mathcal{B}^{(j)}_N$, which can be written in a matrix notation as:

$$\vec{S}_{N+1} = \mathcal{M}\vec{S}_N = \begin{pmatrix} \mathcal{M}_A & \mathcal{M}_B \\[2mm] \mathcal{M}_C & \mathcal{M}_D \end{pmatrix} \vec{S}_N, \qquad (7.35)$$

where $\mathcal{M}_A$, $\mathcal{M}_B$, $\mathcal{M}_C$, $\mathcal{M}_D$ are 3×3 matrices, all of them proportional to $\frac{1}{F^2}$ and therefore $\mathcal{O}(\frac{1}{N_C})$. They are given by

$$\mathcal{M} \;=\; 16\pi \begin{pmatrix} T^{LO} & T^{LO}_B \\[2mm] T^{LO}_C & T^{LO}_D \end{pmatrix} \cdot \begin{pmatrix} J & -A \\[2mm] -A & \frac{q^2}{2}A \end{pmatrix}, \qquad (7.36)$$

where one finds the 3×3 diagonal matrices $A = \mathrm{diag}(A(m_\pi^2),\ A(m_K^2),\ A(m_\eta^2))$ and $B_0 = \mathrm{diag}(B_0(q^2, m_\pi^2, m_\pi^2),\ B_0(q^2, m_K^2, m_K^2),\ B_0(q^2, m_\eta^2, m_\eta^2))$, composed by the one- and two-propagator Feynman integrals given in Appendix A. The 3×3 sub-matrices T^{LO} and $T^{LO}_{B,C,D}$ are defined from the off-shell expression for the $I=0$ scattering

amplitude at LO in $1/N_C$. In this resummation only the scattering through local $\mathcal{L}_{2\chi}$ vertices and scalar resonances in the s-channel will be considered. The scattering amplitude shows then the momentum structure

$$
\begin{aligned}
\mathcal{T}^{LO} = \quad & T^{LO} \; + \; T_B^{LO} \left[p_1 p_2 - \tfrac{q^2}{2} - m_P^2 \right] + T_C^{LO} \left[p_1' p_2' - \tfrac{q^2}{2} - m_P'^2 \right] + \\
& + T_D^{LO} \left[p_1 p_2 - \tfrac{q^2}{2} - m_P^2 \right] \cdot \left[p_1' p_2' - \tfrac{q^2}{2} - m_P'^2 \right] \quad,
\end{aligned}
\tag{7.37}
$$

with p_1, p_2 the incoming momenta and p_1', p_2' the outgoing momenta. The terms with $T_{B,C,D}^{LO}$ only contribute off-shell, and depend on the realization of the chiral group. But later on we will see that at the order considered here they do not influence the final result when the out-going particles are on-shell.

The value for the on-shell amplitude T^{LO} can be found in Appendix F. Moreover the only relevant piece in the recurrence matrix $\mathcal{M}$ is going to be the submatrix

$$
\mathcal{M}_A \; = T^{LO} \cdot B_0 \; - \; T_B^{LO} \cdot A \quad.
\tag{7.38}
$$

This recurrence implies that the SFF at a given number of loops is given by

$$
\vec{S}_{N+1}^{(8)} \; = \; \mathcal{M} \vec{S}_N^{(8)} \; = \; \dots \; = \mathcal{M}^{N+1} \vec{S}_0^{(8)} \quad.
\tag{7.39}
$$

Here and in the following the type-of-current label –octet or singlet– will be omitted.

In order to regularize the real pole of the propagator at LO in $1/N_C$ we must perform the Dyson-Schwinger summation to all numbers of loops:

$$
\vec{S} \; = \; \sum_{N=0}^{\infty} \vec{S}_N \; = \; \sum_{N=0}^{\infty} \mathcal{M}^N \vec{S}_0 \; = \; (1 - \mathcal{M})^{-1} \vec{S}_0 \,.
\tag{7.40}
$$

Using the formula for inverse $2n \times 2n$ matrices which can be found in Appendix E, the resummed on-shell SFF $\vec{\mathcal{F}}$ is then expressed as

$$
\vec{\mathcal{F}} = [1 - \mathcal{M}_A - \mathcal{M}_B (1 - \mathcal{M}_D)^{-1} \mathcal{M}_C]^{-1} [\vec{\mathcal{F}}_0 + \mathcal{M}_B (1 - \mathcal{M}_D) \vec{\mathcal{B}}_0],
\tag{7.41}
$$

with the on-shell tree-level SFF $\vec{\mathcal{F}}_0$ and the off-shell tree-level contributions $\vec{\mathcal{B}}_0$, introduced before in Eqs. (7.29) and (7.30). Notice that either $\mathcal{M}_B$ and $\mathcal{M}_D$ are purely real and only $\mathcal{M}_A$ contains absorptive contributions. The scattering vertices in Eq. (7.38) are given just at LO in $1/N_C$, because just the LO contributions to the imaginary parts were sought.

The NLO terms in the former Eq. (7.41) are of the same order than the NLO contributions in $1/N_C$ of $\mathcal{M}_A$ and $\mathcal{F}_0$:

$$
\begin{aligned}
\mathcal{M}_A \sim \mathcal{O}\left(\tfrac{1}{N_C}\right) \qquad &\gg \qquad \mathcal{M}_B (1 - \mathcal{M}_D)^{-1} \mathcal{M}_C \sim \mathcal{O}\left(\tfrac{1}{N_C^2}\right), \\
\vec{\mathcal{F}}_0 \sim \mathcal{O}(1) \qquad &\gg \qquad \mathcal{M}_B (1 - \mathcal{M}_D) \vec{\mathcal{B}}_0 \sim \mathcal{O}\left(\tfrac{1}{N_C}\right),
\end{aligned}
\tag{7.42}
$$

Therefore, keeping these subleading terms is inconsistent and the Dyson-Schwinger summation becomes, up to the NLO order,

$$\vec{\mathcal{F}}(q^2) \;=\; [1 \,-\, \mathcal{M}_A(q^2)]^{-1}\, \vec{\mathcal{F}}_0(q^2)\,. \tag{7.43}$$

About this point someone could argue that one should keep each independent SFF $\mathcal{F}^{(P)}$ up to the considered order. The inverse matrix is going to produce for each one the factor $\frac{1}{\det(1-\mathcal{M}_A)}$, which contains a denominator with terms $\mathcal{O}(1)$ and $\mathcal{O}\left(\frac{1}{N_C}\right)$, and also other subleading terms $\mathcal{O}\left(\frac{1}{N_C^2}\right)$ and so on. Why not then cutting this denominator at $\mathcal{O}\left(\frac{1}{N_C}\right)$ and dropping off the subleading terms? The reason why this denominator cannot be modified at this level of the calculation is that exact unitarity forbids that kind of manipulations. When one studies a concrete element of the T-matrix the perturbative expansion cannot be cut independently in each matrix element because there are subtle relations among them. What one is allowed to do, is what has been done in Eq. (7.43): The matrix $\mathcal{M}_A$ has a whole series of higher order corrections and one is interested in just its value up to a given order in $1/N_C$, then it is right to cut the whole matrix $\mathcal{M}_A$ at that order before computing each individual matrix element through the inverse matrix $(1 - \mathcal{M}_A)^{-1}$. Otherwise unitarity breaks down and one gets such wrong results as a negative imaginary part for the $\pi\pi$ scattering.

The bare poles of the octet and singlet resonance propagators in $\vec{\mathcal{F}}_0$ become regularised trough the inverse matrix $(1 - \mathcal{M}_A)^{-1}$ in Eq. (7.43), as it happened for the VFF. However as there are two scalar resonances we cannot perform a clear separation of each resonance width. Since there is not a perfect $U(3)$ symmetry, the singlet state may flip to octet and viceversa.

When calculating the correlator of two scalar currents and the partial wave scattering amplitude one sees that they get the same final state interaction through the $(1 - \mathcal{M})^{-1}$ matrix, mixing the on-shell and off-shell intermediate states, and providing the same poles to all the processes. This re-scattering process only depends on the intermediate scattering vertices and on the intermediate two-particle loop. As one evaluates the processes with their final pseudo-scalars on-shell it may be demostrated that, up to the considered order, the relevant pole information from $(1 - \mathcal{M})^{-1}$ is within the sub-matrix $(1 - \mathcal{M}_A)^{-1}$. The absorptive contributions come just from $\mathcal{M}_A$, and they only depend on the on-shell scattering vertices, which therefore do not depend on the realisation of the chiral group. Here we obtain the one loop absorptive contribution, that is, the LO in $1/N_C$ contribution to the imaginary part of the propagator. Nevertheless, the real part is incomplete and ultraviolet divergent. The determination of these infinite pieces will be through a matching with χPT as it was done for the VFF [27, 28, 105].

7.5   Calculation in $n_f = 2$

For simplicity the calculation has been done at first with the contributions from pion loops since kaon and η loops will be quite suppressed at energies below the $K\overline{K}$ threshold production, $s \lesssim 4m_K^2 \simeq (991 \text{ MeV})^2$.

7.5.1   Evaluation for $m_\pi = 0$

In order to get a better understanding of the computation the SFF is calculated first in the massless limit. Later on, the massive case will be analysed.

First we will compute the normalization at $q^2 = 0$ of the SFF for the $SU(2)$ current $(\bar{u}u + \bar{d}d)$:

$$\mathcal{F}(0)|_{m_q=0} = \lim_{m_q \to 0} \left(\frac{\partial}{\partial m_u} + \frac{\partial}{\partial m_d} \right) m_\pi^2 = \lim_{m_q \to 0} \{2B_0 + \mathcal{O}(m_q)\} = 2B_0 \quad . \tag{7.44}$$

The effective current vertex is given by:

$$\begin{cases} \mathcal{F}_0(q^2) = 2B_0 \left\{ 1 + \frac{4c_d c_m}{F^2} \frac{q^2}{M_S^2 - q^2} \right\} = \mathcal{F}(0) \left\{ 1 + \frac{4c_d c_m}{F^2} \frac{q^2}{M_S^2 - q^2} \right\} , \\[2mm] \mathcal{B}_0(q^2) = 2B_0 \frac{4c_d c_m}{F^2} \frac{2}{M_S^2 - q^2} = \mathcal{F}^S(0) \frac{4c_d c_m}{F^2} \frac{2}{M_S^2 - q^2} . \end{cases} \tag{7.45}$$

Connecting this effective current vertex with an effective scattering vertex $\mathcal{T}^{LO}$ with $\pi^+ \pi^-$ and $\pi^0 \pi^0$ loops one may compute iteratively the pion SFF for any number of loops, since we obtain the recurrence relation

$$\mathcal{F}_{N+1}(q^2) = \mathcal{F}_N(q^2) \left[\left(q^2 + \frac{3}{4} \frac{4c_d^2}{F^2} \frac{q^4}{M_S^2 - q^2} \right) \left(\frac{B_0(q^2; 0, 0)}{F^2} \right) \right] \quad ,$$

$$\mathcal{B}_{N+1}(q^2) = \mathcal{F}_N(q^2) \left[\left(\frac{2}{3} + \frac{3}{2} \frac{4c_d^2}{F^2} \frac{q^2}{M_S^2 - q^2} \right) \left(\frac{B_0(q^2; 0, 0)}{F^2} \right) \right] \quad . \tag{7.46}$$

In Eq. (7.46) one has the $I = 0$ scalar resonance with $(\bar{u}u + \bar{d}d)$ quark content in the effective scattering vertex.

As result of this recurrence there arise a geometrical series on the on-shell SFF that can be resummed:

$$\mathcal{F}(q^2) = \sum_{N=0}^{\infty} \mathcal{F}_N(q^2) = \mathcal{F}(0) \frac{1 + \frac{4c_d c_m}{F^2} \frac{q^2}{M_S^2 - q^2}}{1 - \frac{q^2}{F^2} \left[1 + \frac{3}{4} \frac{4c_d^2}{F^2} \frac{q^2}{M_S^2 - q^2} \right] B_0(q^2; 0, 0)} , \tag{7.47}$$

which can be ordered in a more familiar way as:

$$\frac{\mathcal{F}(q^2)}{\mathcal{F}(0)} = \frac{M_S^2 + q^2 \left[\frac{4c_d c_m}{F^2} - 1 \right]}{[M_S^2 + \Delta\Pi_S(q^2)] - q^2 - iM_S\Gamma_S(q^2)} \quad , \tag{7.48}$$

where the real and imaginary parts from loop contribution in $B_0(q^2; 0, 0)$ have been separated. The ultraviolet divergent real part is:

$$\Delta\Pi_S(q^2) = -\frac{q^2}{F^2}\left[M_S^2 + q^2\left(\frac{3}{4}\frac{4c_d^2}{F^2} - 1\right)\right]\text{Re}\left\{B_0(q^2; 0, 0)\right\} \quad , \qquad (7.49)$$

whereas the imaginary part remains finite and takes the value

$$M_S\Gamma_S(q^2) = \frac{q^2}{F^2}\left[M_S^2 + q^2\left(\frac{3}{4}\frac{4c_d^2}{F^2} - 1\right)\right]\text{Im}\left\{B_0(q^2; 0, 0)\right\} =$$

$$\tag{7.50}$$

$$= \frac{q^2}{16\pi F^2}\left[M_S^2 + q^2\left(\frac{3}{4}\frac{4c_d^2}{F^2} - 1\right)\right]\theta(q^2) \quad .$$

When calculating the two-current correlator one finds the same denominator, this is, the same poles in the complex s-plane. More exactly, it generates the same finite width $\Gamma_s(q^2)$.

In order to compare this expression with the experiment it can only be done with the SFF phase-shift, which in the elastic region is equal to the $T^{I=J=0}$ scattering phase-shift due to the Watson theorem [60], and this has been experimentally measured in several works [35, 62]. The function $\Delta\Pi_S(q^2)$ can be fixed by a comparison with the low energy result from χPT in the massless limit which can be found in Eq. (7.12). The expansion in q^2 of the resummed expression gives:

$$\mathcal{F}(q^2) = \mathcal{F}(0)\left[1 + \frac{4c_d c_m}{F^2}\frac{q^2}{M_S^2} + \frac{q^2}{F^2}B_0(q^2; 0, 0) + \mathcal{O}\left(q^4\right)\right] . \qquad (7.51)$$

Here one can again employ the knowledge that one has of the chiral couplings at LO in $1/N_C$; they become saturated by the heavy resonance exchange and the running with the scale comes at NLO in $1/N_C$:

$$\ell_4^r(\mu) = \ell_4\big|_{N_C\to\infty} + \Delta\ell_4(\mu) = \frac{4c_d c_m}{M_S^2} + \Delta\ell_4(\mu), \qquad (7.52)$$

with the subleading term $\Delta\ell_4(\mu)$ being of order $\mathcal{O}(N_C^0)$, so the χPT SFF becomes:

$$\mathcal{F}(q^2)_{\pi\pi} = \mathcal{F}(0)_{\pi\pi}\left[1 + \frac{4c_d c_m}{F^2}\frac{q^2}{M_S^2} + \frac{q^2}{16\pi^2 F^2}\left\{1 - \ln\left(-\frac{q^2}{\mu^2}\right) + 16\pi^2\Delta\ell_4(\mu)\right\}\right] \quad .$$

$$\tag{7.53}$$

Thus the matching between the resummed expression and χPT provides the divergent Feynman integral with a finite value:

$$B_0(q^2; 0, 0) \longrightarrow B_0^r = \frac{1}{16\pi^2}\left\{1 - \ln\left(-\frac{q^2}{\mu^2}\right) + 16\pi^2\Delta\ell_4(\mu)\right\} . \qquad (7.54)$$

Therefore, one has for the phase-shift the finite theoretical value:

$$\delta_0^0(q^2) = \arctan\left\{\frac{M_S\Gamma_S(q^2)}{M_S^2 + \Delta\Pi_S^r(q^2) - q^2}\right\} \quad , \qquad (7.55)$$

where now $B_0(q^2; 0, 0)$ has been replaced by B_0^r within $\Delta\Pi_S(q^2)$ and hence getting $\Delta\Pi_S(q^2)$.

Taking this expression I have performed a fit to the experimental data (Ochs–energy independent sample–[35]). Although the result is scale independent the value of $\Delta\ell_4(\mu)$ depends on the scale μ. For the fit I took the usual reference scale $\mu = 770$ MeV and I performed it for energies below the $K\overline{K}$ threshold, i.e. including the bins of the sample with $\sqrt{q^2} \leq \sqrt{s_{end}} = 970$ MeV. I obtained $M_S = (870 \pm 14)$ MeV, $2c_d/F = 0.67 \pm 0.04$ and $\Delta\ell_4(\mu) = (-4.1 \pm 0.5) \cdot 10^{-3}$, with $\chi^2/\text{dof}= 10.0/16$. Notice that the value for $\Delta\ell_4(\mu)$ is not as small as in the vector case; in this case one would have also naively expected a contribution much more suppressed in comparison with the value of the coupling at LO in $1/N_C$, this is, $|\Delta\ell_4(\mu)| \ll |\ell_4|_{N_C \to \infty} = c_d c_m/M_S^2 \sim 9 \cdot 10^{-3}$, where I have taken $M_S \sim 1$ GeV.

Likewise, the value of the parameters obtained from the fit vary a bit if one changes the final point of the considered range. Actually, it is the size of the errors what changes, since the low energy region is fitted better. The value of χ^2/dof remains essentially unchanged. Thus, the final point s_{end} has been varied in the range $870 \to 970$ MeV. Considering this systematic error the values of the parameters become now $M_S = (870 \pm 14^{+4}_{-21})$ MeV, $2c_d/F = 0.67 \pm 0.04^{+0.17}_{-0.02}$ and $\Delta\ell_4(\mu) = (-4.1 \pm 0.5^{+0.4}_{-2.5}) \cdot 10^{-3}$, for $\mu = 770$ MeV. The comparison of the experimental data and the resummed result in Eq. (7.55), taking the former central values of the fit for the parameters, can be seen in Fig. (7.1).

From this result it is possible to recover the value of the renormalized χPT coupling at the reference scale $\mu = 770$ MeV:

$$\ell_4^r(\mu) = \ell_4|_{N_C \to \infty} + \Delta\ell_4(\mu) = \frac{4c_d c_m}{M_S^2} + \Delta\ell_4(\mu) \simeq 3.5 \cdot 10^{-3}, \qquad (7.56)$$

where I took the central values from the fit for M_S, c_d and $\Delta\ell_4(\mu)$, and the LO in $1/N_C$ value $c_m = F/2$, with $F \simeq 92.4$ MeV. This can be compared with the phenomenological determinations in χPT [8], which give the scale invariant constant $\bar{\ell}_4 = 4.4 \pm 0.3$ (Appendix D), and therefore the renormalized coupling at the reference μ, $\ell_4^r(\mu) = (6.1 \pm 1.9) \cdot 10^{-3}$. A further analysis of the errors in Eq. (7.56) would show that both result are completely compatible within errors. However, it could be hard to estimate the uncertainties coming from assuming the massless pion limit.

When approaching to $s = 1$ GeV^2 this description fails and the other channels have to be considered. In addition, after $\delta_0^0 = 90°$ the experimental phase-shift shows up a large variation in a very narrow range, changing form $\delta_0^0 = 112°$ in $\sqrt{s} = 950$ MeV to $\delta_0^0 = 226°$ in $\sqrt{s} = 1100$ MeV. This cannot be explained just with a $U(2)$ scalar multiplet, where there is only one iso-scalar resonance. It is necessary to consider the whole $U(3)$ multiplet and include also the iso-scalar resonance containing strangeness.

Nevertheless, it seems clear from this analysis that the lightest scalar $q\bar{q}$ meson has a mass $M_S \simeq 870$ MeV, this is, heavier than $\rho(770)$, in agreement with former studies in QCD [91, 92].
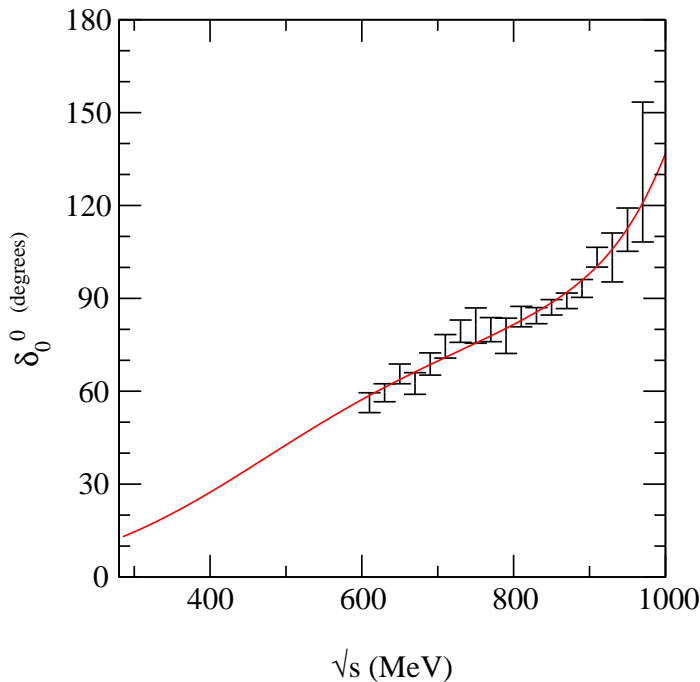
Figure 7.1:   Comparison of the phase-shift δ_0^0 coming from the resummed Eq. (7.55) with Ochs' experimental data–energy independent sample– [35].

At this point it is important to remark a detail about the asymptotic behaviour at high energies. Both the resummed form-factor and the two-current correlator have a good behaviour at short distances. However, every independent diagram with a N number of loops do not accomplish such behaviour since every loop increases the power behaviour by a factor $\frac{q^2}{M_S^2-q^2}(M_S^2 - \frac{1}{4}q^2) \overset{q^2\to\infty}{\sim} q^2$ (where the LO value $4c_d^2 = F^2$ has been taken), as it can be observed from the recurrence in Eq. (7.46). Thus, one finds again the same problem that one found for the one loop VFF where the scattering amplitude grew as $\sim q^2$ due to the t-channel scattering. Here we have found that for $I = J = 0$ the problem arises even when considering only the s-channel scattering. This remarks, once again, the great necessity of further analysis of the scattering amplitudes within an EFT with resonances.

7.5.2   Massive pion case

For completeness I will show here also the theoretical result for the massive pion case. This situation is a bit more complicated since now one finds a mixing between

the on-shell and the off-shell amplitudes when computing the SFF at $N + 1$ loops from the SFF at N loops:

$$\vec{S}_{N+1} \;=\; \mathcal{M} \; \vec{S}_N \qquad , \tag{7.57}$$

that is short for

$$\begin{pmatrix} \mathcal{F}_{N+1} \\ \mathcal{B}_{N+1} \end{pmatrix} = \begin{pmatrix} \mathcal{M}_A & \mathcal{M}_B \\ \mathcal{M}_C & \mathcal{M}_D \end{pmatrix} \begin{pmatrix} \mathcal{F}_N \\ \mathcal{B}_N \end{pmatrix} \qquad , \tag{7.58}$$

where this time $\mathcal{M}_{A,B,C,D}$ are just complex functions, not matrices.

However, as we saw before in the $n_f = 3$ derivation the SFF really only depends on the element $\mathcal{M}_A$:

$$\begin{aligned}
\mathcal{M}_A = & \left(q^2 - \tfrac{1}{2} m_\pi^2 + \frac{3}{4} \frac{4 c_d^2}{F^2} \frac{q^4}{M_S^2 - q^2} \right) \frac{B_0(q^2; m_\pi^2, m_\pi^2)}{F^2} \\[2mm]
& - \left(\frac{2}{3} + \frac{3}{2} \frac{4 c_d^2}{F^2} \frac{q^2}{M_S^2 - q^2} \right) \frac{A(m_\pi^2)}{F^2} \; .
\end{aligned} \tag{7.59}$$

Thus, the resummed SFF will be:

$$\mathcal{F}(q^2) \;=\; \frac{\mathcal{F}_0(q^2)}{1 - \mathcal{M}_A(q^2)} \tag{7.60}$$

where $\mathcal{F}_0(q^2)$ was given before in Eq. (7.16). In it easy to check that in the chiral limit $m_\pi^2 = 0$ one recovers again the result from the former section. Again, through a matching with χPT it would be possible to provide the ultraviolet divergences with a finite value.

7.6   Pion and kaon decay constants: Influence of the scalar resonances.

The study in this section is focused on the computation of how the variation of the quark masses affects the pion and kaon decay constants, F_π and F_K. Lattice calculations have provided information about QCD results for unphysical values of the u/d light quarks [101]. The simulations are forced sometimes to work with masses of nearly the size of the physical strange quark mass or higher. Thus, χPT extrapolations break down and generate large unphysical chiral logarithms, yielding a large bending in the extrapolation [101, 102, 103, 33]. Nonetheless, more than purely numerical values, this work aims to provide a possible way to analyse the Lattice simulations at large quark masses, explaining why the usual linear extrapolations work so well and which are the underlying physical foundations.

Through the inclusion of the first resonance multiplets, with masses $M_R \sim 1$ GeV, one expects to reproduce the physics for the Goldstones up to that range

of momenta and masses. Moreover, at LO in $1/N_C$ only the scalar resonances contribute to F_π and F_K. Since the first multiplet of pseudo-scalar resonances stays at much higher masses, it will not be considered in the calculation and its mixing with the pNGB will be neglected.

7.6.1   Scalar tadpole and field redefinition

Analysing the LO lagrangian one observes the presence of a linear term in the scalar fields, i.e. a scalar tadpole. It is given by the term of $\mathcal{L}_{2S}$ with the coupling c_m, which provides the vertex for the scalar resonance production from a scalar quark current.

Chiral symmetry requires the quark masses to enter in the effective lagrangian only through the tensor $\chi = 2B_0\{s(x) + ip(x)\}$, which appears in the chiral covariant combinations $\chi_\pm = u^\dagger\chi u^\dagger \pm u\chi^\dagger u$. In order to recover physical QCD, the external fields are evaluated at the end of the calculation as $\chi = 2B_0\mathcal{M}$, being $\mathcal{M} = \text{diag}(m_u, m_d, m_s)$ the diagonal matrix with the light quark masses.

The pieces of the lagrangian containing the scalar fields are

$$
\mathcal{L}_R^{\text{Kin}}(S) + \mathcal{L}_{2S} = \frac{1}{2}\langle \partial^\mu S \partial_\mu S \rangle - \frac{1}{2}M_S^2\langle S^2 \rangle + 4B_0 c_m\langle S\mathcal{M} \rangle +
$$
$$
+ \mathcal{O}(S^2\Phi^2, S\Phi^2)\,. \tag{7.61}
$$

Therefore, the scalar field has a non-zero vacuum expectation value (v.e.v.). In order to define the quantum field theory around the minimum one needs to perform the shift:

$$
S = \bar{S} + \frac{4B_0 c_m}{M_S^2}\mathcal{M}\,, \tag{7.62}
$$

where the shifted scalar nonet fields $\bar{S}$ has a zero v.e.v. Nonetheless this shift makes $\bar{S}$ not to be chiral covariant any longer. For the present work this detail is not relevant although other alternative shifts (like $S = \bar{S} + c_m\chi_+$) would restore the explicit covariance. The important detail is that the shift is not equal for all the scalars but proportional to the quark masses and different for each resonance.

The part of the lagrangian containing the vectors, axial-vectors and pseudo-scalar resonances, $\mathcal{L}_R[V, A, P]$, remains unchanged under the shift but the remaining $\mathcal{O}(p^2)$ chiral term $\mathcal{L}_{2\chi}$ and the scalar pieces $\mathcal{L}_S^{\text{Kin}} + \mathcal{L}_{2S}$ become

$$
\mathcal{L}_S^{\text{Kin}} + \mathcal{L}_{2S} + \mathcal{L}_{2\chi} = \mathcal{L}_{\bar{S}}^{\text{Kin}\,'} + \mathcal{L}_{2\bar{S}}^{'} + \mathcal{L}_{2\chi}^{'} - \frac{8B_0^2 c_m^2}{M_S^2}\langle \mathcal{M}^2 \rangle\,, \tag{7.63}
$$

yielding a constant term proportional to $\langle \mathcal{M}^2 \rangle$, a kinetic term structure for $\bar{S}$,

$$
\mathcal{L}_{\bar{S}}^{\text{Kin}\,'} = \frac{1}{2}\langle \nabla^\mu\left(\bar{S} + \frac{4B_0 c_m}{M_S^2}\mathcal{M}\right)\nabla_\mu\left(\bar{S} + \frac{4B_0 c_m}{M_S^2}\mathcal{M}\right)\rangle - \frac{1}{2}\langle M_S^2\bar{S}^2\rangle\,, \tag{7.64}
$$

an interaction lagrangian without tadpoles,

$$\mathcal{L}'_{2\bar{S}} = c_d \langle \bar{S} u_\mu u^\mu \rangle + c_m \langle \bar{S} (\chi_+ - 4B_0 \mathcal{M}) \rangle \tag{7.65}$$

and a modified $\mathcal{O}(p^2)$ χPT term,

$$\mathcal{L}'_{2\chi} = \frac{F^2}{4} \langle C_\phi^{-1} \left[u_\mu u^\mu + \chi_+^{(can)} \right] \rangle, \tag{7.66}$$

provided by the matrix definitions

$$\chi_+^{(can)} = \left(1 + \frac{4c_d c_m}{F^2} \frac{4B_0 \mathcal{M}}{M_S^2} \right)^{-1} \left(1 + \frac{4c_m^2}{F^2} \frac{4B_0 \mathcal{M}}{M_S^2} \right) \chi_+,$$

$$C_\phi^{-1} = \left(1 + \frac{4c_d c_m}{F^2} \frac{4B_0 \mathcal{M}}{M_S^2} \right). \tag{7.67}$$

In order to convert the pNGB kinetic term to the canonical form, one needs to perform a re-scaling C_ϕ on the pNGB fields $u = \exp\left(i\Phi/\sqrt{2}F \right) = \exp\left(iC_\phi^{\frac{1}{2}} \Phi^{(can)}/\sqrt{2}F \right)$.

At LO in $1/N_C$ the resonance couplings are fixed by the QCD short distance constraints [21, 22]: $c_d = c_m = F/2$. Hence, from Eqs. (7.66) and (7.67) one gets for the pion and kaon fields the re-scalings and LO masses

$$\begin{cases} m_\pi^2 = 2B_0 \hat{m}, \\[2mm] C_\pi = \left[1 + \frac{2m_\pi^2}{M_S^2} \right]^{-1}, \end{cases} \qquad \begin{cases} m_K^2 = B_0(\hat{m} + m_s), \\[2mm] C_K = \left[1 + \frac{2m_K^2}{M_S^2} \right]^{-1}. \end{cases} \tag{7.68}$$

7.6.2 F_π and F_K at Leading Order

Since the scalar tadpole has been removed, at LO there is only one diagram contributing to the pion decay constant: the tree-level production of the pNGB from the axial current,

$$\langle 0 | \bar{d} \gamma_\mu \gamma_5 u | P^+(p) \rangle = i\sqrt{2} F C_P^{-\frac{1}{2}} p_\mu, \tag{7.69}$$

and therefore the pion and kaon decay constants are

$$F_\pi = F \left(1 + \frac{2m_\pi^2}{M_S^2} \right)^{\frac{1}{2}}, \qquad F_K = F \left(1 + \frac{2m_K^2}{M_S^2} \right)^{\frac{1}{2}}. \tag{7.70}$$

When $m_P^2 \ll M_S^2$ the decay constants may be expanded in powers of m_P^2, recovering the tree-level χPT result $F_P = F \left[1 + \frac{4L_5}{F^2} m_P^2 + \mathcal{O}(m_P^4) \right]$, with $L_5 = F^2/4M_S^2$ [19, 21] (the $SU(3)$ breaking coupling L_4 is zero at $N_C \to \infty$). This explains why the
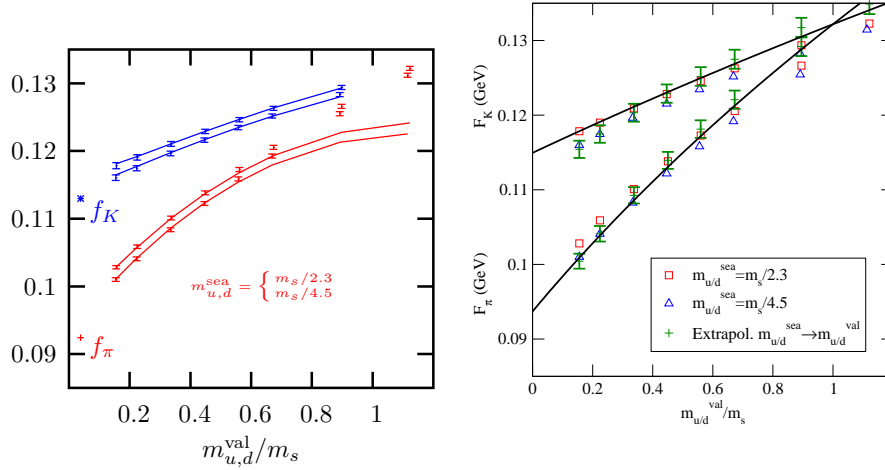
Figure 7.2: **A)** Lattice results for F_π and F_K and χPT extrapolations taken from MILC collaboration [101]. **B)** RχT extrapolations for the values from the fit, $F = 93.7$ MeV, $M_S = 1020$ MeV and the splitting $e_m^S = -0.02$. The kaon mass varies as $m_K^2 = m_K^{Phys.\,2} + (m_\pi^2 - m_\pi^{Phys.\,2})/2$ due to its light quark content. They are shown together with the data for $m_{u/d}^{sea} = m_s/2.3$ (squares), $m_{u/d}^{sea} = m_s/4.5$ (triangles) and the linear extrapolation to the value $m_{u/d}^{sea} = m_{u/d}^{val}$ (error bars).

linear extrapolations work so well. Only near the zero quark mass the LO result in $1/N_C$ gains sizable non-analytic contributions from the one-loop logarithms (NLO in $1/N_C$): $F_\pi = F \left[1 + \frac{4L_5^r(\mu)}{F^2} m_\pi^2 - \frac{m_\pi^2}{16\pi^2 F^2} \ln \frac{m_\pi^2}{\mu^2} + ... \right]$.

The results for F_π and F_K from the Lattice simulations (MILC Collaboration [101]) are shown in the first plot of Fig. (7.2.A). The simulation handles two kinds of quark masses: The sea-quark masses of the fermions within closed loops; and the valence-quark masses of those which are not from the sea. In this simulation the strange quark valence-mass m_s^{val} and the strange quark sea-mass m_s^{sea} take the same value $m_s = m_s^{val} = m_s^{sea}$ and equal to $114\% \times m_s^{Phys}$, being m_s^{Phys} the physical mass of the strange quark. The u/d quark valence-masses $m_{u/d}^{val}$ (isospin limit is assumed) are varied continuously between nearly zero and the physical mass of the strange quark. Finally, the simulation is performed for two values of the sea-masses of the quarks u/d: $m_{u,d}^{sea} = m_s/2.3$ and $m_{u,d}^{sea} = m_s/4.5$

The modifications due to the sea quark mass are much smaller than those from the valence masses, as it is expected in the large-N_C limit, since the closed quark loops would be suppressed by $1/N_C$. Thus, in this work I have generated the matrix elements for equal values of the sea and valence masses, i.e. for $m_{u/d}^{sea} = m_{u/d}^{val}$, through a simple linear extrapolation from the points of the Lattice simulation shown in Fig. (1.B).

The theoretical expressions derived from RχT for F_π and F_K in Eqs. (7.70) were fitted to these extrapolated points. The error in my input data in the fit was a 1 % error, a typical discretization error, but it did not account the uncertainties in the $m_{u/d}^{sea}$ extrapolation to the value $m_{u/d}^{val}$. The variation of the decay constant when changing $m_{u/d}^{sea}$ could be considered as an estimate of this uncertainty. In addition, the errors due to NLO contributions have not been considered. The fit yields the values $F = 94.1 \pm 0.9$ MeV and $M_S = 1049 \pm 25$ MeV, with $\chi^2/\text{dof} = 11.0/13$. This yields for the physical pion and kaon decay constants $F_\pi = 95.8 \pm 0.9$ MeV and $F_K = 113 \pm 1.4$ MeV, in acceptable agreement with the experimental values $F_{\pi+} = 92.4 \pm 0.07 \pm 0.3$ MeV and $F_{K+} = 113.0 \pm 1.0 \pm 0.3$ MeV [82]. One may also estimate the χPT coupling at LO in $1/N_C$, $L_5 = F^2/4M_S^2 = (2.01 \pm 0.10) \cdot 10^{-3}$.

Nevertheless, here the chiral logarithms have not been included. In χPT they produce an important non-analytic effect and a large bending in the F_π curve, since its slope becomes large at small pion mass due to $\frac{dF_\pi}{dm_\pi^2} \sim \ln \frac{m_\pi^2}{\mu}$. The effect of the logs on F_K is much more reduced since the value of the kaon mass does not become small when $m_{u/d} \to 0$. That is the reason for the better agreement of the F_K result. Eventually the NLO calculation in $1/N_C$ (one loop) would introduce this extra non-analytic curvature and the usual one loop result for F_π in χPT would be recovered.

The mass splitting between the masses of the two $I = 0$ scalar resonances can also be studied since they do not contribute equally to F_π and F_K. The resonance multiplet has been considered at first as degenerate in mass. Nonetheless the resonance masses can gain contributions due to the quark masses. In the large-N_C limit, Chiral invariance requires that, at order $\mathcal{O}(m_q)$, the mass splitting enters only through a chiral invariant term [104]:

$$\Delta\mathcal{L}_{m_q} = e_m^S \langle \chi_+ S^2 \rangle, \tag{7.71}$$

being e_m^S an $\mathcal{O}(N_C^0)$ dimensionless constant, independent of the quark masses.

The shift now in the scalar field to re-absorb the tadpole is slightly different:

$$S = \bar{S} + 4B_0 c_m \mathcal{M} \left[M^2 - 8e_m^S B_0 \mathcal{M} \right]^{-1}. \tag{7.72}$$

The mass eigenvalues for the $I = 0$ scalars are not M_S^2 anymore but the two values $\bar{M}_{S_n} \equiv M_S^2 - 8e_m^S B_0 m_{u/d}$, for the state $\left(\frac{1}{\sqrt{2}} \bar{u}u + \frac{1}{\sqrt{2}} \bar{d}d \right)$, and $\bar{M}_{S_s} \equiv M_S^2 - 8e_m^S B_0 m_s$, for $\bar{s}s$. Nonetheless, the physical scalar states will separate away from this ideal mixing and these masses will gain also contributions due to NLO effects in $1/N_C$.

At LO in $1/N_C$ the pNGB masses still remain as given in Eq. (7.68). However the re-scaling factors for pions and kaons change accordingly:

$$C_\pi = \left[1 + \frac{2m_\pi^2}{M_S^2 - 4e_m^S m_\pi^2} \right]^{-1}, \qquad C_K = \left[1 + \frac{2m_K^2}{M_S^2 - 4e_m^S m_K^2} \right]^{-1}, \tag{7.73}$$

which therefore modify the pion and kaon decay constants.

The pion and kaon decay constants depend now on the splitting parameter e_m^S. However the fit to the former data is not sensitive to this coupling, yielding: $F = 93.7 \pm 1.5$ MeV, $M_S = 1020 \pm 80$ MeV and $e_m^S = -0.02 \pm 0.05$, with similar $\chi^2/\text{dof}=$ 10.9/12. It provides an estimate of the scalar masses at large N_C: one gets the values $\bar{M}_{S_n} = 1020 \pm 80$ MeV and $\bar{M}_{S_s} = 1040 \pm 90$ MeV, highly correlated, and their splitting, equal to $\bar{M}_{S_s} - \bar{M}_{S_n} = 20 \pm 40$ MeV. In addition, large OZI-rule violations could occur at NLO of the same size as the quark mass corrections. In the worst case, one would expect them to be of the order of $1/N_C \simeq 33\%$ times the value of the scalar mass at LO in $1/N_C$.

The RχT extrapolation is shown in the second graph of Fig. (7.2.B). Since this effective field theory describes the equal valence and sea mass case, the theoretical result is compared with an emulation of the Lattice data for $m_{u/d}^{sea} = m_{u/d}^{val}$, obtained by linear extrapolation as it was explained before.

7.6.3   Conclusions on the pion and kaon decay constants

RχT has been shown to be an interesting tool to analyse the Lattice data, which usually are generated for non-physical values of the light quark masses. The present work hints that the mesonic resonances may play an important role in the large quark mass extrapolations. This work explores the pion and kaon decay constants, providing successful results. The importance and aim of the present work is not just the decay constant determinations but an alternative idea of how to interpret the Lattice simulations for large unphysical values of the masses, providing a clear explanation of why the usual linear extrapolations yield such a good result. Likewise, this provides solid theoretical foundations for the thechniques based on the underlying QCD. Thus, the $1/N_C$ expansion might be a suitable framework to describe the heavy quark matrix elements (f_B, B_B...) at large values of the u/d quark masses, where a similar linear behaviour has also been observed.

The fact that at low energies RχT recovers χPT ensures that we are introducing the proper low mass behaviour [19, 23, 106]. Former works [102, 103, 33] noticed the necessity of a separation scale Λ where the χPT loops become irrelevant. The resonance masses provide a "natural" scale where the chiral extrapolations fail and where the dynamics of the observable changes drastically.

The fits to the simulations were done for an emulation of the Lattice data, obtained by extrapolating $m_{u/d}^{sea}$ to the value $m_{u/d}^{val}$, that varied in a wide and continuous range between zero and the strange quark mass. For a more proper analysis one would need a simulation with equal sea and valence masses. However, the main dependence comes from the valence-quarks and hence the sea-quark effects are small, since the closed quark loops are suppressed by $1/N_C$. Therefore, the present calculation can be considered an adequate estimate of the hadronic parameters. A further improvement would also be the reduction of the systematic errors that occur in the simulation. For the Lattice data [101] one obtains the values $F = 94.1 \pm 0.9$ MeV and $M_S = 1049 \pm 25$ MeV, and the χPT coupling estimate at LO in $1/N_C$,
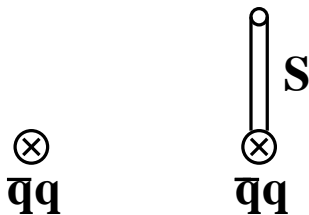
Figure 7.3: Diagrams contributing to the scalar condensate.

$L_5 = (2.01\pm0.10)\cdot10^{-3}$. The scalar mass splitting shows however large uncertainties.

7.7 Quark condensates in RχT

In the former section we saw that the presence of a scalar tadpole produced an important effect in the order parameters F_π and F_K. In this section I am going to show that one can also provide a prediction for the quark condensates at LO in $1/N_C$.

In this case it is even not necessary to perform the field redefinition to remove the tadpole, since one has just two diagrams: The point-like condensate and the diagram creating a scalar . In the F_π case one had to consider an infinity of diagrams since the pion propagator implied the insertion of an arbitrary number of scalar tadpoles. The two diagrams are shown in Fig. (7.3), and provide the value:

$$\langle \bar{q}q \rangle = B_0 F^2 \left\{ 1 + \frac{4c_m^2}{F^2} \frac{4B_0 m_q}{M_S^2} \right\} . \tag{7.74}$$

If now one uses the results derived in the former section for the pNGB masses at LO in $1/N_C$ and the LO values of the scalar couplings, $c_m = F/2$, then one finds:

$$\langle \bar{u}u \rangle = \langle \bar{d}d \rangle = B_0 F^2 \left\{ 1 + \frac{2m_\pi^2}{M_S^2} \right\} ,$$

$$\langle \bar{s}s \rangle = B_0 F^2 \left\{ 1 + \frac{4m_K^2 - 2m_\pi^2}{M_S^2} \right\} . \tag{7.75}$$

Chapter 8

Long distance chiral corrections in B meson amplitudes

We discuss in this chapter the chiral corrections to f_B and B_B with particular emphasis on determining the portion of the correction that arises from long distance physics (this Chapter is essentially based on the publication from Ref. [33]). For very small pion and kaon masses all of the usual corrections are truly long distance, while for larger masses the long distance portion decreases. These chiral corrections have been used to extrapolate lattice calculations towards the physical region of lighter masses. We show in particular that the chiral extrapolation is better behaved if only the long distance portion of the correction is used.

Lattice calculations of B meson properties are presently done with parameters such that the light quark masses are larger than their physical values. In order to make predictions that are relevant for phenomenology, these calculations are extrapolated down to lower quark masses. One of the extrapolation methods uses some results from Chiral Perturbation Theory, and this appears to produce rather large effects due to the chiral corrections. A recent summary of the field [34] noted that this chiral extrapolation is the largest uncertainty (17%) at present in the calculation of the B meson decay constant f_B.

As it was explained in Chapter 3, Chiral perturbation theory is an effective field theory involving pions, kaons and η mesons. These mesons are the lightest excitations in QCD and the effective field theory is designed to describe the effects of long range propagation of these light degrees of freedom. Even in loop diagrams there are long distance effects which are described well by the effective field theory. However, chiral perturbation theory is not a good model of physics at short distances and is not valid for large meson masses. If we consider mesons of variable mass, as the masses become heavier, less and less of the loop corrections are truly long distance.

The chiral corrections are sometimes used in ways that hide the separation of long distance and short distance physics. Consider for example the chiral correction

to the B meson decay constant in dimensional regularization [109, 110, 111]

$$f_B = f_0 \left[1 - \left(\frac{1 + 3g^2}{16\pi^2 F_\pi^2} \right) \frac{3}{8} m_\pi^2 \ln \frac{m_\pi^2}{\mu^2} + ... \right] , \qquad (8.1)$$

where g is the heavy meson coupling to pions. The ellipses denote the kaon and eta contributions as well as analytic terms in the masses that carry unknown coefficients which must be fit. We see that the corrections vanish for massless mesons and grow continuously with large meson masses[1]. This is the opposite of the behavior that one might expect, which would be to have larger chiral corrections when the pions are nearly massless. For very large masses of the "pions", physically we expect that the loop effects must decouple from the observables. The expression of Eq. 1 does not illustrate this decoupling. The key point is that as the mesons become heavier, most of the correction given in Eq. (8.1) comes from short distance physics, which is not a reliable part of the effective field theory. We will show this in more detail below. This behavior is not a problem in principle. The free coefficients in the chiral lagrangian allow one to compensate for the unwanted behavior and correctly match the short distance physics of QCD. However the reliance on Eq. (8.1) at large masses can have a deleterious effect on phenomenology in some applications.

The way that present lattice extrapolations of F_B are performed apply the chiral predictions outside their region of validity. An example is given in Fig. (8.1), describing the results of the JLQCD collaboration [102].

In order to address the issue of the chiral exptrapolation, the lattice data was fit with the function of Eq. (8.1) at large mass and the form is used to extrapolate the results to small values of the mass. The fact that there appears to be a large effect at $m = 0$ does not imply that the chiral correction is large here. Indeed, inspection of Eq. (8.1) shows that the chiral log correction vanishes at zero mass, so the chiral logarithm is not large at the physical masses. Rather, the big effect seen comes from using Eq. (8.1) at large masses. Since the chiral logs grow at large mass, and appear in this formula with a fixed coefficient, normalizing the function at large mass produces a sizeable difference when compared to smaller masses. Since chiral perturbation theory is not applicable at such large masses, this shift is not a valid consequence of chiral perturbation theory.

We will explore the long-distance/short-distance structure of the chiral corrections [113], and show that the undesirable effects described above come from short distance physics that chiral perturbation theory is not able to describe. The application of Eq. (8.1) at large masses then amounts to a bad model of the short distance physics. We will give formulas for the one loop corrections of Eq. (8.1) which *removes* the unwanted short-distance component. At small quark masses, our

---

[1]Note that we keep the B meson mass unchanged, so that when we refer to large and small meson masses, we are always referring to the masses of the chiral particles - pions, kaons and etas - that occur in the loop diagrams.
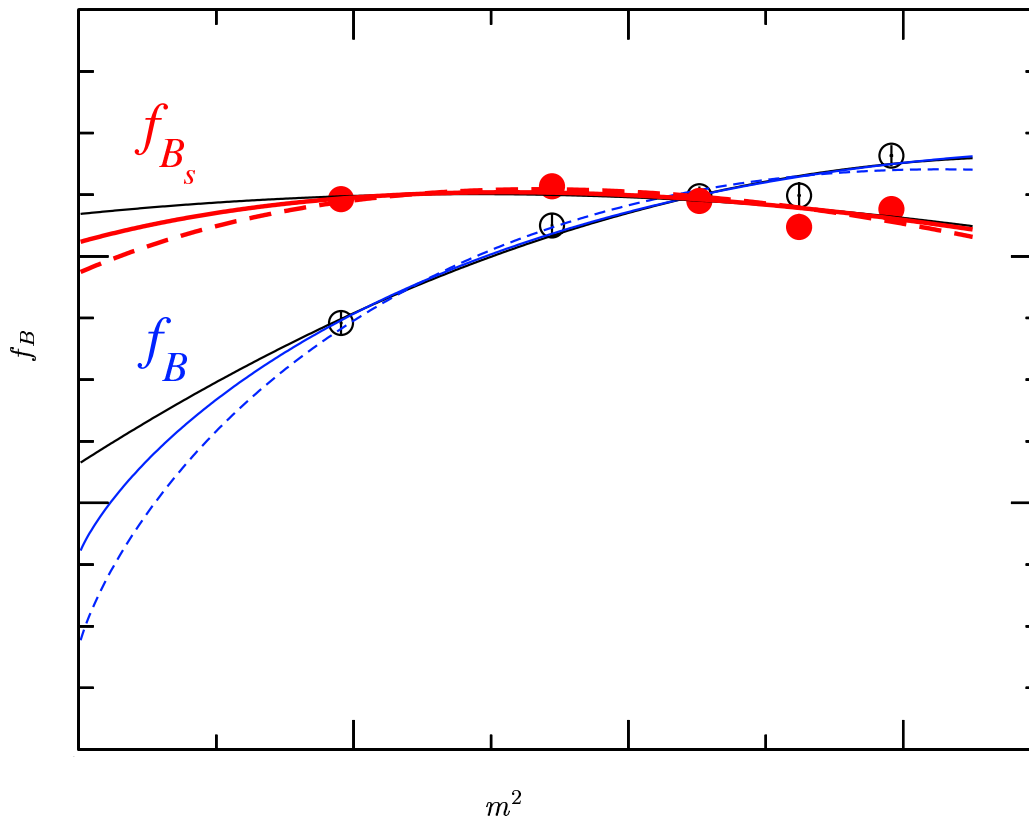
Figure 8.1: Lattice data points for f_B and f_{B_s} and fitted curves with quadratic fit (upper solid curve) and with chiral logs for $g = 0.27$ and $g = 0.59$ (dashed)

method is just a different regularization of the theory, and reproduces the usual chiral corrections. When applied at large quark masses, our formulas must also be considered as a model. However, it is a relatively innocuous model in that it makes no assumptions about short distance physics and it produces a small correction since the loop effect decouples at large mass. When used to extrapolate the lattice results to the physical masses, our results lead to more reasonable estimates of the chiral corrections. Our methods are similar to some work on long distance regularization in baryon chiral perturbation theory [113] and on chiral extrapolations in other processes [114]. In particular, the JLQCD group has explored the use of the Adelaide-MIT approach [114] in the extrapolation of the pion decay constant [102]. Our work describes the rationale and benefits of a modified approach for the heavy-light system.

8.1   A study of the chiral corrections to f_B

The chiral corrections were initially calculated by Grinstein et al [109] (see also [110, 112, 111]). The methods are standard and we will not reproduce the details. However we note that, although there are various Feynman diagrams in the calculation, in the end the loop calculations involve only one loop integral,

$$\mathbf{A}\left(m^2\right) = \int \frac{d^d 4}{i\,(2\pi)^4} \frac{1}{(k^2 - m^2 + i\epsilon)}\,. \tag{8.2}$$

The chiral expansion involves unknown parameters for the reduced decay constant at zero mass ($\bar{f}_0$) and for the slopes (α_1, α_2) parameterizing linear dependence in the masses. The results are [109, 110, 111]

$$f_{B_{u,d}} = \frac{1}{\sqrt{m_B}} \qquad \bar{f}_0 \Bigg[1 + \alpha_1 m_\pi^2 + \alpha_2 (2m_K^2 + m_\pi^2)$$

$$+ \frac{1+3g^2}{4\,F_\phi^2}\left(\tfrac{3}{2}\,\mathbf{A}\left(m_\pi^2\right) + \mathbf{A}\left(m_K^2\right) + \tfrac{1}{6}\,\mathbf{A}\left(m_\eta^2\right) \right) \Bigg], \tag{8.3}$$

and

$$f_{B_s} = \frac{1}{\sqrt{m_B}} \quad \bar{f}_0 \Bigg[1 + \alpha_1 (2m_K^2 - m_\pi^2) + \alpha_2 (2m_K^2 + m_\pi^2)$$

$$+ \frac{1+3g^2}{4\,F_\phi^2}\left(2\,\mathbf{A}\left(m_K^2\right) + \tfrac{2}{3}\,\mathbf{A}\left(m_\eta^2\right) \right) \Bigg], \tag{8.4}$$

where g is the coupling of heavy mesons to pions[2] and F_ϕ is the pseudo-goldstone meson decay constant in the chiral limit[3]. Of course, the integral still needs to be regularized. In dimensional regularization, one absorbs the $1/(d-4)$ divergences into the slopes and finds the residual integral

$$\mathbf{A}^{d.r.}\left(m^2\right) = \frac{1}{16\pi^2} \quad \left[-m^2 - m^2 \ln\frac{m^2}{\mu^2} \right], \tag{8.5}$$

where μ is the arbitrary mass parameter that enters in dimensional regularization. The physical results do not depend on μ as it can be absorbed into a shift in the unknown slope coefficients.

8.2   Cut-off regularization and lattice extrapolation

Let us explore the loop integral and study the long-distance part. In order to do this, we use a cut-off defined in the rest frame of the B meson in order to remove

---

[2]In our numerical work, we will use $g = 0.59$.
[3]We use the normalization such that $F_\pi = 0.0924$ GeV.

the short-distance component. Specifically, we use a dipole cutoff yielding

$$\mathbf{A}\left(m^2, \Lambda^2\right) = \Lambda^4 \int \frac{d^4 k}{i\,(2\pi)^4} \frac{1}{(k^2 - m^2 + i\epsilon)\,(k^2 - \Lambda^2 + i\epsilon)^2}. \tag{8.6}$$

In related contexts, other forms of cut-offs have been studied [113, 114] - qualitatively similar results are found with other forms, although the parameter Λ will have different meanings in each case. We employ a finite value for the cut-off of order the size of the B meson. The integral may be calculated and has the form

$$\mathbf{A}\left(m^2, \Lambda^2\right) = \frac{\Lambda^4}{16\pi^2}\left[\frac{1}{m^2 - \Lambda^2} + \frac{m^2}{\left(m^2 - \Lambda^2\right)^2}\,\ln\frac{m^2}{\Lambda^2}\right]. \tag{8.7}$$

More illuminatingly, this result is shown in Fig. (8.2). In this figure we compare the dimensionally regularized result to the long-distance portion, defined by Eq. (8.7).
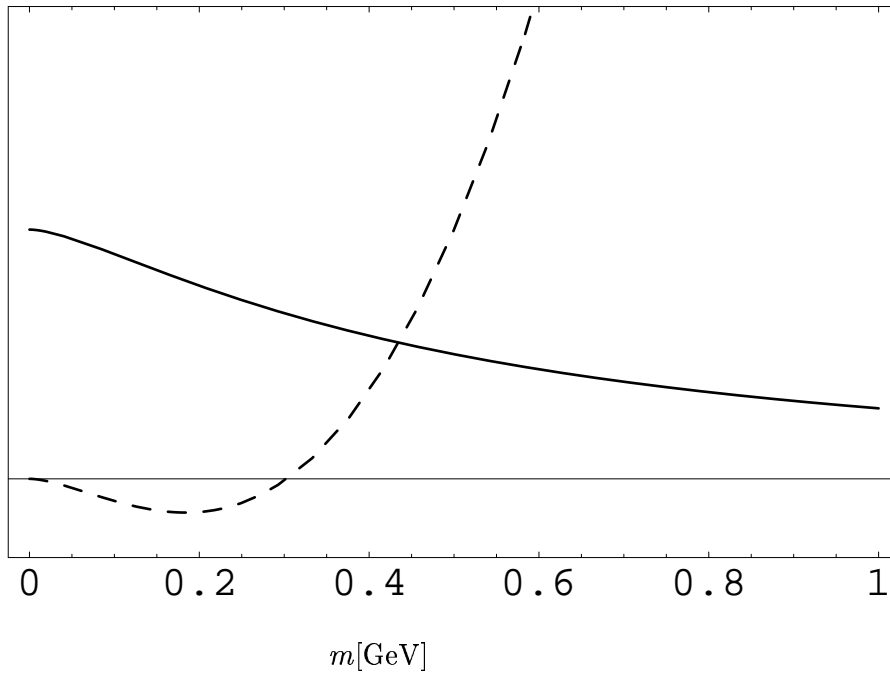

Figure 8.2: Integrals $-\mathbf{A}\left(m^2, \Lambda^2\right)$ with $\Lambda = 500$ MeV and $-\mathbf{A}^{d.r.}\left(m^2\right)$ with $\mu = 500$ MeV (dashed)

The long distance component is seen to have several reassuring features in the cut-off regularization. It is largest when the meson is massless, as one would expect. It is small when the mass is big and exhibits decoupling, vanishing as the mass goes to infinity. It smoothly interpolates between these limits. When comparing it to the dimensionally regularized result, one sees a shift in the intercept at zero mass -

this is not surprising because the regularization corresponds to removing the value when $m = 0$. One also notices that, aside from this shift, both forms have the same logarithmic behavior near $m = 0$. The small curvature noted at the smallest mass values is the nonlinear behavior due to the chiral log factor $m^2 \ln m^2$. Without this term the result would be able to be Taylor expanded about $m = 0$, with the first term being a linear slope in m^2 - the nonlinear behavior is the result of the logarithm.

We also see that the chiral log by itself grows large quickly and has a large curvature at large masses in dimensional regularization. This effect is not mirrored in the long-distance component, so that it is clear that this behavior comes from the short-distance portion of the integral. This is not surprising. In dimensional regularization, there is no scale within the integration aside from the particle's mass, so that the the whole integral scales with $k \sim m$. These short distance effects are the ones which are not reliable calculated by the effective field theory.

These results suggest that we should consider an extrapolation that only includes the long distance loop effects. The short distance effects are provided by the lattice simulation[4]. The truly long distance effects are supplied by chiral perturbation theory. We will use the long distance parts of the loops in performing the matching of the two regions. In our approach this matching is described by the parameter Λ specifying the separation of long and short distances. The residual dependence on this parameter, within some range, is a reflection of the present uncertainty in the matching procedure.

8.3   Long distance regularization of the chiral calculation

At small quark masses, the cut-off treatment of the integral can be promoted to a regularization of chiral perturbation theory. This has been studied in the context of baryon chiral perturbation theory in Ref. [113], where it was called long distance regularization. The use of a cut-off is clearly more painful calculationally than the usual dimensional regularization, but when the masses are small it reproduces the usual one-loop chiral expansion for matrix elements such as we are studying.

In order to regularize the calculation using the cut-off, the divergent pieces are separated in the Feynman integral. The result is

$$\mathbf{A}\left(m, \Lambda\right) = \frac{1}{16\pi^2}\ \left[-\Lambda^2 + m^2 \ln \frac{\Lambda^2}{\mu^2}\right] + \mathbf{A^{ren}}(m^2, \Lambda^2)\,, \qquad (8.8)$$

---

[4]The "smooth matching" procedure of Ref. [111] is another attempt to apply the chiral results only in their region of validity.

where $\mathbf{A^{ren}}(m^2, \Lambda^2)$ is finite in the limit $\Lambda \to \infty$. This residual integral has the form

$$\mathbf{A^{ren}}\left(m^2, \Lambda^2\right) = \mathbf{A^{d.r.}}\left(m^2\right) + \frac{1}{16\pi^2}\left[\frac{m^4}{m^2 - \Lambda^2} + \frac{m^4(m^2 - 2\Lambda^2)}{(m^2 - \Lambda^2)^2}\ln\frac{m^2}{\Lambda^2}\right]. \quad (8.9)$$

We see that there are potentially divergent contributions proportional to Λ^2 and $\ln\Lambda^2$. However, these have exactly the right structure to be absorbed into the chiral parameters. In particular, the renormalization is

$$\begin{aligned}
\bar{f}_0^{ren} &= \bar{f}_0 - \tfrac{8}{3}\,\bar{f}_0 \tfrac{1+3g^2}{64\pi^2 F_\phi^2}\,\Lambda^2 \\
\alpha_1^{ren} &= \alpha_1 + \tfrac{5}{6}\,\tfrac{1+3g^2}{64\pi^2 F_\phi^2}\,\ln\tfrac{\Lambda^2}{\mu^2} \\
\alpha_2^{ren} &= \alpha_2 + \tfrac{11}{18}\,\tfrac{1+3g^2}{64\pi^2 F_\phi^2}\,\ln\tfrac{\Lambda^2}{\mu^2}.
\end{aligned} \quad (8.10)$$

After renormalization, we can express the chiral amplitudes in terms of these parameters plus the logarithmic contribution in the residual integral $\mathbf{A^{ren}}\left(m^2, \Lambda^2\right)$, providing the renormalized observables

$$\begin{aligned}
f_{B_{u,d}} = {}& \frac{1}{\sqrt{m_B}}\,\bar{f}_0^{ren}\left[1 + \alpha_1^{ren} m_\pi^2 + \alpha_2^{ren}(2m_K^2 + m_\pi^2)\right. \\
& \left. + \frac{1+3g^2}{4F_\phi^2}\left(\tfrac{3}{2}\,\mathbf{A^{ren}}\left(m_\pi^2, \Lambda^2\right) + \mathbf{A^{ren}}\left(m_K^2, \Lambda^2\right) + \tfrac{1}{6}\,\mathbf{A^{ren}}\left(m_\eta^2, \Lambda^2\right)\right)\right] (8.11)
\end{aligned}$$

and

$$\begin{aligned}
f_{B_s} = {}& \frac{1}{\sqrt{m_B}}\,\bar{f}_0^{ren}\left[1 + \alpha_1^{ren}(2m_K^2 - m_\pi^2) + \alpha_2^{ren}(2m_K^2 + m_\pi^2)\right. \\
& \left. + \frac{1+3g^2}{4F_\phi^2}\left(2\,\mathbf{A^{ren}}\left(m_K^2, \Lambda^2\right) + \tfrac{2}{3}\,\mathbf{A^{ren}}\left(m_\eta^2, \Lambda^2\right)\right)\right]. \quad (8.12)
\end{aligned}$$

Since at small mass, the residual integral $\mathbf{A^{ren}}\left(m^2, \Lambda^2\right)$ tends to $\mathbf{A^{d.r.}}\left(m^2\right)$, the usual chiral expansion is recovered at $m^2 \ll \Lambda^2$. At small mass, the cut-off is just another way to regularize the calculation.

8.4 The chiral extrapolation of f_B

If we are going to use any meson loop calculation at larger masses in order to match to the lattice, then all treatments are model dependent. We have argued above that the use of chiral logs at these scales amounts to a bad model because it builds in very large and spurious short distance effects. Our calculation above removes the short distance effects in the one loop diagrams. This is then a reasonable formalism to apply to the lattice calculation. The lattice calculation supplies the correct short

distance physics, described there through terms analytic in m^2 (linear behavior, quadratic...). In addition, at smaller masses, our formulas naturally include the chiral logarithms in the regions where they should be valid. This motivates us to use the long-distance loop calculation in the chiral extrapolation for B meson properties.

Let us first fit our expression to a caricature of the lattice data by matching the data at two points. Such a linear extrapolation is appropriate for one loop since we have only the constants and linear counterterms in the one loop expression. This fit is demonstrated in Fig. (8.3), for various values of Λ. We see that the extrapolation is smoother and that there is no large curvature induced at large mass.
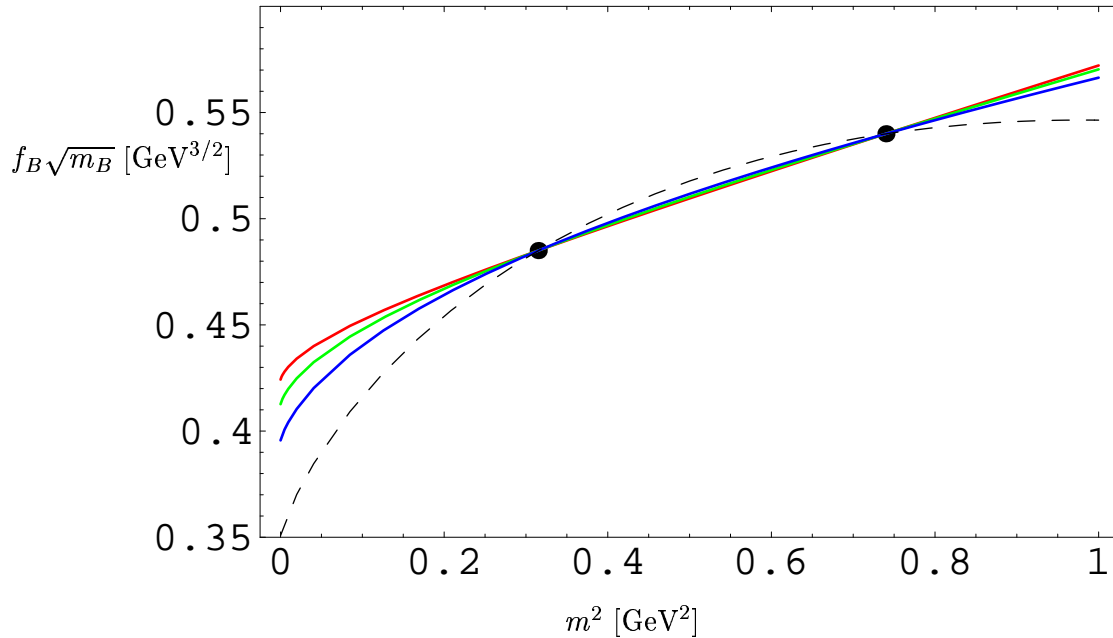

Figure 8.3: $f_B\sqrt{m_B}$ as a function of m^2 fitted to the Lattice data points for $\Lambda = 400, 600, 1000$ MeV and for the result from dimensional regularization, $\Lambda \to \infty$ (dashed)

There is a residual dependence of the extrapolated value on the parameter Λ. This is shown in Fig. (8.4). In the range $\Lambda = 400$ MeV $\to 1000$ MeV, this amounts to a 5% uncertainty in the extrapolated value. The formula used in previous extrapolations corresponds to $\Lambda \to \infty$. It is clear that the loop contributions that arise beyond the scale of $\Lambda = 1000$ MeV are of too short distance to be physically relevant for the effective field theory - there is no reliable chiral physics beyond this scale.

This extrapolation can be systematically improved. Most favorably would be the situation in which the lattice data can be calculated at smaller mass squared - eventually no extrapolation would be needed. Even if the improved data goes only part of the distance to the physical masses, it would remove some of the model de-
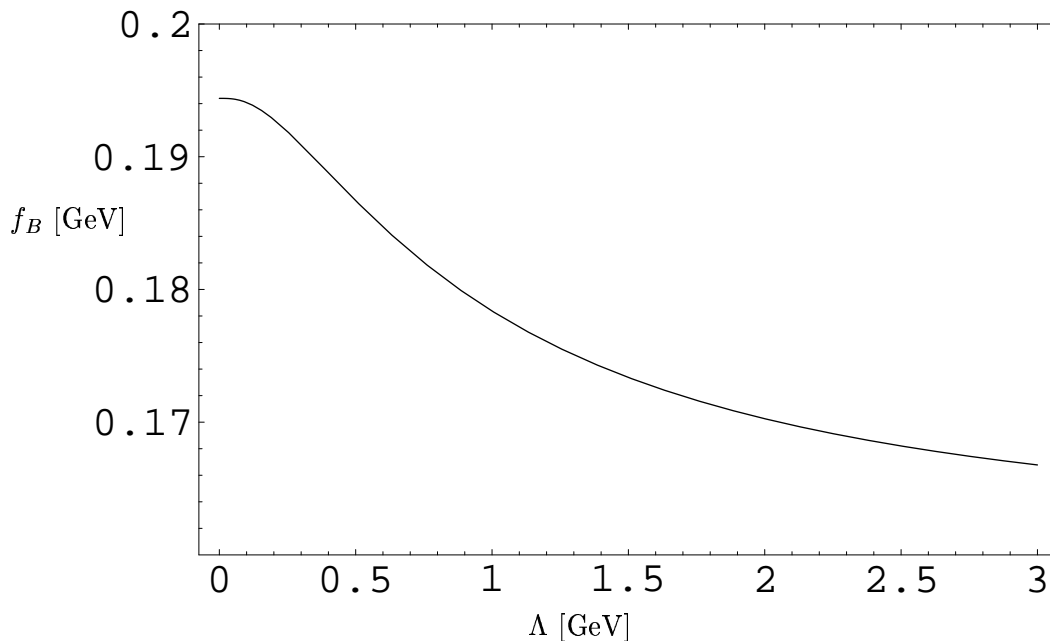
Figure 8.4: f_B at the physical pion mass as a function of Λ

pendence of the result. The extrapolation needed would be smaller and the residual Λ dependence would be smaller. Another way that improvement possibly may be made is with increased precision even at larger masses. As shown by Eq. (8.9) above, the extrapolations for different Λ values differ only at order m^4/Λ^2. If one includes an extra $\mathcal{O}(m^4)$ in the one loop chiral calculation, fitting to a quadratic expression, then the extrapolations will be in closer agreement at this chiral order. Note however that the low mass region is still being extrapolated by a one-loop chiral formula - this procedure is not equivalent to a two-loop result in chiral perturbation theory.

As the lattice data reaches higher precision, it may be that the range of Λ for which a good fit is obtained may shrink. While we are treating Λ as a regularization parameter, it is meant as a rough parameterization of a physical effect - the transition from long-distance to short-distance in the loop calculation. Therefore when using a fit to a given order in the chiral expansion, the lattice data may only be describable with Λ within some range near the scale of this physical effect. Indeed, already the present data is a poor fit for $\Lambda \to \infty$. Of course if one allows arbitrary orders in the chiral expansion, with free parameters at each order, it is always possible to correct the loop effect for any incorrect short distance behavior by adjusting the parameters. However, when using the one loop integral with precise data it may not be possible to obtain good fits for large values of Λ without introducing *several* new parameters at higher orders in the masses. In contrast, simpler fits with fewer parameters may be obtained with Λ within some optimal range.

Our procedure might be criticized as being a model, due to the choice of a sep-

aration function and a separation scale. However, at large masses, the dimensional regularization result is really more of a model as it introduces large and unphysical short distance physics. Our procedure is the "anti-model" because it removes most of that physics. The residual dependence on Λ comes from the ambiguity concerning how much of the short distance physics to remove. The value of Λ from the lattice results, introduced through the dipole cut-off, parametrizes the short distance physics. However, this dependence can itself be adjusted by using the coefficients of the chiral lagrangian. Despite the decoupling of the loop at large mass, we retain all of the correct chiral behavior in the limit of small quark mass.

8.5   Application to B_B

All of the preceding formalism can also be applied to the chiral extrapolation of the B_B parameter for $B - \bar{B}$ mixing. We have reproduced the calculations of Ref. [109, 110] using throughout the method of long distance regularization. As above, only the integral $\mathbf{A^{ren}}$ is needed in the final answer. The chiral formulas after renormalization of the parameters are

$$
B_{B_d} = B_0^{ren} \qquad \left[1 + \beta_1^{ren}\, m_\pi^2 + \beta_2^{ren}\,(2m_k^2 + m_\pi^2) \right.
$$

$$
\left. + \frac{1 - 3g^2}{4\,F_\phi^2}\left(\mathbf{A^{ren}}\left(m_\pi^2, \Lambda^2\right) + \tfrac{1}{3}\,\mathbf{A^{ren}}\left(m_\eta^2, \Lambda^2\right) \right) \right], \qquad (8.13)
$$

$$
B_{B_s} = B_0^{ren} \qquad \left[1 + \beta_1^{ren}\,(2m_K^2 - m_\pi^2) + \beta_2^{ren}\,(2m_k^2 + m_\pi^2) \right.
$$

$$
\left. + \frac{1 - 3g^2}{3\,F_\phi^2}\,\mathbf{A^{ren}}\left(m_\eta^2, \Lambda^2\right) \right], \qquad (8.14)
$$

in the same notation as before. Here the new chiral constants B_0, β_1, β_2 describe the intercept and slope of the chiral expansion. At small masses the usual dimensional regularization results of Ref. [109, 110] are recovered in the limit of small m/Λ, as is seen using Eq. (8.9).

The chiral corrections for B_B are proportional to $1 - 3g^2$, while in the case of f_B the corrections contain the factor $1 + 3g^2$. This modification makes an important change in the result. For the coupling $g = 0.59$ that is favored by recent measurements [115] and supported by recent lattice calculations and theoretical predictions [115], the factor $1 - 3g^2$ almost vanishes. In this case, the one loop chiral corrections are tiny whether one employs the standard scheme or our long-distance regularization methods. (See also [116] for a discussion of this effect). For this reason, we do not display the numerical effect of the chiral extrapolation of B_B. Use of a significantly smaller value of the coupling g would lead to measurable effect in the B_B extrapolation.

8.6 Conclusions

We have presented a method for the extrapolation of lattice data to smaller quark masses. This includes the chiral logarithm in the region where it is valid. It has the advantage that it removes the large and unphysical short distance effects that caused problems in previous methods. There is still some residual model dependence that is visible in the variation of the results on Λ. However the extrapolations are better behaved than previous ones. The residual uncertainty in a linear extrapolation (i.e. with a slope proportional to m^2 and no chiral logarithm) for f_B is about 5% when the cut-off is constrained to the range 400 MeV–1000 MeV. For B_B the uncertainty in the chiral extrapolation is negligible for $g = 0.59$. We would recommend that our method only be applied for values in this range.

The chiral corrections have the effect of producing a slight decrease in the extrapolated values of f_B and B_B when compared to an extrapolation which does not include chiral effects. This is the effect of the non-analytic behavior of the chiral logarithm at long distance. Our estimates suggest that the decrease due to the chiral log puts the chirally corrected result at 0.945 ± 0.025 of the uncorrected extrapolation for f_B. We hope that our method will be applied in future extrapolations of lattice data.

Chapter 9

Discusión y conclusiones

Para concluir esta tesis doctoral voy a resumir brevemente el trabajo realizado. Así mismo plantearé las conclusiones finales una vez han sido mostradas todas las partes del trabajo. Comentaré primero el planteamiento de la acción efectiva. Luego mostraré los resultados para el factor de forma vectorial en la región entorno al pico de la $\rho(770)$, para a renglón seguido comentar el resultado perturbativo cuando uno se aleja de polo de la resonancia. Por último terminaré las conclusiones comentando los resultados obtenidos en los otros dos estudios realizados en esta tesis, el sector de resonancias escalares y el estudio de la constante de desintegración de los mesones B.

9.1 Un lagrangiano efectivo para QCD en la región de las resonancias

Al comienzo del trabajo partimos de la acción de QCD. Al estar trabajando a energías $E \lesssim 2$ GeV se podía prescindir de los sabores de quarks pesados - *charm/bottom/top* y el estudio se realizó sobre QCD con tres sabores ligeros - *up/down/strange*. Aún con esta simplificación la teoría en términos de quarks y gluones se vuelve altamente no-perturbativa a bajas energías. Para estudiarla se necesitan entonces una serie de herramientas alternativas. En esta tesis nos hemos centrado en la construcción de una teoría efectiva para describir las interacciones entre mesones –el octete de pseudo-escalares ligeros y el primer multiplete de resonancias vectoriales, axiales, escalares y pseudo-escalares–. Se ha intentado extender el rango de validez de anteriores teorías efectivas así como calcular el tamaño de las correcciones cuánticas que vienen de los loops.

En este escenario se observa que las masas de los quarks se pueden despreciar en principio e introducirse posteriormente como un parámetro perturbativo. Esto da lugar a que aparezca una nueva simetría en QCD, la simetría quiral. Sin embargo esta simetría se rompe espontáneamente generando una serie de bosones de Nambu-Goldstone.

A partir de las simetrías es posible construir una teoría efectiva, χPT, para describir las interacciones entre los Goldstones. Desafortunadamente esta teoría deja de tener validez al acercarnos a energías del orden de la masa del primer multiplete de resonancias.

Como herramienta alternativa al contaje de momentos que se suele emplear en otras teorías como χPT se empleó una expansión en $1/N_C$, siendo N_C el numero de colores en QCD. El campo está siendo ampliamente trabajado a primer orden en la expansión en $1/N_C$. Sin embargo se echan en falta trabajos que traten de comprobar la consistencia de la teoría al nivel de *loops* [105, 59]. A través del análisis del factor de forma vectorial hasta segundo orden en $1/N_C$ se observaron una serie de patologías que destrozan la conexión del resultado efectivo con el de QCD perturbativo a altas energías. Estos problemas son:

- **Factores de forma con resonancias en los estados finales:** El lagrangiano mínimo que introdujeron Ecker *et al.* [19] se ha mostrado muy eficaz para describir factores de forma a orden árbol con Goldstones en los estados finales. Sin embargo para los casos con dos resonancias en los estados finales este lagrangiano produce factores de forma constantes. Si bien experimentalmente puede no estar claro cómo definir las resonancias, lo que si es esperable es que el comportamiento de sus factores de forma no sea constante y que a altas energías tiendan a cero.

  Este problema parece tener una salida bastante obvia, que es el estudio teórico de estos factores de forma al orden dominante en $1/N_C$ y la introducción de nuevos términos con operadores de tres resonancias, que permitan recobrar la conocida estructura monopolar $\frac{M_R^2}{M_R^2-s}$, como se ha mostrado recientemente en Ref. [106].

- **Comportamiento de las amplitudes de dispersión:** Mediante estudios de analiticidad y unitariedad es bien conocido que las amplitudes de dispersión de dos partículas $\mathcal{T}(s,t)$ deben crecer más despacio que $\sim s^2$ a altas energías. De este modo uno asegura que cada onda parcial de momento angular J permanece acotada. En el caso de RχT uno encuentra que a altas energías las ondas parciales de las amplitudes de dispersión de dos Goldstones yendo a dos Goldstones crecen como $T^J \sim s$. El problema no tiene una solución trivial ya que, por ejemplo en el canal $I = J = 1$, si bien la amplitud en el canal-s obedece un buen comportamiento a altas energías, éste se estropea al considerar también el intercambio de resonancias en el canal-t ya que las contribuciones dadas por el intercambio de vectores y escalares van como $\sim s$ a altas energías. De hecho parece bastante complicado poder llegar a solucionar el problema sin considerar de alguna manera el efecto de la pila infinita de resonancias y posibles espines. Lo que es más, para las amplitudes de dispersión de dos resonancias a dos Goldstones el lagrangiano contiene sólo un término local que va como $\sim s$, $\mathcal{L}_{2\chi}$, y cuyas constantes ya están fijadas.

Así que, por lo tanto, este problema requiere un estudio más complejo que el de los factores de forma. Aquí no es suficiente el estudiar las amplitudes de dispersión a orden árbol y el considerar un número de nuevos operadores, sino que se debe desarrollar una manera de describir el intercambio de mesones en el canal-t de manera que, de modo efectivo, se recupere el comportamiento correcto a altas energías incluso cuando se considera la interacción a primer orden en $1/N_C$.

- **Modos no-físicos de los estados vectoriales:** A altas energías uno encuentra que QCD acepta una descripción perturbativa en términos de partículas de masa cero (en el límite en que despreciamos las masas de los quarks). Por lo tanto de algún modo los grados de libertad extra de los estados vectoriales no puede estar presentes a cortas distancias. Sin embargo, nuestra teoría de resonancias contiene campos masivos de *spin* 1. Al contrario de lo que sucede en el Modelo Estándar la masa de los vectores no ha sido introducida en nuestro lagrangiano a traves de un mecanismo de Higgs, sino mediante un término explícito de masa sin apelar a ninguna simetría extra. En los cálculos a un *loop* se puede observar de manera explícita la propagación de los modos no-físicos de los mesones vectoriales (proyección Ω en el formalismo antisimétrico y longitudinales en el de Proca). Así sucede que al considerar *loops* donde tenemos vectores (y axial-vectores) como estados intermedios la amplitud crecen como una potencia más alta del momento que los *loops* con escalares (y pseudo-escalares), estropeando el comportamiento a altas energías y dando un factor de forma que no se ajusta al que predice QCD a cortas distancias.

  Este problema parece tener también una solución más compleja que el simplemente considerar operadores con mayor número de resonancias y de términos locales de χPT. Las masas de todas las resonancias del espectro de QCD, así como cualquier otra escala de la interacción fuerte, vienen dadas por la escala característica de ruptura de la simetría quiral Λ_χ, de tal modo que el régimen no perturbativo de QCD genera una escala de modo dinámico y que no se encontraba presente inicialmente en la descripción perturbativa de QCD. De este modo se ve como el tema es tremendamente más complicado e interrelacionado de lo que parece; los grados longitudinales de los mesones de *spin* $J \geq 1$ surgen entonces por mecanismo que están todavía por resolver, como son la ruptura espontánea de la simetría quiral y más concretamente el régimen no pertubativo de QCD.

Al estudiar el factor de forma vectorial hasta segundo orden en $1/N_C$ uno encuentra que no se puede aplicar el comportamiento asintótico como se hizo con los factores de forma a piones a primer orden en $1/N_C$. El cálculo del grado superficial de divergencia desarrollado en el capítulo 4 nos hace esperar a priori un comportamiento del factor de forma a un *loop* como $\mathcal{F}(q^2) \sim q^2$ a altas energías.

Realmente el comportamiento que nos da el cálculo es incluso peor y se comporta como $\mathcal{F}(q^2) \sim q^4$, debido a los contribución de la proyección Ω de los propagadores vectoriales en el *loop* con dos propagadores vectoriales (contribuciones V7 y A2 en el Apéndice C). La parte analítica, en la que ha habido que introducir contratérminos subdominantes en $1/N_C$ para renormalizar, no plantea un grave problema ya que los acoplamientos de las resonancias hasta segundo orden en $1/N_C$ se podrían ajustar para que sólo sobrevivieran los términos que van como $\Delta\mathcal{F}(q^2) \sim 1/q^2$, como se hace habitualmente en los cálculos a orden árbol.

El auténtico problema lo plantean los términos no analíticos, los logaritmos $\ln(-s)$, que dependen sólo de los acoplamientos a primer orden en $1/N_C$ y que fueron ya fijados. Por lo tanto no es posible realizar el mismo juego de ajuste de acoplamiento que se utiliza para hacer que los términos analíticos se comporten bien a altas energías.

Resumiendo:

Los problemas anteriormente mencionados producen precisamente ese excesivo crecimiento del factor de forma vectorial a piones a un *loop*. Estos diagramas sólo pueden tener corte absortivo de estados de dos partículas, de modo que nuestros diagramas quedan descompuestos en tres partes: primeramente tenemos una producción de dos mesones a orden árbol que , salvo para la producción del estado $\pi\pi$, se comporta como $\sim s^0$ en lugar de como $\sim 1/s$; segundo, al final estas partículas son dispersadas nuevamente a orden arbol dando un estado final $\pi\pi$, de modo que esta amplitud de dispersión se comporta como $\sim s$ en lugar de como $\sim s^0$; por último, en un tipo de diagrama concreto referido antes –el diagrama V7 del Apéndice C para vectores y el A2 para axial-vectores– se tiene una contribución no nula de la parte en Ω de uno de los dos propagadores vectoriales (y axial-vectoriales) intermedios, de modo que a altas energías va como $\Delta(k)^{\mu\nu,\rho\sigma} \sim i/M_{V,A}^2$ en lugar de como $\Delta(k)^{\mu\nu,\rho\sigma} \sim i/k^2$. Así entiende uno con claridad el origen de las tres potencias extra de q^2 que daba el cálculo en comparación con el resultado obtenido a primer orden en $1/N_C$.

La importancia de este análisis es que semejantes problemas pueden aparecer al estudiar otros observables más complejos: correladores a un *loop* [59], funciones de Green de cuatro puntos [117], otros factores de forma a órdenes superiores [118]... A través del análisis del ejemplo concreto del factor de forma vectorial ha sido posible encontrar las pautas que permiten saber de antemano cual va a ser el orden de divergencia que vamos a obtener en nuestro observable, así como los posibles órdenes extra que pueden surgir por los propagadores de vectores masivos.

Sin embargo es importante reseñar que la Teoría Quiral de Resonancias que se ha desarrollado hasta segundo orden en $1/N_C$ reproduce de modo exacto el predicho por χPT una vez que se va a energías mucho más bajas que la masa de la $\rho(770)$. Se observa que se recupera totalmente el resultado de χPT a un *loop*, dando la relación que existe entre las constantes de bajas energías del lagrangiano quiral y

las constantes de altas energías del lagrangiano de resonancias. Es más, se da la expresión no a primer orden en $1/N_C$ como se venía haciendo hasta ahora, sino hasta segundo orden y para una escala de renormalización cualquiera. Se demuestra de este modo que la pregunta que se planteaba hasta ahora sobre a que escala se produce la saturación por resonancias no tiene en realidad mucho sentido; a cambio lo que se tiene son unos acoplamientos de la teoría de resonancias con un valor concreto para un μ dado y que "corren" de tal manera que a bajas energías las constantes quirales "corran" también y en el modo predicho por χPT.

Es más, el estudio de las renormalizaciones nos permite observar que el tamaño de las correcciones radiativas en los acoplamientos de RχT son realmente subdominantes en comparación con el valor de los acoplamientos a primer orden $1/N_C$.

9.2 Determinación de algunas propiedades de los mesones

En esta tesis se realizaron además algunas determinaciones de los parámetros del lagrangiano quiral y del de resonancias. A través de los análisis fenomenológicos de factores de forma para energías entorno a la masa de las resonancias se pudieron obtener alguna determinanciones de los acoplamientos y masas de los mesones. En los casos con mayor incertidumbre, como en el escalar, se dieron unas buenas estimaciones.

9.2.1 Sector vectorial

Mediante una técnica de vértices efectivos desarrollada en la Ref. [26] se realizaron resumaciones de Dyson con la adaptación que requiere el contaje perturbativo en $1/N_C$. De ese modo, para el vector se obtuvo la masa y anchura polo de valor

$$M_\rho^{\text{pole}} = (764.1 \pm 2.7 \, {}^{+4.0}_{-2.5}) \, \text{MeV} \,, \qquad \Gamma_\rho^{\text{pole}} = (148.2 \pm 1.9 \, {}^{+1.7}_{-5.0}) \, \text{MeV} \,, \quad (9.1)$$

en completo acuerdo con otras determinaciones [82]. El otro modo en que habitualmente se suelen dar estos parámetros es la masa y anchura Breit-Wigner, definidos a partir de la fase compleja de la amplitud de dispersión, y que en nuestro caso valían

$$M_{BW} = (776.0 \pm 1.6 \, {}^{+0.3}_{-0.7}) \, \text{MeV} \,, \qquad \Gamma_{BW} = (156.2 \pm 1.6 \, {}^{+0.3}_{-3.0}) \, \text{MeV} \,. \quad (9.2)$$

De igual modo se obtuvieron determinaciones de las constantes de acoplamiento $\rho(770)$ a fotón, F_V, y $\rho(770)$ a dos piones, G_V,

$$|F_V/F| = 1.696 \pm 0.008 \, {}^{+0.010}_{-0.028} \,, \qquad |G_V/F| = 0.695 \pm 0.004 \, {}^{+0.011}_{-0.019} \,, \quad (9.3)$$

y $F_V G_V > 0$. Este resultado está en completo acuerdo con lo predicho teóricamente a través de análisis de cortas distancias, desviándose menos de un 20 % de la predicción a primer orden en $1/N_C$.

De igual modo, la determinación de los parámetros del lagrangiano a través de un análisis parcial hasta segundo orden (sólo se resuman los diagramas más relevantes),

permite dar una determinación de la constante $L_9^r(\mu)$ de χPT a cualquier escala μ, ya que su *running* es recuperado totalmente salvo correcciones subdominantes en $1/N_C$. El análisis de los datos nos muestra que en efecto esas correcciones son despreciables y que a efectos prácticos el *running* se recupera perfectamente. En concreto para $\mu = 770$ MeV se tiene

$$L_9^r(\mu_0) = (7.04 \pm 0.05\,^{+0.19}_{-0.27}) \cdot 10^{-3}\,. \tag{9.4}$$

9.2.2 Sector escalar

Para el caso del escalar se obtuvieron determinaciones de la masa del primer multiplete de resonancias escalares por dos métodos y aproximaciones diferentes. En un primer lugar se realizó una resumación de Dyson, enlazando con χPT, similar a la que se había hecho anteriormente con el VFF. Aunque teóricamente se mostró la estructura formal de la amplitud para el caso de canales acoplados ($\pi\pi$, $K\overline{K}$ y $\eta_8\eta_8$), a efectos prácticos se realizó el análisis por debajo del umbral $K\overline{K}$ en la teoría de dos sabores (u/d) y en el límite de masa del pion cero. Se hizo un ajuste a los datos experimentales del desfasaje complejo de la amplitud de dispersion en la región elástica [35]. De ahí salieron las determinaciones de la masa (el parámetro del lagrangiano, no la masa polo o Breit-Wigner) y del acoplamiento escalar-pion-pion:

$$M_S = (870 \pm 14^{+\,4}_{-21})\,\text{MeV}\,, \qquad \frac{2c_d}{F} = 0.67 \pm 0.04^{+0.17}_{-0.02}\,. \tag{9.5}$$

Este resultado proporciona la siguiente estimación de la constante de χPT,

$$\ell_4^r(\mu) = \ell_4\big|_{N_C \to \infty} + \Delta\ell_4(\mu) = \frac{4c_d c_m}{M_S^2} + \Delta\ell_4(\mu) \simeq 3.5 \cdot 10^{-3}\,, \tag{9.6}$$

para $\mu = 770$ MeV y tomando $c_m = F/2$, con $F \simeq 92.4$ MeV.

El estudio de otros observables, las constantes de desintegración del pion y del kaón, nos permite extraer alguna información sobre el sector escalar. Para ello, tomé los resultados de las simulaciones en el retículo de los correspondientes elementos de matriz hadrónicos. Estas simulaciones se realizan para distintos valores de las masas *up* y *down*, con lo que uno puede obtener información sobre la dependencia de estos parámetros con la masa de los quarks ligeros.

De este modo, al orden dominante en $1/N_C$ uno puede fijar la masa del multiplete $U(3)$ más ligero de resonancias escalares:

$$M_S = 1049 \pm 25\,\text{MeV}\,. \tag{9.7}$$

Se puede incluso estimar la ruptura de la degeneración de masas entre los dos escalares con $I = 0$ debido a las diferentes masas de los quarks *up/down* y *strange*, pero se comprueba que hay una alta incertidumbre en la determinación. Así mismo,

uno debe tener presente que al siguiente orden en $1/N_C$ pueden aparecer variaciones en la masa del escalar del mismo tamaño que la contribución por masas de quarks.

Lo que queda por tanto bastante claro tanto de los análisis en $n_f = 2$ (resumación de Dyson de piones sin masa) y en $n_f = 3$ (F_π y F_K en el límite $N_C \to \infty$) es que el valor de la masa del primer multiplete de resonancias escalares $q\bar{q}$ tiene $M_S \simeq 1$ GeV, encontrándose por tanto por encima del primer multiplete de vectores, el de la $\rho(770)$.

9.3 Sector de quarks pesados

Por último, se realizó un análisis de los parámetros de los mesones B, la constante de desintegración f_B y la de mezcla B_B, obtenidos a través de simulaciones en el retículo para valores no físicos de las masas de los quarks *up* y *down*. Para altos valores de estas masas se observaba el mismo tipo de comportamiento lineal que en F_π y F_K. Si bien un estudio basado en N_C grande, como en el caso escalar, aún permanece pendiente, uno puede realizar una serie de *Ansatzë* previos para analizar con más claridad el comportamiento y la dependencia de estos parámetros en las masas de los quarks.

De este modo, se introdujo un $cut-off$ suave Λ_{cut}, con estructura dipolar. Se vio que el cambio de régimen logarítmico a lineal ocurría para $\Lambda_{cut} = (400 \to 1000)$ MeV, reproduciéndose así los resultados obetenidos en el retículo. La falta de conocimiento en el valor del parámetro Λ_{cut} producía una incertidumbre en f_B y rebajaba su valor con respecto a las extrapolaciones lineales anteriores en un 0.945 ± 0.025.

Para finalizar, el análisis de la constante de mezcla B_B muestra que en ese caso la influencia de los *loops* es menor ya que hay cancelaciones accidentales entre loops debido al valor del acoplamiento $g_{\pi BB^*} \simeq 0.59$. Por tanto, las extrapolaciones lineales producen prácticamente el mismo resultado que las que consideran las contribuciones a un *loop*.

9.4 Coda

La resolución de QCD parece aún un problema con difícil solución. Sin embargo a través del empleo de técnicas de teorías efectivas y de métodos como la expansión en $1/N_C$ se obtienen resultados que parecen estar en la dirección correcta.

En este trabajo nos hemos centrado principalmente en el estudio de las resonancias de quarks ligeros obteniendo por un lado unos buenos resultados fenomenológicos, y por otro toda una serie de nuevos e interesantes interrogantes. Se comprobó que a bajas energías se proporciona una decripción correcta y al nivel teórico se recupera χPT de modo exacto hasta el orden en $1/N_C$ estudiado, no sólo a orden árbol sino a uno y dos *loops*. Por otro lado, aún parece que estemos lejos de poder recuperar el comportamiento correcto al ir a altas energías pues hay un sinnúmero de problemas aún por trabajar y estudiar.

Como tema accesorio se hizo también un acercamiento al campo de simulaciones en el retículo un campo en claro auge y que promete dar todavía una gran cantidad de resultados interesantes. A través del estudio realizado en el capítulo 8 hice un primer acercamiento al estudio de las interacciones entre mesones ligeros, con componentes *up/down/strange*, y mesones pesados, con componentes *charm* o *bottom*. Se vio así cómo las propiedades de un sector afectan a las del otro y que en un necesitan ser trabajados conjuntamente.

Chapter 10

Agradecimientos

One Coupling to rule them all, One Coupling to find them,
One Coupling to bring them all and strongly bind them
In the Land of Mesons where QCD lies.

Bueno, por una vez seré breve. Querría dar las gracias lo primero a las dos personas de que de un modo más directo han hecho posible que esta tesis existiera (y existiera en el plazo fijada, lo cual no es trivial): Toni y Jorge. Gracias por aguantar el aluvión de lectura que os di los últimos días y por toda la ayuda durante el tiempo aquí. Os habéis ganado medio cielo.

También quería agradecer a mi familia y amigos el apoyo moral dado durante esas etapas en que parece que nada anda por el buen camino y que, porque no decirlo, te sientes el más rematadamente tonto del instituto. Gracias a vosotros por ayudarme a desintoxicar y recordarme que la Física no es todo (a veces uno se llega a obsesionar peligrosamente con ciertos problemas y más de una vez me ha costado dormir porque no paraban de venirme cálculos y cálculos a la cabeza). Muchas gracias a Rueda, a Zaro, a Romeo, a Emilio, por soportar mis tonterias sin sacarnos los ojos en exceso, y a la Vidala, a Velasco y Míriam (lo siento pero ya eres *mejillona* –y yo no–), y a todos los *mejillones* que no han sido excesivamente integristas; a Nachete, a Juan y a Oscar y a todos mis sectarios favoritos (si aprendes a soportar a *Antichriste* todo lo demás son minucias); y a Jeil, una persona realmente honesta (no hay tantas) con quien tan buenas (y elevadas) charlas he tenido; un saludo a Néstor (Alias *violinista loco*), Pascu, Agus y a los amigos de la sala, mis esgrimistas de barra, con quienes tan buenos ratos he pasado en el *Black Sheep* y rondando por Valencia; a Pedro e Irene, para que sigan tan majos (y de paso me inviten a Munich, Je Je), y al resto de amigos del IFIC, Natxo (ahora y familia), Juan (y más familia) y tantos otros que han hecho que el trabajo al final fuera menos trabajo y que han humanizado un poco tanta ecuación y tanta leche (que falta hace). De ultramar, quiero acordarme de los buenos amigos que hice en Amherst e Ithaca, en donde pasé unos meses excelentes y a los que les guardo también un cariño especial. Un saludo

a Yamile, la Miss Colombia, reina de la fiesta y la salsa, y a David y toda la *troupe*; y también un abrazo para Luís y Loren, sin dudarlo, los mejores compañeros que pueda uno tener para una casa; y un beso para mi parejita hispano-alemana, Andi y Rebeca, que sigan y sigan, dondequiera que estén o terminen (volved, volved a casa!!); y quiero acordarme también Betty y Susie (aunque mira que es más bonito Azucena), mis gemelas favoritas (seguro que alguna mente calenturienta empezará a volar en este punto); por último agradecer a John y a Matthias el buenísimo trato que me dieron cuando estuve ahí y el buen ambiente que encontré; y bueno a todo el mundo que seguro me olvido también les envio un fuerte abrazo.

Tan sólo quiero remarcar especialmente a dos personas que considero que son las que más han sufrido y sufren esta profesión (sí, lo juro, yo trabajo) sin comerlo ni beberlo. Por un lado quiero recordar a Silvia, y que dondequiera que esté ahora se encuentre bien y que sepa que sin ella a lo mejor no habría podido conseguirlo. Por otro lado no quiero olvidar a Ramune (lo siento, no he podido encontrar el puntito encima de la *e*). Siento la incomunicación de los últimos meses y los gestos ausentes y pensativos. Seguro que encontraremos el modo de compensartelos. De momento, empecemos por un beso.

Para terminar (*that not least*) dar las gracias a Bordes y a las secretarias (en concreto Alicia) por aguantar mis preguntas y repreguntas sobre procedimientos, papeles, plazos, tramites...

Bueno, pues ahora, a disfrutar un poco el verano y a seguir trabajando... Vaya, me acabo de dar cuenta que ya es casi otoño; habrá que darse prisa.

P.D.: El encabezado es una adaptación particular que me salió una de esas noches interminables, a altas horas, mientras me apresuraba por empaquetar la tesis a tiempo. Lo escribí en ese momento y al final mandé la tesis a imprenta sin haberlo borrado antes. Así quede esta constancia de cómo del poco dormir y del mucho leer (*papers*) se me secó el seso.

Appendix A

Feynman integrals

A.1 Scalar integrals

In the calculation of the one loop diagrams there appeared three kinds of Feynman integrals,

$$A_0(M^2) = \int \frac{dk^d}{i(2\pi)^d} \frac{1}{k^2 + i\epsilon - M^2} \,,$$

$$B_0(q^2; M_a^2, M_b^2) = \int \frac{dk^d}{i(2\pi)^d} \frac{1}{(k^2 + i\epsilon - M_a^2)\left((q-k)^2 + i\epsilon - M_b^2\right)}$$

$$C_0(q^2; M_a^2, M_b^2, M_c^2) =$$

$$\int \frac{dk^d}{i(2\pi)^d} \frac{1}{\left((p_1-k)^2 + i\epsilon - M_a^2\right)\left((p_2+k)^2 + i\epsilon - M_b^2\right)\left(k^2 + i\epsilon - M_c^2\right)} \,,$$

$$\tag{A.1}$$

with $q = p_1 + p_2$, the squared external momenta $p_1^2 = p_2^2 = 0$ and the divergence

$$\lambda_\infty = \frac{2\mu^{d-4}}{d-4} + \gamma_E - \ln 4\pi - 1 = \frac{2}{d-4} + \gamma_E - \ln 4\pi - 1 + \ln \mu^2 \,, \tag{A.2}$$

being $\gamma_E \simeq 0.5772$ the Euler constant.

These integrals for some especific values of the masses are:

$$A_0(M^2) = \frac{M^2}{16\pi^2}\left\{-\lambda_\infty - \ln\frac{M^2}{\mu^2}\right\},$$

$$B_0(q^2; M^2, M^2) = \frac{1}{16\pi^2}\left\{-\lambda_\infty + 1 - \ln\frac{M^2}{\mu^2} - \sigma_M \ln\left(\frac{\sigma_M + 1}{\sigma_M - 1}\right)\right\},$$

$$B_0(q^2; 0, M^2) = \frac{1}{16\pi^2}\left\{-\lambda_\infty + 1 - \ln\frac{M^2}{\mu^2} - \left(1 - \frac{M^2}{q^2}\right)\ln\left(1 - \frac{q^2}{M^2}\right)\right\},$$

$$B_0(q^2; 0, 0) = \frac{1}{16\pi^2}\left\{-\lambda_\infty + 1 - \ln\left(-\frac{q^2}{\mu^2}\right)\right\},$$

$$C_0(q^2; 0, 0, M^2), = -\frac{1}{16\pi^2 q^2}\left\{\mathrm{Li}_2\left(1 + \frac{q^2}{M^2}\right) - \mathrm{Li}_2(1)\right\},$$

$$C_0(q^2; M^2, M^2, 0), = \frac{1}{16\pi^2 q^2}\ln^2\left(\frac{\sigma_M - 1}{\sigma_M + 1}\right)$$

$$\tag{A.3}$$

with $\sigma_M \equiv \sqrt{1 - 4M^2/q^2}$.

The three-propagator integral with two different masses is [47]:

$$C_0(q^2, M^2, M^2, m^2) = \frac{1}{16\pi^2 q^2}\left\{-\widetilde{\mathrm{Li}}_2\left(\frac{q^2 m^2}{(M^2 - m^2)^2}\right) + \right.$$

$$+\widetilde{\mathrm{Li}}_2\left(\frac{q^2 M^2}{(M^2 - m^2)(M^2 - m^2 - q^2)}\right) +$$

$$+\widetilde{\mathrm{Li}}_2\left(-\frac{q^2}{M^2 - m^2}\frac{1 + \sigma_M}{2}\right) - \widetilde{\mathrm{Li}}_2\left(\frac{q^2}{M^2 - m^2 - q^2}\frac{1 - \sigma_M}{2}\right) +$$

$$\left. +\widetilde{\mathrm{Li}}_2\left(-\frac{q^2}{M^2 - m^2}\frac{1 - \sigma_M}{2}\right) - \widetilde{\mathrm{Li}}_2\left(\frac{q^2}{M^2 - m^2 - q^2}\frac{1 + \sigma_M}{2}\right)\right\},$$

$$\tag{A.4}$$

where a new function has been defined:

$$\widetilde{\mathrm{Li}}_2(x) = \mathrm{Li}_2\left(\frac{1}{1 + x}\right), \tag{A.5}$$

with the usual dilogarithm definition

$$\mathrm{Li}_2(y) = -\int_0^1 \frac{dx}{x}\ln(1 - xy) = -\int_0^y \frac{dx}{x}\ln(1 - x). \tag{A.6}$$

There are some properties of the dilogs that may be useful:

$$\mathrm{Li}_2\left(\frac{x - 1}{x}\right) = \mathrm{Li}_2(x) - \frac{\pi^2}{6} + \frac{1}{2}\ln^2 x + \ln x \ln(1 - x) \tag{A.7}$$

$$\mathrm{Im}\{\mathrm{Li}_2(y + i\epsilon)\} = \pi \ln(y)\,\theta(y - 1), \tag{A.8}$$

being $\theta(x)$ the usual step function.

In the calculation we are going to separate the infinite part with λ_∞ and the finite part:

$$\hat{A}_0(M^2) \equiv \quad A_0(M^2) + \frac{M^2}{16\pi^2}\lambda_\infty \quad = -\frac{M^2}{16\pi^2}\ln\frac{M^2}{\mu^2}$$

$$\hat{B}_0(q^2; M^2, M^2) \equiv \quad B_0(q^2; M^2, M^2) + \frac{1}{16\pi^2}\lambda_\infty \quad = \frac{1}{16\pi^2}\left\{1 - \ln\frac{M^2}{\mu^2} \right.$$
$$\left. -\sigma_M \ln\left(\frac{\sigma_M + 1}{\sigma_M - 1}\right)\right\},$$

$$\hat{B}_0(q^2/\mu^2) = \quad B_0(q^2; 0, 0) + \frac{1}{16\pi^2}\lambda_\infty \quad = \frac{1}{16\pi^2}\left\{1 - \ln\left(-\frac{q^2}{\mu^2}\right)\right\}.$$
$$\text{(A.9)}$$

For the Feynman integral with two massive propagators sometimes we will use the function substracted at zero momentum:

$$B_0(q^2; M^2, M^2) = \frac{1}{16\pi^2}\left\{-\lambda_\infty - 1 - \ln\frac{M^2}{\mu^2}\right\} + \overline{J}_{MM}(q^2), \qquad \text{(A.10)}$$

with the substracted function

$$\overline{J}_{MM}(q^2) = \overline{B}_0(q^2; M^2) = \frac{1}{16\pi^2}\left\{2 - \sigma_M \ln\left(\frac{\sigma_M + 1}{\sigma_M - 1}\right)\right\}, \qquad \text{(A.11)}$$

which vanishes at $q^2 = 0$. Likewise, one defines

$$B_0(q^2; 0, M^2) = \frac{1}{16\pi^2}\left\{-\lambda_\infty - \ln\frac{M^2}{\mu^2}\right\} + \overline{J}(q^2; 0, M^2), \qquad \text{(A.12)}$$

with the subtracted function

$$\overline{J}(q^2; 0, M^2) = \frac{1}{16\pi^2}\left\{1 - \left(1 - \frac{M^2}{q^2}\right)\ln\left(1 - \frac{q^2}{M^2}\right)\right\}. \qquad \text{(A.13)}$$

In addition one finds:

$$\left.\frac{d}{ds}\overline{J}(s; 0, M^2)\right|_{s=0} = \frac{1}{32\pi^2 M^2}. \qquad \text{(A.14)}$$

In general one has the subtracted two-propagator Feynman integral,

$$\overline{J}(q^2; M_a^2, M_b^2) \equiv B_0(q^2; M_a^2, M_b^2) - B_0(0; M_a^2, M_b^2), \qquad \text{(A.15)}$$

with the value

$$\overline{J}(q^2; M_a^2, M_b^2) = \frac{1}{32\pi^2}\left\{2 + \left[\frac{M_a^2 - M_b^2}{q^2} - \frac{M_a^2 + M_b^2}{M_a^2 - M_b^2}\right]\ln\frac{M_b^2}{M_a^2}\right.$$
$$\left. -\frac{\lambda^{1/2}(q^2, M_a^2, M_b^2)}{q^2}\ln\left(\frac{[q^2 + \lambda^{1/2}(q^2, M_a^2, M_b^2)]^2 - (M_a^2 - M_b^2)^2}{[q^2 - \lambda^{1/2}(q^2, M_a^2, M_b^2)]^2 - (M_a^2 - M_b^2)^2}\right)\right\},$$
$$\text{(A.16)}$$

with $\lambda(x, y, z) \equiv x^2 + y^2 + z^2 - 2xy - 2xz - 2yz$.

A.2 Tensorial integrals

The loop function $B_{22}^{(P)}$ used in the text is defined through

$$\int \frac{dk^d}{i\,(2\pi)^d} \frac{k^\mu k^\nu}{(k^2 - m_P^2)\,[(q-k)^2 - m_P^2]} \equiv B_{22}^{(P)}\,q^2 g^{\mu\nu} + B_{21}^{(P)}\,q^\mu q^\nu\,, \qquad (\text{A.17})$$

with

$$B_{22}^{(P)} = \frac{1}{192\pi^2}\left[\left(1 - \frac{6m_P^2}{q^2}\right)\left[\lambda_\infty + \ln\left(\frac{m_P^2}{\mu^2}\right)\right] + \frac{8m_P^2}{q^2} - \frac{5}{3} + \sigma_P^3 \ln\left(\frac{\sigma_P + 1}{\sigma_P - 1}\right)\right]\,, \qquad (\text{A.18})$$

The real part of this Feynman integral is divergent, but its imaginary part is finite and takes the value

$$\text{Im}\left\{B_{22}^{(P)}\right\} = -\frac{\sigma_P^3}{192\pi}\,\theta(q^2 - 4m_P^2)\,. \qquad (\text{A.19})$$

Appendix B

Tensor structures in the antisymmetric formalism

We are going to use the definitions $p_{1,2}$ for the momenta of the outgoing Goldstones, and $q = p_1 + p_2$ the momentum of the s–channel vector resonance. One finds the scalar product $q(p_1 - p_2) = 0$ when the external particles are on the mass-shell $(p_1^2 = p_2^2 = m_P^2)$.

In the antisymmetric formalism the vector propagator is given by a four index tensor. The kinetic term of the vector field,

$$\mathcal{L}_V^{Kin} = -\tfrac{1}{2} \partial^\mu V_{\mu\nu} \partial_\lambda V^{\lambda\nu} + \tfrac{1}{4} M_V^2 V_{\mu\nu} V^{\mu\nu} , \tag{B.1}$$

which provides the classical equations of motion,

$$\partial^\mu \partial_\lambda V^{\lambda\nu} - \partial^\nu \partial_\lambda V^{\lambda\mu} + M_V^2 V^{\mu\nu} = 0 , \tag{B.2}$$

implying

$$\partial_\mu \left(\partial^2 + M_V^2 \right) V^{\mu\nu} = 0 . \tag{B.3}$$

The corresponding free propagator in momentum space has the form

$$\langle V^{\mu\nu} V^{\rho\sigma} \rangle_F = \Delta^{\mu\nu,\rho\sigma}(q) = \frac{2i}{M_V^2 - q^2} \mathcal{A}^{\mu\nu,\rho\sigma}(q) + \frac{2i}{M_V^2} \Omega^{\mu\nu,\rho\sigma}(q) =$$

$$= \frac{2i}{M_V^2 - q^2} \left\{ \mathcal{I}^{\mu\nu,\rho\sigma} - \frac{q^2}{M_V^2} \Omega(q)^{\mu\nu,\rho\sigma} \right\} , \tag{B.4}$$

with the antisymmetric tensors

$$\mathcal{A}_{\mu\nu,\rho\sigma}(q) \equiv \frac{1}{2q^2} \left[g_{\mu\rho} q_\nu q_\sigma - g_{\rho\nu} q_\mu q_\sigma - (\rho \leftrightarrow \sigma) \right] ,$$

$$\Omega_{\mu\nu,\rho\sigma}(q) \equiv -\frac{1}{2q^2} \left[g_{\mu\rho} q_\nu q_\sigma - g_{\rho\nu} q_\mu q_\sigma - q^2 g_{\mu\rho} g_{\nu\sigma} - (\rho \leftrightarrow \sigma) \right] , \tag{B.5}$$

$$\mathcal{I}_{\mu\nu,\rho\sigma} \equiv \frac{1}{2} \left(g_{\mu\rho} g_{\nu\sigma} - g_{\mu\sigma} g_{\nu\rho} \right) ,$$

This propagator can easily be related to the usual gauge boson propagator in the SM (the W propagator for instance):

$$\Delta_W^{\mu\nu}(q) \;=\; \frac{i}{M_W^2 - q^2}\, P_T^{\mu\nu}(q) \;+\; \frac{i\xi}{\xi M_W^2 - q^2}\, P_L^{\mu\nu}(q) \;=\;$$

$$\;=\; \frac{i}{M_W^2 - q^2}\, \left\{ g^{\mu\nu} \;-\; \frac{(\xi - 1)q^2}{\xi M_W^2 - q^2}\, P_L^{\mu\nu}(q) \right\} \,,$$

(B.6)

with $P_T^{\mu\nu}(q) = g^{\mu\nu} - q^\mu q^\nu/q^2$ and $P_L^{\mu\nu}(q) = q^\mu q^\nu/q^2$ the usual Lorentz projectors. In the limit $\xi \to \infty$ for the gauge parameter it yields the usual Proca propagator:

$$\Delta_W^{\mu\nu}(q) \;=\; \frac{i}{M_W^2 - q^2}\, P_T^{\mu\nu}(q) \;+\; \frac{i}{M_W^2}\, P_L^{\mu\nu}(q) \;=\;$$

$$\;=\; \frac{i}{M_W^2 - q^2}\, \left\{ g^{\mu\nu} \;-\; \frac{q^2}{M_W^2}\, P_L^{\mu\nu}(q) \right\} \,.$$

(B.7)

The former antisymmetric tensors obey the following properties:

$$\Omega \cdot \mathcal{A} \;=\; \mathcal{A} \cdot \Omega \;=\; 0 \quad,\quad \mathcal{A} \cdot \mathcal{A} \;=\; \mathcal{A} \quad,\quad \Omega \cdot \Omega \;=\; \Omega \quad,\quad \mathcal{A} + \Omega \;=\; \mathcal{I}\,,$$

$$q^\mu\, \Omega_{\mu\nu,\rho\sigma}(q) \;=\; q^\nu\, \Omega_{\mu\nu,\rho\sigma}(q) \;=\; q^\rho\, \Omega_{\mu\nu,\rho\sigma}(q) \;=\; q^\sigma\, \Omega_{\mu\nu,\rho\sigma}(q) \;=\; 0\,.$$

(B.8)

In general, for any antisymmetric tensor $H_{\mu\nu,ab}$ the operator $\mathcal{I}_{cd,\alpha\beta}$ acts like the identity, i.e.

$$H \cdot \mathcal{I} \;=\; \mathcal{I} \cdot H \;=\; H\,.$$

(B.9)

One may then define the antisymmetric inverses $G^{ab,\rho\sigma}$, satisfying

$$H_{\mu\nu,ab} G^{ab,\rho\sigma} \;=\; G_{\mu\nu,ab} H^{ab,\rho\sigma} \;=\; \mathcal{I}_{\mu\nu}^{\rho\sigma}\,.$$

(B.10)

Through these tensors it is possible to rewrite the kinetic term:

$$\mathcal{L}_V^{Kin} \;=\; \sum_{\mu,\nu,\rho,\sigma} \frac{1}{4}\, V_{\mu\nu}\, \left[\partial^2 \mathcal{A}(\partial)^{\mu\nu,\rho\sigma} + M_V^2 \right] V_{\rho\sigma} \;=\;$$

$$\;=\; \sum_{\mu<\nu,\,\rho<\sigma} \frac{1}{2}\, V_{\mu\nu}\, \left[\partial^2 \mathcal{A}(\partial)^{\mu\nu,\rho\sigma} + M_V^2 \right] V_{\rho\sigma}\,,$$

(B.11)

and the equations of motion in Eq. (B.2) can be re-expressed as

$$\left[\partial^2\, \mathcal{A}(\partial)^{\mu\nu,\rho\sigma} \;+\; M_V^2\, \mathcal{I}^{\mu\nu,\rho\sigma} \right] V_{\rho\sigma} \;=\; 0\,.$$

(B.12)

The inverse propagator in momentum space is:

$$\Delta^{-1}(q)^{\mu\nu,\rho\sigma} \;=\; -\frac{i}{2}\, \left(M_V^2 - q^2 \right)\, \mathcal{A}^{\mu\nu,\rho\sigma}(q) \;-\; \frac{i}{2}\, M_V^2\, \Omega^{\mu\nu,\rho\sigma}(q) \;=\;$$

$$\;=\; \frac{i}{2}\, q^2\, \mathcal{A}^{\mu\nu,\rho\sigma}(q) \;-\; \frac{iM_V^2}{2}\, \mathcal{I}^{\mu\nu,\rho\sigma}\,.$$

(B.13)

Other useful relations are

$$q^4 \mathcal{A}_{\mu\nu,\rho\sigma}(q) = -4\Delta^{-1}(q)_{\mu\nu}^{\alpha\beta} \Delta^{-1}(q)_{\alpha\beta,\rho\sigma} - 4i\, M_V^2\, \Delta^{-1}(q)_{\mu\nu,\rho\sigma} +$$

$$+ M_V^4\, \mathcal{I}_{\mu\nu,\rho\sigma}\,,$$

$$\frac{q^\mu (p_1 - p_2)^\nu}{2} - (\mu \leftrightarrow \nu) = \mathcal{I}_{\alpha\beta}^{\mu\nu}\, q^\alpha (p_1 - p_2)^\beta \overset{p_1^2 = p_2^2 = m_P^2}{=} \mathcal{A}_{\alpha\beta}^{\mu\nu}(q)\, q^\alpha (p_1 - p_2)^\beta\,,$$

$$(q^\rho g^{\mu\sigma} - q^\sigma g^{\mu\rho}) = -2\, q^\nu\, \mathcal{I}_{\mu\nu}^{\rho\sigma} = -2\, q^\nu\, \mathcal{A}_{\mu\nu}^{\rho\sigma}(q)\,,$$

$$(q^2 g^{\mu\rho} - q^\mu q^\sigma) = 2\, q_\nu\, \mathcal{A}^{\mu\nu,\rho\sigma}(q)\, q_\sigma\,.$$

(B.14)

Finally it is interesting to consider de matrix element for an outgoing vector of momentum p and polarization $\epsilon_{(i)}$:

$$\langle\, 0 | V^{\mu\nu} | V(p, \epsilon_{(i)})\,\rangle = \epsilon_{(i)}^{\mu\nu} = \frac{i}{M_V} \left(p^\mu \epsilon_{(i)}^\nu - p^\nu \epsilon_{(i)}^\mu \right)\,.$$

(B.15)

Thus, the summation over the physical vector polarizations $\epsilon_{(i=1,2,3)}^\lambda$ for a massive vector $(\epsilon \cdot p = 0)$ yields:

$$\sum_{i=1,2,3} \epsilon_{(i)}^{\mu\nu} \epsilon_{(i)}^{\rho\sigma\,*} = -\frac{2\, p^2}{M_V^2} \mathcal{A}(p)^{\mu\nu,\rho\sigma}\,,$$

(B.16)

where the usual result $\sum_{i=1,2,3} \epsilon_{(i)}^\alpha \epsilon_{(i)}^{\beta\,*} = \left(-g^{\alpha\beta} + \dfrac{p^\alpha p^\beta}{M_V^2} \right)$ has been employed.

Appendix C

Diagrams in the NLO calculations of the VFF
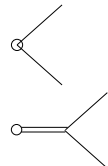
C.1   Detailed diagrammatic calculation

In this appendix I will show the contribution from every single diagram to the VFF up to one loop. In many of them one will find a vector resonance at tree-level in the s-channel. Due to the quantum numbers of the current there cannot be any other intermediate meson. However we will have many different combinations of particles running within the loops. They will be specified for every diagram, both for two and three light quark flavours. In this appendix I provide the particles that run in every loop for the three-flavour case. For $n_f = 2$ one must remove the particles with strangeness and keep just the $I = 0$ states with $\bar{u}u$ and $\bar{d}d$ content.

All the parameters in the next results have been defined in Chapter 4. Likewise, I remind that this calculation has been carried out in the chiral limit and up to NLO in $1/N_C$.

C.1.1   Tree-level Form Factor

The tree-level contributions (TL1,TL2) from the LO lagrangian:

$$
\begin{aligned}
\Delta \mathcal{F}_1^{TL}(q^2) &= 1 \,, \\[2ex]
\Delta \mathcal{F}_2^{TL}(q^2) &= \frac{F_V G_V}{F^2} \frac{q^2}{M_V^2 - q^2} \,.
\end{aligned}
\tag{C.1}
$$

In addition one also has the contribution at tree-level with one vertex from the NLO lagrangian:

$$\Delta\mathcal{F}_3^{TL}(q^2) = -\frac{\widetilde{\ell}_6}{F^2}q^2 + \frac{\widetilde{r}_{V2}}{F^4}q^4 \,,$$

$$\Delta\mathcal{F}_4^{TL}(q^2) = -2\,X_Z\,\frac{F_V G_V}{F^2}\,\frac{q^6}{(M_V^2 - q^2)^2} \,,$$

$$\Delta\mathcal{F}_5^{TL}(q^2) = -\frac{4\sqrt{2}F_V X_G}{F^2}\,\frac{q^4}{M_V^2 - q^2} \,,$$

$$\Delta\mathcal{F}_6^{TL}(q^2) = -\frac{2\sqrt{2}X_F G_V}{F^2}\,\frac{q^4}{M_V^2 - q^2} \,.$$

$$(C.2)$$

C.1.2   Loops with vertices just from $\mathcal{L}_{2\chi}$

The unique diagram which has contributions from only $\mathcal{L}_{2\chi}$ vertices is $(\chi1)$:

$$\Delta\mathcal{F}_1^{\chi}(q^2) = \frac{n_f}{2}\,\frac{q^2}{F^2}\left\{\frac{1}{6}B_0(q^2,0,0) + \frac{1}{144\pi^2}\right\} \,. \qquad (C.3)$$

Within the loops one may find $\pi^+\pi^-$, K^+K^- and $K^0\overline{K}^0$.

C.1.3   Contribution from diagrams with only pNGB and vectors

The diagrams with a loop of two pNGB propagators are (V1,V2,V3):

$$\Delta\mathcal{F}_1^{V}(q^2) = \frac{n_f}{2}\,\frac{F_V G_V}{F^2}\,\frac{q^2}{M_V^2 - q^2}\,\frac{q^2}{F^2}\left\{\frac{1}{6}B_0(q^2,0,0) + \frac{1}{144\pi^2}\right\} \,,$$

$$\Delta\mathcal{F}_2^{V}(q^2) = \frac{n_f}{2}\,\frac{2G_V^2}{F^2}\,\frac{q^2}{M_V^2 - q^2}\,\frac{q^2}{F^2}\left\{\frac{1}{6}B_0(q^2,0,0) + \frac{1}{144\pi^2}\right\} \,,$$

$$\Delta\mathcal{F}_3^{V}(q^2) = \frac{n_f}{2}\,\frac{F_V G_V}{F^2}\,\frac{2G_V^2}{F^2}\,\frac{q^4}{(M_V^2 - q^2)^2}\,\frac{q^2}{F^2}\left\{\frac{1}{6}B_0(q^2,0,0) + \frac{1}{144\pi^2}\right\} \,,$$

$$(C.4)$$

and within the loops there may be $\pi^+\pi^-$, K^+K^- and $K^0\overline{K}^0$.

There are also diagrams with a loop of a pNGB and a resonance propagator attached to just one of the external legs. For every case there is always the symmetric diagram which connects the loop to the other external leg. Here the summation of both is shown (V4,V5):

$$
\Delta \mathcal{F}_4^V(q^2) = \frac{n_f}{2} \frac{2 G_V^2}{F^4} \left\{ -3 A_0(M_V^2) + \frac{M_V^2}{32\pi^2} \right\} ,
$$

$$
\Delta \mathcal{F}_5^V(q^2) = \frac{n_f}{2} \frac{F_V G_V}{F^4} \frac{q^2}{M_V^2 - q^2} \left\{ -\frac{3}{2} A_0(M_V^2) + \frac{M_V^2}{64\pi^2} \right\} .
$$

$$(C.5)$$

The particles in the loop of the π^- leg may be $\pi^- \rho^0$, $\pi^0 \rho^-$, $K^- K^{*0}$ and $K^0 K^{*-}$. For the π^+ leg one may have the conjugate particles.

The next contribution comes from the resonance tadpole (V6):

$$
\Delta \mathcal{F}_6^V(q^2) = \frac{n_f}{2} \frac{1}{F^2} \left\{ \frac{3}{2} A_0(M_V^2) - \frac{M_V^2}{64\pi^2} \right\} .
\qquad (C.6)
$$
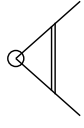
Within the loop there may be $\rho^+(\rho^-)$, $\rho^0, K^{*+}(K^{*-})$ and $K^{*0}(\overline{K}^{*0})$.

There is a diagram with a two resonance propagator loop (V7):

$$
\Delta \mathcal{F}_7^V(q^2) = \frac{n_f}{2} \frac{1}{F^2} \left\{ B_0(q^2, M_V^2, M_V^2) \left[-2 M_V^2 - \frac{q^2}{6} + \frac{q^4}{6 M_V^2} \right] \right.
$$
$$
\left. + A_0(M_V^2) \left[\frac{1}{2} - \frac{q^2}{3 M_V^2} \right] - \frac{7 M_V^2}{64\pi^2} + \frac{q^2}{48\pi^2} - \frac{q^4}{288\pi^2 M_V^2} \right\} .
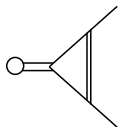$$

$$(C.7)$$

In the loop one finds $\rho^+ \rho^-$, $K^{*+} K^{*-}$ and $K^{*0} \overline{K}^{*0}$.

Finally the last possible type of loops is that with three propagators –the triangles–. There can be a Goldstone-Goldstone-resonance loop coming either directly from an external current or through an intermediate vector resonance (V8,V9):

$$\Delta\mathcal{F}_8^V(q^2) = \frac{n_f}{2}\frac{2G_V^2}{F^4}\left\{C_0(q^2,0,0,M_V^2)\left[-\frac{M_V^6}{q^2}-\frac{5M_V^4}{2}-q^2M_V^2\right]+\right.$$
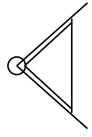$$+B_0(q^2,0,0)\left[-\frac{M_V^4}{q^2}-2M_V^2-\frac{q^2}{12}\right]+A_0(M_V^2)\left[\frac{M_V^2}{q^2}+2\right]$$
$$\left.-\frac{M_V^2}{64\pi^2}-\frac{q^2}{288\pi^2}\right\},$$

$$\Delta\mathcal{F}_9^V(q^2) = \frac{n_f}{2}\frac{2G_V^2}{F^4}\frac{F_VG_V}{f^2}\frac{q^2}{M_V^2-q^2}\times$$

$$\times\left\{C_0(q^2,0,0,M_V^2)\left[-\frac{M_V^6}{q^2}-\frac{5M_V^4}{2}-q^2M_V^2\right]\right.$$
$$+B_0(q^2,0,0)\left[-\frac{M_V^4}{q^2}-2M_V^2-\frac{q^2}{12}\right]+A_0(M_V^2)\left[\frac{M_V^2}{q^2}+2\right]$$
$$\left.-\frac{M_V^2}{64\pi^2}-\frac{q^2}{288\pi^2}\right\}.$$

$$\text{(C.8)}$$

In the loop one finds the combinations $\pi^+\pi^-\rho^0$, $K^-K^+K^{*\,0}$ and $K^0\overline{K}^0K^{*\pm}$.

There is also another available triangle, formed by resonance-resonance-Goldstone (V10):

$$\Delta\mathcal{F}_{10}^V(q^2) = \frac{n_f}{2}\frac{2G_V^2}{F^4}\left\{C_0(q^2,M_V^2,M_V^2,0)\left[\frac{M_V^6}{q^2}+\frac{M_V^4}{2}\right]\right.$$
$$+B_0(q^2,M_V^2,M_V^2)\left[-\frac{M_V^4}{q^2}-\frac{2M_V^2}{3}+\frac{5q^2}{12}\right]+A_0(M_V^2)\left[\frac{M_V^2}{q^2}+\frac{2}{3}\right]$$
$$\left.+\frac{M_V^2}{192\pi^2}-\frac{q^2}{288\pi^2}\right\},$$
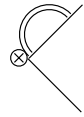
$$\text{(C.9)}$$

Our LO lagrangian does not contain three resonance vertices so the analogous diagram with an intermediate vector resonance is not present. The combinations of particles in the loop are $\rho^+\rho^-\pi^0$, $K^{*+}K^{*-}K^0$ and $K^{*\,0}\overline{K}^{*\,0}K^\pm$.

C.1.4   Contributions including scalars

I will denote the scalar resonances (and also afterwards with the axial-vector and pseudo-scalar resonances) with the same name as the vectors, in order to expose clearly what component of the $U(3)$ multiplet we are talking about. For instance, the $S=1, I=1/2$ scalar will be denote as $S_{K^{*+}}$.
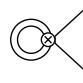
There are also diagrams with a Goldstone and a scalar resonance loop in one of the external legs (S1):

$$\Delta \mathcal{F}_1^S(q^2) \;=\; \frac{n_f}{2} \frac{4c_d^2}{F^4} \left\{ A_0(M_S^2) + \frac{M_S^2}{32\pi^2} \right\} . \qquad (C.10)$$

For this diagram one may find in the loop of the π^- leg the combinations $\eta_8 S_{\rho^-}$, $\eta_1 S_{\rho^-}$, $\pi^- S_{\omega_8}$, $\pi^- S_{\omega_1}$, $K^- S_{K^{*0}}$ and $K^0 S_{K^{*-}}$.
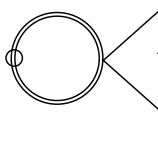
The next contribution is that from the tadpole (S2):

$$\Delta \mathcal{F}_2^S(q^2) \;=\; \frac{n_f}{2} \frac{1}{F^2} \left\{ A_0(M_S^2) \right\} . \qquad (C.11)$$

Within the loop there may be $S_{\rho^+}(S_{\rho^-})$, S_{ρ^0}, $S_{K^{*+}}(S_{K^{*-}})$ and $S_{K^{*0}}(S_{\overline{K}^{*0}})$.
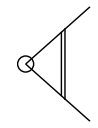
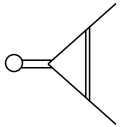One finds also diagrams with one loop of two resonance propagators (S3)

$$\Delta \mathcal{F}_3^S(q^2) \;=\; \frac{n_f}{2} \frac{1}{F^2} \left\{ B_0(q^2, M_S^2, M_S^2) \left[-\frac{2M_S^2}{3} + \frac{q^2}{6} \right] \right.$$
$$\left. + A_0(M_S^2) \left[-\frac{1}{3} \right] - \frac{M_S^2}{24\pi^2} + \frac{q^2}{144\pi^2} \right\} . \qquad (C.12)$$

In the loop one finds $S_{\rho^+} S_{\rho^-}$, $S_{K^{*+}} S_{K^{*-}}$ and $S_{K^{*0}} S_{\overline{K}^{*0}}$.

Finally we have the triangles. There can be a Goldstone-Goldstone-resonance loop coming from both a local current or from a current through a vector resonance (S4,S5):
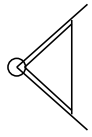
$$\Delta \mathcal{F}_4^S(q^2) \;=\; \frac{n_f}{2} \frac{4c_d^2}{F^4} \left\{ C_0(q^2, 0, 0, M_S^2) \left[-\frac{M_S^6}{q^2} - \frac{M_S^4}{2} \right] \right.$$
$$+ B_0(q^2, 0, 0) \left[-\frac{M_S^4}{q^2} - \frac{q^2}{12} \right] + A_0(M_V^2) \left[\frac{M_S^2}{q^2} \right]$$
$$\left. - \frac{M_S^2}{64\pi^2} - \frac{q^2}{288\pi^2} \right\} ,$$

$$\Delta \mathcal{F}_5^S(q^2) \;=\; \frac{n_f}{2} \frac{F_V G_V}{F^2} \frac{q^2}{M_V^2 - q^2} \frac{4c_d^2}{F^4} \left\{ C_0(q^2, 0, 0, M_S^2) \left[-\frac{M_S^6}{q^2} - \frac{M_S^4}{2} \right] \right.$$
$$+ B_0(q^2, 0, 0) \left[-\frac{M_S^4}{q^2} - \frac{q^2}{12} \right] + A_0(M_V^2) \left[\frac{M_S^2}{q^2} \right]$$
$$\left. - \frac{M_S^2}{64\pi^2} - \frac{q^2}{288\pi^2} \right\} . \qquad (C.13)$$

In the loop one finds the combinations $\pi^+ \pi^- S_{\omega_8}$, $\pi^+ \pi^- S_{\omega_1}$, $K^- K^+ S_{K^{*0}}$ and $K^0 \overline{K}^0 S_{K^{*\pm}}$.

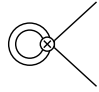Finally, there is also the triangle resonance-resonance-Goldstone (S6):

$$\Delta\mathcal{F}_6^S(q^2) = \frac{n_f}{2}\frac{4c_d^2}{F^4}\left\{C_0(q^2, M_S^2, M_S^2, 0)\left[\frac{M_S^6}{q^2} - \frac{M_S^4}{2}\right]\right.$$
$$+ B_0(q^2, M_S^2, M_S^2)\left[-\frac{M_S^4}{q^2} + \frac{M_S^2}{3} - \frac{q^2}{12}\right] + A_0(M_S^2)\left[\frac{M_S^2}{q^2} - \frac{1}{3}\right]$$
$$\left. + \frac{M_S^2}{192\pi^2} - \frac{q^2}{288\pi^2}\right\} .$$

$$(\text{C.14})$$

The possible combinations of particles within the loop are $S_{\rho^+}S_{\rho^-}\eta_8$, $S_{\rho^+}S_{\rho^-}\eta_1$, $S_{K^{*+}}S_{K^{*-}}K^0$ and $S_{K^{*0}}S_{\overline{K}^{*0}}K^\pm$.
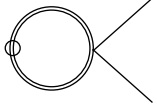
C.1.5   Contribution from axial-vector loops

In this case there are only two contributions. One comes from tadpoles (A1):

$$\Delta\mathcal{F}_1^A(q^2) = \frac{n_f}{2}\frac{1}{F^2}\left\{\frac{3}{2}A_0(M_A^2) - \frac{M_A^2}{64\pi^2}\right\} .$$

$$(\text{C.15})$$

Within the loop there may be $A_{\rho^+}(A_{\rho^-})$, A_{ρ^0}, $A_{K^{*+}}(A_{K^{*-}})$ and $A_{K^{*0}}(A_{\overline{K}^{*0}})$.

There are also diagrams with loops of two resonance propagators (A2):
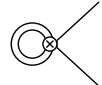
$$\Delta\mathcal{F}_2^A(q^2) = \frac{n_f}{2}\frac{1}{F^2}\left\{B_0(q^2, M_A^2, M_A^2)\left[-2M_A^2 - \frac{q^2}{6} + \frac{q^4}{6M_A^2}\right]\right.$$
$$\left. + A_0(M_A^2)\left[\frac{1}{2} - \frac{q^2}{3M_A^2}\right] - \frac{7M_A^2}{64\pi^2} + \frac{q^2}{48\pi^2} - \frac{q^4}{288\pi^2 M_A^2}\right\} .$$

$$(\text{C.16})$$

In the loop one finds $A_{\rho^+}A_{\rho^-}$, $A_{K^{*+}}A_{K^{*-}}$ and $A_{K^{*0}}A_{\overline{K}^{*0}}$.

C.1.6   Pseudo-scalar resonance loops

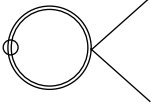Also for the pseudo-scalar there are only two contributions, one coming from tadpoles (P1):

$$\Delta\mathcal{F}_1^P(q^2) = \frac{n_f}{2}\frac{1}{F^2}A_0(M_P^2) .$$

$$(\text{C.17})$$

Within the loop there may be $P_{\rho^+}(P_{\rho^-})$, P_{ρ^0}, $P_{K^{*+}}(P_{K^{*-}})$ and $P_{K^{*0}}(P_{\overline{K}^{*0}})$.

And, to end with, the loop with two resonance propagators (P2):

$$
\begin{aligned}
\Delta\mathcal{F}_2^P(q^2) = \; & \frac{n_f}{2}\frac{1}{F^2}\left\{ B_0(q^2, M_P^2, M_P^2)\left[-\frac{2M_P^2}{3}+\frac{q^2}{6}\right]\right. \\
& \left. + A_0(M_P^2)\left[-\frac{1}{3}\right] - \frac{M_P^2}{24\pi^2} + \frac{q^2}{144\pi^2}\right\},
\end{aligned}
\tag{C.18}
$$

where one finds $P_{\rho^+}P_{\rho^-}$, $P_{K^{*+}}P_{K^{*-}}$ and $P_{K^{*0}}P_{\overline{K}^{*0}}$.

C.2 Limit $q^2 \ll \Lambda_\chi^2$

In this section we will study the low energy limit of each independent diagram in order to recover the one-loop χPT result.

First of all I show the high energy behaviour of every Feynman integral involved in this calculation:

$$
A(M^2) \quad\overset{q^2\to 0}{=}\quad \frac{M^2}{16\pi^2}\left\{-\lambda_\infty - \ln\frac{M^2}{\mu^2}\right\},
\tag{C.19}
$$

$$
B_0(q^2; 0, 0) \quad\overset{q^2\to 0}{=}\quad \frac{1}{16\pi^2}\left\{-\lambda_\infty + 1 - \ln\left(-\frac{q^2}{\mu^2}\right)\right\},
\tag{C.20}
$$

$$
\begin{aligned}
B_0(q^2; M^2, M^2) \quad\overset{q^2\to 0}{=}\quad & \frac{1}{16\pi^2}\left[-\lambda_\infty - 1 - \ln\frac{M_V^2}{\mu^2}\right] + \frac{q^2}{96\pi^2 M^2} + \\
& + \frac{q^4}{960\pi^2 M^4} + \mathcal{O}\left(\frac{q^6}{M^6}\right),
\end{aligned}
\tag{C.21}
$$

$$
\begin{aligned}
C_0(q^2; 0, 0, M^2) \quad\overset{q^2\to 0}{=}\quad & \frac{1}{16\pi^2 M^2}\left[\ln\left(-\frac{q^2}{M^2}\right) - 1\right] + \\
& + \frac{q^2}{64\pi^2 M^4}\left[1 - 2\ln\left(-\frac{q^2}{M^2}\right)\right] + \\
& + \frac{q^4}{144\pi^2 M^6}\left[3\ln\left(-\frac{q^2}{M^2}\right) - 1\right]\mathcal{O}\left(\frac{q^6}{M^8}\right),
\end{aligned}
\tag{C.22}
$$

$$
\begin{aligned}
C_0(q^2; M^2, M^2, 0) \quad\overset{q^2\to 0}{=}\quad & -\frac{1}{16\pi^2 M^2} - \frac{q^2}{192\pi^2 M^4} \\
& - \frac{q^4}{1440\pi^2 M^6} + \mathcal{O}\left(\frac{q^6}{M^8}\right).
\end{aligned}
\tag{C.23}
$$

For simplicity I have expanded the renormalized diagrams and the ultraviolet divergences are hidden just within the renormalised couplings $c^r(\mu)$. To recover the

infinities explicitly one just have to perform the replacement $c^r(\mu) = c^{(B)} - \delta c(\mu)$, where $\delta c(\mu)$ contains the divergence $\lambda_\infty(\mu)$.

$$\Delta \mathcal{F}_1^{TL}(q^2) = 1 \tag{C.24}$$

$$\Delta \mathcal{F}_2^{TL}(q^2) = \frac{F_V G_V}{F^2} \frac{q^2}{M_V^2} + \mathcal{O}\left(\frac{q^4}{M_V^4}\right). \tag{C.25}$$

$$\Delta \mathcal{F}_3^{TL}(q^2) = -\frac{\widetilde{\ell}_6}{F^2} q^2 + \frac{\widetilde{r}_{V2}}{F^4} q^4, \tag{C.26}$$

$$\Delta \mathcal{F}_4^{TL}(q^2) = \mathcal{O}\left(\frac{q^6}{M_V^6}\right), \tag{C.27}$$

$$\Delta \mathcal{F}_5^{TL}(q^2) = \mathcal{O}\left(\frac{q^4}{M_V^4}\right), \tag{C.28}$$

$$\Delta \mathcal{F}_6^{TL}(q^2) = \mathcal{O}\left(\frac{q^4}{M_V^4}\right). \tag{C.29}$$

$$\Delta \mathcal{F}_1^{\chi}(q^2) = \frac{n_f}{2} \frac{q^2}{F^2} \left\{ \frac{1}{6} B_0(q^2, 0, 0) + \frac{1}{144\pi^2} \right\}. \tag{C.30}$$

$$\tag{C.31}$$

$$\Delta \mathcal{F}_1^{V}(q^2) = \mathcal{O}\left(\frac{q^4}{M_V^4}\right), \tag{C.32}$$

$$\Delta \mathcal{F}_2^{V}(q^2) = \mathcal{O}\left(\frac{q^4}{M_V^4}\right), \tag{C.33}$$

$$\Delta \mathcal{F}_3^{V}(q^2) = \mathcal{O}\left(\frac{q^6}{M_V^6}\right), \tag{C.34}$$

$$\Delta \mathcal{F}_4^{V}(q^2) = \frac{n_f}{2} \frac{2G_V^2}{F^4} \left\{ -3 A_0(M_V^2) + \frac{M_V^2}{32\pi^2} \right\}, \tag{C.35}$$

$$\Delta \mathcal{F}_5^{V}(q^2) = \frac{n_f}{2} \frac{F_V G_V}{F^4} \left\{ -\frac{3}{2} A_0(M_V^2) + \frac{M_V^2}{64\pi^2} \right\} \frac{q^2}{M_V^2} + \mathcal{O}\left(\frac{q^4}{M_V^4}\right). \tag{C.36}$$

$$\Delta \mathcal{F}_6^{V}(q^2) = \frac{n_f}{2} \frac{1}{F^2} \left\{ \frac{3}{2} A_0(M_V^2) - \frac{M_V^2}{64\pi^2} \right\} \tag{C.37}$$

$$\Delta \mathcal{F}_7^{V}(q^2) = \frac{n_f}{2} \left\{ \frac{M_V^2}{64\pi^2 F^2} \left[1 + 6 \ln \frac{M_V^2}{\mu^2} \right] + \frac{q^2}{96\pi^2 F^2} \left[1 + 3 \ln \frac{M_V^2}{\mu^2} \right] \right\} + $$

$$+ \; \mathcal{O}\left(\frac{q^4}{M_V^4}\right) . \tag{C.38}$$

$$\Delta\mathcal{F}_8^V(q^2) \;=\; \frac{n_f}{2}\frac{2G_V^2}{F^2}\frac{q^2}{1152\pi^2 F^2}\left[25 + 6\ln\left(\frac{M_V^2}{\mu^2}\right)\right] + \mathcal{O}\left(\frac{q^4}{F^2 M_V^2}\right), \tag{C.39}$$

$$\Delta\mathcal{F}_9^V(q^2) \;=\; \mathcal{O}\left(\frac{q^4}{F^2 M_V^2}\right), \tag{C.40}$$

$$\Delta\mathcal{F}_{10}^{TL}(q^2) \;=\; -\frac{n_f}{2}\frac{2G_V^2}{F^2}\frac{q^2}{1152\pi^2 F^2}\left[47 + 30\ln\left(\frac{M_V^2}{\mu^2}\right)\right] + \mathcal{O}\left(\frac{q^4}{F^2 M_V^2}\right), \tag{C.41}$$

$$\Delta\mathcal{F}_1^S(q^2) \;=\; \frac{n_f}{2}\frac{4c_d^2}{F^4}\left\{A_0(M_S^2) + \frac{M_S^2}{32\pi^2}\right\}, \tag{C.42}$$

$$\Delta\mathcal{F}_2^S(q^2) \;=\; \frac{n_f}{2}\frac{1}{F^2}\left\{A_0(M_S^2)\right\}, \tag{C.43}$$

$$\Delta\mathcal{F}_3^S(q^2) \;=\; \frac{n_f}{2}\frac{M_S^2}{16\pi^2 F^2}\ln\left(\frac{M_S^2}{\mu^2}\right) - \frac{n_f}{2}\frac{q^2}{96\pi^2 F^2}\left[1 + \ln\left(\frac{M_S^2}{\mu^2}\right)\right] +$$

$$+ \; \mathcal{O}\left(\frac{q^4}{F^2 M_S^2}\right), \tag{C.44}$$

$$\Delta\mathcal{F}_4^S(q^2) \;=\; \frac{n_f}{2}\frac{4c_d^2}{F^2}\frac{q^2}{1152\pi^2 F^2}\left[6\ln\left(\frac{M_S^2}{\mu^2}\right) - 11\right] + \mathcal{O}\left(\frac{q^4}{F^2 M_S^2}\right), \tag{C.45}$$

$$\Delta\mathcal{F}_5^S(q^2) \;=\; +\mathcal{O}\left(\frac{q^4}{F^2 M_R^2}\right). \tag{C.46}$$

$$\Delta\mathcal{F}_6^S(q^2) \;=\; \frac{n_f}{2}\frac{4c_d^2}{F^2}\frac{q^2}{1152\pi^2 F^2}\left[6\ln\left(\frac{M_S^2}{\mu^2}\right) + 7\right] + \mathcal{O}\left(\frac{q^4}{F^2 M_S^2}\right), \tag{C.47}$$

$$\Delta\mathcal{F}_1^A(q^2) \;=\; \frac{n_f}{2}\frac{1}{F^2}\left\{\frac{3}{2}A_0(M_A^2) - \frac{M_A^2}{64\pi^2}\right\}, \tag{C.48}$$

$$\Delta\mathcal{F}_2^A(q^2) \;=\; \frac{n_f}{2}\frac{M_A^2}{94\pi^2 F^2}\left[1 + 6\ln\left(\frac{M_A^2}{\mu^2}\right)\right] + \frac{n_f}{2}\frac{q^2}{96\pi^2 F^2}\left[1 + 3\ln\left(\frac{M_A^2}{\mu^2}\right)\right] +$$

$$+ \; \mathcal{O}\left(\frac{q^2}{F^2 M_A^2}\right). \tag{C.49}$$

$$\Delta\mathcal{F}_1^P(q^2) \;=\; \frac{n_f}{2}\frac{1}{F^2}A_0(M_P^2), \tag{C.50}$$

$$\Delta \mathcal{F}_2^P(q^2) \;=\; \frac{n_f}{2} \frac{M_P^2}{16\pi^2 F^2} \ln\left(\frac{M_P^2}{\mu^2}\right) - \frac{n_f}{2} \frac{q^2}{96\pi^2 F^2}\left[1 + \ln\left(\frac{M_P^2}{\mu^2}\right)\right] +$$

$$+\; \mathcal{O}\left(\frac{q^4}{F^2 M_P^2}\right) . \tag{C.51}$$

C.3   Limit $q^2 \gg \Lambda_\chi^2$

In this section I will study the high energy behaviour of each independent diagram and I will observe how some cancellations between different diagrams occur.

First of all here I show the high energy behaviour of every Feynman integral involved in this calculation:

$$A(M^2) \quad \overset{q^2 \to \infty}{=} \quad \frac{M^2}{16\pi^2}\left\{-\lambda_\infty - \ln\frac{M^2}{\mu^2}\right\} , \tag{C.52}$$

$$B_0(q^2; 0, 0) \quad \overset{q^2 \to \infty}{=} \quad \frac{1}{16\pi^2}\left\{-\lambda_\infty + 1 - \ln\left(-\frac{q^2}{\mu^2}\right)\right\} , \tag{C.53}$$

$$B_0(q^2; M^2, M^2) \quad \overset{q^2 \to \infty}{=} \quad B_0(q^2; 0, 0) + \frac{M^2}{16\pi^2 q^2}\left[2\ln\left(-\frac{q^2}{M^2}\right) + 2\right] + \tag{C.54}$$

$$+ \frac{M^4}{16\pi^2 q^4}\left[2\ln\left(-\frac{q^2}{M^2}\right) - 1\right] +$$

$$+ \frac{M^6}{16\pi^2 q^6}\left[4\ln\left(-\frac{q^2}{M^2}\right) - \frac{10}{3}\right] + \mathcal{O}\left(\frac{M^8}{q^8}\right) ,$$

$$C_0(q^2; 0, 0, M^2) \quad \overset{q^2 \to \infty}{=} \quad \frac{1}{16\pi^2 q^2}\left[\ln\left(\frac{q^2}{M^2}\right)\left\{-\frac{1}{2}\ln\left(\frac{q^2}{M^2}\right) + \right. \tag{C.55}$$

$$\left. + \ln\left(-\frac{q^2}{M^2}\right)\right\} - \frac{\pi^2}{6}\right] +$$

$$+ \frac{M^2}{16\pi^2 q^4}\left[\ln\left(-\frac{q^2}{M^2}\right) + 1\right] + \mathcal{O}\left(\frac{M^4}{q^6}\right) ,$$

$$C_0(q^2; M^2, M^2, 0) \quad \overset{q^2 \to \infty}{=} \quad \frac{1}{16\pi^2 q^2}\ln^2\left(-\frac{q^2}{M^2}\right) \tag{C.56}$$

$$- \frac{M^2}{4\pi^2 q^4}\ln\left(-\frac{q^2}{M^2}\right) + \mathcal{O}\left(\frac{M^4}{q^6}\right) .$$

The contribution from each diagram is:

$$\Delta \mathcal{F}_1^{TL}(q^2) \;=\; 1 , \tag{C.57}$$

$$\Delta \mathcal{F}_2^{TL}(q^2) \;=\; -\frac{F_V G_V}{F^2} - \frac{F_V G_V}{F^2} \frac{M_V^2}{q^2} + \mathcal{O}\left(\frac{M_V^4}{q^4}\right). \tag{C.58}$$

$$\Delta \mathcal{F}_3^{TL}(q^2) \;=\; -\frac{\widetilde{\ell}_6}{F^2} q^2 + \frac{\widetilde{r}_{V2}}{F^4} q^4, \tag{C.59}$$

$$\Delta \mathcal{F}_4^{TL}(q^2) \;=\; 2 X_Z \frac{F_V G_V}{F^2} \left\{ -q^2 - 2M_V^2 + \mathcal{O}\left(\frac{M_V^4}{q^2}\right) \right\}, \tag{C.60}$$

$$\Delta \mathcal{F}_5^{TL}(q^2) \;=\; \frac{4\sqrt{2} F_V X_G}{F^2} \left\{ q^2 + M_V^2 + \mathcal{O}\left(\frac{M_V^4}{q^2}\right) \right\}, \tag{C.61}$$

$$\Delta \mathcal{F}_6^{TL}(q^2) \;=\; \frac{2\sqrt{2} X_F G_V}{F^2} \left\{ q^2 + M_V^2 + \mathcal{O}\left(\frac{M_V^4}{q^2}\right) \right\}, \tag{C.62}$$

$$\Delta \mathcal{F}_1^\chi(q^2) \;=\; \frac{n_f}{2} \left\{ \frac{1}{6} B_0(q^2,0,0) + \frac{1}{144\pi^2} \right\} \frac{q^2}{F^2}, \tag{C.63}$$

$$\Delta \mathcal{F}_1^V(q^2) \;=\; \frac{n_f}{2} \frac{F_V G_V}{F^2} \left\{ \frac{1}{6} B_0(q^2,0,0) + \frac{1}{144\pi^2} \right\} \times$$
$$\times \left\{ -\frac{q^2}{F^2} - \frac{M_V^2}{F^2} - \frac{M_V^4}{q^2 F^2} + \mathcal{O}\left(\frac{M_V^6}{q^4 F^2}\right) \right\}, \tag{C.64}$$

$$\Delta F_2^V(q^2) \;=\; \frac{n_f}{2} \frac{2 G_V^2}{F^2} \left\{ \frac{1}{6} B_0(q^2,0,0) + \frac{1}{144\pi^2} \right\} \times$$
$$\times \left\{ -\frac{q^2}{F^2} - \frac{M_V^2}{F^2} - \frac{M_V^4}{q^2 F^2} + \mathcal{O}\left(\frac{M_V^6}{q^4 F^2}\right) \right\}, \tag{C.65}$$

$$\Delta \mathcal{F}_3^V(q^2) \;=\; \frac{n_f}{2} \frac{F_V G_V}{F^2} \frac{2 G_V^2}{F^2} \left\{ \frac{1}{6} B_0(q^2,0,0) + \frac{1}{144\pi^2} \right\} \times$$
$$\times \left\{ \frac{q^2}{F^2} + \frac{2 M_V^2}{F^2} + \frac{3 M_V^4}{q^2 F^2} + \mathcal{O}\left(\frac{M_V^6}{q^4 F^2}\right) \right\}, \tag{C.66}$$

$$\Delta \mathcal{F}_4^V(q^2) \;=\; \frac{n_f}{2} \frac{2 G_V^2}{F^4} \left\{ -3 A_0(M_V^2) + \frac{M_V^2}{32\pi^2} \right\}, \tag{C.67}$$

$$\Delta \mathcal{F}_5^V(q^2) \;=\; \frac{n_f}{2} \frac{F_V G_V}{F^4} \frac{q^2}{M_V^2 - q^2} \left\{ -\frac{3}{2} A_0(M_V^2) + \frac{M_V^2}{64\pi^2} \right\}, \tag{C.68}$$

$$\Delta \mathcal{F}_6^V(q^2) \;=\; \frac{n_f}{2} \frac{1}{F^2} \left\{ \frac{3}{2} A_0(M_V^2) - \frac{M_V^2}{64\pi^2} \right\}, \tag{C.69}$$

$$\Delta \mathcal{F}_7^V(q^2) \;=\; \frac{n_f}{2} \frac{1}{96\pi^2} \left\{ \frac{q^4}{M_V^2 F^2} \left[\frac{2}{3} - \ln\left(-\frac{q^2}{\mu^2}\right) \right] + \right.$$

$$\frac{3q^2}{F^2} \left[1 + \ln\left(-\frac{q^2}{\mu^2}\right) \right] +$$

$$\left. + \frac{M_V^2}{F^2} \left[12 \ln\left(-\frac{q^2}{\mu^2}\right) - 3 \ln\left(\frac{M_V^2}{\mu^2}\right) - \frac{51}{2} \right] \right\} +$$

$$+ \; \mathcal{O}\left(\frac{M_V^4}{q^2 F^2}\right) , \tag{C.70}$$

$$\Delta \mathcal{F}_8^V(q^2) \;=\; \frac{n_f}{2} \frac{2G_V^2}{F^2} \frac{1}{96\pi^2} \left\{ \frac{q^2}{F^2} \left[-\frac{5}{6} + \frac{1}{2} \ln\left(-\frac{q^2}{\mu^2}\right) \right] + \right.$$

$$+ \frac{M_V^2}{F^2} \left[3 \ln^2\left(\frac{q^2}{M_V^2}\right) + 12 \ln\left(-\frac{q^2}{M_V^2}\right) \right.$$

$$\left. -6 \ln\left(-\frac{q^2}{M_V^2}\right) \ln\left(\frac{q^2}{M_V^2}\right) + \pi^2 - \frac{27}{2} \right] +$$

$$\left. + \mathcal{O}\left(\frac{M_V^4}{q^2 F^2}\right) \right\} , \tag{C.71}$$

$$\Delta \mathcal{F}_9^V(q^2) \;=\; \frac{n_f}{2} \frac{2G_V^2}{F^2} \frac{F_V G_V}{F^2} \frac{1}{96\pi^2} \left\{ \frac{q^2}{F^2} \left[\frac{5}{6} - \frac{1}{2} \ln\left(-\frac{q^2}{\mu^2}\right) \right] + \right.$$

$$+ \frac{M_V^2}{F^2} \left[-3 \ln^2\left(\frac{q^2}{M_V^2}\right) - 12 \ln\left(-\frac{q^2}{M_V^2}\right) + \right.$$

$$\left. +6 \ln\left(-\frac{q^2}{M_V^2}\right) \ln\left(\frac{q^2}{M_V^2}\right) - \pi^2 + \frac{27}{2} \right] +$$

$$\left. + \frac{M_V^2}{F^2} \left[\frac{5}{6} - \frac{1}{2} \ln\left(-\frac{q^2}{\mu^2}\right) \right] + \mathcal{O}\left(\frac{M_V^4}{q^2 F^2}\right) \right\} , \tag{C.72}$$

$$\Delta \mathcal{F}_{10}^V(q^2) \;=\; \frac{n_f}{2} \frac{2G_V^2}{F^2} \frac{1}{96\pi^2} \left\{ \frac{q^2}{F^2} \left[-\frac{5}{2} \ln\left(-\frac{q^2}{\mu^2}\right) + \frac{13}{6} \right] \right.$$

$$\left. + \frac{M_V^2}{F^2} \left[9 \ln\left(-\frac{q^2}{M_V^2}\right) + 1 \right] \; \mathcal{O}\left(\frac{M_V^4}{q^2 F^2}\right) \right\} , \tag{C.73}$$

$$\Delta \mathcal{F}_1^S(q^2) \;=\; \frac{n_f}{2} \frac{4c_d^2}{F^4} \left\{ A_0(M_S^2) + \frac{M_S^2}{32\pi^2} \right\} , \tag{C.74}$$

$$\Delta\mathcal{F}_2^S(q^2) \;=\; \frac{n_f}{2}\frac{1}{F^2}\left\{A_0(M_S^2)\right\}, \tag{C.75}$$

$$\Delta\mathcal{F}_3^S(q^2) \;=\; \frac{n_f}{2}\frac{1}{96\pi^2}\left\{\frac{q^2}{F^2}\left[-\ln\left(-\frac{q^2}{\mu^2}\right)+\frac{5}{3}\right]+\right.$$
$$\left.+\frac{M_S^2}{F^2}\left[6\ln\left(-\frac{q^2}{\mu^2}\right)-1\right]+\mathcal{O}\left(\frac{M_S^4}{q^2F^2}\right)\right\}, \tag{C.76}$$

$$\Delta\mathcal{F}_4^S(q^2) \;=\; \frac{n_f}{2}\frac{4c_d^2}{F^2}\frac{1}{96\pi^2}\left\{\frac{q^2}{F^2}\left[-\frac{5}{6}+\frac{1}{2}\ln\left(-\frac{q^2}{\mu^2}\right)\right]\right.$$
$$\left.-\frac{3}{2}\frac{M_S^2}{F^2}+\mathcal{O}\left(\frac{M_S^4}{q^2F^2}\right)\right\}, \tag{C.77}$$

$$\Delta F_5^S(q^2) \;=\; \frac{n_f}{2}\frac{F_V G_V}{F^2}\frac{4c_d^2}{F^2}\frac{1}{96\pi^2}\left\{\frac{q^2}{F^2}\left[\frac{5}{6}-\frac{1}{2}\ln\left(-\frac{q^2}{\mu^2}\right)\right]+\frac{M_S^2}{F^2}\left[\frac{3}{2}\right]+\right.$$
$$\left.+\frac{M_V^2}{F^2}\left[\frac{5}{6}-\frac{1}{2}\ln\left(-\frac{q^2}{\mu^2}\right)\right]+\mathcal{O}\left(\frac{M_S^4}{q^2F^2}\right)\right\}, \tag{C.78}$$

$$\Delta\mathcal{F}_6^S(q^2) \;=\; \frac{n_f}{2}\frac{4c_d^2}{F^2}\frac{1}{96\pi^2}\left\{\frac{q^2}{F^2}\left[-\frac{5}{6}+\frac{1}{2}\ln\left(-\frac{q^2}{\mu^2}\right)\right]+\right.$$
$$\left.+\frac{M_S^2}{F^2}\left[\frac{3}{2}-3\ln\left(-\frac{q^2}{M_S^2}\right)\right]+\mathcal{O}\left(\frac{M_S^4}{q^2F^2}\right)\right\}. \tag{C.79}$$

$$\Delta\mathcal{F}_1^A(q^2) \;=\; \frac{n_f}{2}\frac{1}{F^2}\left\{\frac{3}{2}A_0(M_A^2)-\frac{M_A^2}{64\pi^2}\right\}, \tag{C.80}$$

$$\Delta\mathcal{F}_2^A(q^2) \;=\; \frac{n_f}{2}\frac{1}{96\pi^2}\left\{\frac{q^4}{M_A^2 F^2}\left[\frac{2}{3}-\ln\left(-\frac{q^2}{\mu^2}\right)\right]+\right. \tag{C.81}$$

$$\tag{C.82}$$

$$+\frac{3q^2}{F^2}\left[1+\ln\left(-\frac{q^2}{\mu^2}\right)\right]+ \tag{C.83}$$

$$\tag{C.84}$$

$$\left.+\frac{M_A^2}{F^2}\left[12\ln\left(-\frac{q^2}{\mu^2}\right)-3\ln\left(\frac{M_A^2}{\mu^2}\right)-\frac{51}{2}\right]\right\}+ \tag{C.85}$$

$$\tag{C.86}$$

$$+\;\mathcal{O}\left(\frac{M_A^4}{q^2F^2}\right). \tag{C.87}$$

$$\Delta\mathcal{F}_1^P(q^2) \;=\; \frac{n_f}{2}\frac{1}{F^2}A_0(M_P^2), \tag{C.88}$$

$$\Delta \mathcal{F}_2^P(q^2) \quad = \quad \frac{n_f}{2} \frac{1}{96\pi^2} \left\{ \frac{q^2}{F^2} \left[-\ln\left(-\frac{q^2}{\mu^2} \right) + \frac{5}{3} \right] + \right.$$

$$\left. + \frac{M_P^2}{F^2} \left[6\ln\left(-\frac{q^2}{\mu^2} \right) - 1 \right] + \mathcal{O}\left(\frac{M_P^4}{q^2 F^2} \right) \right\} . \quad \text{(C.89)}$$

It is good to make now some remarks about these results.

The combination of the diagrams $\chi 1$, V1, V2 and V3 produces a cancellation up to order $\sim M_R^4/q^2 F^2$ when using the LO values $F_V = 2G_V = F\sqrt{2}$. In this diagrams the intermediate state is $\pi\pi$ and both the pion form factor and the $\pi\pi \to \pi\pi$ scattering amplitude in the s-channel behave adequately at high energies. Thus, the asymptotic behaviour of the summed one-loop diagrams is the proper one, $\sim 1/q^2$.

The resonance tadpoles are constant and proportional to squared mass of the resonances (V6,S2,A1,P1). The same happens with the topologies with the loop over one of the external legs (V4,S1). The analogous vector loop with an intermediate vector resonance (V5) is just $q^2/(M_V^2 - q^2)$ times a constant factor proportional to M_V^2. Therefore, all these contributions do not have absorptive cuts and are analytic so they can be cancel by choosing appropriate values of the RχT couplings.

The summation of the NGB-NGB-resonance triangles with and without an intermediate vector (V8 plus V9 for vector loops, and S4 plus S5 for the scalar loops) cancel up to order $\sim M_V^2/F^2$. In this case one has again a $\pi\pi$ intermediate state. The good behaviour of the pion form factor at tree-level provides the former cancellation that reduces the asymptotic behaviour from $\sim q^2$. However, the $\pi\pi \to \pi\pi$ scattering through exchange of resonances in the t-channel shows the bad behaviour $\sim q^2/F^2$ instead of being bound, so summed one-loop diagrams behaves as $\sim const$ instead of the desirable $\sim 1/q^2$ behaviour.

The case of the other kind of triangles, the resonance-resonance-NGB loop, is worse. One finds only 1PI triangles (V10,S6) and the lagrangian from Ecker *et al.* [19] does not provide the analogous diagram with an intermediate vector resonance that could cancel the order $\sim q^2/F^2$ terms, showing therefore this behaviour at high energies. One should study and implement the right short distance limits to the form factor to resonances and the scattering amplitudes $RR \to \pi\pi$, adding the required pieces to the lagrangian. Thus, similar situations are found for the diagrams S3 and P2.

Finally, the diagrams V7 and A2 produce a cut of two vectors and two axial-vectors. They receive non-zero contributions from the projection-Ω of the propagator.

C.4 Ω–contribution in the diagrams V7 and A2

In these two diagrams there was a one loop structure with two spin-1 propagators. In the rest of diagrams where we had before a spin-1 particle always the Ω–projection
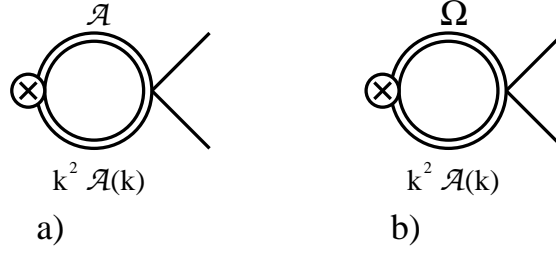
Figure C.1: Contributions to the diagrams V7 and A2 from: a) Just the $\mathcal{A}$–projections of the spin-1 propagators; b) contributions coming from the Ω-projection of one of them. There are no contributions from the Ω-projections of both propagators.

of the vector (or axial-vector) propagator vanished due to the form of the vertices. For simplicity, I will consider now on just the vector-vector diagram V7.

However, in this case, one finds that the Ω projection in one of the two vector propagators survive. Thus, it is possible to split the result of the diagram in two pieces, that coming from just the physical $\mathcal{A}$-projection of the propagators, and that "contaminated" with contributions from the Ω-projection of one of the propagators. We realised during the thesis that the important part of the VFF when analysing the short distance behaviour is the absorptive contribution of the diagrams. Thus, only the logarithms are analysed in this section.

The contribution to V7 from just the $\mathcal{A}$–projection is (diagram a in Fig. (C.1)),

$$\Delta \mathcal{F}_7^V (q^2)^{absor-\mathcal{A}} = \frac{n_f}{2} \frac{B_0(q^2; M_V^2, M_V^2)}{F^2} \left[-2 M_V^2 - \frac{q^2}{6} + \frac{q^4}{6 M_V^2} \right] + $$
$$+ \frac{n_f}{2} \frac{B_0(q^2; 0, M_V^2)}{F^2} \left[-\frac{M_V^4}{6 q^2} + \frac{M_V^2}{6} + \frac{q^2}{6} - \frac{q^4}{6 M_V^2} \right] , \tag{C.90}$$

and the Ω–projection (diagram b in Fig. (C.1)),

$$\Delta \mathcal{F}_7^V (q^2)^{absor-\Omega} = \frac{n_f}{2} \frac{B_0(q^2; 0, M_V^2)}{F^2} \left[\frac{M_V^4}{6 q^2} - \frac{M_V^2}{6} - \frac{q^2}{6} + \frac{q^4}{6 M_V^2} \right] . \tag{C.91}$$

The summation of both contributions gives again the absorptive logarithm in $\Delta \mathcal{F}_7^V (q^2)$.

The first thing to notice is that each individual contribution contains an un-physical cut of a mass M_V particle and a massless state, in addition to the physical cut in $B_0(q^2; M_V^2, M_V^2)$. This is because when splitting the vector propagator in $\Delta(q) = \frac{2i}{M_V^2 - q^2} \mathcal{A}(q) + \frac{2i}{M_V^2} \Omega(q)$, the part in $\mathcal{A}(q)$ contains two poles, $q^2 = M_V^2$ and $q^2 = 0$ (within the $\mathcal{A}(q)$ definition in Eq. (B.5)).

However, the second pole, in $q^2 = 0$, is fictitious. It is generated due to the special way of splitting the propagator. Once both parts are summed up the fake pole disappears, and just the $q^2 = M_V^2$ state remains.

This annoying situation only occurs in one of the two propagators. Due to the form of the vertices the other propagator is always contracted with suitable momentum structures, in such a way that its Ω–projection vanishes and also the q^2 pole in $\mathcal{A}(q)$.

As result of this, in order to recover the physical result with only a two-massive-particle absorptive cut one must sum up both contributions. This means that the extra spin–1 state found in the Ω–projection is essential to recover the physical result.

However, whereas at energies of the mass of the resonances and below including the Ω–projection is crucial, at high q^2 the Ω–projection spoils the short distance behaviour with an order q^4 term: The expression in Eq. (C.90) becomes,

$$\mathcal{F}_7^V(q^2)^{absor-\mathcal{A}} \quad \overset{q^2\to\infty}{=} \quad \frac{n_f}{2} \frac{q^2}{96\pi^2 F^2} \left[1 + \ln\left(-\frac{q^2}{M_V^2}\right)\right] +$$

$$+ \frac{n_f}{2} \frac{M_V^2}{96\pi^2 F^2} \left[11\lambda_\infty - \frac{25}{2} - \ln\frac{M_V^2}{\mu^2} + 12\ln\left(-\frac{q^2}{\mu^2}\right)\right] + \mathcal{O}\left(\frac{1}{q^2}\right),$$
$$\text{(C.92)}$$

and the expression in Eq. (C.91) turns out to be,

$$\mathcal{F}_7^V(q^2)^{absor-\Omega} \quad \overset{q^2\to\infty}{=} \quad \frac{n_f}{2} \frac{q^4}{96\pi^2 M_V^2 F^2} \left[-\lambda_\infty + 1 - \ln\left(-\frac{q^2}{\mu^2}\right)\right] +$$

$$+ \frac{n_f}{2} \frac{q^2}{96\pi^2 F^2} \left[\lambda_\infty - \ln\frac{M_V^2}{\mu^2} + 2\ln\left(-\frac{q^2}{\mu^2}\right)\right] + \qquad \text{(C.93)}$$

$$+ \frac{n_f}{2} \frac{M_V^2}{96\pi^2 F^2} \left[\lambda_\infty - \frac{5}{2} + \ln\frac{M_V^2}{\mu^2}\right] + \mathcal{O}\left(\frac{1}{q^2}\right).$$

The form factor scales then as $\sim q^4$ at high energies due to the contributions from the Ω–projection of the propagator. These extra degrees of freedom should be removed somehow from the calculation in order to recover the $\mathcal{F} \sim q^2$ behaviour expected from the naive superficial degree of divergence analysis.

Summarising

- **Low and intermediate energies:** Both $\mathcal{A}$– and Ω–components of the propagator contribute to the amplitude in such a way that unphysical cuts are canceled out.

- **High energies:** The $\mathcal{A}$–projection, corresponding to the degrees of freedom of our spin–1 meson, gives a well behaved form-factor. However, the addition

of the Ω–component spoils the form-factor, increasing the behaviour at large momenta by one extra power of q^2.

Appendix D

Couplings of the effective lagrangian

D.1 χPT couplings of $\mathcal{L}_{4\chi}$ in $SU(2)_R \otimes SU(2)_L$

The χPT lagrangian at $\mathcal{O}(p^4)$ –given in the $U(\phi)$ formalism– is [8]:

$$
\begin{aligned}
\mathcal{L}_{4\chi} \;=\; & \ell_1 (D^\mu U^\dagger D_\mu U)^2 + \ell_2 (D_\mu U^\dagger D_\nu U)(D^\mu U^\dagger D^\nu U) \\
& + \ell_3 (\chi^\dagger U)^2 + \ell_4 (D^\mu \chi^\dagger D_\mu U) \\
& + \ell_5 (U^\dagger F^{\mu\nu} F_{\mu\nu} U) + \ell_6 (D^\mu U^\dagger F_{\mu\nu} D^\nu U) \\
& + \ell_7 (\widetilde{\chi}^\dagger U)^2 + h_1 \chi^\dagger \chi + h_2 F_{\mu\nu} F^{\mu\nu} + h_3 \widetilde{\chi}^\dagger \widetilde{\chi} \quad .
\end{aligned}
\tag{D.1}
$$

There are also a pair of terms allowed by the symmetry but they can be removed through the employment of the EOM of the $\mathcal{O}(p^2)$ χPT lagrangian.

This set of coupling removes the ultraviolet divergences of the processes up to $\mathcal{O}(p^4)$ through the renormalizations:

$$
\ell_i \;=\; \frac{\gamma_i}{32\pi^2} \, \lambda_\infty(\mu) \;+\; \ell_i^r(\mu),
\tag{D.2}
$$

being ℓ_i and $\ell_i^r(\mu)$ the bare and renormalized couplings respectively. The constants γ_i have been put together into Table (D.1) [8].

It is possible to express the renormalized couplings $\ell_i^r(\mu)$ in terms of the scale invariant conbinations $\bar{\ell}_i$:

$$
\bar{\ell}_i \;=\; \frac{32\pi^2}{\gamma_i} \, \ell_i^r(\mu) \;-\; \ln \frac{m_\pi^2}{\mu^2} \quad .
\tag{D.3}
$$

When integrating out the $\rho(770)$ the $\mathcal{O}(p^4)$ couplings gain contributions [8], that can be found In Table (D.1) (in Ref. [8] one finds the notation $F_V \to F_\rho$, $G_V \to G_\rho$, $F \to F_\pi$).

i	$\bar{\ell}_i$	γ_i	$\bar{\ell}_i^\rho$
1	-1.7 ± 1.0	$1/3$	$-\frac{96\pi^2 G_V^2}{M_\rho^2} \simeq -6.8$
2	6.1 ± 0.5	$2/3$	$\frac{48\pi^2 G_V^2}{M_\rho^2} \simeq 3.4$
3	2.9 ± 2.4	$-1/2$	0
4	4.4 ± 0.3	2	0
5	13.0 ± 0.9	$-1/6$	$\frac{48\pi^2 F_V^2}{M_\rho^2} \simeq 13.6$
6	$16.0 \pm 0.5 \pm 0.7$	$-1/3$	$\frac{96\pi^2 F_V G_V}{M_\rho^2} \simeq 13.6$

Table D.1:   Value of the constants $\bar{\ell}_i$, γ_i and $\bar{\ell}_i^\rho$. The experimental values of ℓ_1 and ℓ_2 have been taken from Ref [79], ℓ_3 comes from Ref [8], and ℓ_4, ℓ_5, ℓ_6 have been obtained in the recent study of Ref. [17]. For the constants $\bar{\ell}_i$ from the $\rho(770)$ saturation the value $M_\rho = 770$ MeV was consider, together with the $N_C \to \infty$ relations $F_V = 2G_V = F\sqrt{2}$.

When working at $\mathcal{O}(p^6)$ [17, 16] one defines the combinations k_i of couplings ℓ_i:

$$k_i = \left(4\ell_i^r - \gamma_i \frac{1}{16\pi^2} \ln \frac{m_\pi^2}{\mu^2}\right) \frac{1}{16\pi^2} \ln \frac{m_\pi^2}{\mu^2} = \frac{1}{16\pi^2}\left(2\gamma_i\bar{\ell}_i + \ln\frac{m_\pi^2}{\mu^2}\right)\frac{1}{16\pi^2}\ln\frac{m_\pi^2}{\mu^2} \quad . \tag{D.4}$$

D.2 χPT couplings in $SU(3)_R \otimes SU(3)_L$

At $\mathcal{O}(p^2)$ the χPT lagrangian is identical to the two flavour case. However, the $\mathcal{O}(p^4)$ lagrangian for $n_f = 3$ contains a few more terms [9] and it was given before in Eq. (3.26) in the $U(\phi)$ formalism (Eq. (3.38) if expressed through $u(\phi)$).

This constants remove the ultraviolet divergences at $\mathcal{O}(p^4)$ through the renormalizations:

$$L_i = \frac{\Gamma_i}{32\pi^2}\lambda_\infty + L_i^r(\mu) \quad , \qquad H_i = \frac{\Gamma_i^H}{32\pi^2}\lambda_\infty + H_i^r(\mu), \tag{D.5}$$

where $\Gamma_1^H = -\frac{1}{8}$ and $\Gamma_2^H = \frac{5}{24}$, and the constants Γ_i can be found in Table (D.2). Notice that the couplings L_3 and L_7 are not renormalized at this chiral order and, consequently, are scale independent.

Through the renormalization in Eq. (D.5), the running of the renormalized couplings is given by the Γ_i:

$$\mu \frac{d L_i^r}{d\mu} = -\frac{\Gamma_i}{16\pi^2} . \tag{D.6}$$

Table D.2: Phenomenological values of the $\mathcal{O}(p^4)$ renormalized couplings for $\mu = 770$ MeV [6]. The last column shows the source.

i	Γ_i	$L_i^r(\mu) \times 10^3$	Source
1	$\frac{3}{32}$	0.4 ± 0.3	K_{e4}, $\pi\pi \to \pi\pi$
2	$\frac{3}{16}$	1.4 ± 0.3	K_{e4}, $\pi\pi \to \pi\pi$
3	0	-3.5 ± 1.1	K_{e4}, $\pi\pi \to \pi\pi$
4	$\frac{1}{8}$	-0.3 ± 0.5	Regla de Zweig
5	$\frac{3}{8}$	1.4 ± 0.5	F_K/F_π
6	$\frac{11}{144}$	-0.2 ± 0.3	Zweig Rule
7	0	-0.4 ± 0.2	Gell-Mann–Okubo, L_5, L_8
8	$\frac{5}{48}$	0.9 ± 0.3	$m_{K^0} - m_{K^+}$, L_5, $(m_s - \hat{m})/(m_d - m_u)$
9	$\frac{1}{4}$	6.9 ± 0.7	$\langle r^2 \rangle_V^\pi$
10	$-\frac{1}{4}$	-5.5 ± 0.7	$\pi \to e\nu\gamma$

Finally, it is possible to recover χPT for $n_f = 2$ by performing the limit $m_s \gg m_{u/d}$, providing the next relation of $SU(2)$ and $SU(3)$ couplings [9]:

$$
\begin{aligned}
\ell_1^r &= 4L_1^r + 2L_3 - \tfrac{1}{24}\nu_K \quad, \\
\ell_2^r &= 4L_2^r - \tfrac{1}{12}\nu_K \quad, \\
\ell_3^r &= -8L_4^r - 4L_5^r + 16L_6^r + 8L_8^r - \tfrac{1}{18}\nu_\eta \quad, \\
\ell_4^r &= 8L_4^r + 4L_5^r - \tfrac{1}{2}\nu_K \quad, \\
\ell_5^r &= L_{10}^r + \tfrac{1}{12}\nu_K \quad, \\
\ell_6^r &= -2L_9^r + \tfrac{1}{6}\nu_K \quad, \\
\ell_7^r &= \tfrac{f^2}{2B_0 m_s}\left(1 + \tfrac{10}{3}\bar{\mu}_\eta\right) + 4\left(L_4^r - L_6^r - 9L_7 - 3L_8^r + \tfrac{1}{8}\nu_K\right) \quad, \\
h_1^r &= 8L_4^r + 4L_5^r - 4L_8^r + 2H_2^r - \tfrac{1}{2}\nu_K \quad, \\
h_2^r &= -\tfrac{1}{4}L_{10}^r - \tfrac{1}{2}H_1^r - \tfrac{1}{24}\nu_k \quad, \\
h_3^r &= 4L_8^r + 2H_2^r - \tfrac{1}{2}\nu_K - \tfrac{1}{3}\nu_\eta + \tfrac{1}{96\pi^2} \quad,
\end{aligned}
\tag{D.7}
$$

where $\nu_P \equiv \frac{1}{32\pi^2}(\ln\frac{m_P^2}{\mu^2} + 1)$ and $\bar{\mu}_\eta \equiv \frac{1}{32\pi^2}\frac{m_\eta^2}{f^2}\ln\frac{m_\eta^2}{\mu^2}$.

D.3 Resonance couplings and masses

In Chapter 4 the RχT lagrangian was introduced, including vector, axial-vector, scalar and pseudo-scalar resonances. This lagrangian in Eqs. (4.7) and (4.8) provides the interaction between the resonances of resonances and the Goldstones. Although this work has introduced the resonances as degenerated $U(n_f)$ multiplets, former works separated explicitly the singlet component R_1 [19]. For vectors and axial-vectors there is no difference but for the lagrangian for the scalar and pseudo-scalar resonances:

$$
\mathcal{L}_{\text{Kin}}(R = S, P) = \tfrac{1}{2}\langle \nabla^\mu R \nabla_\mu R - M_R^2 R^2 \rangle + \tfrac{1}{2}\left\{ \partial^\mu R \partial_\mu R - M_{R_1}^2 R^2 \right\}, \tag{D.8}
$$

and

$$
\begin{aligned}
\mathcal{L}_{2S} &= c_d \langle S u_\mu u^\mu \rangle + c_m \langle S \chi_+ \rangle + \tilde{c}_d \, S_1 \langle u_\mu u^\mu \rangle + \tilde{c}_m \, S_1 \langle \chi_+ \rangle, \\
\mathcal{L}_{2P} &= i d_m \langle P \chi_- \rangle + i \tilde{d}_m \, P_1 \langle \chi_- \rangle \ .
\end{aligned}
\tag{D.9}
$$

In the large N_C limit $U(1)_A$ anomaly disappears and one has $M_{S_1} = M_S$, $\tilde{c}_d = \sqrt{3} c_d$, $\tilde{c}_m = \sqrt{3} c_m$ and $\tilde{d}_m = \sqrt{3} d_m$. The singlet fields could be then put together with the rest of fields in the matrix $R_{U(3)} = R_{SU(3)} + R_1 \frac{1}{\sqrt{3}} \mathcal{I}$.

The vector couplings F_V and G_V for the $\rho(770)$ can be obtained from $\Gamma(\rho^0 \to e^+ e^-) = (6.9 \pm 0.3)$ KeV and $\Gamma(\rho \to \pi\pi) = (153 \pm 2)$ MeV [19], respectively, yielding

$$
\begin{aligned}
F_V &\simeq 154 \text{ MeV} \quad , \tag{D.10} \\
G_V &\simeq 69 \text{ MeV} \quad , \tag{D.11}
\end{aligned}
$$

taking the mass $M_\rho = 770$ MeV. In addition, through the QCD short distance constraints one may also give a prediction for these couplings at LO in $1/N_C$ [23]:

$$
\begin{aligned}
F_V &= F\sqrt{2} \quad \simeq 132 \text{ MeV} \quad , \tag{D.12} \\
G_V &= F/\sqrt{2} \quad \simeq 66 \text{ MeV} \quad . \tag{D.13}
\end{aligned}
$$

The knowledge in the scalar sector is poorer. Recently, a analysis of the $K\pi$ scattering provided [76]:

$$
\begin{aligned}
c_d &= (30 \pm 10) \text{ MeV} \quad , \tag{D.14} \\
c_m &= (43 \pm 14) \text{ MeV} \quad , \tag{D.15}
\end{aligned}
$$

where c_d and c_m were left free. In addition, the fit gave the mass for the K_0^* vector $(I = \frac{1}{2}, \ J = 0)$ $M_{K_0^*} = 1.4$ GeV. Moreover, imposing the constraint $c_d = c_m$ to the fit one obtains [76]

$$
c_d = c_m \simeq 45.4 \text{ MeV} \quad , \tag{D.16}
$$

in reasonable agreement with the theoretical prediction provided by the QCD short-distance constraints [76, 21]:

$$
c_d = c_m = \frac{F}{2} \simeq 46.2 \text{ MeV} \quad . \tag{D.17}
$$

The experimental determination of the scalar singlet parameters $\tilde{c}_d$, $\tilde{c}_m$ and M_{S_1} is rather complicated, due to the actual controversy on the asignement of the 0^{++} states to the observed experimental spectrum. It is not clarified yet the degree of mixing between the singlet and octet channels [104]. However, through large N_C arguments, one expects them to form a degenerate $U(3)$ multiplet (Zweig Rule).

D.4 Contributions from the resonances to $\mathcal{L}_{4\chi}$ at LO in $1/N_C$

From the integration of the resonances, much heavier that the Goldstones $(m_\pi, m_K, m_\eta \ll M_R)$, one obtains their contribution to the χPT couplings at low energies [19]. The first contribution comes at $\mathcal{O}(p^4)$, so $\mathcal{L}_{2\chi}$ is not influenced by the presence of resonances.

The saturation hypothesis states that at LO in $1/N_C$ the $\mathcal{O}(p^4)$ χPT coupling constants are given just from the integration of the resonances. Since the saturation is at LO in $1/N_C$, i.e. at tree-level, one does not have a scale where this occurs. The modifications due to the running are subleading in $1/N_C$ and one expects them to be small, and to essentially reproduce the experimental values $L_i^r(\mu)$, for $\mu = 770$ MeV, in Table (D.2). In the vector case the saturation fulfill reasonably well the experimental L_i for any value of $\mu = (0.5 \to 1)$ GeV. However, in the scalar channel one has important logarithm contributions, for instance for the coupling L_5.

At LO in $1/N_C$ one has the resonance lagrangian in Eq. (D.9) yields the contributions

$$
\begin{aligned}
L_1 &= \frac{G_V^2}{8M_V^2} - \frac{c_d^2}{6M_S^2} + \frac{\tilde{c}_d^2}{2M_{S_1}^2} \quad, \\
L_2 &= \frac{G_V^2}{4M_V^2} \quad, \\
L_3 &= -\frac{3G_V^2}{4M_V^2} + \frac{c_d^2}{2M_S^2} \quad, \\
L_4 &= -\frac{c_d c_m}{3M_S^2} + \frac{\tilde{c}_d \tilde{c}_m}{M_{S_1}^2} \\
L_5 &= \frac{c_d c_m}{M_S^2} \quad, \\
L_6 &= -\frac{c_m^2}{6M_S^2} + \frac{\tilde{c}_m^2}{2M_{S_1}^2} \\
L_7 &= \frac{d_m^2}{6M_P^2} - \frac{\tilde{d}_m^2}{2M_{P_1}^2} \quad, \\
L_8 &= \frac{c_m^2}{2M_S^2} - \frac{d_m^2}{2M_P^2} \quad, \\
L_9 &= \frac{F_V G_V}{2M_V^2} \quad, \\
L_{10} &= -\frac{F_V^2}{4M_V^2} + \frac{F_A^2}{4M_A^2} \quad, \\
H_1 &= -\frac{F_V^2}{8M_V^2} - \frac{F_A^2}{8M_A^2} \quad,
\end{aligned}
\tag{D.18}
$$

$$H_2 \quad = \quad \frac{c_m}{M_S^2} + \frac{d_m^2}{M_P^2} \quad .$$

In the large N_C limit, when the multiplets become degenerated and $\widetilde{c}_i = c_i/\sqrt{3}$, $\widetilde{d}_i = d_i/\sqrt{3}$, one observes that $L_4 = L_6 = L_7 = 0$, receiving just contributions subleading in $1/N_C$. Thus, one can beheld in Table (D.2) that they are in fact experimentally suppressed.

Appendix E

Matrix relations

E.1 $SU(N)$ algebra

One can find the main properties of the $SU(N)$ algebras in many reviews. Here I show the most interesting ones that have being used in this work and that have been extracted from Ref. [1].

$SU(N)$ is the group of $N \times N$ unitary matrices, $UU^\dagger = U^\dagger U = 1$, with $\det U = 1$. The generators of the $SU(N)$ algebra, T^a $(a = 1, 2, \ldots, N^2 - 1)$, are hermitian, traceless matrices satisfying the commutation relations

$$[T^a, T^b] = i f^{abc} T^c \,, \tag{E.1}$$

the structure constants f^{abc} being real and totally antisymmetric.

The fundamental representation $T^a = \lambda^a/2$ is N-dimensional. For $N = 2$, λ^a are the usual Pauli matrices, while for $N = 3$, they correspond to the eight Gell-Mann matrices:

$$\lambda^1 = \begin{pmatrix} 0 & 1 & 0 \\ 1 & 0 & 0 \\ 0 & 0 & 0 \end{pmatrix}, \lambda^2 = \begin{pmatrix} 0 & -i & 0 \\ i & 0 & 0 \\ 0 & 0 & 0 \end{pmatrix}, \lambda^3 = \begin{pmatrix} 1 & 0 & 0 \\ 0 & -1 & 0 \\ 0 & 0 & 0 \end{pmatrix},$$

$$\lambda^4 = \begin{pmatrix} 0 & 0 & 1 \\ 0 & 0 & 0 \\ 1 & 0 & 0 \end{pmatrix}, \lambda^5 = \begin{pmatrix} 0 & 0 & -i \\ 0 & 0 & 0 \\ i & 0 & 0 \end{pmatrix}, \lambda^6 = \begin{pmatrix} 0 & 0 & 0 \\ 0 & 0 & 1 \\ 0 & 1 & 0 \end{pmatrix},$$

$$\lambda^7 = \begin{pmatrix} 0 & 0 & 0 \\ 0 & 0 & -i \\ 0 & i & 0 \end{pmatrix}, \lambda^8 = \frac{1}{\sqrt{3}} \begin{pmatrix} 1 & 0 & 0 \\ 0 & 1 & 0 \\ 0 & 0 & -2 \end{pmatrix}. \tag{E.2}$$

They satisfy the anticommutation relation

$$\left\{\lambda^a, \lambda^b\right\} = \frac{4}{N}\,\delta^{ab}\,I_N \,+\, 2d^{abc}\,\lambda^c\,, \tag{E.3}$$

where I_N denotes the N-dimensional unit matrix and the constants d^{abc} are totally symmetric in the three indices.

For $SU(3)$, the only non-zero (up to permutations) f^{abc} and d^{abc} constants are

$$\frac{1}{2}f^{123} = f^{147} = -f^{156} = f^{246} = f^{257} = f^{345} = -f^{367} = \frac{1}{\sqrt{3}}f^{458} = \frac{1}{\sqrt{3}}f^{678} = \frac{1}{2}\,,$$

$$d^{146} = d^{157} = -d^{247} = d^{256} = d^{344} = d^{355} = -d^{366} = -d^{377} = \frac{1}{2}\,, \tag{E.4}$$

$$d^{118} = d^{228} = d^{338} = -2d^{448} = -2d^{558} = -2d^{688} = -2d^{788} = -d^{888} = \frac{1}{\sqrt{3}}\,.$$

The adjoint representation of the $SU(N)$ group is given by the $(N^2-1)\times(N^2-1)$ matrices $(T_A^a)_{bc} \equiv -if^{abc}$. The relations

$$\mathrm{Tr}\left(\lambda^a\lambda^b\right) = 4T_F\,\delta_{ab}\,, \qquad\qquad T_F = \frac{1}{2}\,,$$

$$\left(\lambda^a\lambda^a\right)_{\alpha\beta} = 4C_F\,\delta_{\alpha\beta}\,, \qquad\qquad C_F = \frac{N^2-1}{2N}\,, \tag{E.5}$$

$$\mathrm{Tr}(T_A^a T_A^b) = f^{acd}f^{bcd} = C_A\,\delta_{ab}\,, \qquad C_A = N\,,$$

define the $SU(N)$ invariants T_F, C_F and C_A. Other useful properties are:

$$\left(\lambda^a\right)_{\alpha\beta}\left(\lambda^a\right)_{\gamma\delta} = 2\delta_{\alpha\delta}\delta_{\beta\gamma} - \frac{2}{N}\delta_{\alpha\beta}\delta_{\gamma\delta}\,; \qquad\qquad \mathrm{Tr}\left(\lambda^a\lambda^b\lambda^c\right) = 2(d^{abc} + if^{abc})\,;$$

$$\mathrm{Tr}(T_A^a T_A^b T_A^c) = i\,\frac{N}{2}f^{abc}\,; \qquad \sum_b d^{abb} = 0\,; \qquad d^{abc}d^{ebc} = \left(N - \frac{4}{N}\right)\delta_{ae}\,; \tag{E.6}$$

$$f^{abe}f^{cde} + f^{ace}f^{dbe} + f^{ade}f^{bce} = 0\,; \qquad\qquad f^{abe}d^{cde} + f^{ace}d^{dbe} + f^{ade}d^{bce} = 0\,.$$

E.2 3×3 matrices

For 3 matrices A, B, C, the Cayley-Hamilton theorem states:

$$\begin{aligned}
&ABC + ACB + BAC + BCA + CAB + CBA \\
&-AB\langle C\rangle - AC\langle B\rangle - BC\langle A\rangle - CA\langle B\rangle - CB\langle A\rangle \\
&-A\langle BC\rangle - B\langle AC\rangle - C\langle AB\rangle - \langle ABC\rangle - \langle ACB\rangle \\
&\quad +A\langle B\rangle\langle C\rangle + B\langle A\rangle\langle C\rangle + C\langle A\rangle\langle B\rangle \\
&+\langle A\rangle\langle BC\rangle + \langle B\rangle\langle AC\rangle + \langle C\rangle\langle AB\rangle - \langle A\rangle\langle B\rangle\langle C\rangle = 0\,,
\end{aligned} \tag{E.7}$$

$$\langle AB^\dagger AB^\dagger\rangle = -2\langle AA^\dagger BB^\dagger\rangle + \tfrac{1}{2}\langle AA^\dagger\rangle\langle BB^\dagger\rangle + \langle AB^\dagger\rangle^2 \quad .$$

For 3×3 hermitian matrices one has:

$$
\begin{aligned}
B^2 A + B A B + A B^2 = \quad & \langle A \rangle B^2 + \{A, B\} \langle B \rangle \\
& + (\langle AB \rangle - \langle A \rangle \langle B \rangle) B + \langle AB^2 \rangle \mathcal{I} \\
& \tfrac{1}{2} (A - \langle A \rangle \mathcal{I}) (\langle B^2 \rangle - \langle B \rangle^2) - \langle B \rangle \langle AB \rangle \mathcal{I} .
\end{aligned}
\tag{E.8}
$$

For traceles 3×3 matrices A_i we have:

$$
\langle A_1 A_2 A_3 A_4 \rangle + \langle A_1 A_3 A_2 A_4 \rangle + \langle A_1 A_4 A_3 A_2 \rangle +
$$

$$
+ \langle A_1 A_2 A_4 A_3 \rangle + \langle A_1 A_3 A_4 A_2 \rangle + \langle A_1 A_4 A_2 A_3 \rangle
\tag{E.9}
$$

$$
- \langle A_1 A_2 \rangle \langle A_3 A_4 \rangle - \langle A_1 A_3 \rangle \langle A_2 A_4 \rangle - \langle A_1 A_4 \rangle \langle A_2 A_3 \rangle = 0 .
$$

E.3 $2n \times 2n$ Matrices

In order to calculate the re-scattering we had to invert matrices. Sometimes, as it happened in the vector case with the tree level scattering amplitude, we had to handle matrices with zero determinant and therefore at first, non invertible. This problem is solved just adding to the matrix an infinitesimal matrix ϵ with provides a non zero determinant. We just can work this way during the calculations and take the limit $\epsilon \to 0$ at the end.

This algebraic operation for 2×2 matrices is given by

$$
M = \begin{pmatrix} a & b \\ c & d \end{pmatrix} \longrightarrow M^{-1} = \frac{1}{det(M)} M^* = \frac{1}{ad - bc} \begin{pmatrix} d & -b \\ -c & a \end{pmatrix}, \tag{E.10}
$$

where $det(...)$ denotes the determinant of the matrix and $M^* \equiv \{M^a\}^T$ is defined as the transposed adjoint matrix.

In a more general way, the inverse of a $2n \times 2n$ matrix $M = \begin{pmatrix} A & B \\ C & D \end{pmatrix}$ is

$$
\begin{aligned}
M^{-1} &= \begin{pmatrix} (A - BD^{-1}C)^{-1} & -(A - BD^{-1}C)^{-1} BD^{-1} \\ -(D - CA^{-1}B)^{-1} CA^{-1} & (D - CA^{-1}B)^{-1} \end{pmatrix} = \\
&= \begin{pmatrix} C^{-1}D(AC^{-1}D - B)^{-1} & -A^{-1}B(D - CA^{-1}B)^{-1} \\ -(AC^{-1}D - B)^{-1} & (D - CA^{-1}B)^{-1} \end{pmatrix},
\end{aligned}
\tag{E.11}
$$

where A, B, C, D are any general $n \times n$ matrices.

E.4 Properties of the dimension 1 projectors

The matrix for the scattering amplitude at LO in $1/N_C$ in the $I = J = 1$ channel could be given in terms of a dimension one projector times a factor. Thus, it would be interesting to have a look on some of the properties of the projectors.

Consider a matrix $H = \lambda \, \vec{u}_\lambda \vec{u}_\lambda^\dagger$, with $|\vec{u}_\lambda| = 1$ and being therefore $\lambda = \text{tr}(T)$ the unique non-zero eigenvalue.

It obeys

$$
\begin{aligned}
H^2 &= \text{Tr}(H)\, H, & \text{(E.12)} \\
\det(1 - H) &= 1 - \text{tr}(H), & \text{(E.13)} \\
(1 - H)^{-1} &= \frac{1}{1 - \text{tr}(H)} + \frac{1}{1 - \text{tr}(H)}\,(H - \text{tr}(H)). & \text{(E.14)}
\end{aligned}
$$

Notice that if H is proportional to a dimension one projector and A, B are arbitrary matrices, then $H' = AHB$ is as well proportional to a dimension one projector with its non-zero eigenvalue equal to $\lambda' = \text{tr}(H')$ corresponding to its normalized eigenvector $\vec{u}'_\lambda$ (that is not necessarily equal to $\vec{u}_\lambda$), and obeys

$$
\begin{aligned}
H' \cdot H &= \lambda'\, H' \cdot (\vec{u}_\lambda'^\dagger A^{-1} \vec{u}'_\lambda) B^{-1}, & \text{(E.15)} \\
\det(1 - H') &= 1 - \lambda', & \text{(E.16)} \\
(1 - H')^{-1} &= \frac{1}{1 - \lambda'} + \frac{1}{1 - \lambda'}\,(H' - \lambda'). & \text{(E.17)}
\end{aligned}
$$

Therefore, when we multiply the former inverse matrix $(1 - H)^{-1}$ by the eigenvector $\vec{u}_\lambda$, or by a matrix $H \cdot B$ on the right, with B any matrix, one finds

$$
\begin{aligned}
(1 - H)^{-1}\, \vec{u}_\lambda &= \frac{1}{1 - \lambda}\, \vec{u}_\lambda, & \text{(E.18)} \\
(1 - H)^{-1} \cdot (H \cdot B) &= \frac{1}{1 - \lambda}\,(H \cdot B). & \text{(E.19)}
\end{aligned}
$$

$$
\text{(E.20)}
$$

So therefore the effect of the inverse matrix in these cases is completely equivalent to just multiplying by a number,

$$
(1 - H)^{-1} \sim \frac{1}{1 - \lambda}. \tag{E.21}
$$

All this can be applied to the scattering amplitudes. In the isospin limit, the matrix $\left[\Sigma^{-1} T_{\text{LO}}^{I=J=1} \Sigma^{-1}\right]_{s-channel}$, is proportional to a dimension-one projector, being $\left[T_{\text{LO}}^{I=J=1}\right]_{s-channel}$ the $\pi\pi$ and $K\overline{K}$ $I = J = 1$ partial wave scattering amplitude. The subspcript $s - channel$ denotes that only the local scattering and the exchange of a vector in the s-channel have been considered. The exchanges in the t-channel have been left appart. In the study carried on before in Chapter 5 I applied the properties of H', taking the matrices $H = \left[\Sigma^{-1}\, T_{\text{LO}}^{I=J=1}\, \Sigma^{-1}\right]_{s-channel}$, $A = \mathcal{I}$ and $B = (-192\pi B_{22})$. The matrix $H' = H \cdot B$ was just the recurrence matrix $\mathcal{M}$ from N loops to $N + 1$ and the vector $\vec{u}'_\lambda$ was simply the tree-level VFF $\vec{\mathcal{F}}_0$.

E.5   Physical eigenstate decomposition

A general hermitian $n \times n$ matrix H can always be expanded in terms of its eigenstate spectral decomposition. This is the sum over the dimension one projectors $H = \sum_{i=1}^{n} \lambda_i P_i$. These projectors have the form $P_i = \vec{u}_i \vec{u}_i^\dagger$ with the unitary vector $\vec{u}_i$ marking the P_i projecting direction corresponding to the eigenvalue λ_i.

With this decomposition we have the inverse matrix relations

$$(1 - H)^{-1} = 1 + \sum_i \frac{1}{1 - \lambda_i}\, \lambda_i P_i, \tag{E.22}$$

$$(1 - H)^{-1} H = \sum_i \frac{1}{1 - \lambda_i}\, \lambda_i P_i, \tag{E.23}$$

$$(1 - H)^{-1} \vec{u}_j = \frac{1}{1 - \lambda_j}\, \vec{u}_j. \tag{E.24}$$

However in the physical problem this hermitian matrix was also multiplied by a matrix of Feynman integrals $B = \mathrm{diag}(B_{(1)}, B_{(2)}, ...)$ which became proportional to the identity in the $U(3)$ limit. Then the former relations get modified when we have $(1 - HB)^{-1}$. If H is only considered at the leading order we have

$$(1 - HB)^{-1} \simeq \prod_i (1 - \lambda_i P_i B)^{-1}, \tag{E.25}$$

$$(1 - HB)^{-1} H \simeq \sum_j \left[\prod_{i \neq j} (1 - \lambda_i P_i B)^{-1} \right] \frac{1}{1 - \lambda_j \mathrm{tr}(P_j B)} \lambda_j P_j, \tag{E.26}$$

$$(1 - HB)^{-1} \vec{u}_j \simeq \left[\prod_{i \neq j} (1 - \lambda_i P_i B)^{-1} \right] \frac{1}{1 - \lambda_j \mathrm{tr}(P_j B)} \vec{u}_j. \tag{E.27}$$

These relations turn exact in the $U(3)$ limit when B becomes proportional to the identity or when H is proportional to a given dimension one projector.

The tree-level scattering amplitude coming from the exchange of an intermediate bare propagator in the s-channel is in general given by the structure $\mathcal{T}_{fi} = V_f \cdot \frac{\alpha}{M^2 - q^2} \cdot V_i$. The factors $V_{f,i}$ depend on the channel for the initial (i) and final (f) state. Therefore we can express it in the matrix way $\mathcal{T} = \frac{\alpha}{M^2 - q^2} \vec{V} \vec{V}^T$, with the real vector $(\vec{V})_K = V_k$. When we work with a scattering with angular momentum J, usually this scattering is projected in the J partial wave:

$$\mathcal{T} \quad \longrightarrow \quad T^J = C\, \Sigma^J\, \mathcal{T}\, \Sigma^J, \tag{E.28}$$

with C a constant provided by the partial wave normalisation.

So both $\mathcal{T}$ and T^J are hermitian matrices proportional to dimension one projectors: $T = \lambda^{\mathcal{T}} \vec{u}_{\mathcal{T}} \vec{u}_{\mathcal{T}}^\dagger$, with $\vec{u}_{\mathcal{T}} = \frac{\vec{V}}{|\vec{V}|}$, and $T^J = \lambda^T \vec{u}_T \vec{u}_T^\dagger$, with $\vec{u}_T = \frac{\Sigma^J \vec{V}}{|\Sigma^J \vec{V}|}$.

E.5.1   Only One resonance Tree-level Scattering

If we only handle tree-level scatterings through a unique resonance exchange in the s-channel, then the observables are described by the re-scattering matrix $[1 + T^J(L+\Delta)]^{-1}$, so applying the former reasoning,

$$[1 + T^J(L+\Delta)]^{-1} = 1 - \frac{1}{1+\mathrm{tr}(T^J(L+\Delta))} T^J(L+\Delta). \qquad (\text{E.29})$$

Thus the re-summed scattering yields

$$[1 + T^J(L+\Delta)]^{-1}T^J = \frac{1}{1+\mathrm{tr}(T^J(L+\Delta))} T^J. \qquad (\text{E.30})$$

The form factor is provided by an initial vertex consisting in an intermediate bare propagator in the s-channel, i.e. $\vec{\mathcal{F}}_0 = \frac{\beta}{M^2-q^2}\vec{V} = \frac{\beta}{M^2-q^2}|\vec{V}|\vec{u}_\mathcal{T}$. Then, the re-summed form factor is

$$\vec{\mathcal{F}} = [1 + \Sigma^{-J}T^J(L+\Delta)\Sigma^J]^{-1} \vec{\mathcal{F}}_0 = \frac{1}{1+\mathrm{tr}(T^J(L+\Delta))} \vec{\mathcal{F}}_0. \qquad (\text{E.31})$$

The assumption that there are only tree-level interactions through a bare propagator is right when you are close to the resonance, i.e. $q^2 \simeq M^2$. The Dyson-Schwinger summation handles the bare real pole in the right way, regularising the tree-level pole in the tree-level T^J or in $\mathcal{F}_0$ with the tree-level pole in $\mathrm{tr}(T^J(L+\Delta))$.

E.5.2   Resonance + Background

When we are close to a resonance the rest of interactions (local, other resonances...) act like a background. The total tree-level scattering $T = T^R + T^{Bg}$ is then composed by the term T^R with the real pole $s = M_R^2$, and the background T^{Bg}, which is regular at energies $s \sim M_R^2$:

$$[1 + T(L+\Delta)]^{-1} =$$

$$= [1 + T^{Bg}(L+\Delta)]^{-1} \times [1 + T^R(L+\Delta)\cdot\{1+T^{Bg}(L+\Delta)\}^{-1}]^{-1}. \qquad (\text{E.32})$$

Appendix F

Partial wave amplitudes

The partial wave projection consists in the decomposition of the scattering amplitude in terms of Legrende Polynomials of the scattering angle:

$$\mathcal{O}(s,t) \;=\; \sum_{J=0}^{\infty} 32\pi^2 (2J+1)\; P^J(cos\theta)\; \mathcal{O}^J(s)\;, \tag{F.1}$$

with the first two polynomia being $P^0(x) = 1$ and $P^1(x) = x$.

F.1   Scattering with I=J=1

The $I = J = 1$ scattering allows the final and inital states $\pi\pi$ and $K\overline{K}$. The corresponding partial wave scattering amplitudes at LO in $1/N_C$ can be put together into the matrix

$$T_{LO}^{I=J=1} \;=\; \Sigma\;\cdot\; \frac{q^2}{96\pi F^2}\; \left[1 + \frac{2G_V^2}{F^2}\frac{q^2}{M_V^2 - q^2}\right] \begin{pmatrix} 1 & -\dfrac{1}{\sqrt{2}} \\ -\dfrac{1}{\sqrt{2}} & \dfrac{1}{2} \end{pmatrix} \cdot \Sigma\;, \tag{F.2}$$

where $\Sigma = \text{diag}(\sigma_\pi, \sigma_K)$, being $\sigma_P = \sqrt{1 - 4m_P^2/q^2}$, and only the s-channel scattering is considered. In this result the initial and final states are given in the charge basis.

One can observe that, up to the kinematic Σ factors (proportional to the identity in the equal mass limit), the scattering amplitude is proportional to the projector

$$P_{|8\rangle}^{1^{(1)}} \;=\; \frac{2}{3} \begin{pmatrix} 1 & -\dfrac{1}{\sqrt{2}} \\ -\dfrac{1}{\sqrt{2}} & \dfrac{1}{2} \end{pmatrix}\;, \tag{F.3}$$

in the direction

$$|8\rangle^{1^{(1)}} \;=\; \sqrt{\frac{2}{3}}|\pi\pi\,\rangle^{1^{(1)}} - \sqrt{\frac{1}{3}}|K\overline{K}\,\rangle^{1^{(1)}} \;=\; \sqrt{\frac{2}{3}} \begin{pmatrix} 1 \\ -\dfrac{1}{\sqrt{2}} \end{pmatrix}\;, \tag{F.4}$$

where one has the $\pi\pi$ and $K\overline{K}$ states in the isospin and angular momentum basis.

The T-scattering operator acting over an incoming octet $1(1^{--})$ state produces only an outgoing octet $1(1^{--})$ state. This is the reason for the particular form of the matrix of the partial wave scattering amplitude. Likewise, it is easy to check that the VFF for pions and kaons at tree level is essentially the vector $|\mathbf{8}\rangle^{1(1)}$, i.e. the vector quark current generates just an octet state.

F.2   Scattering with $I = J = 0$

For $SU(3)$ one can find in this channel the states $\pi\pi$, $K\overline{K}$ and $\eta_8\eta_8$. Their partial wave scattering amplitudes are given by the symmetric matrix

$$
\begin{aligned}
T_{LO}^{I=J=0} = \frac{1}{F^2} &\begin{pmatrix} \left[q^2 - \frac{m_\pi^2}{2}\right] & \left[\frac{\sqrt{3}q^2}{4}\right] & \left[\frac{m_\pi^2}{2\sqrt{3}}\right] \\ \dots & \left[\frac{3q^2}{4}\right] & \left[\frac{3q^2}{4} - \frac{2m_K^2}{3}\right] \\ \dots & \dots & \left[\frac{m_\eta^2}{2} + \frac{2\Delta_{K\pi}}{9}\right] \end{pmatrix} + \\[2em]
+ \frac{1}{F^2}\frac{q^4}{M_8^2 - q^2} &\begin{pmatrix} \frac{1}{4} & -\frac{1}{4\sqrt{3}} & -\frac{1}{4\sqrt{3}}\left(1 + \frac{2\Delta_{K\pi}}{3q^2}\right) \\ .. & \frac{1}{12} & \frac{1}{12}\left(1 + \frac{2\Delta_{K\pi}}{3q^2}\right) \\ \dots & \dots & \frac{1}{12}\left(1 + \frac{2\Delta_{K\pi}}{3q^2}\right)^2 \end{pmatrix} + \\[2em]
+ \frac{1}{F^2}\frac{q^4}{M_1^2 - q^2} &\begin{pmatrix} \frac{1}{2} & \frac{1}{\sqrt{3}} & \frac{1}{2\sqrt{3}} \\ \dots & \frac{2}{3} & \frac{1}{3} \\ \dots & \dots & \frac{1}{6} \end{pmatrix},
\end{aligned}
\tag{F.5}
$$

where $\Delta_{K\pi} = (m_K^2 - m_\pi^2)$ and the values of the scalar couplings at LO in $1/N_C$, $c_d = c_m = F/2$, have been considered. This result is given for the final and initial states in the charge basis and only the s-channel scattering has been considered.

Bibliography

[1] "Aspects of quantum chromodynamics", A. Pich, Proc. 1999 ICTP Summer School in Particle Physics (Trieste, Italy, 21 June- 9 July 1999), eds. G. Senjanović and A. Yu. Smirnov, The ICTP Series in Theoretical Physics – Vol. 16 (World Scientific, Singapore, 2000) 53-102; hep-ph/0001118.

[2] "QCD and Resonance Physics: Applications", M.A. Shifman, A.I. Vainshtein, V.I. Zakharov; *Nucl. Phys.* B **147** (1979) 448. "QCD and Resonance Physics: Sum Rules", M.A. Shifman, A.I. Vainshtein, V.I. Zakharov; *Nucl. Phys.* B **147** (1979) 385. "Condensates in Quantum Chromodynamics", B.L. Ioffe, *Phys. Atom. Nucl.* **66** (2003) 30-43.

[3] "Light Quark Masses in QCD from Local Duality", C.A. Domínguez, E. de Rafael; *Ann. Phys.* **174** (1987) 372. "Four-Quark Operators and Non-Leptonic Weak Transitions", A. Pich. E. de Rafael; *Nucl. Phys.* B **358** (1991) 311.

[4] "Chiral-Symmetry Breakdown in Large-N Chromodynamics", S. Coleman, E. Witten; *Phys. Rev. Lett.* **45,2** (1980) 100.

[5] "A Planar Diagram Theory for Strong Interactions", G. 't Hooft, *Nucl. Phys.* B **72** (1974) 461. "A Two-Dimensional Model for Mesons", G. 't Hooft, *Nucl. Phys.* B **75** (1974) 461. "Baryons in the $1/N_C$ Expansion", E. Witten, *Nucl. Phys.* B **160** (1979) 57.

[6] "Effective Field Theory", A. Pich, Proc. Les Houches Summer School of Theoretical Physics –Probing the Standard Model of Particle Interactions– (Les Houches, France, 28 July – 5 September 1997), eds. R. Gupta et al. (Elsevier Science B.V., Amsterdam, 1999), Vol. II, 949-1050, hep-ph/9806303.

[7] "Phenomenological Lagrangians", S. Weinberg, *Physica* **96A** (1979) 327.

[8] "Chiral Perturbation Theory to One Loop", J. Gasser and H. Leutwyler, *Annals Phys.* **158** (1984) 142.

[9] "Chiral Perturbation Theory: Expansions in the Mass of the Strange Quark", J. Gasserand H. Leutwyler, *Nucl. Phys.* B **250** (1985) 465.

[10] *Effective Lagrangian for Standard Model,* A. Dobado, A. Gómez-Nicola, A.L. Maroto, J.R. Peláez; Springer-Verlag Berlin Heidelberg (1997).

[11] "Heavy Quarks and Longlived Hadrons", T. Appelquist, H.D. Politzer; *Phys. Rev.* D **12** (1975) 1404.

[12] "On the foundations of Chiral Perturbation Theory", H. Leutwyler (Bern U.), *Annals Phys.* **235** (1994) 165-203.

[13] *Dynamics of the Standard Model,* J.F. Donoghue, E. Golowich, B.R. Holstein; Cambridge University Press.

[14] "Chiral Perturbation Theory", G. Ecker, *Prog. Part. Nucl. Phys.* **35** (1995) 1.

[15] "Chiral Perturbation Theory", A. Pich, *Rep. Prog. Phys.* **58** (1995) 563.

[16] "The Mesonic Chiral Lagrangian of Order p^6", J. Bijnens, G. Colangelo, G. Ecker; *JHEP* **9902** (1999) 020.

[17] "The Vector and Scalar Form Factors of the Pion to Two Loops", J. Bijnens, G. Colangelo, P. Talavera; *JHEP* **9805** (1998) 014.

[18] "τ Decays and Chiral Perturbation Theory", G. Colangelo, M. Finkemeier, R. Urech; *Phys. Rev.* D **54,7** (1996) 4403.

[19] "The Role of Resonances in Chiral Perturbation Theory" G. Ecker, J. Gasser, A. Pich, E. de Rafael; *Nucl. Phys.* B **321** (1989) 311.

[20] "Large N_C in Chiral Perturbation Theory", R. Kaiser and H. Leutwyler, *Eur. Phys. J.* C **17** (2000) 623-649; "Pseudoscalar decay constants at large N_C", R. Kaiser and H. Leutwyler, proceedings of *Workshop on Methods of Nonperturbative Quantum Field Theory,* Adelaide, Australia, 2-13 Feb 1998, hep-ph/9806336

[21] "Colourless Mesons in a Polychromatic World", A. Pich, Proc. Workshop on *The Phenomenology of Large–N_C QCD* (Tempe, Arizona, 9–11 January 2002), ed. R. Lebed (World Scientific, Singapore 2002); ArXiv:hep-ph/0205030.

[22] "Strangeness Changing Scalar Form Factors", M. Jamin, J.A. Oller and A. Pich, *Nucl. Phys.* B **622** (2002) 279.

[23] "Chiral Lagrangians for Massive Spin-1 Fields" G. Ecker, J. Gasser, H. Leutwyler, A. Pich, E. de Rafael; *Phys. Lett.* B **223** 3,4 (1989) 425.

[24] *An Introduction to Quantum Field theory*,
M.E. Peskin, D.V. Schroeder; Collæge Press, University of Beijing.

[25] *The quantum theory of fields: Volume I, foundations*, S. Weinberg, Cambridge University Press, 1995.

[26] "Hadronic Off-Shell Width of Meson Resonances"
D. Gómez Dumm, A. Pich, J. Portoles; *Phys. Rev.* D **62** (2000) 054014-1.

[27] "Effective Field Theory Description of the Pion Form Factor",
F. Guerrero, A. Pich; *Phys. Lett.* B **412** (1997) 382.

[28] "Pion and Kaon Vector Form-Factors", J.A. Oller, E. Oset and J.E. Palomar, *Phys. Rev.* D **63** (2001) 114009.

[29] "Finite-Width Corrections to the Vector-Meson-Dominance Prediction for $\rho \to e^+e^-$", G.J. Gounaris and J.J. Sakurai, *Phys. Rev. Lett.* **21** (1968) 244.

[30] "Chiral Perturbation Theory and Final State Theorem", T.N. Truong, *Phys. Rev. Lett.* **61** (1988) 2526.
"Unitarized Chiral Perturbation Theory for Elastic Pion-Pion Scattering", A. Dobado, M.J. Herrero and Tran N. Truong, *Phys. Lett.* **B** 235 (1990) 134.
"The Inverse Amplitude Method and Chiral Perturbation Theory to Two Loops", T. Hannah, *Phys. Rev.* D **55** (1997) 5613.
"Meson Meson Scattering within One Loop Chiral Perturbation Theory and its Unitarization", A. Gómez Nicola and J.R. Peláez, *Phys. Rev.* D **65** (2002) 054009.
"The Inverse Amplitude Method in $\pi\pi$ Scattering in Chiral Perturbation Theory to Two Loops", J. Nieves, M. Pavón Valderrama and E. Ruiz Arriola, *Phys. Rev.* D **65** (2002) 036002.

[31] "Bethe-Salpeter Approach for Unitarized Chiral Perturbation Theory", J. Nieves and E. Ruiz Arriola, *Nucl. Phys.* A **679** (2000) 57.

[32] "N/D Description of Two Meson Amplitudes and Chiral Symmetry",
J.A. Oller, E. Oset; *Phys. Rev.* D **60** (1999) 074023.

[33] "Long Distance Chiral Corrections in B-Meson Amplitudes", J.J. Sanz-Cillero, J.F. Donoghue and Andreas Ross, *Phys. Lett.* B **579** (2004) 86-98.

[34] "Phenomenology from Lattice QCD", L. Lellouch, *Nucl. Phys. Proc. Suppl.* **117** (2003) 127-144.

[35] "Die Bestimmung von $\pi\pi$-Streuphasen auf del Grundlage einer Amplitudeanalyse der Reaktion $\pi^- p \to \pi^- \pi^+ n$ bei 17 GeV/c Primärimpuls",
W. Ochs; Ph.D. Thesis (U.Munich, 1973).

[36] "Restrictions on Symmetry Breaking in Vector - Like Gauge Theories",
C. Vafa and E. Witten, *Nucl. Phys.* B **234** (1984) 173.

[37] "Theoretical Chiral Dynamics", H. Leutwyler, talk given at the 3rd Workshop
on Chiral Dynamics –Chiral Dynamics 200: Theory and Experiment, Newport
News, Virginia 17-22 Jul 2000; hep-ph/0011140.

[38] "The Standard Model of Electroweak Interactions", A. Pich, lectures given
at CERN Academic Training, Geneva, Switzerland 15-26 Nov 1993; hep-
ph/9412274.

[39] "Flavor Dynamics", A. Pich, talk given at 23rd International Meeting on Fun-
damental Physics: The Top Quark, Heavy Flavour Physics and Symmetry
Breaking, Comillas, Spain 22-26 May 1995; hep-ph/9601202.

[40] "Low-Energy Expansion of Meson Form Factors",
J. Gasser, H. Leutwyler; *Nucl. Phys.* B **250** (1985) 517.

[41] "Spectrum of QCD and chiral lagrangian of the strong and weak interactions",
J.F. Donoghue, C. Ramirez and G. Valencia, *Phys. Rev.* D **39,7** (1989) 1947-
1955.

[42] "Low energy hadron physics from effective chiral lagrangians with vector
mesons", U.G. Meissner, *Phys. Rep.* **161** (1988) 213.

[43] M. Bando, T. Kugo and K. Yamawaki, *Phys. Rep.* **164** (1988) 217.
"Hidden Local Symmetry at loop", M. Harada and K. Yamawaki, *Phys. Rep.*
381 (2003) 1-233.
"Hidden Local Symmetry at one loop", M. Harada and K. Yamawaki, *Phys.
Lett.* B **297** (1992) 151-158.

[44] "The hadronic cross-section in the resonance energy region", J. Portoles and
P.D. Ruiz-Femenia, talk given at *Workshop on Hadronic Cross-Section at Low-
Energy* (SIGHAD03), Pisa, Italy, 8-10 Oct 2003. published in *Nucl. Phys. Proc.
Suppl.* **131** (2004) 170-175.

[45] "One Loop Corrections for e^+e^- annihilation into $\mu^+\mu^-$ in the Weinberg
Model",
G. Passarino, M. Veltman; *Nucl. Phys.* B **160** (1979) 151.

[46] "Extensión de ChPT a Energías Superiores",
F. Guerrero; Ph.D. Thesis (U. Valencia, 1998).

[47] "Renormalització de RχT: Factor de Forma Vectorial del pió", I. Rosell, *trabajo
de investigación de tercer ciclo* (U. Valencia 2004)

[48] S. Weinberg, *Phys.Rev. Lett.* **18** (1967) 507.

[49] M.A. Shiftman, A.I. Vainstein and V.I. Zahkarov, *Nucl. Phys.* B **147** (1979) 385, 448.
M. Jamin and M. Münz, *Z. Phys.* C **66** (1995) 633.
M. Golterman and S. Peris, *Phys. Rev.* D **61** (2000) 034018.
M. Knecht and E. de Rafael, *Phys. Lett.* B **424** (1998) 335.
M. Knecht, S. Peris and E. de Rafael, *Phys. Lett.* B **443** (1998) 255.
M. Golterman*et al.*, *JHEP* **024** (2002).
S. Peris, hep-ph/0204181.

[50] "Exclusive processes and the exclusive-inclusive connection in Quantum Chromodynamics", S.J. Brodsky and G.P. Lepage, presented at Workshop on Current Topics in High Energy Physics, Cal Tech., Pasadena, Calif., Feb 13-17, 1979.
"Exclusive processes in perturbative Quantum Chromodynamics", G.P. Lepage and S.J. Brodsky, *Phys. Rev.* D **22,9** (1980) 2157.
"Asymptotic behaviour of composite particle form-factors and the renormalization group", A. Duncan and A. H. Mueller, *Phys. Rev.* D **21** (1980) 1636.
"Asymptotics of pion electromagnetic form-factor in scale invariant quark model", A.V. Efremov and A.V. Radyushkin (Moscow State U.), *Teor.Mat.Fiz.* **30** (1977) 168-182.

[51] " Asymptotic limits and structure of the pion form-factor", J.F. Donoghue and Euy Soo Na, *Phys. Rev.* D **56** (1997) 7073-7076.

[52] "Spectral Function Sum Rules in Quantum Chromodynamics"
E. Floratos, S. Narison and E. de Rafael; *Nucl. Phys.* B **155** (1979) 115.

[53] "Semileptonic Decays of Pseudoscalar Particles $(M \to M' + l + \nu_l)$ and Short-distance Behaviour of Quantum Chromodynamics"
C. Bourrely, B. Machet and E. de Rafael; *Nucl. Phys.* B **189** (1981) 157.

[54] "Asymptotic behaviour and subtractions in the Mandlestam representation", Marcel Froissart, *Phys. Rev.* **123** (1961) 1053-1057.

[55] "Matching long and short distance in large N_C QCD", S. Peris, M. Perrottet and E. de Rafael, *JHEP* **9805** (1998) 011.
"tests of large N_C QCD from hadronic tau decay", S. Peris, B. Phily and E. de Rafael, *Phys. Rev. Lett.* **86** (2001) 14-17.
"Analytic approaches to kaon physics", E. de Rafael, *Nucl. Phys. Proc.Suppl.* **119** (2003) 71-83.

[56] "On the Solution of Certain Singular Integral Equations of Quantum Field Theory",
R. Omnès; *Nuovo Cimento* **8** (1958) 316.

[57] "Singular Integral Equations", N. I. Muskhelishvili, (Noordhoof, Gronigen, 1953).

[58] "Introduction to Chiral Perturbation Theory" , S. Scherer, to be edited by J.W. Negele and E. Vogt. In *Negele, J.W. (ed.) et al.: Advances in Nuclear Physics*, **vol. 27** 277-538; ArXive hep-ph/0210398

[59] " An example of resonance saturation at one loop" , O. Cata and S. Peris, *Phys. Rev.* D **65** (2002) 056014.

[60] "Some General Relations Between the Photoproduction and Scattering of π Mesons",
K. M. Watson; *Phys. Rev.* 95 (1954) 228.

[61] " Final State Interactions in Kaon Decays"
E. Pallante, A. Pich; *Nucl. Phys.* B **592** (2001) 294.

[62] " $\pi\pi$ Partial Wave Analysis from Reactions $\pi^+ P \to \pi^+\pi^-\Delta^{++}$ and $\pi P \to K^+ K^- \Delta^{++}$ at 7.1 GeV/c",
S. D. Protopopescu, M. Alston-Garnjost, A. Barbaro-Galtieri, S. M. Flatte, J. H. Friedman, T. A. Lasinski, G. R. Lynch, M. S. Rabin, F. T. Solmitz; *Phys. Rev.* D **7** (1973) 1279.

[63] "Vector Form Factor of the Pion from Unitarity and Analyticity: A model-Independent Approach", A. Pich and J. Portolés, *Phys. Rev.* D **63** (2001) 093005.

[64] "Hadronic Contributions to the $g - 2$ of the Muon", J.A. Casas, C. López and F.J. Yndurain, *Phys. Rev.* D **32** (1985) 736.
"Precision Determination of the Pion Form Factor and Calculation of the Muon $g - 2$", J.F. De Trocóniz and F.J. Yndurain, *Phys. Rev.* D **65** (2002) 093001.

[65] "Measurement of the Spectral Functions of the Vector Current Hadronic Tau Decays", ALEPH Collaboration (R. Barate et al.), *Z. Phys.* C **76** (1997) 15.

[66] "A Measurement of the Space-like Pion Electromagnetic Form Factor", NA7 Collaboration (S.R. Amendolia et al.), *Nucl. Phys.* B **277** (1986) 168.

[67] "Measurement of $e^+e^- \to \pi^+\pi^-$ Cross Section with CMD-2 around ρ Meson", CMD-2 Collaboration (R.R. Akhmetshin et al.), *Phys. Lett.* B **527** (2002) 161;
" Reanalysis of hadronic cross-section measurements at CMD-2" , CMD-2 Collaboration (R.R. Akhmetshin *et al.*), *Phys. Lett.* B **578** (2004) 285-289.

[68] "Hadronic Structure in the Decay $\tau^- \to \pi^-\pi^0\nu_\tau$", CLEO Collaboration (S. Anderson et al.), *Phys. Rev.* D **61** (2000) 112002.

[69] "Measurement of the Strong Coupling Constant $\alpha(s)$ and the Vector and Axial Vector Spectral Functions in Hadronic Tau Decays", OPAL Collaboration (K. Ackerstaff et al.), *Eur. Phys. J.* C **7** (1999) 571.

[70] "MINUIT a System for Function Minimization and Analysis of the Parameter Errors and Correlations", F. James and M. Roos, *Comput. Phys. Commun.* **10** (1975) 343.

[71] "$\pi\pi$ Scattering", G. Colangelo, J. Gasser and H. Leutwyler, *Nucl. Phys.* B **603** (2001) 125.

[72] "Effective Theory calculation of resonant high-energy scattering", M. Beneke, A.P. Chapovsky, A. Signer and G. Zanderighi, *Nucl. Phys.* B **686** (2004) 205-247.

[73] "Study of the Resumation of Chiral Logarithms in the Exponentiated Expression for the Pion Form-Factor",
F. Guerrero; *Phys. Rev.* D **57** (1998) 4136. hep-ph/9801305.

[74] "Tau Decay Determination of the strange Quark Mass", A. Pich, J. Prades, *Nucl. Phys. Proc. Suppl* **86** (2000) 236-241.

[75] "Strange Quark Mass from the Invariant Mass Distribution of Cabibbo-Suppressed Tau Decays",
S. Chen, M. Davier, E. Gamiz, A. Hocker, A. Pich and J. Prades, *Eur. Phys. J.* C **22** (2001) 31-38.

[76] "S-Wave $K\pi$ Scattering in Chiral Perturbation Theory with Resonances",
M. Jamin, J. A. Oller, A. Pich; *Nucl. Phys.* B **587** (2000) 331-362.

[77] "The Decay of a Light Higgs Boson", J.F. Donoghue, J. Gasser and H. Leutwyler, *Nucl. Phys.* B **343** (1990) 341.

[78] "Light Higgs Particle in Decays of K and η Mesons", H. Leutwyler and M.A. Shifman, *Nucl. Phys.* B **343** (1990) 369;
"The decay $\eta \to \pi^0 H^0$ in two Higgs doublet models with a light scalar", J. Prades and A. Pich, *Phys. Lett.* B **245** (1990) 117;
"Bounds on a light scalar in two Higgs doublet models", A. Pich, J. Prades and P. Yepes, *Nucl. Phys.* B **388** (1992) 31.

[79] "K(l4) Decays Beyond One Loop", J. Bijnens, G. Colangelo, J. Gasser; *Nucl. Phys.* B **427** (1994) 427. hep-ph/9403390.

[80] "Short Distance Current Correlators: Comparing Lattice Simulations to the Instanton Liquid", T. DeGrand. *Phys. Rev.* D **64** (2001) 094508.

[81] "Charm Quark Mass from QCD Sum Rules for the Charmonium System",
M. Eidemuller, M. Jamin; *Phys. Lett.* B **498** (2001) 203. hep-ph/0010334.

[82] "Review of Particle Physics", Particle Data Group; *The European Physical Journal* C **15,1-4** (2000).

[83] "Structure of Phenomenological Lagrangians. 2",
C.G. Callan, Jr., S. Coleman, J. Wess, B. Zumino; *Phys. Rev.* **177** (1969) 2247.

[84] "Structure of Phenomenological Lagrangians. 1",
S. Coleman, J. Wess, B. Zumino. *Phys. Rev.* **177** (1969) 2239.

[85] "Chiral Perturbation Theory and Final State Theorem",
T.N. Truong; *Phys. Rev. Lett.* **61** (1988) 2526.

[86] "The Inverse Amplitude Method and Chiral Perturbation Theory to Two Loops",
T. Hannah, *Phys. Rev.* D **55** (1997) 5613.

[87] "On Analytic Properties of Vertex Parts in Quantum Field Theory",
L.D. Landau; *Nucl. Phys.* **13** (1959) 181.

[88] "Electromagnetic Form-Factor in the Timelike Region",
L.M. Barkov, A.G. Chilingarov, S.I. Eidelman, B.I. Khazin, M.Yu. Lelchuk,
V.S. Okhapkin, E.V. Pakhtusova, S.I. Redin, N.M. Ryskulov, Yu.M. Shatunov,
A.I. Shekhtman, B.A. Shvarts, V.A. Sidorov, A.N. Skrinsky, V.P. Smakhtin,
E.P. Solodov; *Nucl. Phys.* B **256** (1985) 365.

[89] R.P. Feynman, *Phys. Rev.* **56** (1939 340;
H. Hellman, *Einführung in die Quantenchemie*, Deuticke Verlag (Leipzig, 1937);
S.T. Epstein, *Amer. J. Phys.* **22** (1954) 613.

[90] "Determination of the Elements V_{us} and V_{ud} of the Kobayashi-Maskawa Matrix",
H. Leutwyler, M. Roos; *Z. Phys.* C **25** (1984) 91.

[91] "Ground States $q\bar{q}$ Mass Spectrum in QCD", H.J. Munczek, A.M. Nemirovsky;
Phys. Rev. D **28** (1983) 181.

[92] "Numerical Estimates of Hadronic Masses in a Pure $SU(3)$ Gauge Theory",
H. Hamber, G. Parisi; *Phys. Rev. Lett.* **47, 25** (1981) 1792.

[93] "Precise Relations between the Spectra of Vector and Axial Vector Mesons",
S. Weinberg; *Phys. Rev. Lett.* **18** (1967) 507.

[94] "Study of the Three Prong Tau Decays and Determination of A1 Parameters",
DELCO Collaboration (W. Ruckstuhl et al.); *Phys. Rev. Lett.* **56** (1986) 2132.

[95] "Evidence for the Electromagnetic Production of the A1",
M. Zielinski, D. Berg, C. Chandlee, S. Cihangir, T. Ferbel, J. Huston, T. Jensen,

F. Lobkowicz, T. Ohshima, P. Slattery, P. Thompson, B. Collick, S. Heppelmann, M. Marshak, E. Peterson, K. Ruddick, A. Jonckheere, C.A. Nelson, Jr.; *Phys. Rev. Lett.***52** (1984) 1195.

[96] "Absorption and Dispersion od Pions at Finite Temperature", A. Schenk; *Nucl. Phys.* B **363** (1991) 97.

[97] "The Octet Model and its Clebsch-Gordan Coefficients" , J.J. De Swart, *Review of Modern Physics* **35, 4** (1963) 916.

[98] "Hadronic Contributions to the $g - 2$ of the Muon", J.A. Casas, C. López and F.J. Yndurain, *Phys. Rev.* D **32** (1985) 736.
"Precision Determination of the Pion Form Factor and Calculation of the Muon $g - 2$", J.F. De Trocóniz and F.J. Yndurain, *Phys. Rev.* D **65** (2002) 093001.

[99] "The $\pi\pi$ Interaction", J.L. Peterson, Yellow Report CERN 77-04 (1977).

[100] "Pion and Kaon Electromagnetic Form Factors", J. Bijnens and P. Talavera, *J. High Energy Phys.* **03** (2002) 046.

[101] "Lattice QCD meets experiment in hadron physics", C. Davies and P. Lepage, talk given at Hadron 03:10th International Conference on Hadron Spectroscopy, Aschaffenburg, Germany 31 Aug - 6 Sep 2003; ArXiv:hep-ph/0311041;
"High Precision Lattice QCD Confronts Experiment", HPQCD Collaboration, UKQCD Collaboration, MILC Collaboration and Fermilab Lattice Collaboration (C.T.H. Davies et al.), *Phys. Rev. Lett.* **92** (2004) 022001.

[102] "Chiral Extrapolation of light-light and heavy-light decay constants in unquenched QCD" , S. Hashimoto *et al.* [JLQCD Collaboration], *Nucl. Phys. Proc. Suppl.* **119** (2003) 332-334;

[103] "Chiral Extrapolation of Lattice Moments of Proton Quark Distributions" , W. Detmold *et al.*, *Phys. Rev. Lett.* **87** (2001) 172001.

[104] "Meson Resonances, Large N_C and Chiral Symmetry", V. Cirigliano, G. Ecker, H. Neufeld and A. Pich, *JHEP* **0306:012** (2003).

[105] "Rho meson properties in the chiral theory framework" , J.J. Sanz-Cillero and A. Pich, *Eur. Phys. J.* C **27** (2003) 587-599.

[106] "Quantum Loops in the Resonance Chiral Theory: The Vector Form Factor" , I. Rosell, A. Pich and J.J. Sanz-Cillero, hep-ph/0407240 (*submitted to JHEP*).

[107] "Pion and Kaon decay constants: Lattice vs. Resonance Chiral Theory" , J.J. Sanz-Cillero; hep-ph/0408080 .

[108] "Heavy quark physics and lattice QCD", N. Yamada, *Nucl. Phys. Proc. Suppl.* **119** (2003) 93-104;
"Lattice results relevant to the CKM matrix determination", D. Becirevic, talk given at 31st International Conference on High Energy Physics (ICHEP 2002), Amsterdam, The Netherlands, 24 -31 Jul 2002, published in *Amsterdam 2002, ICHEP*, 493-498; arXiv:hep-ph/0211340.

[109] "Chiral perturbation theory for $f_D(s)$ / f_D and $B_B(s)$ / B_B", B. Grinstein, E. Jenkins, A. V. Manohar, M. J. Savage and M. B. Wise, *Nucl. Phys.* B **380**, 369 (1992).

[110] "Quenched Chiral Perturbation Theory for Heavy-light Mesons", S. R. Sharpe and Y. Zhang, *Phys. Rev.* D **53**, 5125 (1996).

[111] "B → pi and B → K transitions in standard and quenched chiral perturbation theory", D. Becirevic, S. Prelovsek and J. Zupan, *Phys. Rev.* D **67**, 054010 (2003).

[112] "Chiral corrections and lattice QCD results for f_{B_s}/f_{B_d} and $\Delta m_{B_s}/\Delta m_{B_d}$", D. Becirevic, S. Fajfer, S. Prelovsek and J. Zupan, *Phys. Lett.* B **563** (2003) 150-156.

[113] "Improving the convergence of SU(3) baryon chiral perturbation theory", J. F. Donoghue and B. R. Holstein; ArXiv:hep-ph/9803312;
"SU(3) baryon chiral perturbation theory and long distance regularization", J. F. Donoghue, B. R. Holstein and B. Borasoy, *Phys. Rev.* D **59**, 036002 (1999).

[114] "Nucleon magnetic moments beyond the perturbative chiral regime", D. B. Leinweber, D. H. Lu and A. W. Thomas, *Phys. Rev.* D **60**, 034014 (1999);
"Incorporating chiral symmetry in extrapolations of octet baryon magnetic moments", E. J. Hackett-Jones, D. B. Leinweber and A. W. Thomas, *Phys. Lett.* B **489**, 143 (2000);
"Systematic correction of the chiral properties of quenched QCD", R. D. Young, D. B. Leinweber, A. W. Thomas and S. V. Wright; ArXiv:hep-lat/0111041.

[115] "First measurement of Gamma(D*+)", S. Ahmed *et al.* [CLEO Collaboration], *Phys. Rev. Lett.* **87**, 251801 (2001);
"First lattice QCD estimate of the g(D* D pi) coupling", A. Abada D. Becirevic, P. Boucaud, G. Herdoiza, J.P. Leroy, A. Le Yaouanc, O. Pene, J. Rodriguez-Quintero, *Phys. Rev.* D **66**, 074504 (2002);
"g-hat coupling (g(B* B pi), g(D* D pi)): A quark model with Dirac equation", D. Becirevic and A. L. Yaouanc, *JHEP* **9903**, 021 (1999);
"D* D pi form factor revisited", F. S. Navarra, M. Nielsen and M. E. Bracco, *Phys. Rev.* D **65**, 037502 (2002).

[116] "B0 - anti-B0 mixing in quenched lattice QCD", S. Aoki *et al.* [JLQCD Collaboration], *Phys. Rev.* D **67**, 014506 (2003);
"B meson B-parameters and the decay constant in two-flavor dynamical QCD", N. Yamada *et al.* [JLQCD Collaboration], *Nucl. Phys. Proc. Suppl.* **106**, 397 (2002).

[117] "Four-point correlator constraints on electromagnetic chiral parameters and resonance effective lagrangians", B. Ananthanarayan and B. Moussallam, *JHEP* **0406** (2004) 047.

[118] "$\tau \to \pi\pi\pi\nu_\tau$ decays in the Resonance Effective Theory", D. Gomez Dumm, A. Pich and J. Portoles, *Phys. Rev.* D **69** (2004) 073002;
"$\tau \to \pi\pi\pi\nu_\tau$: Theory versus experiment", D. Gomez Dumm, A. Pich and J. Portoles, Talk given at 10th International QCD Conference (QCD 03), Montpellier, France, 2-9 Jul 2003, hep-ph/0312211.